Stratigraphy, Sedimentology, and Diagenesis of Ordovician Outliers, Northern Ottawa–Bonnechere Graben, Central Ontario

by

He Kang

A thesis submitted to the Faculty of Graduate and Postdoctoral Affairs in partial fulfillment of the requirements for the degree of

Master of Science

in

Earth Sciences

Carleton University
Ottawa, Ontario

Abstract

Several Ordovician outliers along or near the northern Ottawa–Bonnechere graben are bounded by Precambrian rocks of the Canadian Shield. Correlation of outlier stratigraphy reveals that these remnant bodies form part of a once expansive Late Ordovician phase of the St. Lawrence Platform extending into the craton interior from the Laurentian margin. Integrating litho-, bio-, and chemostratigraphic data sets, four outliers (Deux Rivières, Brent Crater, Cedar Lake, and Manitou Islands) preserve Turinian strata, whereas a fifth (Owen Quarry outlier) illustrates how local downfaulting has preserved lower Chatfieldian strata. Each outlier documents a unique depositional succession but, in common, record shallow-water depositional environments during net transgression. Local diagenetic records reveal the roles of surface marine, shallow-burial, and deep-burial alteration of limestone. Several dolomite types are present: fabric-selective, pervasive replacement, and local fracture/paleovoid-fill. Isotope (C, O, Sr) signatures identify interaction of dolomitizing fluids with a ^{87}Sr-enriched reservoir, and very negative $\delta^{18}O$ values of dolomite suggest either elevated temperature or meteoric influence. Dolomite shows basement-related, stratabound, and fault/fracture-related spatial distributions. Early-stage dolomitization may be related to Mg derived from marine or meteoric waters whereas late-stage dolomitization, including hydrothermal saddle dolomite, likely involves brines that migrated along Paleozoic-Precambrian boundary, then refocused along vertical faults and fractures. In general, this study demonstrates stratigraphic and sedimentary connectivity in the Laurentia craton interior during the early Late Ordovician, and dolomitization that may be related to local and regional fluid migration.

Acknowledgements

First and foremost, I'd like to thank my thesis supervisor, George R. Dix for giving me the opportunity to work on this great project, and all the support and guidance through the completion of the thesis. For staffs of Carleton University, I'd like to thank Tim Mount for making thin-sections, Peter Jones for conducting microprobe analysis, Shuangquan Zhang for supervision of strontium isotope analysis, and Jianqun Wang for SEM analysis. Quarry owner and Ontario Parks are thanked for allowance of doing field work and field help from the latter. GSC-Ottawa is thanked for access of logging Brent Crater core and XRD analysis of clay samples. Queen's Facility for Isotope Research (Queen's University) and G.G. Hatch Stable Isotope Laboratory (University of Ottawa) contributed to carbon and oxygen isotope analysis. Sandy McCracken (GSC-Calgary) is thanked for processing and identifying conodont fauna. Yuefeng Shen (Laval University) helped with identification of cyanobacteria and algae. I also want to thank my committee members André Desrochers and Claudia Schröder-Adams for their time reviewing my thesis and the comments that improved this thesis.

I'd like to thank my office mates Nkechi Oruche and Wilder Greenman for all the help and discussions. Faculty members, staffs, and fellow graduate students at the Department of Earth Sciences, Carleton University are thanked for making my stay in the department enjoyable.

Thanks to my friends for their accompany during my time in Ottawa. Finally, I want to thank my family members in China who have been consistent support during my stay in Canada, with special thanks to my father Yili Kang who introduced me to the field of geology.

Table of Contents

List of Tables

List of Figures

List of Appendices

Chapter 1 Introduction

1.1 Paleozoic outliers, Ontario

The Ottawa–Bonnechere graben (OBG; Kay, 1942) forms a northwest-trending basement structure extending over at least 650 km from near Montreal (Quebec) in the east to Lake Nipissing (Ontario) in the west (Fig. 1.1). A northern extension, the Timiskaming graben, extends northward from its intersection with the OBG axis near Mattawa, Ontario, and contains the large Timiskaming outlier in the region of New Liskeard (Hume, 1925; Dix et al., 2007). The OBG is of multi-generational origin (Bleeker et al., 2011), cross-cutting both Paleozoic strata and lithotectonic elements of the Mesoproterozoic Grenville Province in the east, and the rocks of the Archean Superior Province and Paleoproterozoic Southern Province in the northwest. Igneous activity at around 590 Ma began with intrusion of large mafic dykes that lie approximately parallel to the later OBG structural axis (Kamo et al., 1995). Local syenitic intrusions followed (Bleeker et al., 2011). The graben is fault-bounded with left-stepping *en échelon* segments for which latest activity appears mostly younger than the Ordovician. But faults were likely initiated as early as ~ 577 Ma and reactivated several times later in the Phanerozoic (Dix and Al Rodhan, 2006; Salad Hersi and Dix, 2006; Dix and Joliceour, 2011; Bleeker et al., 2011).

Paleozoic outliers occur along the axis of the northern OBG and Timiskaming graben within the Canadian Shield (Fig. 1.1). They lie beyond the northwestern erosional limit of continuous Paleozoic cover in eastern and southern Ontario (Fig. 1.1) that forms part of the regional St. Lawrence Platform of eastern Laurentia (Caley and Liberty, 1957;

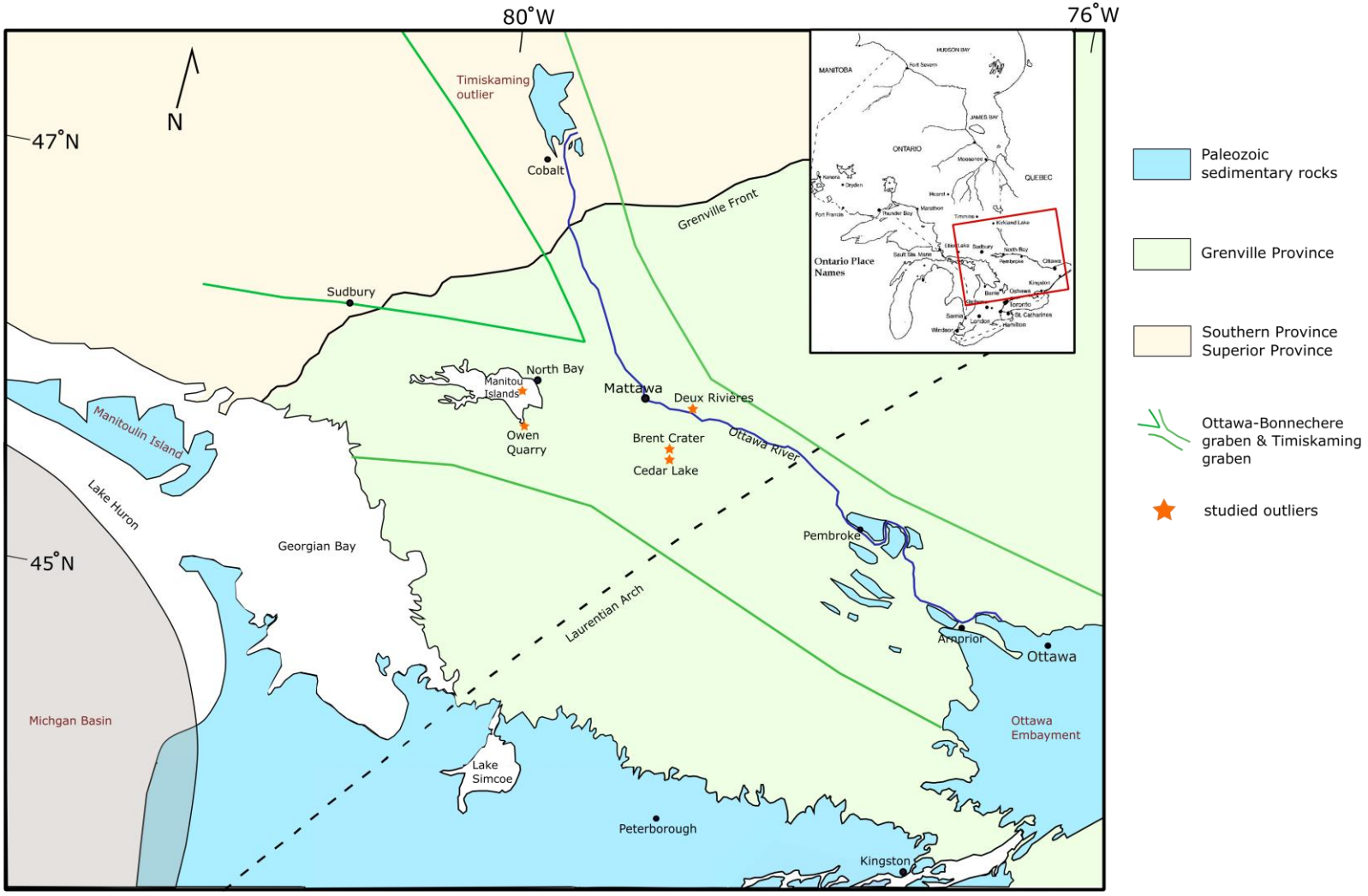

Figure 1.1. Summary map of the Ottawa–Bonnechere graben, related geological features, and location of studied outliers. Modified after Bleeker et al., 2011.

Sanford, 1993a). In general, outlier stratigraphy suggests that they are the erosional remnants of a once more expansive Ordovician succession that extended deep into the Laurentian interior (Hume, 1925; Caley and Liberty, 1957).

A brief history of previous geological work related to the outliers is summarized here. Logan (1847) is the first to refer to the Deux Rivières section on his famous journey along the Ottawa River into the Canadian interior. Goodwillie (1893) mentioned Trentonian sedimentary rocks on Little Manitou Island and Great Manitou Island in Lake Nipissing, and the abundance of fossils. Barlow (1899) indicated that Blackriveran and Trentonian limestone and sandstone outcropped near Mattawa and on Manitou Islands. He also summarized previous paleontological work on all the above sites. Caley and Liberty (1957) confirmed the same age range of these outcrops, and interpreted a more expansive Paleozoic sea that connected St. Lawrence Lowlands with Hudson Bay Lowland area and the Arctic region. Colquhoun (1958) studied the stratigraphy and paleontology of outliers near Mattawa and on Manitou Islands and compared them to rocks elsewhere in Ontario and eastern Quebec.

A small dolostone outlier exposed at an abandoned quarry immediately south of Lake Nipissing (Fig. 1.1) is named after the current owner, Terry Owen. General lithologies and fossil types were previously described by Satterly (1943), Colquhoun (1958), and Lumber (1971).

The only formal geological information about Paleozoic rocks exposed along the north shore of Cedar Lake in Algonquin Park is from a map published by Ford et al. (1984). There is, however, a website with location and images of what is referred to as the Brent Limestone Cliff (http://www.mcelroy.ca/notes/brent_limestone_cliff.html).

The most enigmatic Paleozoic outlier is not even exposed, but underlies the limits of Brent Crater, an impact structure discovered by aerial photographs (Grieve, 2006). Most attention has been directed to studies of the impact breccia, but details of the overlying sedimentary facies recovered from core were published by Lozej and Beales (1975). They interpreted the sedimentary fill to represent deposits of an initial saline lake succeeded by about 150 m (500 ft) of marine sedimentary rocks of Blackriveran-Trentonian age. Grahn and Ormö (1995) found Late Ordovician chitinozoans at the base of the sedimentary section, however, that suggested that the impact structure may have occurred within an Ordovician shallow sea.

1.2 Statement of research intent

The principal goal of this thesis is to integrate existing and new data from widely distributed Ordovician outliers along the northern OBG to evaluate what stratigraphic and sedimentary commonalities, if any, may exist, and develop a better understanding of Late Ordovician deposition within the interior of Laurentia. The structure of the thesis includes, first, separate chapters for each outlier in which there are descriptions and interpretations of stratigraphy, depositional environments, and aspects of diagenesis defined petrographically and geochemically. Where relevant, the characters and origins of dolomitization are presented and discussed. Second, within the Discussion chapter, these geographically separated outliers are placed into regional stratigraphic (litho-, chemo-, and bio-) frameworks, and compared to those defined for the St. Lawrence Platform in southern and eastern Ontario (McFarlane, 1992; Salad Hersi, 1997; El Gadi, 2001), and the larger Timiskaming outlier (Russel, 1984) to the north. Finally, the study

will examine the origins of dolomitization that appears to have affected all localities but to different extents.

1.3 Geological setting

1.3.1 St. Lawrence Platform

Sedimentary rocks outcropping along the Ottawa–Bonnechere graben are part of the larger St. Lawrence Platform (Fig. 1.2) that developed along eastern Laurentia (Kay, 1942; Sandford, 1993a). The St. Lawrence Platform borders the Canadian Shield, and is in turn bounded on the southeast to east by the Appalachian orogen (Sanford, 1993a).

The sedimentary succession in the central St. Lawrence Platform contains Sloss (1988)'s Sauk and Tippecanoe I cratonic sequences, now referred to as megasequences. Local expression of the Sauk Megasequence (latest Proterozoic to early Middle Ordovician in age; Dix, 2012) records sedimentation during rifting of Rodinia and deposition associated with the interior of an epicontinental trailing-margin platform bordering the developing Iapetan Ocean basin (Sloss, 1988). Local expression of the Tippecanoe I Megasequence (Middle Ordovician–early Silurian; Ettensohn and Brett, 2002) records foreland-basin sedimentation during closing of Iapetan Ocean related to subduction and collision along the ancient southern margin of Laurentia (Sanford, 1993b). Subsequent erosion has removed latest Ordovician through early Silurian age sediment, if deposited. Middle to Upper Ordovician sedimentary sequences in Ottawa Embayment, Kingston area, Lake Simcoe area, Manitoulin Island area, northern New York State, and Timiskaming outlier are summarized in Table 1.1.

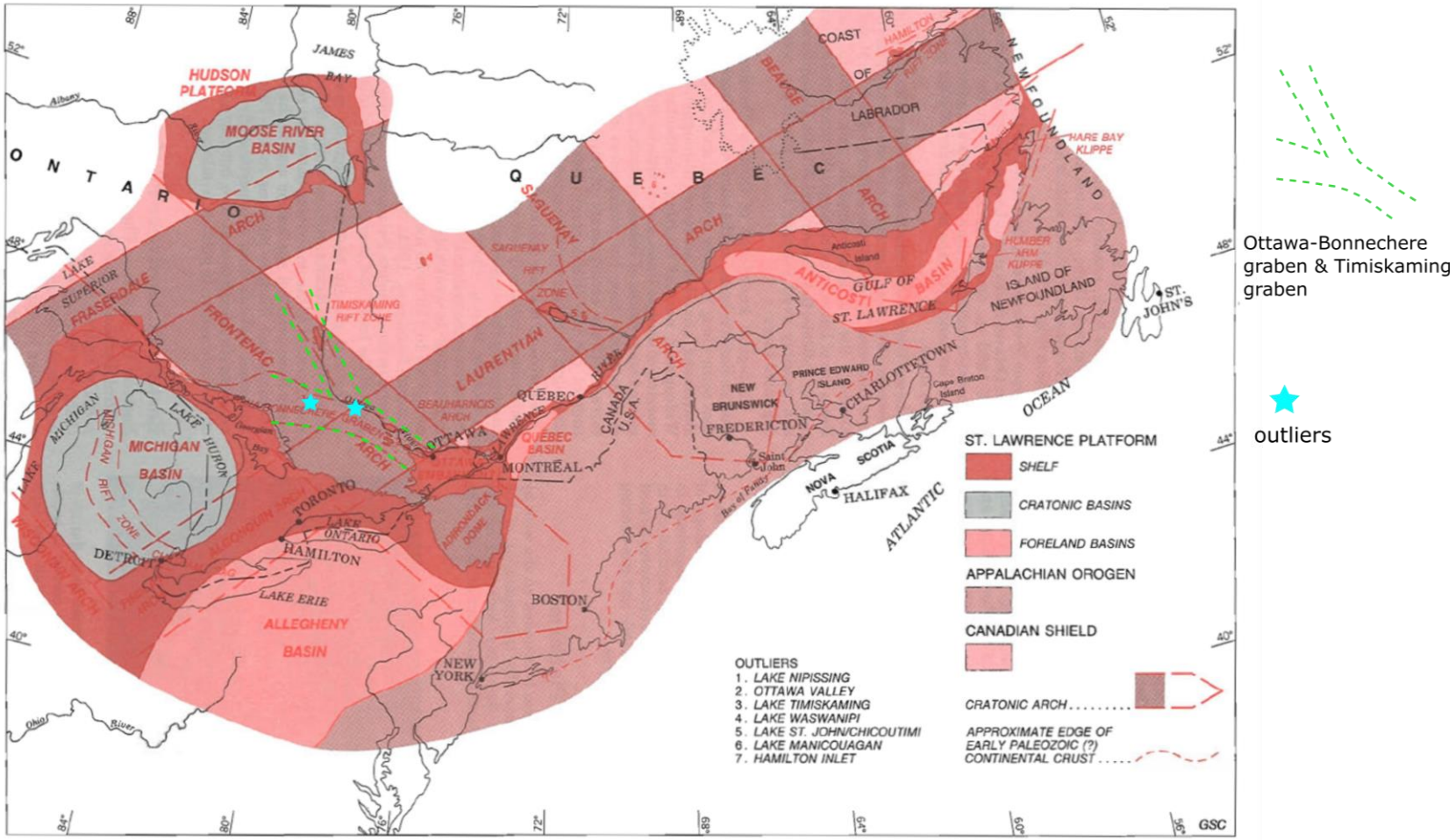

Ottawa-Bonnechere graben & Timiskaming graben

outliers

Figure 1.2. Tectonic elements of St. Lawrence Platform (Sanford, 1993a). Also shown: general boundary of the Ottawa–Bonnechere graben (dashed green lines) and areas of studied outliers (blue stars).

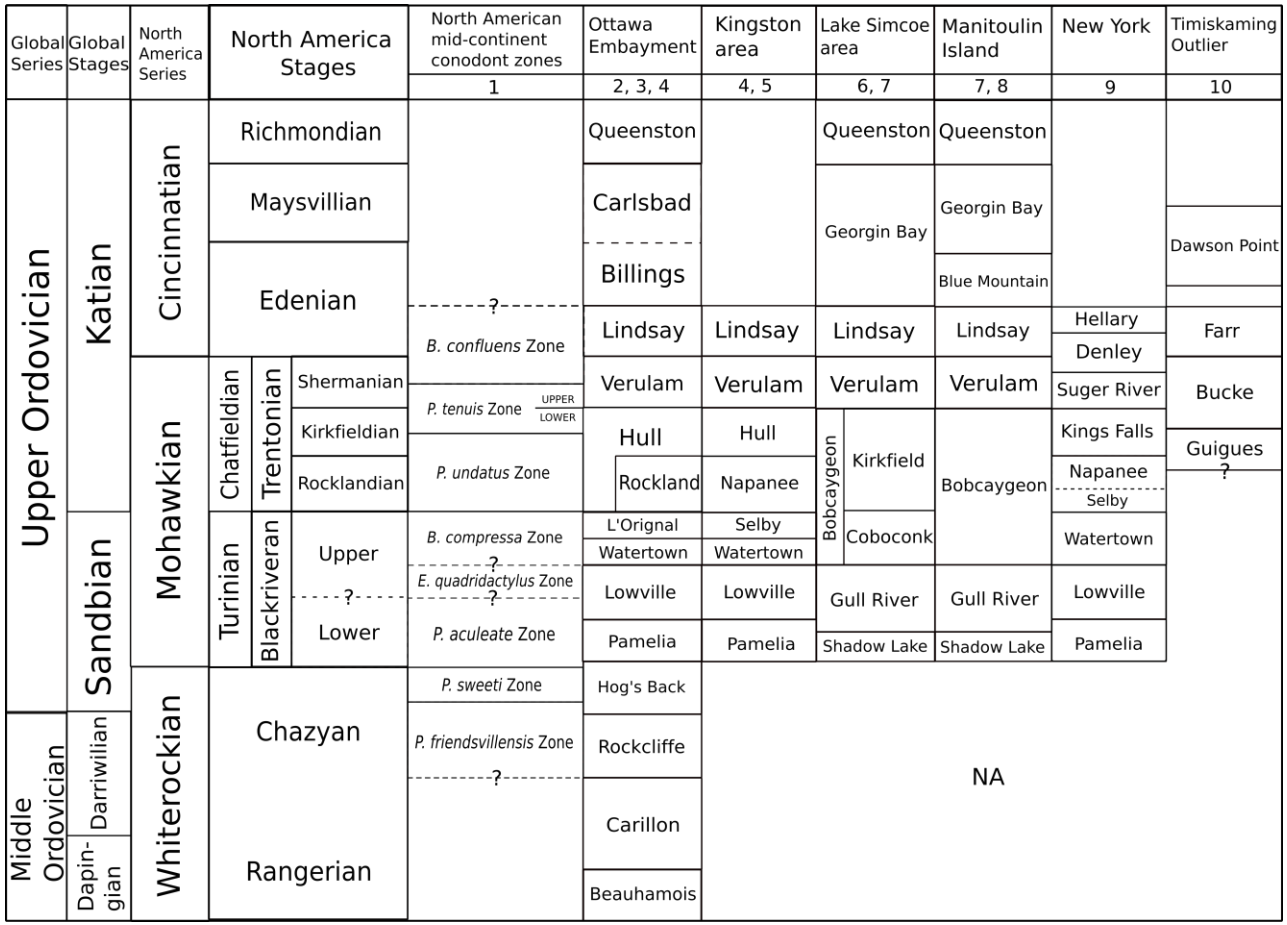

Table 1.1. Regional Middle and Upper Ordovician sedimentary sequences in part of Central and Western St. Lawrence Platform. References: 1, Sweet, 1979; 2, Bleeker et al., 2011; 3, Salad Hersi, 1997; 4, Oruche et al., (submitted to Canadian Journal of Earth Sciences); 5, McFarlane, 1992; 6, Melchin et al., 1994; 7, Noor, 1989; 8, Brunton et al., 2009; 9, Cameron and Mangion, 1977; 10, Stott, 1991.

1.3.2 Ottawa Embayment

Most of eastern Ontario is underlain by a relatively continuous but well-faulted sedimentary platform succession that defines the Ottawa Embayment being bordered along its western limit by Precambrian rocks of Frontenac Arch (Fig. 1.2), and along its northern limit by Precambrian rocks of the Laurentian Highlands. Northwest of Arnprior (Fig. 1.1), relatively narrow Paleozoic outliers define an *en échelon* pattern illustrating down-faulted Paleozoic cover separated by Precambrian basement.

The Tippecanoe Megasequence I in Ottawa Embayment records four stages of platform development (Bleeker et al., 2011). The first stage is represented by the Carillon Formation of Beekmantown Group: a mostly dolomitic tectonostratigraphic unit repletes with seismites and synsedimentary fractures, marking onset of regional seismic activity with foreland basin development. The second stage is represented by the Rockcliffe Formation: a tide- and wave-dominated siliciclastic estuarine system denoting regional sea level fall (Bleeker et al., 2011). The third stage is represented by the Hog's Back Formation marking regional flooding and shallowing with re-establishment of a carbonate platform. The fourth stage is represented by the Ottawa Group: the final stage of the foreland carbonate platform development, characterizing an overall deepening upward (peritidal to open shelf) carbonate-dominated platform succession.

The Ottawa Group contains the important tectonostratigraphic division recognized across eastern North America (Keith, 1988). The lower part of the Ottawa Group succession (Pamelia through L'Orignal formations; Table 1.1) documents peritidal through shallow protected subtidal environments characteristic of regional Blackriveran rocks whereas the remaining succession (Rockland through Lindsay formations) contains

coarser skeletal-rich facies, less mud, and increased presence of siliciclastic fines. This latter succession corresponds to Trentonian strata of eastern North America that record the effects of a regional (eastern Laurentia) environmental change associated with plate-boundary re-organization during the early Chatfieldian (Ettensohn, 2008; Lavoie, 2008). Overall the succession deepens upward, from shallow subtidal to deeper-water ramp (Salad Hersi and Dix, 2000; Gabadeyan and Dix, 2013). The local stratigraphic nomenclature and character of the Black River-Trenton boundary is being revised as part of the PhD project of Nkechi Oruche at Carleton University.

1.3.3 Paleogeography and Paleoceanography

During the Late Ordovician period, Laurentia straddled the equator, with the Ottawa Valley region lying at ~ 15-20°S (Fig. 1.3; Cocks and Torsvik, 2011). In the early Late Ordovician, despite a tropical latitude, the stratigraphic transition from Blackriveran to Trentonian strata appears to correspond lithically with a facies transition similar to warm-to-temperate water (Brookfield, 1988). This local transition is regionally expressed through the St. Lawrence Platform, though diachronously from east to west across the Laurentian margin (Lavoie, 1994). This Canadian expression is repeated elsewhere along the length of the Laurentian epicontinental foreland margin in the United States (Ettensohn, 2008). Temperate-water carbonates with presence of chert and phosphate indicate the transition coincided with increased influence of upwelling that moved cool oceanic waters onto the Laurentian craton (Pope and Steffen, 2003). Ettensohn (2010) concluded that landward migration of deep cool oceanic waters was an oceanographic change driven by ongoing Taconic orogenesis. Structure, tectonics, and paleogeography

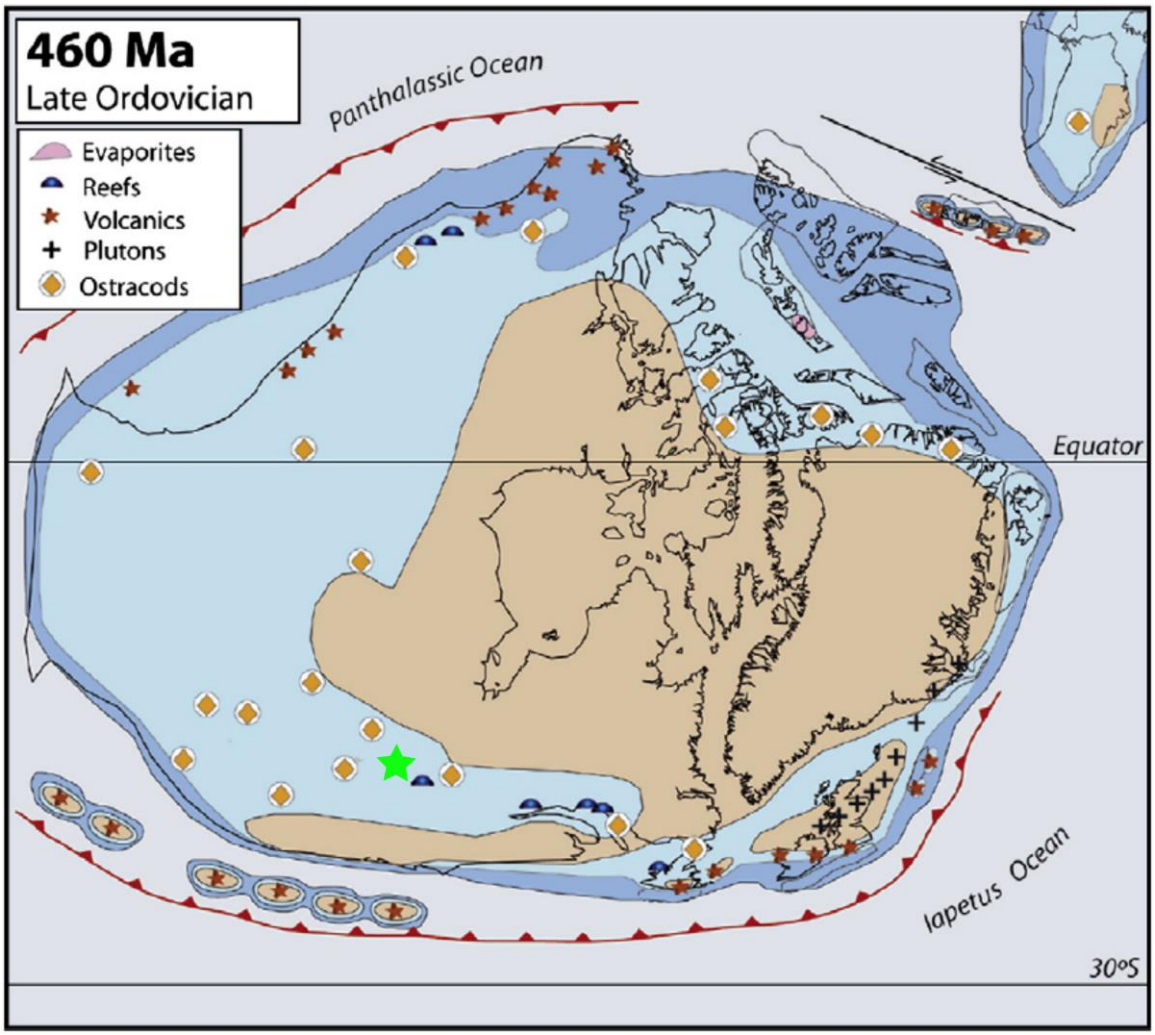

Figure 1.3. Paleogeography of Laurentia in early Late Ordovician (Cocks and Torsvik, 2011). Study area is represented by green star.

in combination may have led to the abrupt breakup of a warm-water platform (defined in Blackriveran time) into several smaller platforms with temperate-water sedimentary and faunal regimes (Ettensohn, 2010). Another explanation from Narbonne and James (2017) is that in a foreland basin the ultimate control is subsidence that drags the platform down through the upper oceanic thermocline. Thus, the ancient ramp was temperature-stratified with a shallow thermocline such initial Blackriveran strata accumulated above this interface and, with subsidence, Trentonian strata accumulated below the interface.

1.4 Methodology

1.4.1 Field methods

Field work was conducted in three parts. First, on October 30th and 31th, 2015, a visit was made to the Owen quarry, located south of Lake Nipissing, ~ 2 km NW of Nipissing District center. Detailed field work included mapping lithostratigraphy, distribution of calcite veins, and collecting and defining presence and types of skeletal fossils and trace fossils. Dunham's (1962) and Embry and Klovan's (1971) classifications were used for rock descriptions. The spatial and structural relationship between the dolostone outcrop and nearby Precambrian rocks was examined. Rock samples were collected for petrographic, geochemical, and paleontological analysis. On this visit, the Manitou Islands were visited on a half day reconnaissance trip (due to weather/wave limitations) to examine the general geology and potential mapping sites.

The second stage of field research was conducted between June 13th and 15th, 2016. The stops included outcrops along the shoreline of Cedar Lake and the Ottawa River near Deux Rivières, and the Manitou Islands in Lake Nipissing. As the targets were

all close to a body of water, the author canoed or took a power boat to reach the outcrops. Field mapping included investigation of distribution of outcrops, lithostratigraphy, sedimentary facies, and the spatial relationship of Paleozoic cover with the Precambrian basement.

The third part of my field work involved logging the Brent Crater core #1–59, from May 30th to June 1st, and on June 6th, 2016, housed at the Geological Survey of Canada storage facility at Tunney's Pasture, Ottawa. Core was photographed and examined for lithostratigraphy and fossil types. Representative samples were collected for more detailed petrographic and geochemical analyses. Due to limited sampling allowed, this work relies heavily on prior extensive petrographic analysis of Lozej and Beales (1975).

1.4.2 Laboratory methods

Standard unpolished thin-sections were made at the Department of Earth Sciences, Carleton University, and at Vancouver Petrographics Ltd. Thin-sections were stained at Carleton University using Alizarin Red-S and potassium ferrocyanide solutions to differentiate dolomite and calcite, and relative iron content (Evamy, 1969). Petrographic analysis of composition and texture used Dunham's (1962) and Embry and Klovan's (1971) classifications for limestone; Sibley and Greg's (1987) and Mazzullo's (1992) classifications for dolomite; and Dott's (1964) for sandstone.

Apart from standard thin-section petrography, cathodoluminesence (CL) of samples was examined at Carleton University using a Nuclide ELM-2 luminoscope with operating conditions of 12 kV, 50 mA, and 40 mTorr. This analysis provides a relative

sense of changing Fe/Mn ratios and resulting zonation commonly associated with calcite and dolomite crystals (Machel, 1985).

Three clay samples were analyzed using X-ray powder diffraction (XRD) analysis at Geological Survey of Canada, Ottawa. Bulk samples are micronized using a McCrone mill in isopropyl alcohol until a grain size of about 5-10 μm is obtained. The samples are dried and then back pressed into an aluminum holder to produce a randomly oriented specimen. Clay size material was separated using centrifuge. 40 mg air-dried clay is suspended in distilled water and pipetted onto glass slides. They are air-dried overnight to produce oriented mounts. X-ray patterns of the pressed powders or air-dried samples are recorded on a Bruker D8 Advance Powder Diffractometer equipped with a Lynx-Eye Detector, Co Kα radiation set at 40 kV and 40 mA. Clay samples are also X-rayed following saturation with ethylene glycol and heat treatment (550 °C for 2 hours). Data were analyzed using the freeware program *MacDiff*. XRD of one sandstone sample was conducted at State Key Laboratory of Oil and Gas Reservoir Geology and Exploitation of Southwest Petroleum University, China, using X'Pert PRO MPD, with mineral identification using X'Pert High Score.

Scanning electron microprobe (SEM) analysis (Carleton University) examined textures of sandstone, siltstone, and carbonate rocks. This was carried out using a Tescan Vega-II XMU SEM with Oxford Inca Energy 250X EDS elemental analysis.

Electron microprobe analysis was conducted at Carleton University to study dolomite and calcite geochemistry using polished thin-sections. A Camebax MBX Electron Microprobe equipped with four wavelength WDX X-ray spectrometers was used to analyze weight percentage of Ca, Mg, Fe, Mn, Ba, Sr, Na, and Si in the carbonate

minerals. The minimum detection limits (MDL) for the corresponding oxides are CaO, MgO: 0.02 wt %; FeO, MnO: 0.04 wt %; BaO: 0.05 wt %; Na_2O, SrO, SiO_2: 0.03 wt %.

Powders processed for isotope analysis were obtained from rock through microdrilling. $\delta^{18}O$ and $\delta^{13}C$ ratios of calcite and dolomite were determined at Queen's Facility for Isotope Research at Queen's University. Approximately 1 mg of powdered material with 100% anhydrous phosphoric acid was heated at 72°C for 4 hours. The CO_2 released was analyzed using a Thermo-Finnigan Gas Bench coupled to a Thermo-Finnigan Delta^{Plus} XP Continuous-Flow Isotope-Ratio Mass Spectrometer (CF-IRMS). $\delta^{18}O$ and $\delta^{13}C$ values are reported using the delta (δ) notation in permil (‰), relative to Vienna Pee Dee Belemnite (VPDB) and Vienna Standard Mean Ocean Water (VSMOW) respectively, with precisions of 0.2‰. A few samples were also analyzed at G.G. Hatch Stable Isotope Laboratory of the University of Ottawa. Samples were weighed into exetainers, 0.1 mL of H_3PO_4 (S.G. 1.91) is added to the side, exetainers are capped and helium-flushed while horizontal. Reaction at 25°C for 24 hrs (calcite) or 50°C for 24 hrs (dolomite) was followed by extraction under continuous flow. The measurements were performed on a Delta XP and a Gas Bench II, both from Thermo Finnigan. Analytical precision (2 sigma) is ± 0.1‰.

Strontium isotope analysis of calcite and dolomite samples was carried out at the Isotope Geochemistry & Geochronology Research Centre (IGGRC) at Carleton University. Carbonate was dissolved in 2.5N HC1, and run through columns of Teflon resin to separate Strontium. Sr with H_3PO_4 are loaded onto a single Ta filament, and run by Thermo Finnigan Triton TI thermal ionization mass spectrometer at temperatures of 1240–1350°C.

Chapter 2 Deux Rivières Outlier

2.1 Local and general geology

The outlier occurs along the north (Quebec) shore of the Ottawa River ~ 6 km northwest of Deux Rivières, Ontario, and extends over 690 meters (between 46° 16.875' N 78° 21.711' W and 46° 16.595' N 78° 21.392' W). The outlier is geographically bounded by biotite-potassium feldspar-quartz-plagioclase gneiss of Mesoproterozoic age, and overlain disconformably by unconsolidated Quaternary (glacial-derived) deposits (Lumbers, 1976). The Paleozoic-Precambrian contact is not exposed. Exposure of the Paleozoic section is thickest (17 m) at the northwestern end of the outlier (Fig. 2.1A). Strata dip shallowly (4°) to the east to a vertical fault (with offset of < 50 cm down to the east), then continue eastward with a nearly horizontal attitude before gradually disappearing below the waterline.

2.2 Lithostratigraphy and facies

A 17-meter-thick composite section was measured and subdivided on the basis of lithology, fossil content, and sedimentary structures (Fig. 2.2). The lower 7.55 meters (Units 1-3) consist of interbedded carbonate and siliciclastic rocks; namely, silty dolomudstone and sandy dolowackestone; limestones of bioclastic mud/wacke/packstone, sandy bioclastic grainstone, and ooid-bearing grainstone; and feldspathic arenite. The upper 10.3 meters (Units 4-6) form a carbonate succession including peloidal packstone, ooid- and oncolite-bearing grainstone, and crystalline dolostone. The following summarizes lithofacies types, their associations, and fossil content of each unit; and interpreted depositional environments. Details are summarized in Table 2.1.

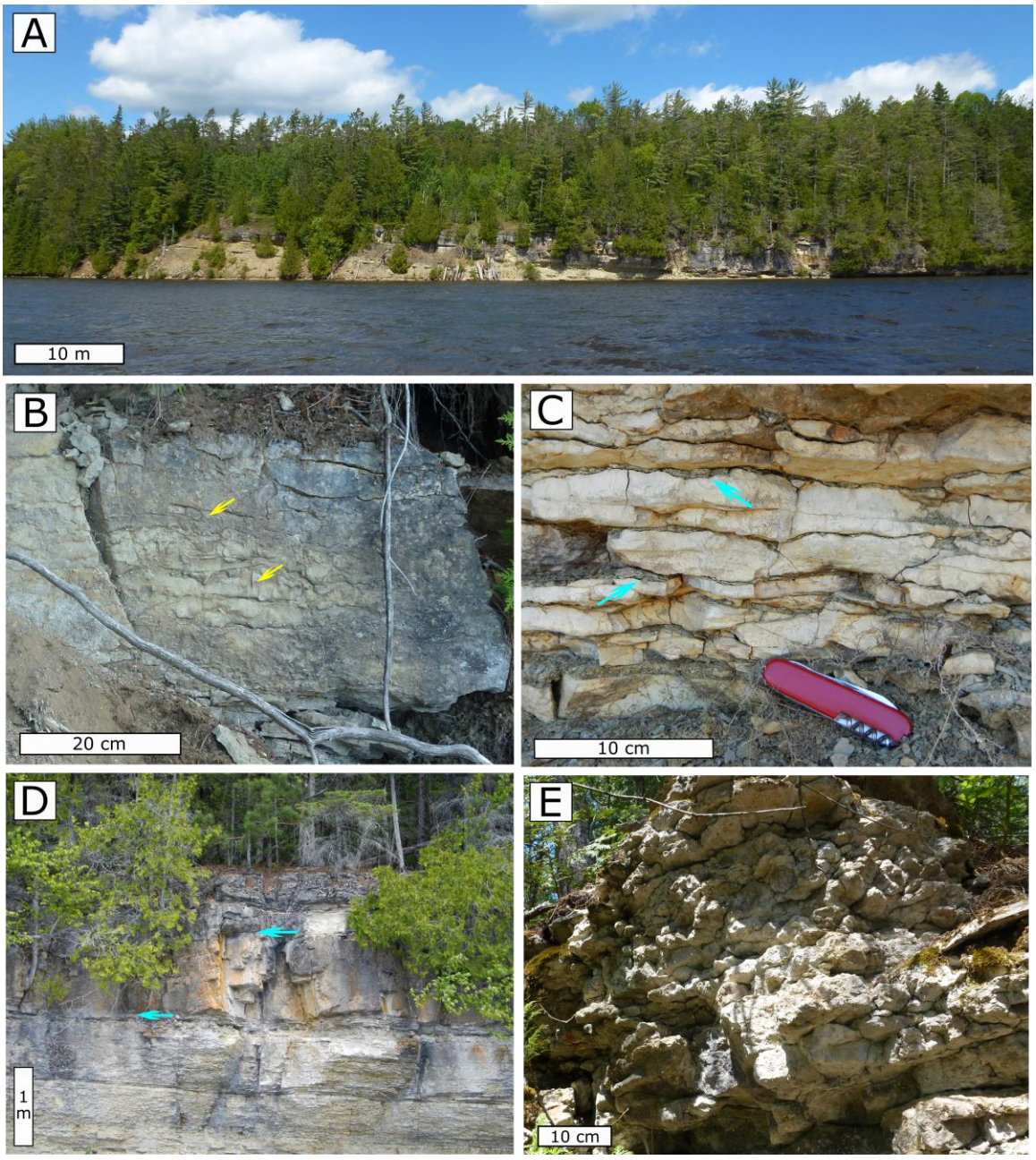

Figure 2.1. Field photos of the Deux Rivières outlier. A) River view of the main outcrop, showing gentle stratal dip (left to right) to the southeast. B) Bioclastic dolomudstone of Unit 1a with abundant vertical burrows (arrows). C) Lower part of Unit 3c shows thin shale layers (arrows) between lime mudstone beds. D) Dolostone (Unit 4b) with boundaries indicated by arrows; thickness of this unit is 1 meter. E) Unit 6, an oncolite-bearing grainstone exhibiting nodular weathering texture; this unit is set back ~ 6 m from the river outcrop (A).

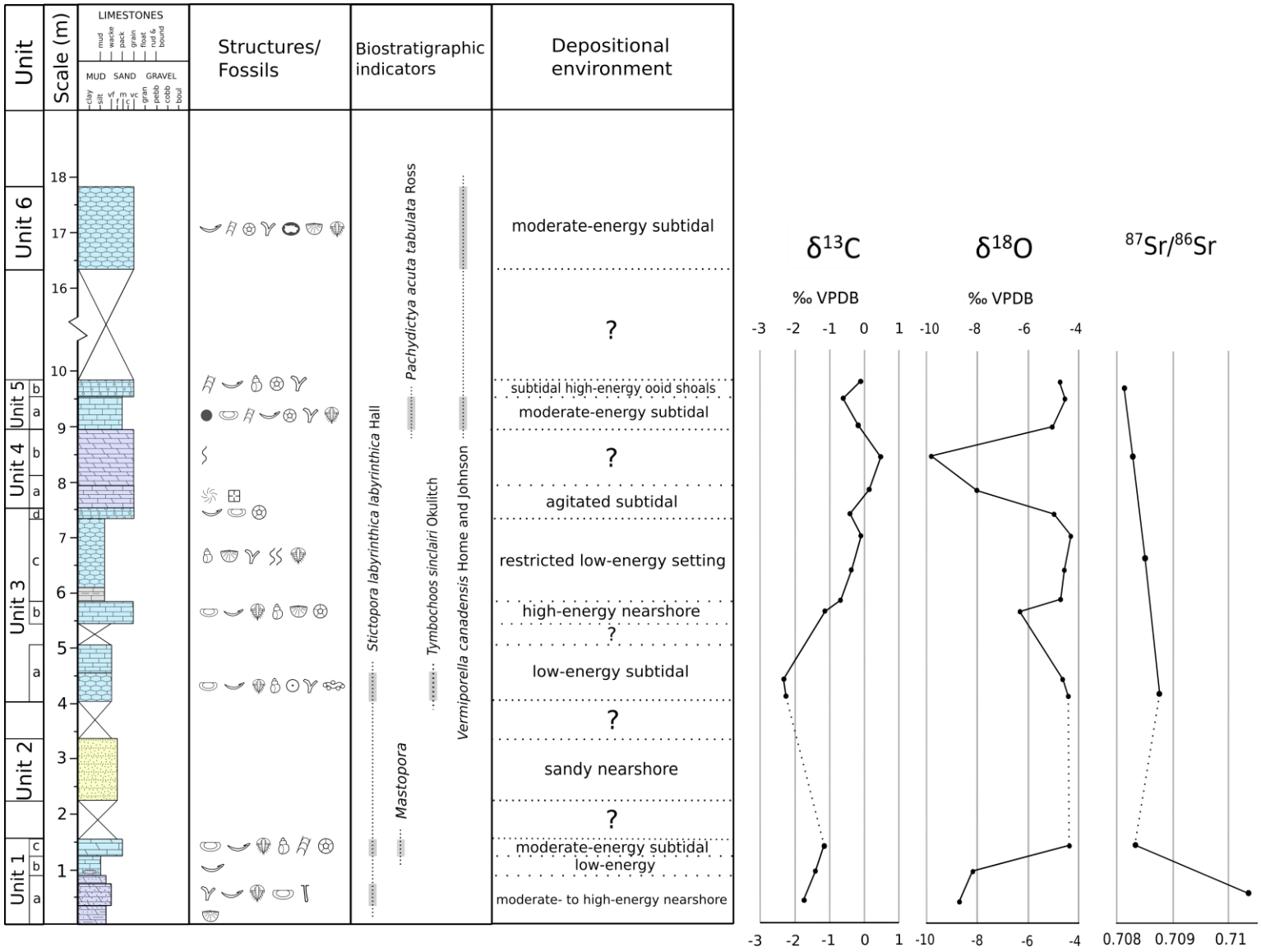
Unit
Scale (m)
LIMESTONES
mud
wacke
pack
grain
float
rud &
bound
MUD
SAND
GRAVEL
clay
silt
vf
f
m
c
vc
gran
pebb
cobb
boul
Structures/
Fossils
Biostratigraphic
indicators
Depositional
environment
Unit 1
Unit 2
Unit 3
Unit 4
Unit 5
Unit 6
Stictopora labyrinthica Hall
Mastopora
Pachydictya acuta tabulata Ross
Tymbochoos sinclairi Okulitch
Vermiporella canadensis Horne and Johnson
moderate-energy subtidal
?
subtidal high-energy ooid shoals
moderate-energy subtidal
?
agitated subtidal
restricted low-energy setting
high-energy nearshore
?
low-energy subtidal
?
sandy nearshore
?
moderate-energy subtidal
low-energy
moderate- to high-energy nearshore
δ13C
δ18O
87Sr/86Sr
‰ VPDB
‰ VPDB
-3 -2 -1 0 1
-10 -8 -6 -4
0.708 0.709 0.71

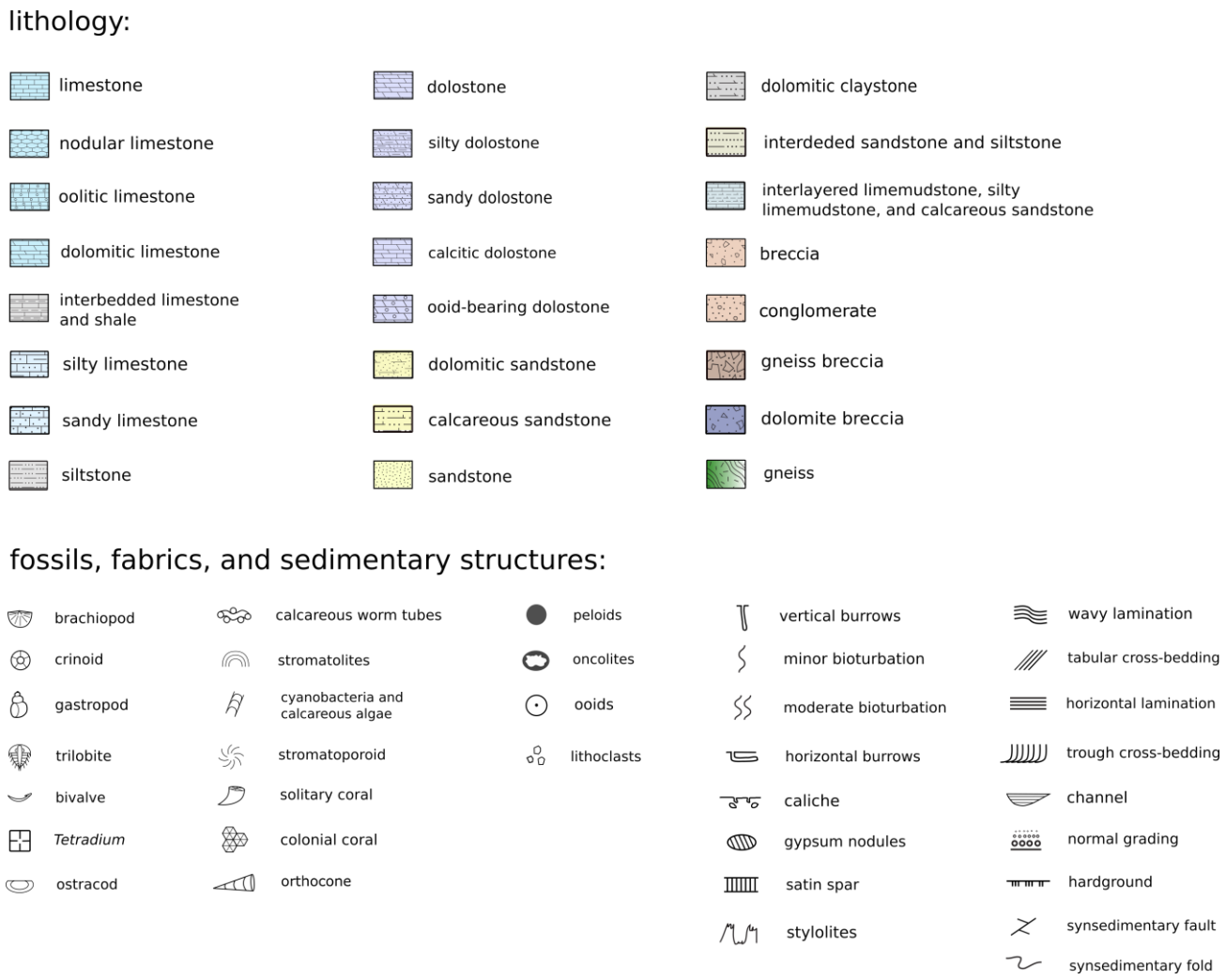

Figure 2.2. Stratigraphic attributes of the Deux Rivières outlier (composite section).

Lithofacies types	lithology	Sedimentary features	Fossils and other textural attibutes	Depositional environment	References
L1a	lime mudstone with dolostone nodules	thin-bedded	bivalves	low-energy	1
L1b	horizontally-burrowed lime mudstone	thin-bedded, horizontally-burrowed, claystone at the lower part	gastropods, bivalves, brachiopods, bryozoans, and trilobites	low-energy subtidal environment, with short-lived sea level fluctuations or fluctuations in terrigenous sediment input	2, 3
L2	nodular bioclastic wackestone	horizontal to sub-horizontal burrows	fragmented crinoid ossicles, bivalves, ostracodes, trilobites, gastropods, bryozoans, calcareous worm tubes (*Tymbochoos sinclairi* Okulitch), and transported ooids; < 1% quartz grains	low-energy, protected environment adjacent to shoals	4, 5
L3a	dolomitic bioclastic packstone	medium-bedded, light brown	brachiopods, ostracodes, bivalves, crinoids, trilobites, gastropods, cyanobacteria (*Hedstroemia*), and calcareous algae (*Mastopora*)	moderate-energy, normal-marine, warm-water subtidal environment	5, 6, 7, 8
L3b	peloidal packstone	thin-bedded	calcareous algae (*Vermiporella canadensis* Horne and Johnson), crinoids, bryozoans, trilobites, ostracodes, and bivalves	warm-water, stenohaline, subtidal protected shallow-marine environments with moderate water circulation; similar to SMF16 NON-LAMINATED of Flügel (2010)	5, 7, 8
L4a	sandy bioclastic grainstone	thin-bedded	bivalves, brachiopods; blackened crinoids and ostracodes; dolomitized bivalves; dolostone fragments; quartz, feldspar, chlorite, muscovite, glauconite, apatite, titanite, zircon	high-energy nearshore setting proximal to siliciclastic source	9
L4b	ooid-bearing grainstone	thin-bedded, light grey	gastropods, bivalves, calcified cyanobacteria (*Hedstroemia*), bryozoans, and crinoid ossicles	normal-marine, subtidal, high-energy carbonate shoals; similar to SMF 15-C of Flügel (2010)	5
L4c	oncolite-bearing grainstone	thin-bedded, nodular, light grey	brachiopods, crinoids, trilobite, cyanobacteria (*Hedstroemia, Girvanella*), calcareous algae (*Vermiporella canadensis* Horne and Johnson), bryozoans, and bivalves	warm-water, normal-marine, moderate-energy subtidal environment	5, 8, 10

D1a	silty dolomudstone	thin-bedded, greenish grey	very scarce brachiopods	close to source of siliciclastic input, probably not open marine	9
D1b	sandy bioclastic dolomudstone	vertically-burrowed, medium-bedded, vertical burrows *Skolithos*	blackened ostracodes, bivalves, trilobites, and bryozoans; 40-200 μm, planar-s dolomite	elevated wave or current energy, close to source of siliciclastic input, probably not open marine	11
D3	calcitic crystalline dolostone	thin-bedded	stromatoporoids and *Tetradium* sp.	agitated, normal-marine, subtidal bioherm/biostrome buildup	12, 13, 14
D4	crystalline dolomite	medium-bedded, light brown	50-2000 μm, planar-s dolomite	unknown	
S	feldspathic arenite	brownish yellow, medium-bedded, planar-laminated	80-200 μm quartz and potassium feldspar grains, minor kaolinite and chlorite; no skeletal material	sand-dominated shallow marine environment, powerful combined flows	15, 16

Table 2.1. Summary of lithofacies types in Deux Rivières outlier. References: 1, James and Jones, 2016; 2, Noor, 1989; 3, Melchin, 1994; 4, Steele-Petrovich and Bolton, 1998; 5, Flügel, 2010; 6, Liu et al., 2016; 7, Mamet et al., 1984; 8, Aguirre and Riding, 2005; 9, Goldhammer, 2003; 10, Blackwell et al., 1984; 11, MacEachern et al., 2010; 12, Walker, 1972; 13, Kapp, 1975; 14, Webby, 2004; 15, Plint, 2010; 16, Borer and Harris, 1991.

Unit 1

Description

Unit 1, the lowermost unit, is 1.55 m thick, and divided into three successive lithofacies associations (1a-1c; Fig. 2.2) that document an upsection transition from dolostone to limestone with increased benthic fauna diversity and abundance, and decreased siliciclastic content. All bedding contacts are abrupt and planar.

The lowermost 35 cm (Unit 1a) consist of thin-bedded greenish silty dolomudstone with scarce brachiopods (lithofacies D1a), and is overlain by 40 cm of medium-bedded sandy bioclastic dolomudstone (lithofacies D1b). The dolomudstone contains very scarce blackened (pyritized) fragmented benthic skeletal fossils, including the cryptostomatid bryozoan *Stictopora labyrinthica labyrinthica* Hall, trilobites, bivalves, and ostracodes. Siliciclastic grains (3-5%) are 80-720 μm in size, subrounded to rounded in shape, and mostly quartz in composition, but with a trace amount of potassium feldspar. This lithofacies contains a common occurrence of vertical burrows, *Skolithos* (Fig. 2.1B), up to 1 cm in diameter, although any connection to a defined paleosurface is unclear. Unit 1b consists of 35 cm of thin-bedded lime mudstone with small (cm-scale) dolostone nodules (lithofacies L1a). Unit 1c, the uppermost division of this interval, consists of medium-bedded dolomitic bioclastic packstone (lithofacies L3a) with abundant fragmented benthic skeletal material, including crinoid ossicles and echinoderm fragments, gastropods, ostracodes, bivalves, trilobites, cryptostomatid bryozoans (*Stictopora labyrinthica labyrinthica* Hall), calcified cyanobacterium *Hedstroemia*, and calcareous algae *Mastopora*; and trace amount (1%) of sand-size siliciclastics grains. Intergranular void space is filled mostly with micrite.

Paleoenvironment interpretation

There appears to be two distinct environmental associations. Unit 1a contains attributes often associated with moderate to high-energy nearshore settings: 1) the common presence of siliciclastic sediment suggests that carbonate accumulation occurs near an available supply; 2) the varying grain size (silt to sand) of siliciclastics grains identifies variation in either transport energy or depositional energy; 3) the vertical trace fossil *Skolithos* isp. is indicative of mobility of sediment under elevated wave or current energy enabling a loose or shifting substrate (MacEachern et al., 2010); and, (4) a low diversity of benthic fauna and absence of crinoids suggest the environment may not have been of normal-marine salinity (Flügel, 2010).

The notable upsection reduction of siliciclastic content into Unit 1c illustrates either a removal of the availability of the sediment source, or a reduced capacity for its transport. Both are accommodated by a net rise in sea level sequestering siliciclastics to a more seaward setting. Initial carbonate deposition (Unit 1b) identifies a relatively quiet water environment, replaced upsection by bioclastic packstone (Unit 1c) representing a moderate-energy subtidal environment. A high-diversity fossil assemblage, including crinoidal debris, identifies a normal-marine setting (Flügel, 2010). The calcified cyanobacterium, *Hedstroemia*, is common to many Ordovician platform successions associated with both open and restricted marine facies (Mamet et al., 1984; Liu et al., 2016). Ordovician dasycladacean algae (including *Mastopora*) are common on shallow well-lit platforms (Mamet et al., 1984) and favorable in warm-water environments (Aguirre and Riding, 2005).

In summary, Unit 1 documents transgression and back-stepping of a siliciclastic source associated with increase in accommodation space. Carbonate accumulation shifts from nearshore to moderate-energy normal-marine setting. The origin of dolomite (discussed in more detail below) may be related to proximity to a nearshore setting or greater permeability of sand-bearing sediment.

Unit 2

Description

Unit 2 is composed of 1.1 meters of medium-bedded planar-laminated feldspathic arenite (lithofacies S). The unit boundaries are not exposed with sub- or superjacent strata. Sand grains exhibit a relatively well sorted, fine-grained (80-200 μm) texture. The grains are angular to sub-rounded, with potassium feldspar more angular than quartz (Fig. 2.3A). SEM analysis shows that K-feldspar grains are dissolved to a moderate degree. Authigenic clay occurs in intergranular pore space. From XRD analysis, the feldspathic arenite contains < 5% of clay minerals, consisting of kaolinite (~ 60%) and chlorite (~ 40%). The unit appears to be barren of skeletal macrofossils.

Paleoenvironmental interpretation

The overall fine-grained texture of sub-rounded, well-sorted sand grains suggests either grain segregation at source, during transport, or during deposition. Planar lamination of very fine- to fine-grained arenites can be indicative of the lower or upper

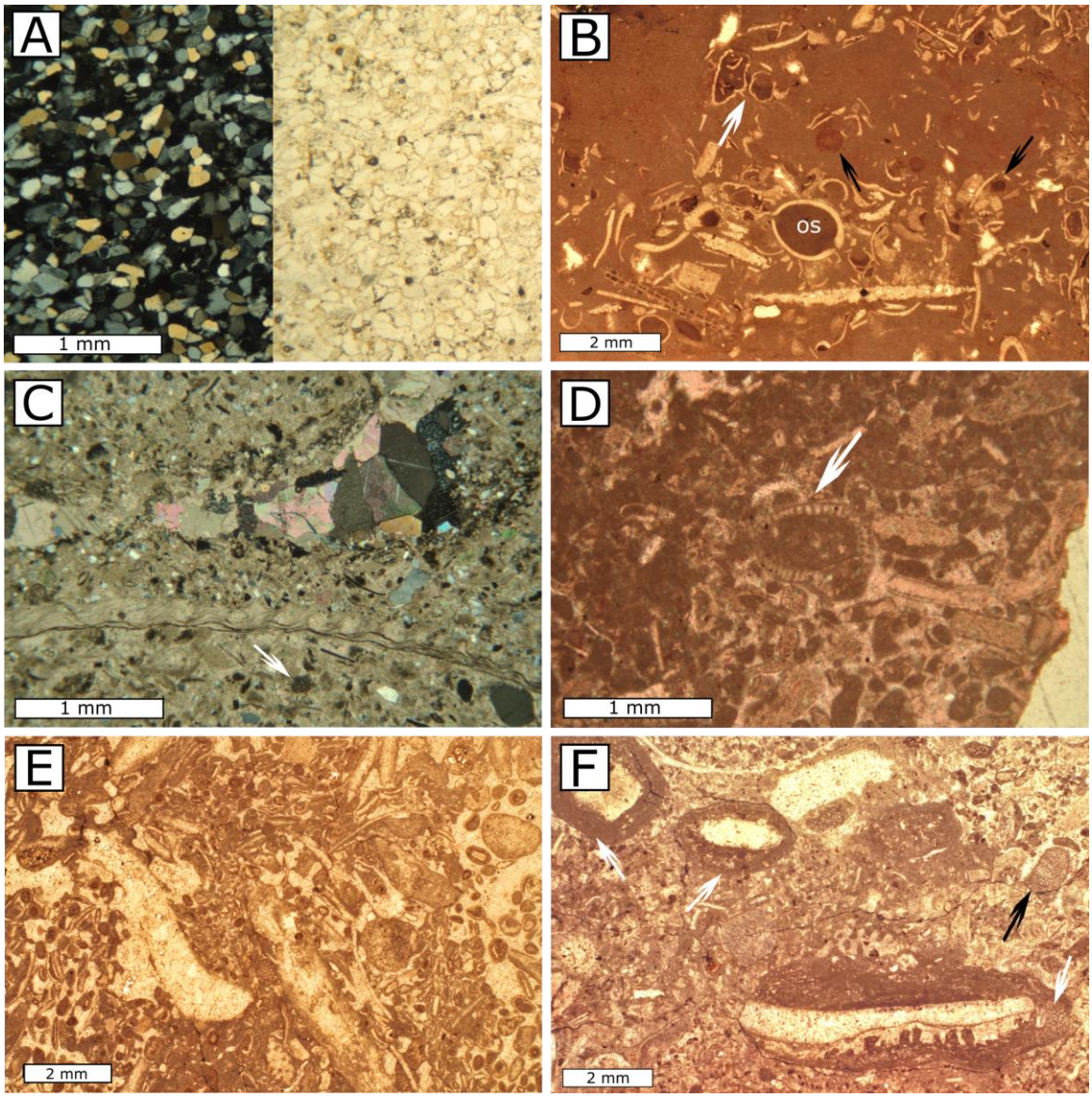

Figure 2.3. Thin-section photomicrographs of representative lithofacies, Deux Rivières outlier. A) Photo pair illustrating fine-grained feldspathic arenite with chlorite cement (lithofacies S); left: cross polarised light; right: plane polarised light. B) Bioclastic wackestone (lithofacies L2) with transported ooids (blue arrows), ostracodes (os), and calcareous worm tubes (white arrow); plane-polarized light image; C) Sandy bioclastic grainstone (lithofacies L4a) with dolostone clasts (arrow); cross-polarized light image. D) Peloidal packstone (lithofacies L3b) with dasycladacean algae *Vermiporella canadensis* Horne and Johnson (arrow); plane-polarized light image. E) Ooid-bearing grainstone with abundant bioclasts (lithofacies L4b); plane-polarized light image. F) Oncolite-bearing grainstone (lithofacies L4c) with *Girvanella* coated oncolites (white arrow) and fragmented bioclasts including cyanobacterium *Hedstroemia* aggregate (black arrow); plane-polarized light image.

flow regime, or combined (wave + current) flows (Plint, 2010). The lithofacies doesn't define a unique depositional environment, but its significance will be discussed later in context of its stratigraphic position.

Unit 3

Description

Unit 3 is 3.5 meters thick, and divided into four subunits (3a-3d; Fig. 2.2). It contains interbedded bioclastic mud/wackestone and sandy/bioclastic grainstone. The lower two divisions contain significant amount (< 10%) of siliciclastic grains and fragmented skeletal material. All bedding contacts are abrupt and planar.

The first (lower) division, Unit 3a, consists of 20 cm of nodular bioclastic wackestone (lithofacies L2). This lithofacies contains fragmented bioclasts including crinoid ossicles, bivalves, trilobites, and cryptostomatid bryozoans *Stictopora labyrinthica labyrinthica* Hall. In addition, there are fragmented radial ooids, disarticulated ostracode shells, fragmented aggregations of calcareous worm tubes (*Tymbochoos sinclairi* Okulitch), and trace amount (< 1%) of quartz grains. There is an abundance of cm-scale horizontal to sub-horizontal burrows.

Unit 3b is 40 cm thick and consists of thin-bedded sandy bioclastic grainstone (lithofacies L4a). It contains large bivalves and brachiopods; and fragments of blackened (pyritized) ostracodes and crinoid ossicles, and dolomitized bivalve shells (Fig. 2.3B). This lithofacies also contains abundant (~ 10%) siliciclastic grains (quartz and potassium feldspar) as well as dolostone rock fragments, and trace amount of chlorite, muscovite, apatite, titanite, and zircon. The siliciclastic grains exhibit a bimodal texture: subangular

to rounded, fine- to medium-grained sand-size sediment of mostly quartz, feldspar, and dolomite; and angular to subrounded silt of quartz and feldspar.

Unit 3c is 1.5 m thick, and consists of thin-bedded horizontally-burrowed lime mudstone (lithofacies L1b). The lime mudstone contains scarce cm-size whole shells of brachiopods and gastropods, and fragmented bryozoans, bivalves, and trilobites. Horizontal burrows are tiny, millimeter-scale in width. In addition, interbeds of calcareous shale are prominent in the lower 30 cm (Fig. 2.1C) but gradually disappear upsection.

The uppermost division of this unit (Unit 3d) is 20 cm thick and consists of thin-bedded ooid-bearing grainstone (lithofacies L4b) with crinoid ossicles, and disarticulated bivalve and ostracode shells.

Paleoenvironmental interpretation

There appears to be a succession of four distinct environmental associations. Unit 3a represents deposition in a quiet subtidal environment. Horizontal burrows identify a stable seafloor with available food source, and likely infer fairweather conditions (MacEachern et al., 2010). Within this division are clasts that are normally associated with higher energy conditions. Calcareous worm tubes *Tymbochoos* build-ups are relatively common in lower Upper Ordovician carbonate rocks (Pamelia and Lowville formations) of eastern Ontario, but are mostly associated with tidal channel and carbonate shoal facies where there are periodic or constant flows (Steele-Petrovich and Bolton, 1998). Rare radial ooids represent transport from a setting of relatively constant wave agitation but also elevated salinity (Flügel, 2010). Rare transported crinoid debris

illustrate a stenohaline (normal-marine) source (Flügel, 2010). The host wackestone likely represents deposition in a protected environment, one that may have not been of normal-marine condition but formed adjacent to a higher energy normal- to hypersaline marine (shoal, tidal-influenced) setting.

The sandy bioclastic grainstone of Unit 3b represents a high-energy nearshore setting: 1) the abundance of siliciclastic sediments suggests that carbonate accumulation occurs near a ready supply; 2) absence of lime mud indicates a high energy depositional environment; and 3) the rare occurrence of crinoidal detritus may suggest that the environment is not normal-marine.

The burrowed lime mudstone of Unit 3c represents a low-energy environment. A low diversity of benthic fauna and absence of crinoids suggest that the environment is not open marine. The upsection loss of shale interbeds demonstrates decreasing influence of siliciclastic fines either through diminished transport related to net rise of fluctuating sea level (Noor, 1989) or changing patterns of riverine/storm influence from shore relative to carbonate production (Melchin et al., 1994).

The low-energy setting was followed by facies of Unit 3d that records establishment of a high-energy, normal-marine, subtidal environment enabling ooid production. The ooid-bearing grainstone may represent deposition in a carbonate shoal lying beside restricted lagoon (Unit 3c).

In summary, the lithofacies succession of Unit 3 illustrates periodic or episodic changes in sea level that allows temporary progradation of a siliciclastic source. Yet, overall, carbonate production shifts from an initial nearshore environment to a higher-energy offshore setting.

Unit 4

Description

Unit 4 consist of 1.4 m of very hard crystalline dolostone and divided into two lithofacies associations (4a and 4b; Fig. 2.2). A lower division, Unit 4a, consists of 40 cm of thin-bedded calcitic crystalline dolostone (lithofacies D3) with domal 10-20 cm stromatoporoids and local *Tetradium* in its lower 20 cm. Unit 4b (Fig. 2.1D) is composed of 1 m of medium-bedded finely to coarsely crystalline dolomite (lithofacies D4). No other sedimentary features nor siliciclastic grains were observed.

Paleoenvironmental interpretation

In the Late Ordovician, stromatoporoids and *Tetradium* colonies are typical of normal-marine, agitated, shallow platform settings (Walker, 1972; El Gadi, 2001; Webby, 2004; Flügel, 2010). Unfortunately, the upper division of this unit doesn't provide enough information for environmental analysis.

Unit 5

Description

Unit 5 is 90 cm thick, and divided into two lithofacies associations (5a and 5b; Fig. 2.2). Unit 5a consists of 60 cm of thin-bedded peloidal packstone (lithofacies L3b). Moderately sorted peloids form the dominant framework component in this lithofacies. They are spherical to elongated, and the size ranges from 80 μm to 550 μm. The peloidal packstone contains diverse benthic skeletal material including crinoid ossicles, ostracodes, bivalves, cryptostomatid bryozoans *Pachydictya acuta tabulata* Ross, and calcareous

algae *Vermiporella canadensis* Horne and Johnson (Fig. 2.3D). The wavy bedding planes appear to be in part stylolitic, hence not depositional in origin. The upper division of Unit 5 is composed of 30 cm of thin-bedded ooid-bearing grainstone (lithofacies L4b) with fragmented benthic skeletal material including crinoid ossicles, bivalves, gastropods, bryozoans, and cyanobacteria *Hedstroemia* (Fig. 2.3E). Ooids are spherical to elongate, moderately well sorted, varying in size from 250 μm to 650 μm. The composition of ooids cores are mostly calcite mud and fragmented bioclasts. Most ooids display a concentric organization of thin laminaes whereas some display radial fabrics.

Paleoenvironmental interpretation

This unit documents two distinct depositional settings. The lower division (Unit 5a) represents deposition in a warm-water, moderate-energy, normal-marine, subtidal environment: 1) abundant crinoid ossicles indicate a stenohaline environment; 2) Ordovician dasycladacean algae are common on shallow platforms (Mamet et al., 1984); and 3) modern and ancient dasycladacean algae favor a warm-water environment (Aguirre and Riding, 2005). A comparable lithofacies (*SMF16 NON-LAMINATED* of Flügel, 2010) is diagnostic of protected shallow-marine environments with moderate water circulation. This setting is replaced by a high-energy, stenohaline, subtidal setting defined by facies of Unit 5b: 1) the abundance of well-sorted ooids and coated grains indicates an agitated environment; and 2) the common presence of crinoid ossicles suggests a normal salinity. This ooid-bearing grainstone resembles lithofacies *SMF 15-C* of Flügel (2010), and characterizes high-energy oolitic shoals as found today along the margins and extending into the interior of carbonate platforms (Ball et al., 1967). Differences in ooid

fabric suggest aragonitic origin for the concentrically laminated ooids and Mg-calcite origin for ooids with radial fabrics (James and Jones, 2016). In summary, Unit 5 documents an upsection increase in depositional energy within a normal-marine subtidal setting.

Unit 6

Description

This unit forms a separate escarpment set back from the main outcrop section along the shoreline, and is separated stratigraphically by ~ 6 meters of covered interval overlying Unit 5. The lower and upper boundaries of the unit are not exposed. Unit 6 consists of 1.5 m of thin-bedded nodular oncolite-bearing grainstone (lithofacies L4c) with a diverse benthic biota assemblage (Fig. 2.1E). Calcified cyanobacterium (such as *Girvanella*) coats fragmented brachiopods, bryozoans, and trilobites to form oncolites (Fig. 2.3F). The oncolites are large, 1.5 to 8 mm in length. Benthic skeletal material includes crinoid ossicles, bryozoans, brachiopods, trilobites, calcareous algae *Vermiporella canadensis* Horne and Johnson, and the cyanobacterium *Hedstroemia*.

Paleoenvironmental interpretation

Facies attributes of Unit 6 represent deposition in a warm-water, normal-marine, moderate-energy subtidal environment: 1) crinoid ossicles support a stenohaline environment; 2) *Girvanella*-coated oncolites form in environment with moderate wave action (Blackwell et al., 1984). According to Flügel (2010), the slowly growing *Girvanella* oncolites are considered indicators of reduced sedimentation in water depths

of at least ten meters; and 3) dasycladacean algae preferably grow in warm-water environment (Aguirre and Riding, 2005).

Summary of depositional environments

A summary of depositional environments is shown in Fig 2.2. The outlier's lithofacies succession documents net transgression from siliciclastic-bearing to carbonate depositional systems with a superimposed higher order of sea level fluctuations. The facies attributes of units 1 through 3 suggest that deposition occurred in a relatively nearshore setting in which fluctuations in sea level resulted in abrupt influx of relatively coarse-grained siliciclastic material with a relative drop in sea level, and abrupt set-back or shoreward sequestering of siliciclastic with relative rise in sea level.

Accumulation of Unit 2, the feldspathic arenite, documents progradation of siliciclastic source across the older carbonate platform in response to a drop in sea level. A good analogy is found in the continental to shoreface siliciclastic rocks of the Yates Formation in the Permian basin (SW USA), where stratigraphy reveals high-order progradational (seaward) migration of lagoonal to tidal flat siliciclastic sediments bounded by transgressive carbonate systems (Borer and Harris, 1991; Andreason, 1992). In the Deux Rivières outlier, Unit 3 documents return of carbonate deposition, and accumulation shifting from a nearshore environment to more open-marine setting.

Normal-marine, siliciclastic-free, moderate- to high-energy subtidal facies characterizes the upper three units (Units 4-6) of the outlier. Net transgression culminated in formation of ooid grainstone shoals (Units 3d and 5b) that today characterize (mostly) the highest energy and shallowest (< 5 m) subtidal water depth on a platform (Ball et al.,

1967). It remains unknown if Unit 6 represents a continuation of this transgression, resulting in accumulation of deeper water oncolite-bearing grainstone (Flügel, 2010) or whether there is some higher order variation in facies succession within the covered interval.

2.3 Biostratigraphic indicators and age of outlier

Biostratigraphic indicators

Conodonts were recovered from Unit 5b (McCraken, 2017), and several macrofossil groups are valuable for interpretation of the age of this outlier, their stratigraphic distribution illustrated in Fig. 2.2.

Conodonts

Of the six conodont species (not shown in Fig. 2.2) four are of stratigraphic significance: *Belodina compressa* (Branson & Mehl), *Plectodina aculeata* (Stauffer), *Curtognathus* sp. and *Erismodus* sp. Together, they identify a relatively long-range time interval extending from the *Belodina compressa* to lower *Plectodina tenuis* zones (McCracken, 2017; Table 1.1). This corresponds globally to the upper Turinian and much of the Chatfieldian stages and regionally encompasses the upper Blackriveran to mid-Trentonian successions of eastern North America (Table 1.1).

Bryozoans

The bryozoan *Stictopora labyrinthica labyrinthica* Hall (Fig. 2.4A) appears in Units 1a, 1c, and 3a (Fig. 2.2) and is known to be restricted to the Lowville-Watertown

interval of northern New York State (Ross, 1964). The bryozoan *Pachydictya acuta tabulata* Ross (Fig. 2.4B), found in Unit 5a, ranges from the upper Watertown Formation into unspecified lower Trentonian strata of northern New York State (Ross, 1964).

Calcareous worm tubes

Tymbochoos sinclairi Okulitch (Fig. 2.4C), found in Unit 3a (Fig. 2.2), is a genus commonly associated with the Pamelia and Lowville formations in the Ottawa Valley (Salad Hersi, 1997; Steele-Petrovich and Bolton, 1998) and the Kingston area (McFarlane, 1992). Calcareous worm tubes of unknown species occur in younger (Coboconk to Verulam formations) strata in the Lake Simcoe area (El Gadi, 2001).

Calcareous algae and cyanobacterium

Calcareous algae observed in this succession include dasycladacean algae *Vermiporella canadensis* Horne and Johnson (Fig. 2.4D) and *Mastopora* sp. (Fig. 2.4E). Calcareous algae *Vermiporella* sp. and *Mastopora* sp. are found in Sandbian- and Katian-age strata globally (Percival, 1999; Shen and Neuweiler, 2016). Although the algae are of a long age range, their occurrence is strongly influenced by environment (temperature, salinity, sun light etc.), and can be used as biostratigraphic markers in regional correlation. *Vermiporella* sp. is observed in upper Gull River to Coboconk formations in the Lake Simcoe area, central Ontario (El Gadi, 2001), and the Lowville to Watertown formations in northern New York State (Walker, 1972). *Mastopora* sp. was recorded from the lower Turinian (Swain et al., 1966) Chambersburg limestone in Virginia (Osgood and Fischer, 1960).

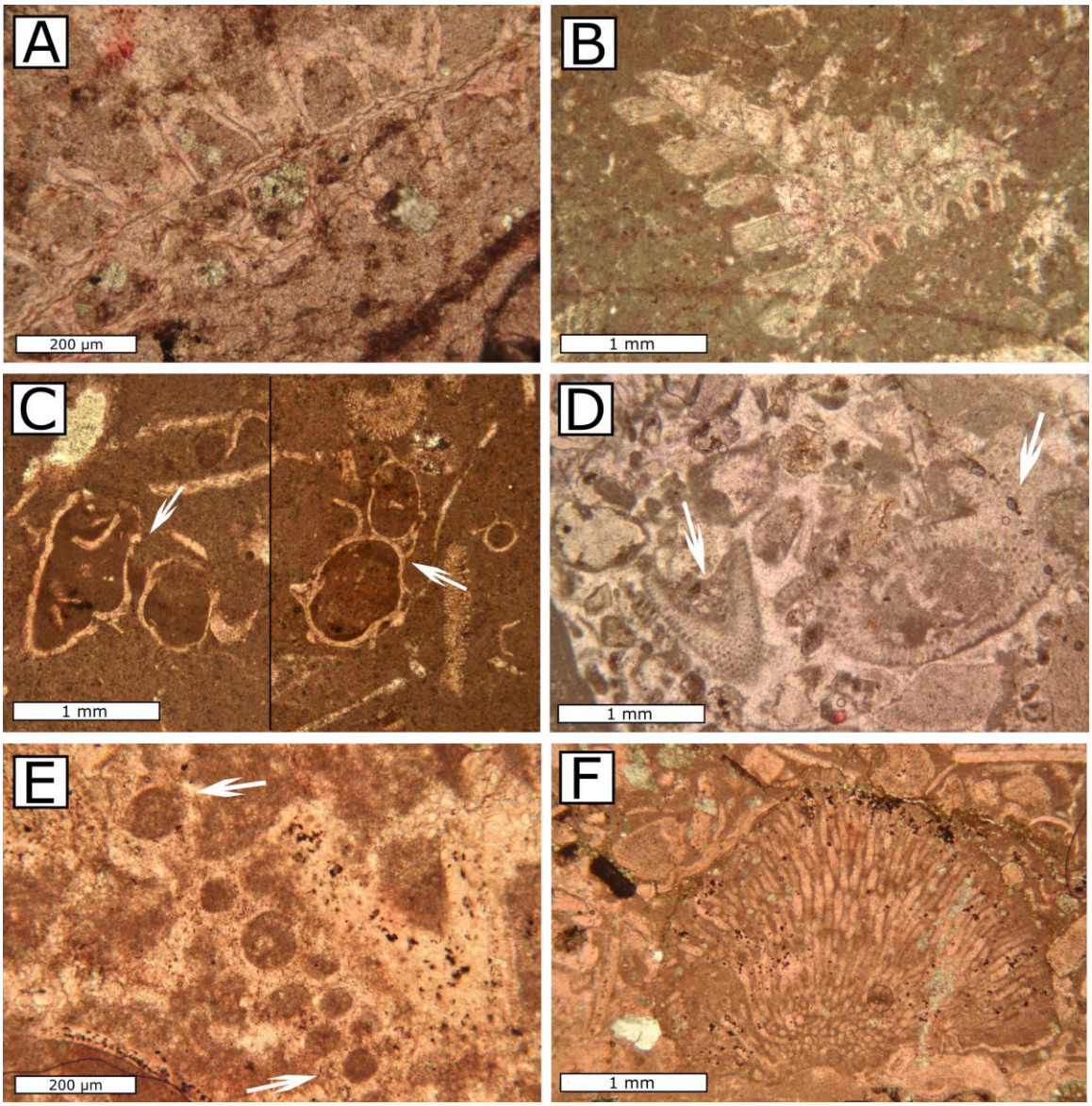

Figure 2.4. Age-significant fossils in Deux Rivières outlier. All images are plane-polarized light photomicrographs of stained thin-sections. A) The cryptostomatid bryozoan *Stictopora labyrinthica labyrinthica* Hall. B) The cryptostomatid bryozoan *Pachydictya acuta tabulata* Ross. C) Photo pair illustrating different attributes of the calcareous worm tubes *Tymbochoos sinclairi* Okulitch (arrows). D) fragments of the calcareous algae *Vermiporella canadensis* Horne and Johnson (arrows). E) Fragments of the calcareous algae *Mastopora* sp. (arrows). F) Domal colony of the calcified cyanobacteria *Hedstroemia*.

Cyanobacterial types include *Hedstroemia* and *Girvanella*. However, these species have very long age ranges and are not of chronostratigraphic importance. *Hedstroemia* sp. (Fig. 2.4F) has been recorded from Lowville to Chaumont (Watertown) strata in southern Quebec and eastern Ontario (Guilbault and Mamet, 1976); in the upper Gull River to Coboconk formations in the Lake Simcoe area, central Ontario (El Gadi, 2001); and in the Lowville to Watertown formations of northern New York State (Walker, 1972). *Girvanella* (Fig. 2.3F), ranging globally from Precambrian through Permian (Nitecki et al., 2004), has been documented from Lowville to Watertown formations in northern New York State (Walker, 1972).

Age of outlier

The conodont assemblage defines the outlier to be of likely late Blackriveran (Turinian) to mid-Trentonian (Chatfieldian) age. Combining the occurrence of bryozoans, calcareous algae, and worm tubes, Units 1-5 strata are probably equivalent to the Blackriveran (Lowville to Watertown) interval of New York State. The bioclastic oncolite-bearing grainstone facies of Unit 6 is very similar to that of the Coboconk (Lower Bobcaygeon) Formation of central and southern Ontario (Melchin, 1994; Noor, 1989; Grimwood et al., 1999; El Gadi, 2001), which is age-equivalent to the Watertown Formation in New York State. In summary, lithostratigraphic and biostratigraphic information suggests that the outlier is equivalent to the upper Turinian (Blackriveran) succession of southern and eastern Ontario, and northern New York State.

Colquhoun (1958) reported a fossil assemblage from limestone blocks found about 1.2 km southeast of the outlier in an area now flooded, along the south shore of the

Ottawa River. He mentioned that the rocks were probably removed from an original position higher along the shoreline due to construction of the railroad along the same shore. The source, if preserved, has not been found. On the basis of the macrofossil assemblage, Colquhoun (1958) suggested that the host rock was likely equivalent to the lower Trentonian Rockland Formation. If the age assessment is correct, it suggests that the original limestone was positioned stratigraphically above the present highest limit of the Deux Rivières outlier stratigraphy. More discussion about the regional stratigraphic position of this outlier can be found in Chapter 7.

2.4 Diagenesis

2.4.1 Introduction

Post-depositional (diagenetic) transformation of sediment to rock represented in the Deux Rivières outlier is described from petrographic and geochemical analyses. The post-depositional events represent surface (seafloor), shallow burial, and deep burial alteration wherein the top of the deep-burial zone is defined by onset of chemical compaction (pressure solution) of low-Mg calcite, a process typically beginning by depths of > 300 meters (Neugebauer, 1991). Fig. 2.5 illustrates the interpreted relative timing and burial depth of diagenetic features.

2.4.2 Petrography

Limestone

Surface to near-surface alteration

Three features found in the limestone strata characterize seafloor to near-surface alteration: burrows, micrite envelopes, and automicrite (Table 2.2). Burrows include horizontal (Fig. 2.6A), sub-horizontal burrows, and vertical *Skolithos* (Fig. 2.1B). Horizontal and sub-horizontal burrows are filled with micrite. Micrite envelopes are the result of repeated cycles of boring, vacation of the boring once the microbe dies, and filling of the boring with micrite (James and Jones, 2016). They form thin (20-40 μm) layers on skeletal grains in grainstone lithofacies (Fig. 2.6B). The grains are likely bivalve fragments that were dissolved following development of the micrite envelope, and the paleo-void space filled with blocky calcite cement I. The CL color of intraskeletal and interskeletal calcite (blocky calcite cement I) is dull whereas micrite envelopes have an orange CL color.

Clots of intergranular micrite adjoining skeletal clasts in ooid-bearing grainstone are interpreted to be an example of automicrite (Fig. 2.6B). It has the same orange CL color as micrite envelopes. Automicrite is considered a product primarily the result of microbial activity (Keim and Schlager, 1999), and represents an early type of cement.

Fragments of blackened (pyritized) ostracodes and crinoid ossicles are represented by an opaque black color. This alteration is interpreted to have formed under reducing conditions in the peritidal zones, with subsequent marine exposure due to shallow-subsurface reworking by fairweather or storm waves and currents (Strasser, 1984).

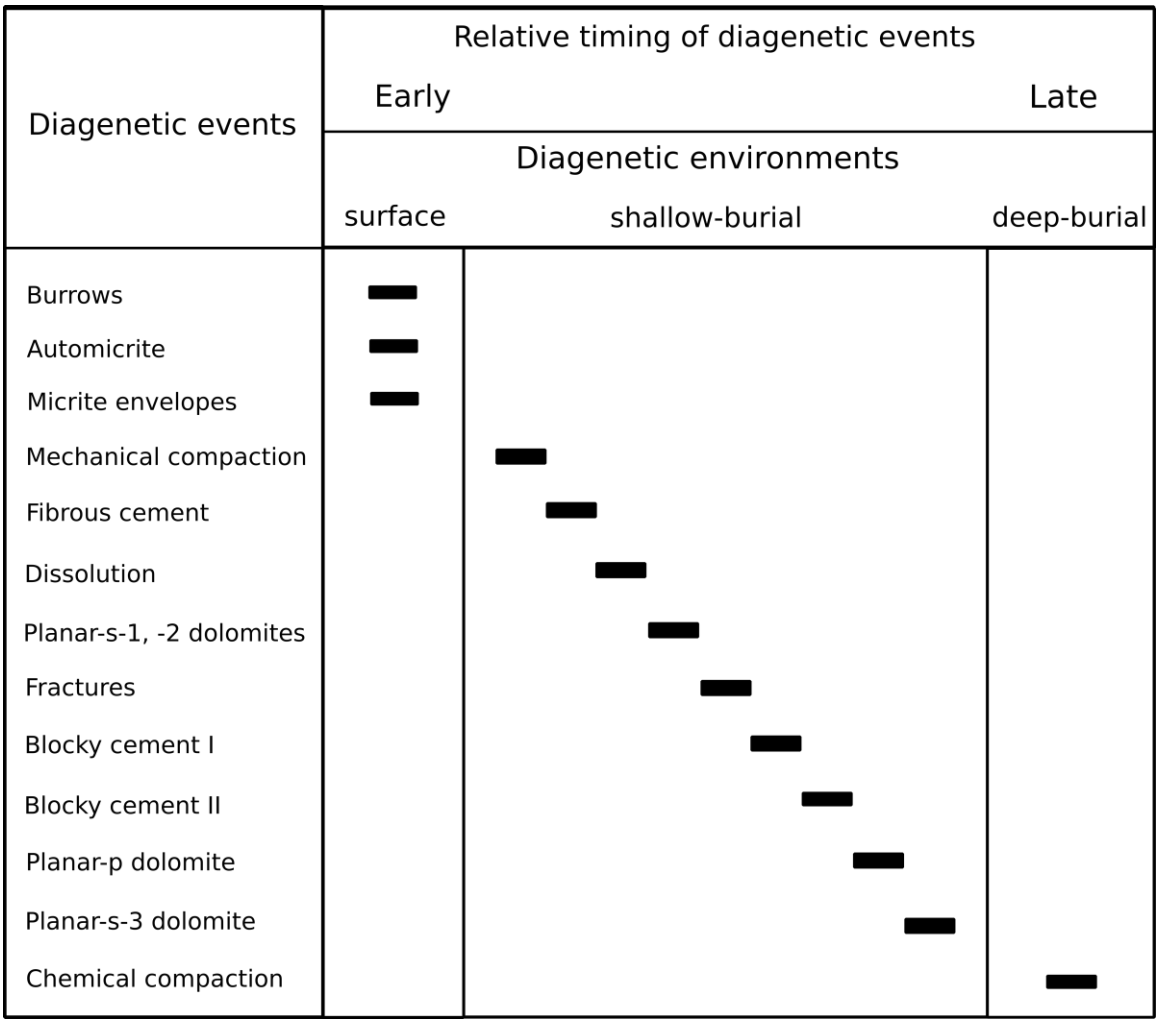

Figure 2.5. Diagenetic events and their relative timing within the Deux Rivières outlier, based on petrographic and geochemistry study of samples.

Cement type	Crystal size	Spatial distribution	CL characteristic
microbial envelopes	< 5 μm	coat bivalve fragments	orange
automicrite	< 5 μm	connect primary grains	orange
fibrous cement	10-100 μm wide, 60-700 μm long	rims coat primary grains	dull
blocky cement I	150-3500 μm	inter-grain and moldic pore space	dull, some are zoned
blocky cement II	400 μm-2 mm	vuggy pore space	orange
vein calcite	20-800 μm	fracture	orange

Table 2.2. Summary of petrographic characteristics of diagenetic calcite in the Deux Rivières outlier limestones.

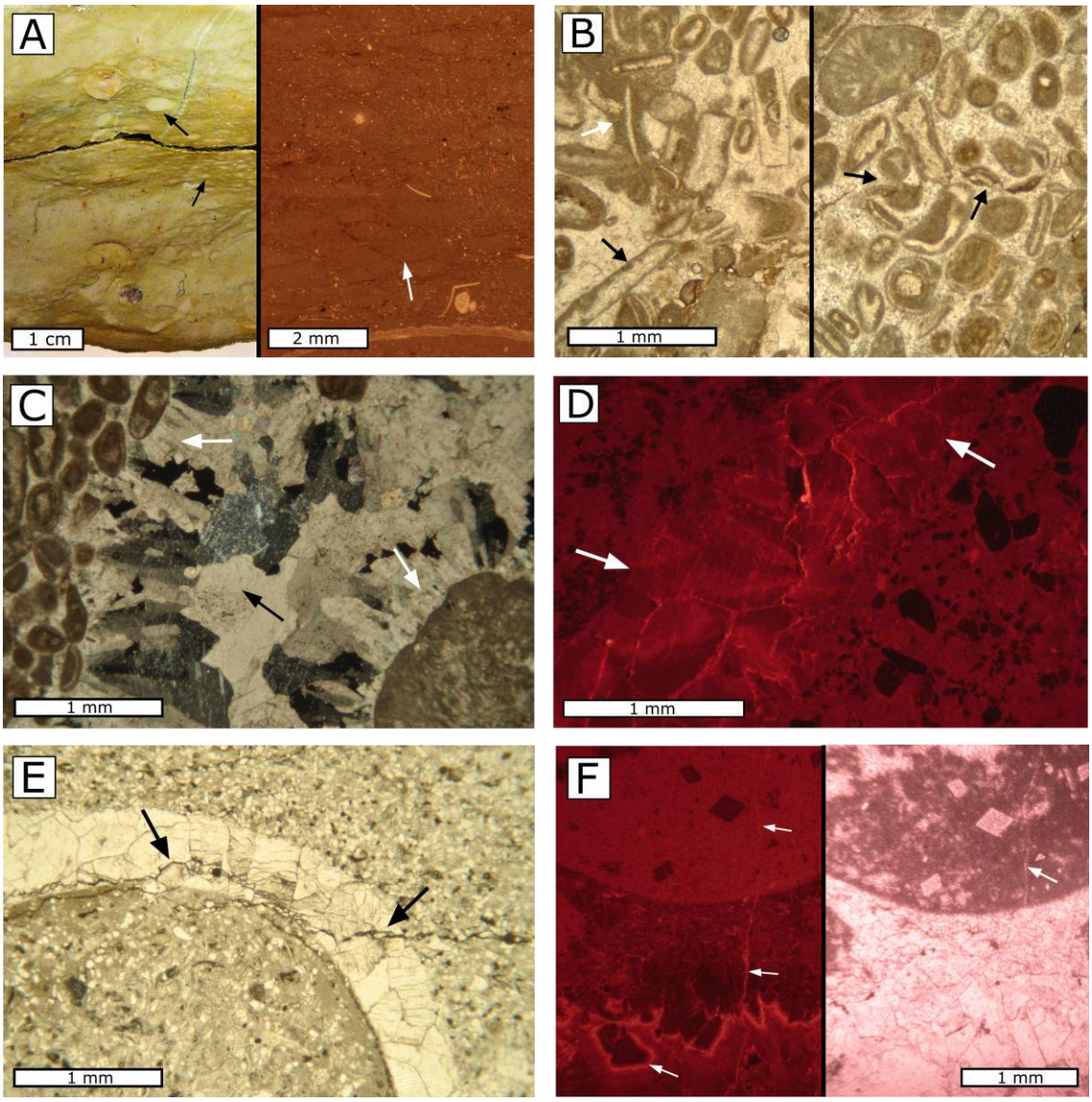

Figure 2.6 Thin-section photomicrographs of limestone diagenetic features at Deux Rivières outlier. A) Hand specimen (left photo) and thin-section of the same lithofacies (right photo, planar-polarized light photo) illustrating horizontal burrows (arrows). B) Photo pair illustrating diagenesis features of ooid-bearing grainstone under plane-polarized light; left: automicrite (white arrow) and micrite envelope (black arrow); right: mechanical compaction represented by breakage of ooids (arrows). C) Fibrous cement (white arrows) and blocky cement I (black arrow) in ooid-bearing grainstone, cross-polarized light image. D) Cathodoluminescence (CL) image of zoned blocky cement I (arrows). E) Stylolite (arrows) cross-cuts blocky cement I in sandy bioclastic grainstone, plane-polarized light image. F) Photo pair illustrating orange-luminescent calcite (arrows) precipitated in fracture and along blocky cement I; left: CL image, right: plane-polarized image.

Shallow-burial diagenesis

Several different features characterize diagenetic alteration in the shallow-burial zone, and are illustrated in paragenetic order (Fig. 2.5). Evidence of mechanical compaction is noted from breakage of ooids (Fig. 2.6B) in Unit 5. Framework grain fracturing does not occur in more muddy facies. Fibrous calcite (Table 2.2) cement is the first stage of burial cementation, and forms isopachous rims around ooids, other coated grains including fragments of cyanobacterium aggregates (e.g., *Girvanella*) and bivalves. The elongated crystals range in length from 60 to 700 μm, and in width from 10 to 100 μm (Fig. 2.6C). Fibrous cement has a dull luminescence.

Secondary porosity includes moldic porosity and vuggy porosity. Moldic porosity is developed in ooid-bearing grainstone, sandy bioclastic grainstone, and calcitic crystalline dolostone through dissolution of aragonitic skeletal material such as bivalves (Fig. 2.6D, E), gastropods, and stromatoporoids. Subsequent cement consists of two stages of equigranular mosaics of calcite cement (Table 2.2) that bracket a period of dissolution. The first stage (blocky cement I) has small to large crystals, 150 μm to 3.5 mm, filling intergranular pore space and secondary porosity. The cement has a dull luminescence, rarely with some brighter zones (Fig. 2.6D). This cement postdates fibrous calcite cement (Fig. 2.6C) in ooid-bearing grainstone. Blocky cement II is represented by relatively large (400 μm to 2 mm) calcite crystals that fill vuggy void space. It has a distinctive orange luminescence, and is developed in lime mudstone (Unit 3c) and ooid-bearing grainstone (Unit 5b).

Vertical and horizontal/subhorizontal calcite microveins are locally developed, and composed of sparry calcite. There are two types of veins. First, in sandy bioclastic

grainstone of Unit 3b, microveins are 80-800 μm in width, and filled with dull-luminencent calcite with brighter zones; an attribute similar to blocky calcite I that fills paleo-molds. Second, microveins in calcitic crystalline dolostone (Fig. 2.6F) of Unit 4a and peloidal packstone of Unit 5a are 20-80 μm in width. They are filled with orange-luminescent calcite.

Deep-burial diagenesis

Horizontal (bedding parallel) stylolites cross-cut all the above diagenetic features (Fig. 2.6E). Stylolites are sinuous, and best developed in grainstone (e.g. sandy bioclastic and ooid-bearing facies) and packstone.

Dolostone

Four types of dolomite are recognized on the basis of petrographic attributes as summarized in Table 2.3. Planar-p (Mazzullo, 1992) dolomite is characterized by porphyrotopic or small patches of dolomite rhombs that range in size from 40 to 500 μm (Fig. 2.7A, B). These are mostly associated with intraskeletal micrite enclosed by stromatoporoids, and crystals often contain small (5-25 μm) micritic domains (Fig. 2.7A, B) possibly illustrating enclosed micrite matrix. Planar-p dolomite forms a local replacement of microvein calcite (Fig. 2.7A). In this case, dolomite crystals are non-luminescent.

There are three different types of planar-s dolomite, or dolomitic mosaics with subhedral crystal shapes. First, planar-s-1 dolomite occurs in bioclastic packstone of Unit 1c. Dolomite crystals are 40-200 μm in size, and form clusters that partially replace both

skeletal grains and micrite within burrows (Fig. 2.7C). Crystals have dull and bright luminescent zones (Fig. 2.7D). There is a moderate degree of local dedolomitization in which crystals are partially replaced by Fe-poor (pink staining) calcite (Fig. 2.7C). A thin calcite microvein cross-cuts dolomite crystals, and is filled with the same calcite associated with dedolomitization. Planar-s-1 dolomite mosaics are also cross-cut by stylolites, indicating that this dolomite predates deep-burial diagenesis.

Second, planar-s-2 dolomite occurs in Unit 1a. Crystals are 40-200 μm in size (Fig. 2.7E), and display a dull luminescence. Dolomite crystals form a crystalline mosaic that replaces the whole rock. Benthic skeletal carbonate fragments (bryozoans, trilobites, bivalves, and ostracodes) can be recognized based on preserved outlines of differentially darkened (pyritized) grains.

And, third, planar-s-3 dolomite makes up all of Unit 4b. Most of the dolomite crystals are coarse-grained, ranging from 50 to 2000 μm in size. Within the crystalline mosaic, crystals have cloudy (inclusion-rich) cores, often of a defined rhombohedral shape, and clear rims. There is no abrupt boundary separating core and rim (Fig. 2.7F). Dolomite crystals show undulose extinction under cross-polarized light, and are non-luminescent precluding better discrimination between core and rim. Dolomite crystals replace microvein calcite (Fig. 2.7F), and are intersected by stylolites. Secondary intercrystalline porosity is locally well developed.

Unit 2 feldspathic arenite

The feldspathic arenite has a visible moderate intergranular porosity (Fig. 2.8A, B). However, SEM analysis shows additional microporosity related to incomplete

		Dolomite type				
		planar-p	planar-e	planar-s	nonplanar	nonplanar-c
	textual attributes	Porphyrotopic scattered crystals	Dolomite crystals are mostly euhedral and crystal-supported	Subhedral to anhedral crystal mosaics	Anhedral crystals boundaries; mosaics	Saddle dolomite
Outliers	Deux Rivières	Intraskeletal micrite (stromatoporoids); crystal size (c) = 40-500 μm	none	1 replaces skeletons & micrite in burrows; c = 40-200 μm 2 whole-rock replacement; c = 40-200 μm 3 whole-rock replacement; inclusion-rich core & clear rim; c = 40-2000 μm	none	none
	Brent Crater	none	1 replaces matrix; c = 20-150 μm 2 replaces matrix; black core; c =10-60 μm	none	none	none
	Cedar Lake	none	none	whole-rock replacement; c = 20-80 μm	whole-rock replacement & fills microveins; c = 80-800 μm	none

		planar-p	planar-e	planar-s	nonplanar	nonplanar-c
Outliers	Great Manitou Island	none	none	1 in burrows, intraskeletal void, and clay; c = 80-400 μm 2 replaces bacteria? c = 5-40 μm 3 whole-rock replacement; cloudy core and clear rim; c = 80-1200 μm	replaces limestone; forms cement in sandstone; c = 80-1200 μm	fills secondary (moldic) void space; c = 400-1600 μm
	Little Manitou Island	replaces matrix & skeletons; c = 80-500 μm	none	in burrows & intraskeletal void space; c = 80-150 μm	replaces limestone; forms cement in sandstone; c = 80-1200 μm	none
	Owen Quarry	inclusions in planar-s and nonplanar dolomite; c = 40-800 μm	none	Whole-rock replacement; c = 40-400 μm	1 whole-rock replacement; cloudy core and clear rim; c = 80-2000 μm 2 microveins; is Fe-rich; c = 100-800 μm	fills secondary (moldic, vuggy) void space, and microveins; c = 400-2000 μm

Table 2.3. Dolomite types, their textural attributes and distribution in outliers.

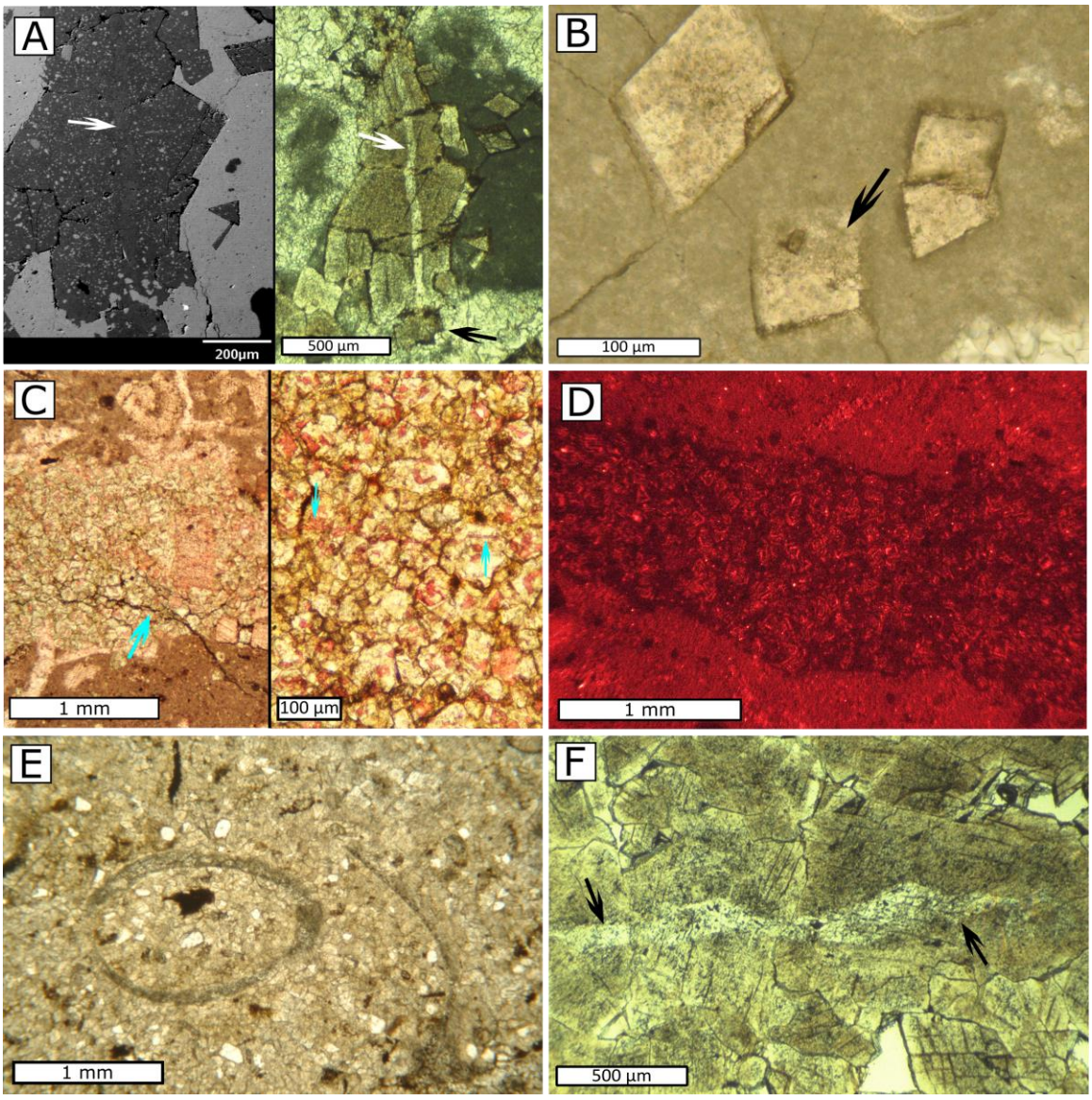

Figure 2.7. Thin-section photomicrographs of dolomite diagenetic features at Deux Rivières outlier. A) Photo pair illustrating planar-p dolomite; left: back-scattered image of dolomite (dark grey) with abundant calcite inclusions (light grey), arrow indicates vein calcite replaced by dolomite; right: planar-p dolomite replaces vein calcite (white arrow) and blocky cement I (black arrow), plane-polarized image. B) Planar-p dolomite with calcite inclusions that resemble micrite (arrow), plane-polarized image. C) Photo pair illustrating dolomitic bioclastic packstone, plane-polarized light image of stained thin section; left: planar-s-1 dolomite (arrow) is truncated by stylolite; right: dedolomitization of dolomite, dolomite grains are truncated by vein calcite (arrows). D) CL image of dull and bright zones of planar-s-1dolomite. E) Bioclastic dolomudstone composed of planar-s-2 dolomite and blackened ostracodes fragments, plane-polarized light image. F) Planar-s-3 dolomite replaces vein calcite (arrows), plane-polarized image.

secondary dissolution of potassium feldspar grains (Fig. 2.8C). Intergranular void space is occupied by variable amount of light brown (in plane-polarized light) clay giving the sandstone its brownish hue. The clay forms thin coatings on framework grains (Fig. 2.8B). SEM shows that chlorite crystals, 1-2 μm in size, form crystal rosettes on sand grain surfaces (Fig. 2.8D). XRD analysis indicates that kaolinite is also present but is not visually confirmed.

2.4.3 Geochemistry

Limestone

Major and minor elemental composition

Limestone samples possess a relatively homogeneous geochemical character among calcite cements and skeletal material. All calcite types are low-Mg (< 2.2 mol %) calcite, with low concentrations of Fe, Mn, Ba, and Sr (< 0.2 mol %) (Table 2.4).

Stable (C, O) isotopes

Sampling was conducted as part of a chemostratigraphic transect through the outlier. $\delta^{13}C$ and $\delta^{18}O$ values of micrite, or the finest carbonate fraction available in a given unit, were measured to generate a chemostratigraphic section (Fig. 2.2). $\delta^{13}C_{VPDB}$ values of micrite range from -2.3‰ to 0.5‰. There is an upsection increase in $\delta^{13}C$ values from less than -1‰ in Unit 1 through Unit 3b, to greater than -1‰ in Unit 3c through Unit 5. This range partially overlaps with the $\delta^{13}C$ range of Turinian marine brachiopod shells, -1‰ to 0‰ VPDB (Qing and Veizer, 1994; Shield et al., 2003)

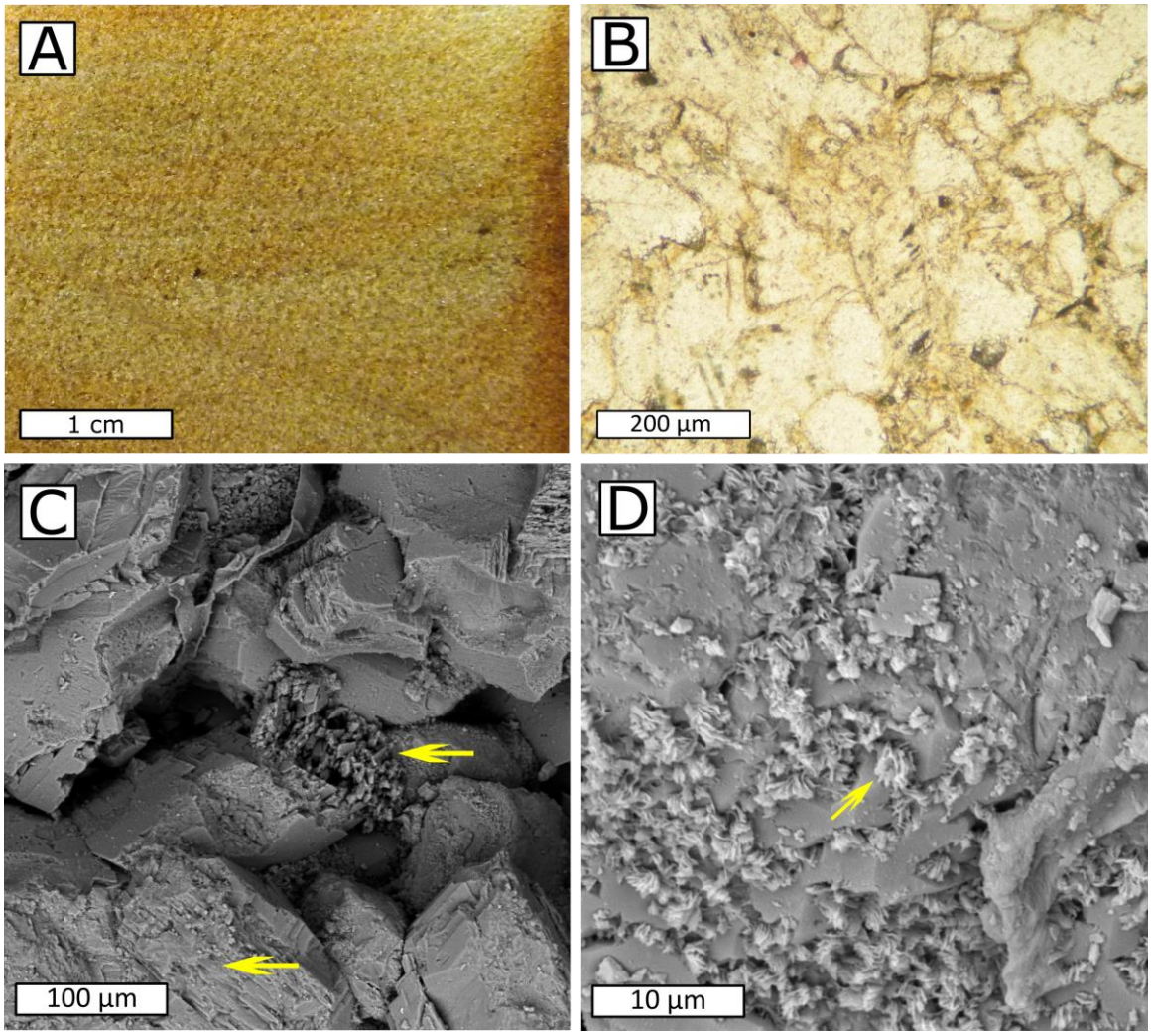

Figure 2.8. Photograph of diagenetic attributes of feldspathic (lithofacies S1) at Deux Rivières outlier. A) Slabbed rock sample showing light brown color of arenite. B) Intergranular clay (brown), plane-polarized light image of thin section. C) Differential dissolution of potassium feldspar grains (arrows), secondary electron photomicrograph. D) Chlorite rosettes (arrow) on sand grain surfaces, secondary electron photomicrograph.

$\delta^{18}O_{VPDB}$ values of micrite are between -4.3‰ and -5‰. This range lies within the $\delta^{18}O$ range of Turinian marine brachiopod shells, -4‰ to -6‰ VPDB (Qing and Veizer, 1994; Shield et al., 2003). As such, it may allow identification of temperature of early marine diagenesis. The equilibrium relationship between $\delta^{18}O$ of calcite, temperature, and $\delta^{18}O$ of water (Fig. 2.9) is adopted from James and Jones (2016; their Fig. 23.4). The relationship is based on equilibrium fractionation where oxygen isotopes in the carbonate-water-biocarbonate system obey rules of kinetic fractionation (O'Neil et al., 1969). Shield et al. (2003) estimated a seawater $\delta^{18}O$ value of -1‰ to -3‰ SMOW for this time period. Calcite with $\delta^{18}O$ values between -4.3‰ and -5‰ VPDB would have formed in water with temperature between 20°C and 33°C.

Strontium isotope ratios

Strontium isotope ratios ($^{87}Sr/^{86}Sr$) of limestone (micrite and grains) samples were determined, and illustrated in Fig. 2.2. The lowermost limestone exposed in this succession (Unit 1c) has a relatively low $^{87}Sr/^{86}Sr$ value (0.70832). The isotope ratio increases upsection for ~ 3 meters and reaches a maximum value (0.70877) for the outlier section in Unit 3a, then decreases gradually, reaching a minimum value (0.70813) in Unit 5b (Fig. 2.2). Overall, there is net decrease in $^{87}Sr/^{86}Sr$ values moving upsection. According to Edwards et al. (2015), $^{87}Sr/^{86}Sr$ for global Turinian seawater ranges from 0.70797 to 0.7082. The upsection decrease in $^{87}Sr/^{86}Sr$ values in the outlier reveals, therefore, values initially more positive than contemporary seawater whereas the value associated with Unit 5b is indistinguishable from that of Turinian seawater.

Type	Distribution	$CaCO_3$	$MgCO_3$	$FeCO_3$	$MnCO_3$	$BaCO_3$	$SrCO_3$
Blocky calcite I	Unit 3b	98.24%	1.60%	n.d.*	0.05%	0.00%	0.06%
Blocky calcite I	Unit 3b	98.50%	1.11%	0.20%	0.14%	0.05%	n.d.
Blocky calcite I	Unit 4a	98.25%	1.62%	0.02%	0.05%	n.d.	0.07%
Blocky calcite I	Unit 4a	97.66%	2.20%	n.d.	n.d.	0.03%	0.08%
Vein calcite	Unit 4a	98.64%	0.96%	0.15%	0.17%	n.d.	0.05%
Planar-p dolomite	Unit 4a	53.05%	42.45%	3.15%	1.27%	n.d.	0.04%
Planar-p dolomite	Unit 4a	52.66%	42.19%	3.65%	1.47%	n.d.	0.03%
Planar-p dolomite (replacing vein calcite)	Unit 4a	52.23%	42.24%	4.09%	1.39%	n.d.	n.d.
Planar-s-3 dolomite (core)	Unit 4b	50.28%	48.65%	1.02%	0.04%	n.d.	0.01%
Planar-s-3 dolomite (core)	Unit 4b	51.09%	47.91%	0.85%	0.09%	n.d.	0.02%
Planar-s-3 dolomite (rim)	Unit 4b	50.13%	48.59%	1.10%	0.14%	0.03%	0.01%

* n.d. = not detected

Table 2.4. Major and minor elemental composition of calcite and dolomite in Deux Rivières outlier. Values are illustrated in molecular percentage.

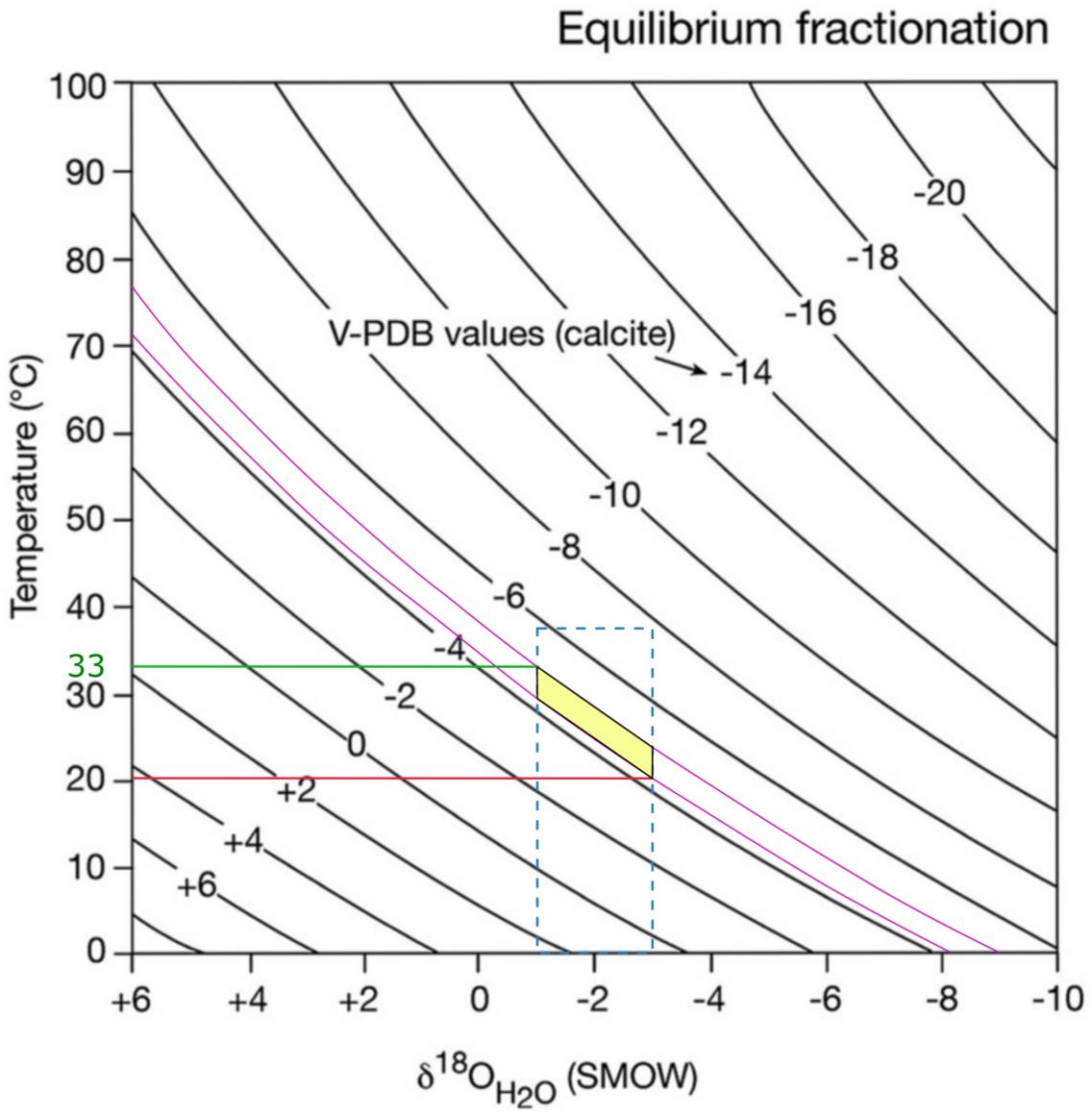

Figure 2.9. Equilibrium relationship between $\delta^{18}O$ of calcite, temperature, and the $\delta^{18}O$ of water, modified after James and Jones (2016). $\delta^{18}O$ of seawater is assumed to range from -1‰ to -3‰ SMOW (Shield et al., 2003). $\delta^{18}O$ of Deux Rivières outlier limestones ranges from -4.3‰ to -5‰ VPDB. The plot shows that calcite is precipitated from water with temperature between 20°C and 33°C.

The most elevated ratio is associated with a limestone sample from Unit 3a immediately above the feldspathic arenite of Unit 2. This more positive ratio demonstrates more abundant ^{87}Sr. Diagenetic fluids interacting with siliciclastics interbedded in a carbonate succession, or positioned along a migration pathway leading to the carbonate succession will, in general, inherit more radiogenic ^{87}Sr than seawater. Influence of crystalline basement rock (see below) is also a possibility although the elevated Sr-isotope value lies directly above a siliciclastic unit. Thus, the overall decrease in $^{87}Sr/^{86}Sr$ values moving upsection may indicate a simple decrease in the abundance of siliciclastic material within the depositional system. The upsection reduction in siliciclastic content is also a function of net transgression, backstepping the siliciclastic source, resulting in establishment of a clean carbonate depositional system as represented by Unit 5b; the unit that records the expected seawater $^{87}Sr/^{86}Sr$ value.

Dolostone

Major and minor elements

Only planar-p dolomite and planar-s-3 dolomite were measured for major and minor elemental composition (Table 2.3) due to limited availability of polished thin-sections. Planar-s-3 dolomite ($Ca_{50-51}Mg_{48}Fe_{01}$) is more stoichiometric than planar-p dolomite ($Ca_{52-53}Mg_{42}Fe_{03-04}Mn_{01}$), with lower Mg, Fe, and Mn content. These two types of dolomite are Fe-bearing, with planar-p dolomite having up to 4.09 mol % $FeCO_3$.

Stable (C, O) isotopes

C and O isotope ratios of planar-s-1 and planar-s-3 dolomites were measured. The other two types of dolomite were not sampled because their small proportion of the host rock precluded effective clear separation during sampling. $\delta^{13}C$ values of dolomite are similar to those of calcite. Planar-s-1 dolomite of Unit 1a has a $\delta^{18}O_{VPDB}$ value of -8.73‰, and planar-s-3 dolomite of Unit 4b has a $\delta^{18}O_{VPDB}$ value of -9.82‰. The latter value is either an average of two possible endmember compositions represented by the inclusion-rich core and inclusion-free rim dolomites that make up the host fabric; or, the value represents mostly the latter (rim) dolomite phase that may have altered an earlier (core) phase of dolomite.

Strontium isotopes

Strontium isotope ratios of planar-s-1 and planar-s-3 dolomites were measured. Planar-s-1 dolomite of Unit 1a has $^{87}Sr/^{86}Sr$ value of 0.71035, whereas planar-s-3 dolomite of Unit 4b has $^{87}Sr/^{86}Sr$ value of 0.70827. The strontium isotope ratio of planar-s-1 is very high compared to other analyzed samples in the succession. It suggests that the fluid from which dolomite precipitated was originally enriched in ^{87}Sr, a product of either interaction with siliciclastics in the succession or the Precambrian basement. The surrounding biotite-potassium feldspar-quartz-plagioclase gneiss also contains intrusive monzonite and granitic dikes (Lumbers, 1976). According to Davis et al. (1968) and Krogh and Davis (1969), granitic and gneissic rocks in the Grenville Province have $^{87}Sr/^{86}Sr$ values higher than 0.7200. Diagenetic fluid interacting with basement rocks would have a similar elevated Sr isotope ratio. Thus, mixing between fluids enriched

from interacting with basement rocks and a less enriched fluid would produce planar-s-1 dolomite. Interaction of fluid with siliciclastics will incorporate more ^{87}Sr within the fluid.

In contrast, planar-s-3 dolomite has a comparable $^{87}Sr/^{86}Sr$ value as Turinian seawater and sub- and superjacent limestone. Given the core-rim differentiation of this dolomite fabric, the resulting "seawater" signature is either fortuitous as a mean value or represents a predominantly marine-derived fluid source.

2.4.4 Discussion

Apart from burial depth, environment of diagenesis is also defined on the basis of fluid chemistry and the distribution of that fluid in the pores (Longman, 1980). Thus, the shallow-burial environment can be subdivided into the marine phreatic zone and freshwater burial zones.

Limestone

Evidence of limestone diagenesis in the marine environment includes petrographic and geochemical evidence. First, automicrite, micrite envelopes, and blackened (pyritic) grains illustrate surface and near-surface alteration. Second, geochemical evidence supports a largely marine to near-surface marine-derived diagenetic framework: 1) the $\delta^{13}C$ value range partially overlaps with the Turinian marine calcite range; 2) the $\delta^{18}O$ value of micrite lies within the range of Turinian marine calcite; and 3) the upsection decrease in $^{87}Sr/^{86}Sr$ values approaches a Turinian seawater value in Unit 5b as siliciclastic material is gradually removed from the depositional system.

Shallow-burial diagenesis documents a shift from a marine phreatic environment to a freshwater burial environment. Isopachous fibrous cement represents a marine phreatic environment (Longman, 1980), whereas input of meteoric-derived fluids is represented by dissolution of aragonitic skeletal material and precipitation of blocky calcite in moldic and intergranular pore space (Longman, 1980). A deep-burial (> 300 m) diagenesis feature is represented by formation of stylolites.

Dolostone

All types of dolomite predate formation of stylolites, indicating that they precipitated in a marine or shallow-burial zone. They also require a source of Mg^{2+}. Planar-p and planar-s-2 dolomites are dealt with first as there are no related isotopic data.

Patches of planar-s-2 dolomite, mostly in burrows, suggest a time- or Mg-supply-limited origin of dolomite formation (Machel and Mountjoy, 1987). Its prominent association with burrows suggests that it is possibly linked to near-surface flushing by marine or marine-derived pore fluids (Gingras et al. 2004). Dedolomitization of planar-s-2 dolomite is a process of replacement calcite along a dissolution-precipitation front (James and Jones, 2016). It is commonly associated with movement of Ca- and sometimes sulphate-rich fluids (Back et al., 1983). Thus, it represents a distinct diagenetic environment from that of the host dolomite.

Planar-p dolomite replaces blocky cement I and calcite veins, and is interpreted to be an entirely burial diagenetic feature post-dating meteoric diagenesis and fracturing. Dolomite crystals have abundant relics of calcite micrite and are non-stoichiometric. An interesting potential analog (petrographically, and its biotic association) of planar-p

dolomite is shallow-burial dolomite of Devonian stromatoporoid-coral boundstone in southern Manitoba (Chou and Longstaffe, 1995). This dolomite appears to have formed in response to marine-derived fluids. If there is a similarity between theses dolomites, then it suggests re-introduction of marine-derived fluids in the Deux Rivières outlier following interpreted meteoric/fracturing events.

From C, O isotope values alone, there remains great uncertainty in the composition of original fluid from which such dolomite can precipitate but some possibilities are illustrated. First, let's assume that dolomite precipitated from seawater ($\delta^{18}O$ value: -1‰ to -3‰ SMOW; Shield et al., 2003). Using the dolomite-water fractionation equation of Land (1983), the estimated temperature range for planar-s-2 dolomite is 65 to 78°C, and for planar-s-3 dolomite is 72 to 86°C (Fig. 2.10). These are unrealistically elevated temperatures if dolomites were co-precipitate with marine calcite given the estimated surface ocean temperature of the early Late Ordovician didn't exceed 35°C (Herrmann and Haupt, 2010). However, it may be realistic if dolomitization was the result of a heated fluid with an isotopic composition of seawater.

Second, let's assume that dolomite did form over a similar temperature range as marine limestone, estimated broadly to have been 20 to 33°C (Fig. 2.9). In this case, planar-s-1 and planar-s-3 dolomites should have values that range between 0 and 2‰ (Fig 2.10), or -1 to -2‰ according to the ~ 3‰ enrichment of dolomite relative to marine calcite (James and Jones, 2016). If there was marine dolomite, any record of it has been removed through subsequent diagenetic alteration in the presence of ^{18}O-depleted fluids. Instead, at the above marine temperatures, the registered fluid composition ranges from -9.5‰ to -13.5‰ SMOW (Fig. 2.10).

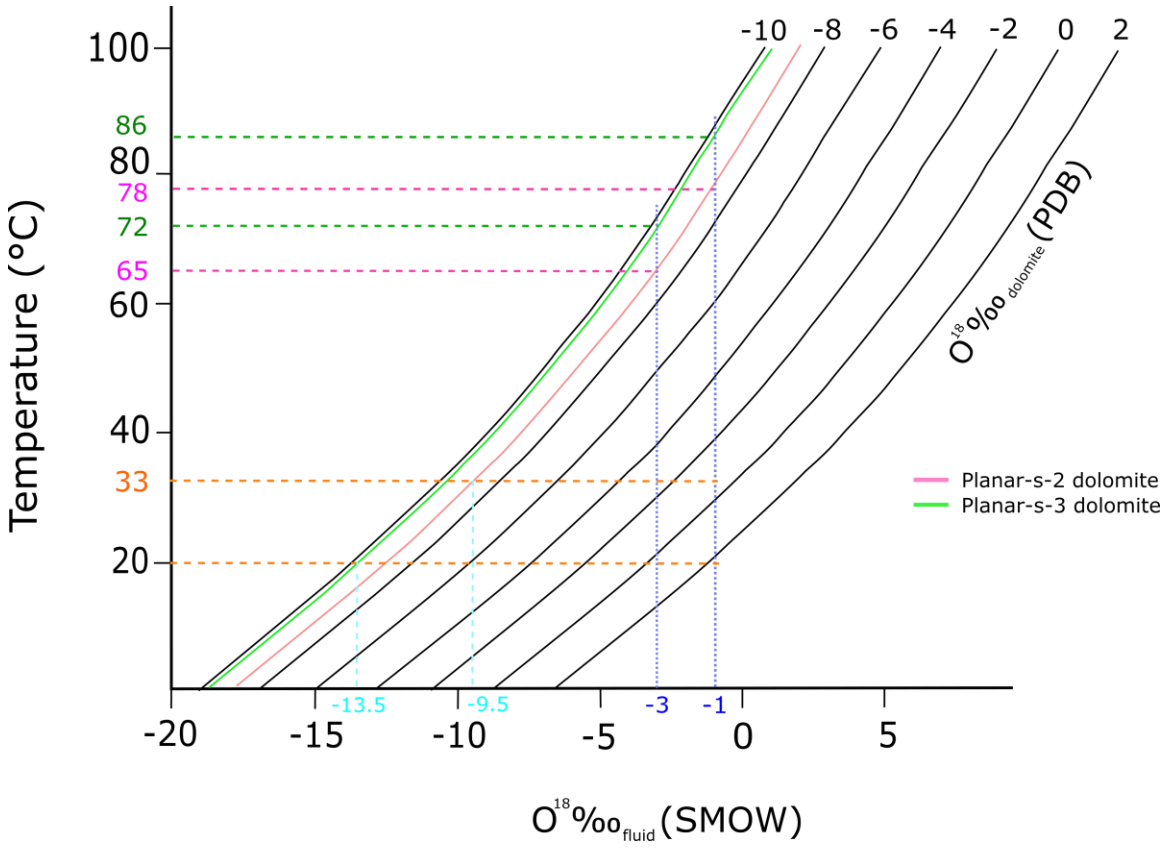

Figure 2.10. Estimated formation temperature and fluid $\delta^{18}O$ value of Planar-s-2, -3 dolomites at Deux Rivières outlier. The plot is modified after Nurkhanuly (2012), whose values are calculated using the equation: $10^3 \ln \alpha = 3.2 \times 10^2 T^{-2} - 3.3$ (Land, 1983).

The above calculations, when integrated with stratigraphic distribution of dolomite and its isotope values, allow for further interpretation of the origin(s) of planar-s-1 and planar-s-3 dolomites.

First, assume that dolomite precipitated from fluid with more negative $\delta^{18}O$ values than Late Ordovician seawater. Both planar-s-2 and planar-s-3 dolomites are stratigraphically-bounded, Unit 1a and Unit 4b, respectively. According to petrographic analysis (Fig. 7A, F), the cloudy cores of planar-s-3 dolomite resembles in size and shape to crystals of planar-p dolomite. As suggested by Chou and Longstaffe (1995), early-stage microcrystalline dolomite can act as nuclei for later dolomite. Planar-s-3 dolomite may have precipitated around and altered planar-p dolomite (poorly ordered). The reasons for the stratigraphically restricted distribution of planar-s-3 dolomite may include: 1) high porosity of the precursor limestone; and 2) presence of earlier-stage dolomite, probably planar-p dolomite. Thus, the distribution of planar-s-2 and planar-s-3 dolomites may record hydraulic flow restricted to a bounded aquifer. If correct, this implies a secondary (burial) origin.

A common conodont color alteration index (CAI) of 1.5 was reported both by Legall et al. (1981) from an uncertain stratigraphic position in the outlier, and by McCracken (2017) from Unit 5. Such a value reflects maximum burial temperature of 60°C (Legall et al., 1981). Excluding any influence of significantly elevated fluid temperature, such as local hydrothermal fracture flow, the origin of planar-s-2 and planar-s-3 dolomites is best related to migration of ^{18}O-depleted meteoric-derived fluids during sea level variation or during later burial diagenesis. This is accommodated by the strongly negative $\delta^{18}O$ and enriched $^{87}Sr/^{86}Sr$ value of planar-s-2 dolomite. For planar-s-3

dolomite, the combination of a strongly negative $\delta^{18}O$ but a marine-like (Turinian) $^{87}Sr/^{86}Sr$ ratio is problematic with a meteoric model unless, in a bounded aquifer, progressive (downflow) dolomitization results in the Sr-isotope ratio eventually approaching the composition of the original marine limestone (Banner, 1995).

There is a second possible origin, however. Assume that dolomite precipitated from a marine-like fluid but at a higher temperature than that of a shallow marine environment. McCracken's (2017) conodont material came from the limestone unit above restricted planar-s-2 and planar-s-3 dolomites. Porous conduits within a shallowly buried succession might allow passage of hotter fluids with minimal influence on sub- or superjacent strata, as documented in the field and modelled (Gomez-Rivas et al., 2011; Lapponi et al., 2011; Hollis et al., 2017). As the outlier is fault-bound along its northwest limit and cross-cut by a fault in the center, both a heat source and movement of Mg-rich (marine-like) fluids up along some structure, then in permeable units may have occurred. For example, a Devonian seaway was likely present along the trace of Ottawa–Bonnechere graben (McCracken et al., 2000) potentially allowing for structurally controlled circulation of marine fluids well after the Late Ordovician. Planar-s-3 dolomite stands out from the other dolomites in forming very hard (crystalline) dolomite. Whether this might be related to this origin remains unclear.

Unit 2 feldspathic arenite

SEM analysis remains inconclusive as to whether kaolinite is detrital or authigenic. It can be readily transported from the continental environment, or form when

marine sediments are subaerially exposed and under the influence of meteoric recharge, where aluminosilicate minerals such as feldspar are dissolved (Worden and Morad, 2003).

The origin of chlorite is also unclear. Two relevant processes for chlorite authigenesis (Anjos et al., 2003) are considered: 1) replacement of clay-mineral precursors such as smectites, berthierine/verdine clays, and kaolinites; and 2) direct precipitation from magnesian brines associated with the mesodiagenesis of evaporitic/carbonate rocks. Given the presence of dolomitizing fluids within the stratigraphic section, chlorite may be a record of migration of these brines through the sandstone.

Chapter 3 Brent Crater

3.1 Introduction

The Brent impact structure (46° 05' N, 78° 29' W) lies within the northern part of Algonquin Provincial Park, Ontario. The present surface morphology of this heavily wooded region displays a 60-meter-deep center of a circular (~ 3 km diameter) depression with a central dome. The orientation of two lakes emphasize the circular structure (Fig. 3.1A). The crater lies within a region underlain by an igneous-metamorphic basement complex of the Grenville province, consisting of granodioritic gneisses and minor amphibolites (Grieve, 2006). An east-west-trending fault system associated with the Ottawa–Bonnechere graben lies ~ 3 km to the south of the crater, but doesn't deform the circular expression of the crater (Murray and Gust, 1970). The present-day crater and central dome is underlain by relatively thick (30-45 m) Pleistocene glacial-derived deposits (Lozej and Beals, 1975), with small outcrops of gneiss and limestone along the crater's margin.

As part of a Canadian government initiative, core was recovered from 12 drill holes between 1955 and 1967 (Lozej and Beals, 1975). Of these, core 1-59 (Fig. 3.1B) is located near the center of the crater, and recovered two distinct lithic successions beneath Quaternary glacial-derived sediment: a lower (~ 787 m) shocked-metamorphosed and breccia sequence, and an upper ~ 259 m thick sedimentary succession (Millman et al., 1960; Lozej and Beales, 1975). The age of the impact event is only broadly defined: an age of 450-500 Ma (or Late Cambrian through Late Ordovician) of impact melt rock is based on K-Ar dating (Hartung et al. 1971) whereas a pre-late Turinian (455 Ma), or Late Ordovician, age of the lower part of the sedimentary sequence is based on

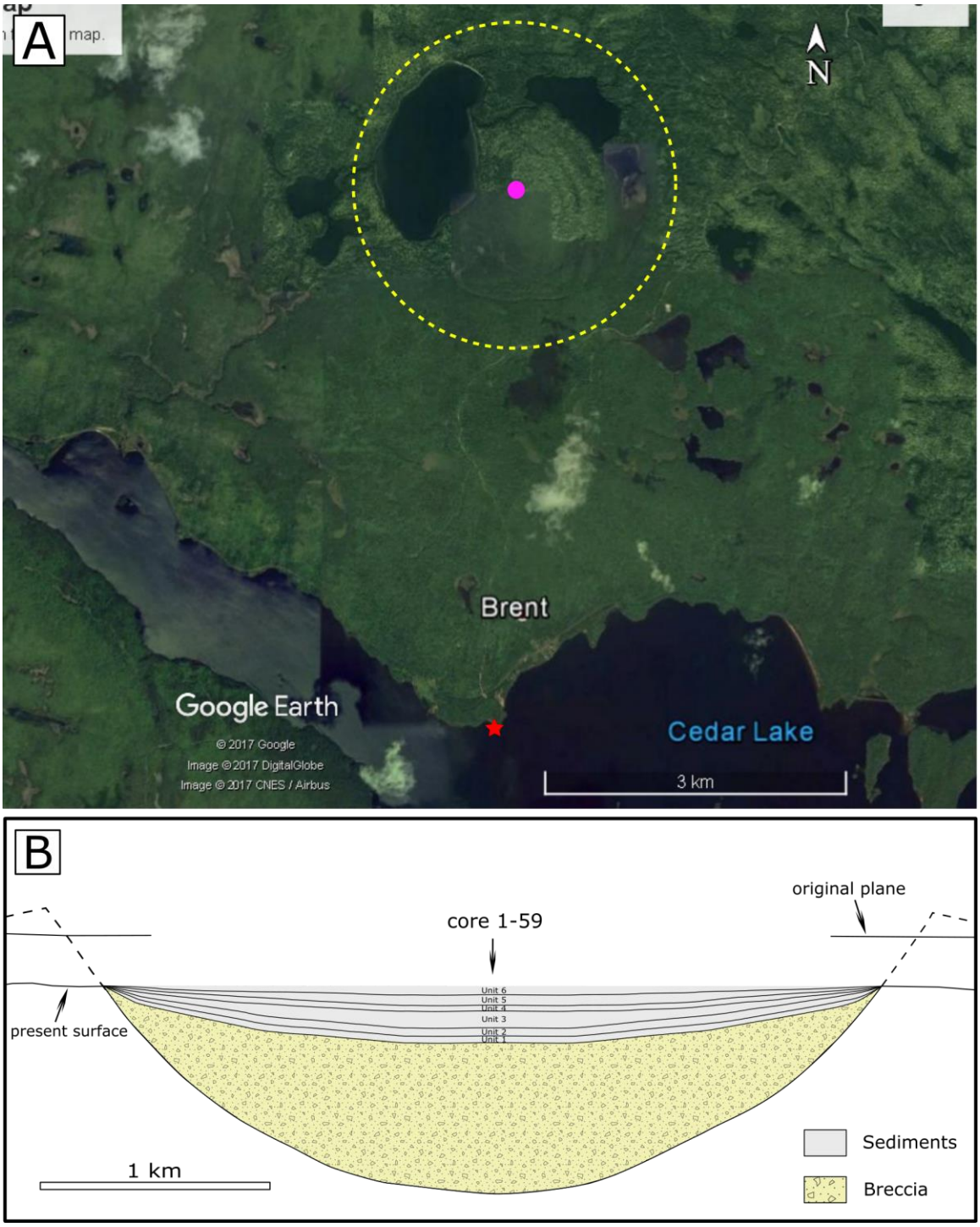

Figure 3.1. Location and general geometry of Brent Crater and Cedar Lake outlier. A) Location map derived from Google Earth showing estimated original crater rim (yellow dashed line; Grieve, 2006), location of core 1-59 (purple circle), and location of the Cedar Lake outlier (red star). B) Interpretation of the cross-sectional geometry of Brent Crater (after Grieve, 2006).

biostratigraphic information (Grahn and Ormö, 1995). In my study, the 251-m-thick sedimentary succession was examined from core 1-59, and will be described based on the author's own examination, but integrating work of Lozej and Beales (1975).

3.2 Lithostratigraphy and facies

The sedimentary succession is subdivided on the basis of lithology, fossil content, and sedimentary structures (Fig. 3.2). The lower 140 meters (Units 1-4) contain finely interlaminated sandstone, siltstone, dolostone, and lime mudstone. The upper 111 meters (Units 5-6) consist of thick alternating units of marine carbonates and siliciclastics. Lithofacies types, their associations, and fossil content are described and summarized in Table 3.1. For comparison with Lozej and Beales' (1975) dataset, metric and imperial units of measure are shown in Fig. 3.2. However, reference to a specific sedimentary feature or boundary is provided here in imperial units enabling direct correlation with core boxes and the work of Lozej and Beales (1975).

Unit 1

Description

The lowest unit of sedimentary fill is ~ 30 m thick, and divided into two subunits (Fig. 3.2). The lower Unit 1a consists of ~ 10 meters of interlaminated medium-grained feldspathic arenite and greenish siltstone (lithofacies S3a). A single 1-cm horizontal burrow was noted at 837.75 feet. Medium-grained sand fills the burrow whereas the burrow occurs in siltstone. There is a 6 mm-thick interval of wave-rippled cross-

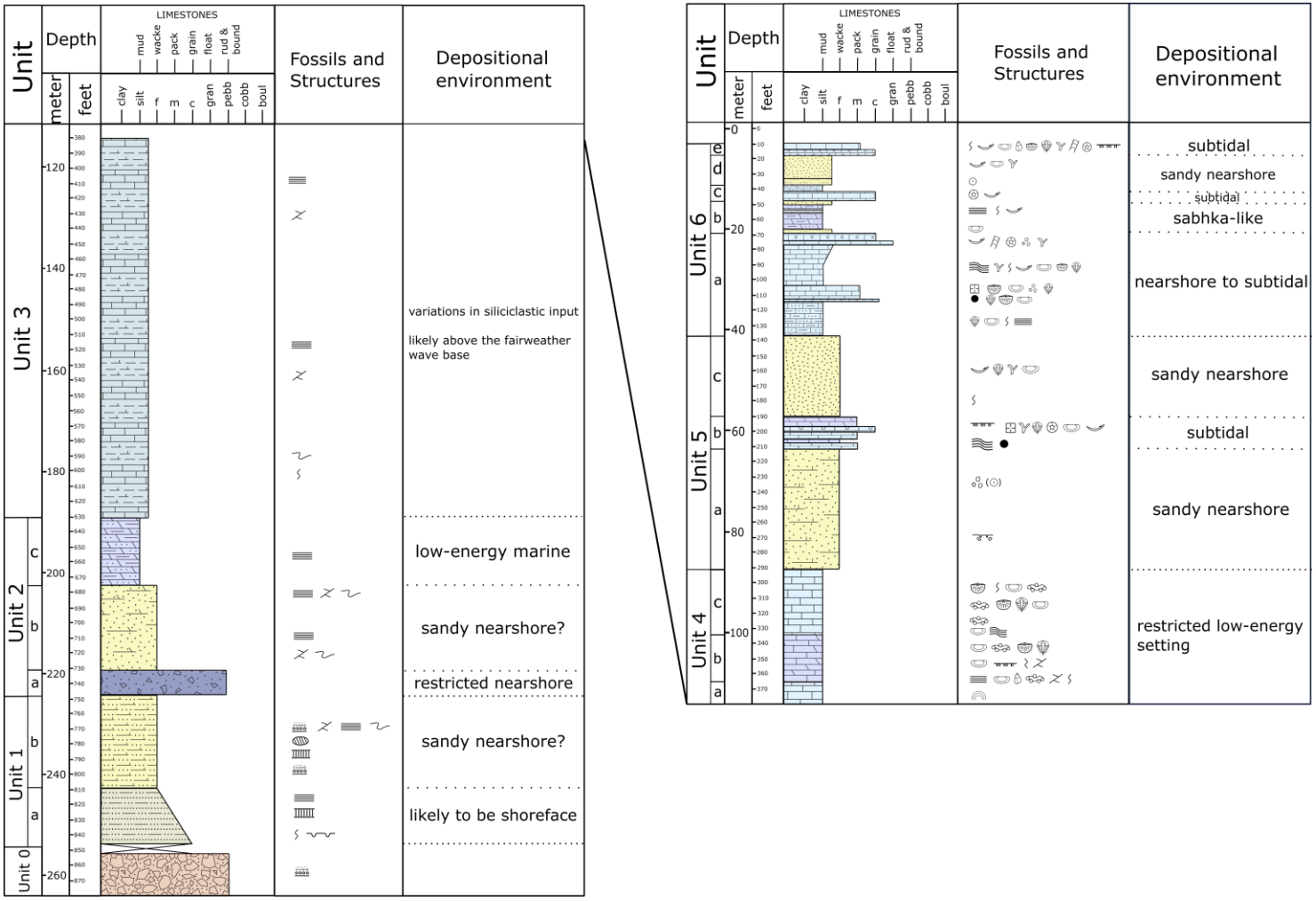

Figure 3.2. Stratigraphic attributes of the sedimentary fill of core 1-50, Brent Crater. Legend is in Fig. 2.2.

Litho-facies	lithology	Sedimentary features	Fossils and other textural attributes	Depositional environment	References
L1a	dolomitic lime mudstone or pure lime mudstone with silty laminaes	synsedimentary folds and faults		non-stenohaline, close to a source of siliciclastics; high slope declivity or earthquake activities	1, 2, 3
L1b	stromatolitic lime mudstone		at least 10 cm of microbial buildups; ostracode shells	non-stenohaline peritidal environment	4
L1c	dolomitic lime mudstone	non-laminated to weakly-laminated, hardground	scarce ostracodes and calcareous worm tubes *Tymbochoos sinclairi* Okulitch	non-stenohaline peritidal environment, intertidal?	5, 6
L1d	pure to silty lime mudstone	wispy discontinuous laminaes, synsedimentary folds and faults	scarce ostracodes, calcareous worm tubes *Tymbochoos sinclairi* Okulitch, and *Lingula* brachiopod	intertidal zone, rapid deposition and sedimentation where oversteepened slopes lead to instability	1, 2, 5, 6
L1e	wavy sandy bioclastic lime mudstone	wavy-laminated	bivalves and trilobites, < 10% sand grains	non-stenohaline, close to a source of siliciclastics	6, 7
L2a	greenish bioclastic wackestone		trilobites	non-stenohaline	6
L2/L3	bioclastic wacke/packstone		fragmented trilobite, bryozoans, ostracodes, and brachiopod	non-stenohaline	6
L3a	peloidal packstone	horizontal burrows	very scarce trilobites	probably tidal flat	6
L3b	*Tetradium*-bearing packstone		fragmented *Tetradium*, bivalves, and ostracodes	restricted environment behind a reef	6
L3c	bioclastic packstone with 3-D burrows	burrows up to 5 cm in size	bryozoans, brachiopods, crinoid ossicles, ostracodes, gastropods, bivalves, and fragments of cyanobacterium aggregates *Hedstroemia*; < 5% quartz sands	normal-marine, subtidal environment	6
L4a	ooid-bearing pack/grainstone		concentric ooid and coated grains; fossils include fragmented bivalves, crinoid ossicles, and cyanobacterium	normal-marine, high-energy subtidal environment	6
L4b	crinoidal grainstone		crinoid ossicles and bivalves	normal-marine, high-energy subtidal environment	6
L5	bryozoan-bivalve float/rudstone		bryozoans and bivalves	low-energy, shallow-water setting with rapid burial	8
D1	silty dolosmudstone	horizontal burrows		low-energy, close a ready source of siliciclastics	

S1a	quartz arenite		dominant size of sand grains is 88-125 μm, some larger (350-710 μm) grains are present. 350-500 μm, spheroidal, concentric pyritic ooid (?)	sand grains undergone several cycles of weathering, erosion, transportation, and deposition.	9
S1b	feldspathic arenite and siltstone	massive	moderately sorted, clay cement, dominant grains are 80-150 μm in size	good grain segregation	9
S2	red and green lithic wacke		lithoclasts (limestone and metamorphic rocks), quartz and feldspar grains (larger ones are 250-2000 μm in size, smaller ones are 20-60 μm in size)	rapid deposition close to a ready source of lithic material; first cycle material that is recently eroded	9
S3a	interlaminated medium-grained feldspathic arenite and greenish siltstone	interlaminated, wave ripple, burrows	gypsum cement, satin spar layers	combined flow, middle shoreface zone	10
S3b	fine-grained calcareous arenite with silt and clay laminaes	normal grading, synsedimentary folds and faults	satin spar layers	waning transport or reduction in transport energy, high slope declivity or earthquake activities	1, 2
S3c	dolomitic sandstone interlayered with thin siltstone laminaes	synsedimentary folds and faults	rare dolostone breccia	variation in siliciclastics supply, high slope declivity or earthquake activities	1, 2
S4	interlaminated siltstone, silty lime mudstone, and lime mudstone	synsedimentary folds and faults, horizontal burrows	silt grains include quartz, feldspar, and pyrite	stable seafloor below the fairweather wave base; episodic control on terrigenous material input; high slope declivity or earthquake activities	1, 2, 11
C	framework- and matrix-supported monomictic dolostone breccia		dolostone clasts: 2 mm to 2 cm	local soft sediment deformation	

Table 3.1. Summary of lithofacies types in Brent Crater sedimentary fill. References: 1, Boggs, 2011; 2, Mayall, 1983; 3, Whalen et al., 2013; 4, Tucker and Wright, 2008. 5, Steele-Petrovich and Bolton, 1998; 6, Flügel, 2010; 7, Goldhammer, 2003; 8, Lavoie, 1995; 9, Selley, 2000; 10, Plint, 2010; 11, MacEachern et al., 2010.

laminated sediment (Fig. 3.3A) at 830.5 feet. The ripple lamination has a relatively symmetrical external form but unidirectional dip of internal lamination identifying deposition under combined flow (Plint, 2010). Horizontal to sub-horizontal layers, 1 cm thick, of satin spar (silky, fibrous gypsum) occur at and above 825 feet. Though originally described as evaporite beds, all of these occurrences appear to be horizontal fracture-fill deposits sub-parallel to bedding. Gypsum cement in sandstone (Fig. 3.3B) also occurs at a depth of 810 feet.

The overlying Unit 1b is ~ 18 meters thick. It is composed of mainly fine-grained calcareous arenite with silt and clay laminae (lithofacies S3b). Several fining upward intervals (Fig. 3.3C) are present consisting of fine- to medium-grained arenite, then siltstone. Satin spar layers of 1 to 4 cm thick are present. There are synsedimentary folds and faults in the upper part of Unit 1b.

Paleoenvironmental interpretation

The laminated (feldspathic sandstone and siltstone) character of Unit 1 identifies high-order alteration of depositional/transport energy, and likely rapid deposition indicated by the feldspathic character of the sediment that suggests there had been little weathering. Within the single burrow, the difference in grain-size of its fill versus the surrounding sediment suggests that colonization of the substrate occurred following silt accumulation and prior or during the onset of sand accumulation. This highlights differential (temporal) transport of silt versus sand. Evidence for combined flow reveals the interaction of oscillatory and unidirectional transport common in shoreface settings

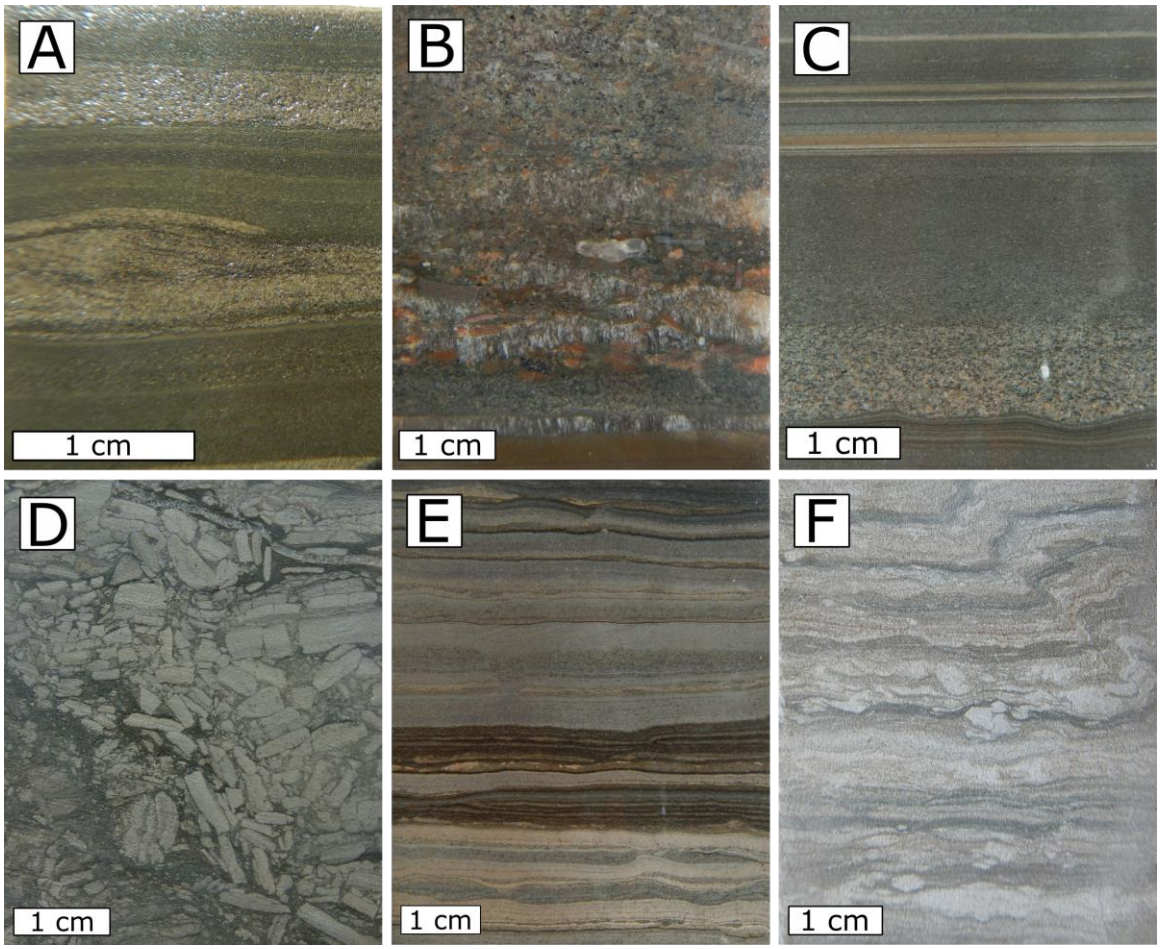

Figure 3.3.Photo of slabbed core samples of core 1-59, Units 1-3. A) Wave-rippled sandstone of Unit 1a. B) Gypsiferous sandstone of Unit 1a. C) Fining upward interval occurs in Unit 1b. D) Dolostone breccia of Unit 2a. E) Dolomitic sandstone interlayered with thin siltstone laminaes of Unit 2b. F) Disrupted interlaminated siltstone, silty lime mudstone, and lime mudstone of Unit 3.

(Plint, 2010). Rippled sandstone, for example, is common near the middle shoreface zone (Plint, 2010). Since the earliest non-marine burrows were reported to occur in fluvial environments in Early Cambrian (Kennedy and Droser, 2011), the presence of the burrow itself cannot identify a specific depositional environment.

Normal grading that characterizes Unit 1b reflects either individual episodes of waning transport, such as associated with gravity-flow transport, or a composite record of progressive reduction in transport energy/deposition (Boggs, 2011). The co-presence of synsedimentary deformation structures in Unit 1 suggests the role of unstable substrate that may be related to rapid deposition along an oversteepened gradient (Boggs, 2011). Whalen et al. (2013), for example, reported that the extent of soft-sediment deformation in the post-impact fill of the much larger Chicxulub impact crater in Mexico is associated with changes in slope declivity during basin fill of the crater. Of course, seismicity related to earthquake tremors will also induce soft-sediment deformation (Mayall, 1983); the recurrence period of tremors likely elevated in a recent impact zone.

The proposed re-interpretation of gypsum as fracture fill and a diagenetic origin of gypsum cement in sandstone is significant. For Lozej and Beales (1975), the satin spar formed the foundation for their interpreted initial (post-impact) playa-sabkha lake environment confined within the crater walls. With gypsum as a diagenetic product, sub-parallel fractures likely formed due to migration of evaporated sea water through sediment casing fracture expansion (Pettijohn et al., 1972), the initial depositional environment may have been a marine siliciclastic basin with initial basin fill related to transport of siliciclastics across an unstable substrate.

Unit 2

Description

Unit 2 is ~ 35 m thick, and divided into three subunits (Fig. 3.2). The lowest subunit (Unit 2a) is ~ 9 m thick, and composed of framework- and matrix-supported monomictic dolostone breccia (lithofacies C; Fig. 3.3D) with a dolomitic siltstone matrix. The size of the clasts ranges from 2 mm to 2 cm. The upper 1.3 meters of this subunit consist of an apparent single bed of dolostone.

Unit 2b is ~ 13 m thick, and consists of dolomitic sandstone interlayered with thin siltstone laminae (lithofacies S3c; Fig. 3.3E). Dolomitic layers are horizontal to sub-horizontal. Rare dolostone breccia is present. Small-scale synsedimentary faults and folds are common.

Unit 2c is ~ 14 m and consists of dolomitic lime mudstone to pure lime mudstone with silty laminae (lithofacies L1a). Moving upsection, intervals of massive lime mudstone occurs and the amount of synsedimentary deformation structures decreases.

Paleoenvironmental interpretation

The monomicitic breccia may be a result of local soft sediment deformation rather than the evaporite solution breccias suggested by Lozej and Beals (1975). The overlying well stratified Unit 2b with synsedimentary deformation features and appearance of sandstone reflects an abrupt variation in siliciclastic sediment supply into a carbonate basin. The occurrence of soft sediment deformation structures suggests, again, the possible role of earthquake activity or slope declivity (Mayall, 1983; Boggs, 2011). The

upsection decrease in deformation structures and change to well stratified lime mudstone suggest transition of the basin into a relatively quiet marine setting (Raaf et al., 1965).

Unit 3

Description

Unit 3 is ~ 75 m thick (Fig. 3.2), and consists of interlaminated siltstone, silty lime mudstone, and lime mudstone (lithofacies S4). Synsedimentary folds (Fig. 3.3F) and faults reappear in this unit. No macrofossil remains were noted, but cm-scale horizontal burrows occur preferentially in silt-dominated layers. Moving upsection, the abundance and thickness of siltstone layers decrease. A thin-section from 627 feet shows that the silt grains include quartz, feldspar, and spheroidal to irregular-shaped pyrite (Fig. 3.4A).

Paleoenvironmental interpretation

Burrows concentrated in siltstone layers probably reflect the greater abundance of organic material associated with fine-grained siliciclastic sediment. Horizontal burrows support a relatively stable seafloor and available food sources such as found commonly at water depth above the fairweather wave base (MacEachern et al., 2010). Alternating siliciclastic silt and carbonate stratigraphy indicates some rhythmic or episodic control on terrigenous material input (e.g. related to storm transport or sea level variation and lateral shifting of depositional systems in the basin) and/or turning on, then off of carbonate mud accumulation. Abundant soft-sediment deformation structures suggest elevated slope declivity or earthquake activity (Mayall, 1983; Boggs, 2011).

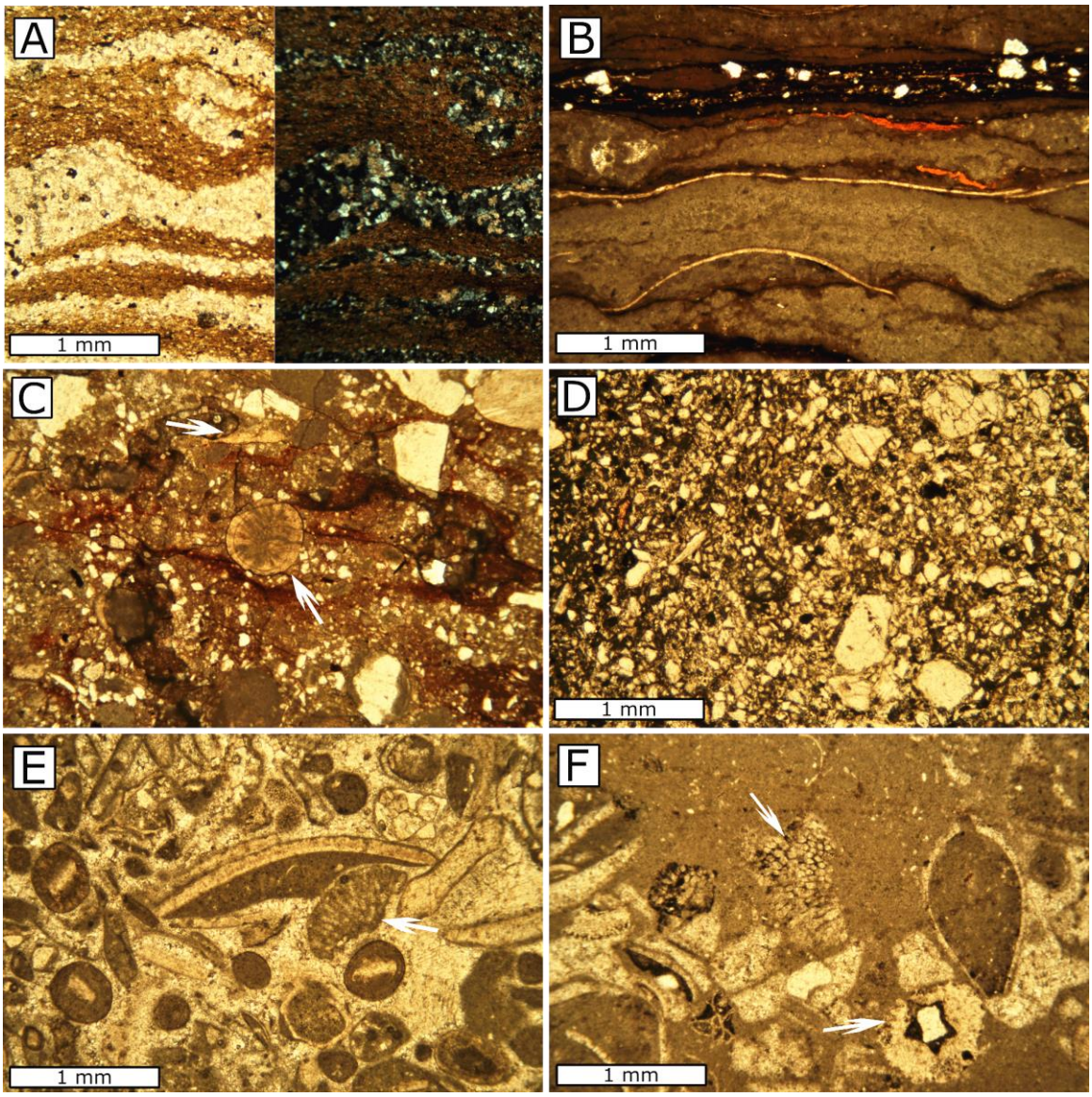

Figure 3.4. Thin-section photomicrograph of representative lithofacies of Brent Crater sedimentary fill. Photo B-F are all taken under plane-polarized light. A) Photo pairing illustrating interlaminated siltstone, silty lime mudstone, and lime mudstone of Unit 3; left: plane-polarized image, right: cross-polarized image. B) Stromatolitic lime mudstone of Unit 4a. C) Red and green lithic wacke of Unit 5a; arrow indicates limestone clasts. D) Feldspathic arenite of Unit 5c. E) ooid-bearing grainstone of Unit 6a; arrow indicates fragments of cyanobacterium (?). F) Bioclastic packstone of Unit 6e with cyanobacterium aggregates *Hedstroemia* (upper arrow) and crinoid ossicles (lower arrow).

Unit 4

Description

Unit 4 is ~ 27 m thick, and divided into three lithofacies associations (Fig. 3.2). The lower 4.5 m (Unit 4a) consist of stromatolitic lime mudstone (lithofacies L1b; Fig. 3.5A) with presence of ostracode shells. The stromatolites, or microbial buildups, exhibit a synoptic relief of at least 10 cm. A thin-section from 380 feet shows some thin broad but unidentified shell fragments (Fig. 3.4B).

Unit 4b is 9 m thick, and consists of non-laminated to weakly-laminated dolomitic lime mudstone (lithofacies L1c). Scarce ostracode shells and calcareous worm tubes (*Tymbochoos sinclairi* Okulitch) are present (Fig. 3.5B).

The upper division, Unit 4c, is composed of ~ 14 m of pure to silty lime mudstone (lithofacies L1d). Wispy discontinuous laminaes are present at the lower part of this division. The dominant fossil types include remains of the above similar calcareous worm tubes and ostracodes. Syn-depositional folds and faults are present. Bioturbation occurs at the top of this unit along with the skeletal remains of the inarticulate brachiopod *Lingula* sp..

Paleoenvironmental interpretation

The presence of microbial carbonate in Unit 4a suggests sediment trapped and bound by activity of microbes, likely cyanobacteria. These structures are commonly found in intertidal and subtidal environments (Tucker and Wright, 2008). The otherwise low diversity of benthic skeletal biota and absence of crinoids may suggest that the depositional environment was not stenohaline (Flügel, 2010).

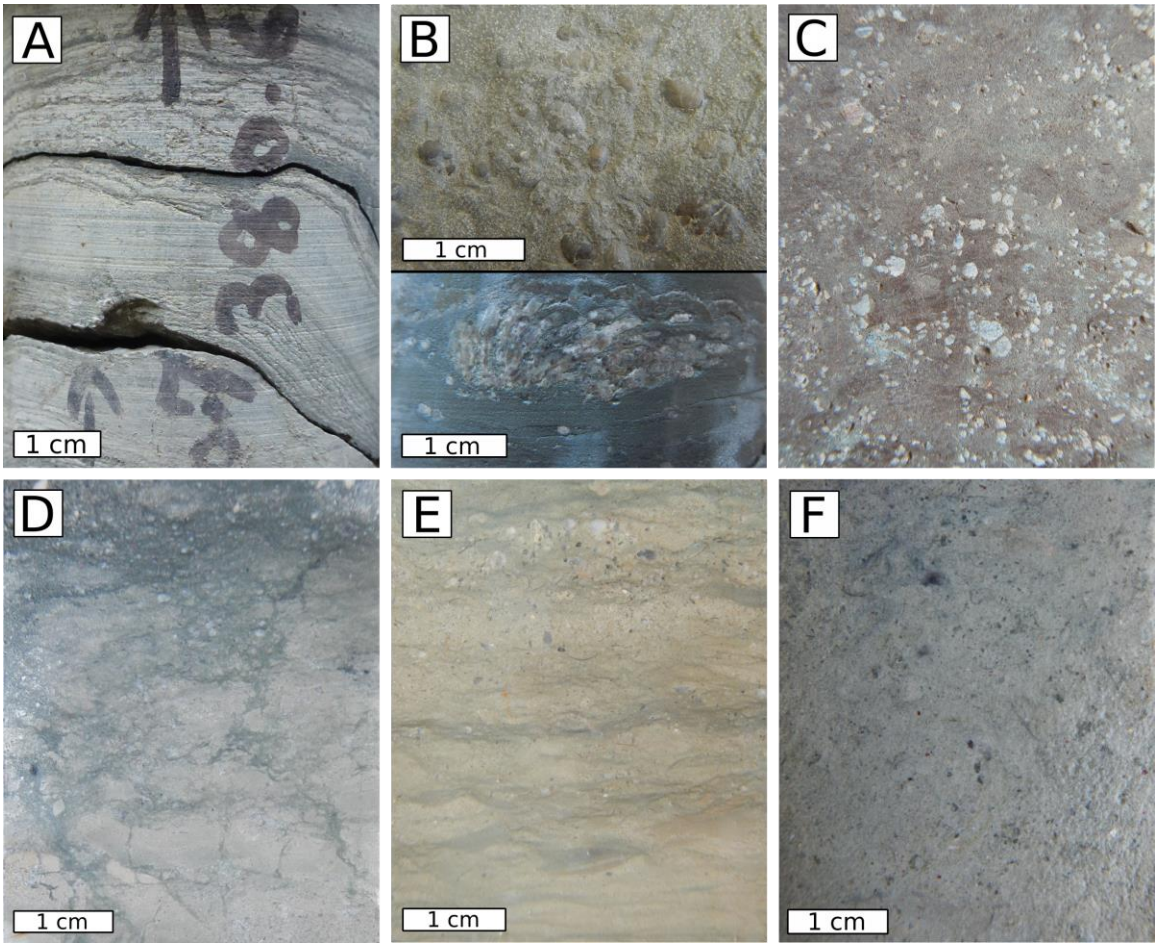

Figure 3.5. Photos of slabbed core samples of core 1-59, Units 4 and 5. A) Stromatolitic lime mudstone of Unit 4a. B) Photo pair illustrating lime mudstone of Unit 4b; upper: ostracode shells, lower: calcareous worm tubes *Tymbochoos sinclairi* Okulitch. C) Red and green lithic wacke of Unit 5a. D), Caliche developed in Unit 5a separates limestone and sandstone. E) Wavy lime mudstone at the bottom of Unit 5b. F) Feldspathic arenite of Unit 5c.

Facies of Units 4b and 4c suggest a similar depositional environment. *Tymbochoos* build-ups are relatively common in Upper Ordovician carbonate rocks in eastern Ontario, but are mostly associated with high-energy tidal channel and carbonate shoal facies influenced by periodic or constant current or wave activity (Steele-Petrovich and Bolton, 1998). The low abundance and diversity of benthic biota, and absence of crinoids, may indicate elevated salinity (Flügel, 2010). The predominant muddy facies suggests a quiet-water setting. The presence of worm tubes may illustrate transport from higher energy shoals. The appearance of an inarticulate brachiopod and bioturbation at the top of the section provides little environmental restriction, as both could be of nearshore to outer shelf-slope environments (Percival, 1978). The common presence of synsedimentary deformation structures in Unit 4c illustrates the continued role of unstable substrate.

Unit 5

Description

Unit 5 is ~ 46 m thick, and divided into three lithofacies associations (Fig. 3.2). The lower Unit 5a is about half of the entire unit and consists mostly of red and green lithic wacke (lithofacies S2; Fig. 3.5C). At the depth of 268 feet, the base of this unit rests abruptly on a greenish lime mudstone with downward tapering fractures illustrating *in situ* brecciation, downward migration of overlying sand into the fractures, and local block rotation (Fig. 3.5D). A sample collected at 232 feet for microscopic analysis reveals reworked ooid- and bioclasts (ostracodes)-bearing sand-size limestone lithoclasts (Fig. 3.4C) that make up > 30% of the framework grains. Other lithoclastic grains include

felsic metamorphic rock lithologies. The lithoclastic framework grains range in size from 250 to 2000 μm, and the matrix is 20-60 μm in size. In general, larger grains are more rounded than smaller grains.

Unit 5b is ~ 6.3 m thick, and consists of carbonate rocks. The base of Unit 5b is marked by the appearance of wavy lime mudstone with scarce bivalves and trilobites (lithofacies L1e) fragments and < 10% sand grains (Fig. 3.5E). The lower part of this unit is composed of greenish silty lime mudstone and dolostone whereas the upper part of this unit is mainly wackestone with fossils including fragmented *Tetradium* coral, crinoid ossicles bryozoans, bivalves, and trilobites (Lozej and Beales, 1975). A thin ooid-bearing grainstone with irregular contact with lime mudstone is present at 202 feet.

Unit 5c is ~ 16 m thick, and consists of fine-grained feldspathic arenite and siltstone (lithofacies S1b; Fig. 3.5F). A thin-section from 139.2 feet reveals a moderately sorted, very fine-grained feldspathic arenite with clay cement (Fig. 3.4D). The dominant grains are 80-150 μm in size, with minor 300-1200 μm grains. Larger grains are subangular to subrounded, whereas smaller grains are angular to subangular.

Paleoenvironmental interpretation

Fractures and block rotation forming the base of Unit 5a is interpreted to mark an erosional paleosurface where exposure has initiated an early stage of caliche (see Fig.4b in James, 1972). Unit 5a represents rapid deposition (with little reworking) close to a ready source of lithic material. However, appearance of limestone lithoclasts and reworked ooid demonstrate transport from existing rock sources. This is the first appearance of ooids in the core. Unit 5b facies demonstrate transgression and marine

carbonate deposited across the once siliciclastic setting. The occurrence of *Tetradium* and crinoid ossicles identifies a normal-marine environment (Flügel, 2010). The thin ooid-bearing grainstone unit illustrates a short-lived high-energy deposition. Re-appearance of siliciclastics forming Unit 5c defines a phase of regression. However, the sediments are much better sorted, forming a fine-grained arenite and siltstone, reflecting good grain segregation either at source, during transport, or during deposition. In summary, Unit 5 records fluctuations in siliciclastic supply, back-stepping of a siliciclastic source from Unit 5a to 5b, and deposition of more reworked siliciclastic facies from Unit 5b to 5c.

Unit 6

Description

Unit 6 is ~ 38 m thick, and divided into five subunits (Fig. 3.2). The lowest division (Unit 6a) is ~ 20.4 m thick, consisting entirely of bioclastic limestone. A thin-section reveals ~ 3% quartz sand admixed within the upper 1 meter of this subunit. Lithofacies reflect a varied assemblage, in ascending order: greenish bioclastic wackestone (lithofacies L2a) with fragmented trilobites (Fig. 3.6A); peloidal packstone (lithofacies L3a); *Tetradium*-bearing packstone (lithofacies L3b) with fragments of *Tetradium* colonies, bivalves, and ostracodes (Fig. 3.6B); bioclastic wacke/packstone with fragmented trilobites, bryozoans, ostracodes, and brachiopods (lithofacies L2/L3); bryozoan-bivalve float/rudstone (lithofacies L5; Fig. 3.6C); and ooid-bearing pack/grainstone (lithofacies L4a). The latter facies contains abundant ooids with concentric layers and pellets (Fig. 3.4E). Fossils include fragmented bivalves, crinoid ossicles, and small shrub-like microbial buildups, probably *Hedstroemia*.

Unit 6b is ~ 6.6 m thick. It is composed mostly of greenish laminated silty dolomudstone with horizontal burrows (lithofacies D1; Fig. 3.6D). Two thin beds of calcareous arenite bound the dolostone interval at the top and bottom. Unit 6c consists of ~ 2.7 m of varied facies of limestone, in ascending order: crinoidal grainstone (lithofacies L4b) with bivalves, then the lithology becomes sandy lime mudstone.

Unit 6d is ~ 6.3 m thick, and consists of quartz arenite (lithofacies S1a). The dominant size of sand grains is 88-125 μm, and some larger (350-710 μm) grains are present. Quartz grains illustrate frosted texture. At depth of 36 feet, spheroidal concentrically laminated pyrite grains (350-500 μm in size) were noted. These likely represent differentially blackened (pyritic) grains that were probably originally ooids.

The uppermost division (Unit 6e) is ~ 2.4 m thick, and consists of bioclastic wacke/packstone and ooid-bearing grainstone (Fig. 3.6E). The uppermost lithofacies is a bioclastic packstone that includes abundant benthic skeletal material (lithofacies L3c; Fig. 3.4F): bryozoans, brachiopods, crinoid ossicles, ostracodes, gastropods, bivalves, and fragments of the cyanobacterium *Hedstroemia*. Less than 5% quartz sand grains are present. A large (up to 5 cm) 3-D burrow network is present (Fig. 3.6F).

Paleoenvironmental interpretation

Overall, the lithofacies succession of Unit 6 illustrates periodic or episodic changes in sea level driving lateral changes in position (relative to the core) of nearshore siliciclastics and offshore carbonates.

First, Unit 6a represents initial deposition in a transgressive shallow-marine environment illustrated by decreased amount of siliciclastic sediment moving upsection

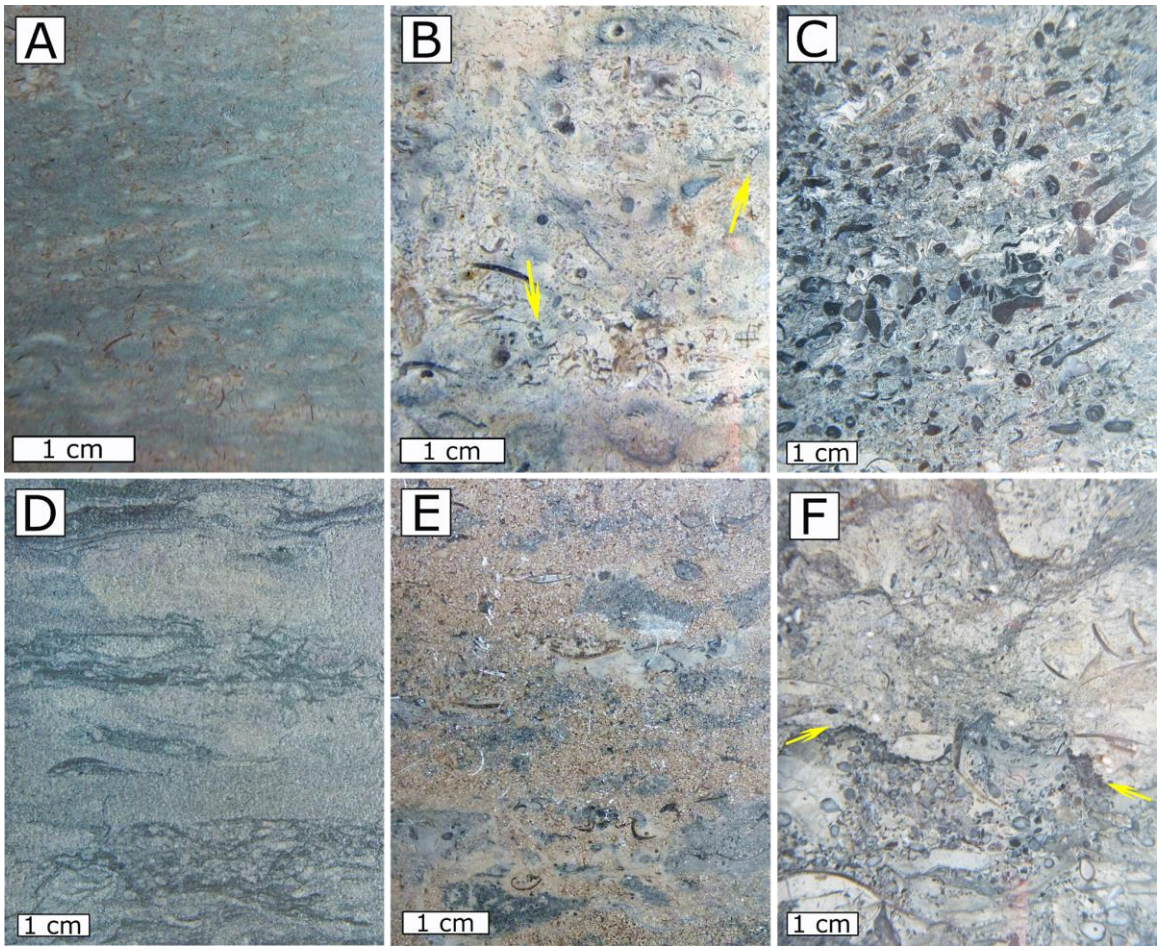

Figure 3.6. Photos of slabbed core samples of core 1-59, Unit 6. A) Greenish bioclastic wackestone at the bottom of Unit 6a. B) *Tetradium*-bearing packstone of Unit 6a; arrows indicate *Tetradium* fragments. C) Bryozoan floatstone Unit 6a. D) Greenish laminated sandy/silty dolomudstone of Unit 6b. E) Ooid-bearing grainstone of Unit 6e. F) 3-D burrows occurs in the bioclastic packstone of Unit 6e; arrows indicate hardground.

indicating back-stepping of a siliciclastic source. The upward transition into packstone with fragments of *Tetradium* may identify coral reworked into a shallow-water restricted environment with a low biota diversity and absence of crinoid ossicles. Moving upsection appearance of crinoid ossicles in the capping ooid-bearing pack/grainstone illustrates net shallowing and development of a high-energy shoals (Flügel, 2010). Overall this succession suggests a cycle of transgression, then stillstand with carbonate accumulation catching up to near sea level.

Further shallowing could result in accumulation of silty dolostone and arenite of subdivision 6b, a restricted environment in which there is greater input of siliciclastics. The low diversity and abundance of benthic biota, absence of crinoid ossicles, and appearance of dolomite may reflect precipitation under sabhka conditions (Flügel, 2010).

Unit 6c documents renewed transgression and establishment of a normal-marine lithofacies, crinoidal grainstone. Increased siliciclastic material in the upper part of subdivision 6c suggests initial stage of regression with appearance of siliciclastic fine-grained fraction. The transition from subdivision 6c into quartz arenite of subdivision 6d defines culmination of regression with well sorted sand. The frosted texture of sand grains likely suggests aeolian origin of quartz.

The uppermost division (Unit 6e) records renewed back-stepping of the siliciclastic source and return to carbonate production. The appearance of ooid-bearing grainstone indicates high-energy ooid shoals along the margins and extending into the interiors of carbonate platforms (Ball et al., 1967). Common presence of crinoid ossicles suggests the depositional environment is of normal salinity (Flügel, 2010). Ordovician cyanobacteria *Hedstroemia* is associated with both open and restricted marine facies

(Mamet et al., 1984; Liu et al., 2016). The presence of quartz sand in the bioclastic packstone suggests that the depositional environment is close to a ready siliciclastic source.

Summary of depositional environments

A summary of depositional environments is shown in Fig. 3.2. The entire sedimentary record of core 1-59 can be divided into two general divisions (Units 1-3 and Units 4-6) distinct in their facies associations. The lower three units are dominated by highly-laminated stratigraphy of mostly unfossiliferous (with the exception of burrows) deposits of sandstone, dolomitic sandstone, dolomudstone, siltstone, silty lime mudstone, and lime mudstone. These three units likely represent deposition in a nearshore environment with variation of siliciclastic input. Abundant soft sediment deformation structures, including dolostone breccia may indicate either high slope steepness or earthquake events.

Units 4 through 6 reflect thicker alternations of siliciclastic and fossiliferous carbonate rocks. Some of these alterations can be related to backstepping of siliciclastic input related to transgression and accumulation of carbonate sediment. Within the overall carbonate succession, there is evidence for greater circulation and normal salinity moving upsection. In general, Unit 6 documents net transgression with high-order sea level fluctuations. The whole preserved succession ends with a capping stenohaline, subtidal deposit.

3.3 Biostratigraphic indicators and age of sedimentary fill

Microfossils

Microfossils (conodonts and chitinozoans) were recovered and identified from core 1-59 by Grahn and Ormö (1995). Fragments of the chitinozoan *Conochitina schopfi* were recovered from a depth of ~ 245 m (Unit 1a), and better-preserved forms occurred in strata between ~ 93 and 80 m (here, Units 4c-5a). *Conochitina schopfi* (Taugourdeau, 1965) was originally described from the Upper Ordovician Simpson Group strata in Oklahoma, USA, where it occurs in the Pooleville Member, but absent in the overlying Corbin Ranch Member (Grahn and Ormö, 1995). According to Karim and Westrop (2002), the Pooleville Member lies within the lower half of equivalent Blackriveran strata, whereas the Corbin Ranch Member straddles the Black River-Trenton boundary.

Several conodont species were recovered by Grahn and Ormö (1995) in strata between ~ 20 and 70 m (here, Units 5a to 6a). They identify the uppermost part of the *Belodina compressa* conodont zone that brackets the Black River-Trenton boundary (Table 1.1).

Macrofossils

Cryptostomid bryozoan fragments in Unit 6e are identified as either *Stictopora labyrinthica labyrinthica* Hall or *Stictopora labyrinthica tabulata* Ross (Fig. 3.7A). These fossils are found in Lowville and Watertown formations of northern New York State (Ross, 1964). Fragments of calcareous worm tubes *Tymbochoos sinclairi* Okulitch (Fig. 3.7B) in Unit 6e are characteristic fauna of the Pamelia and Lowville formations of eastern Ontario (Salad Hersi, 1997; Steele-Petrovich and Bolton, 1998) and the Kingston

area (McFarlane, 1992). Dasycladacean algae (Fig. 3.7C) occur in Unit 6e whereas the cyanobacterium *Hedstroemia* (Fig. 3.7D) was observed in Unit 6a-6e. As mentioned in Chapter 2, despite long-ranging forms, occurrence of dasycladacean algae and cyanobacterium may be used for local regional correlation: the above forms occur in the Lowville/Upper Gull River and Watertown/Coboconk formations of Ontario, northern New York State, and southern Quebec (Walker, 1972; Guilbault and Mamet, 1976; El Gadi, 2001).

Summary

Combining microfossil and macrofossil assemblage information, the sedimentary succession of Brent Crater appears to be of Blackriveran age. The uppermost unit (Unit 6) represents an age similar to that of the Lowville-Watertown interval to the southeast. More discussion about correlation with extrabasinal stratigraphy is in Chapter 7.

3.4 Diagenesis

Only limited sampling of this small-diameter core was allowed resulting in few thin-sections and preclusion of a comprehensive analysis of diagenesis. The ~ 500 thin-sections mentioned by Lozej and Beals (1975), and presumably housed at University of Toronto, could not be traced. However, the following summarizes information associated with Unit 6 limestone and dolostone.

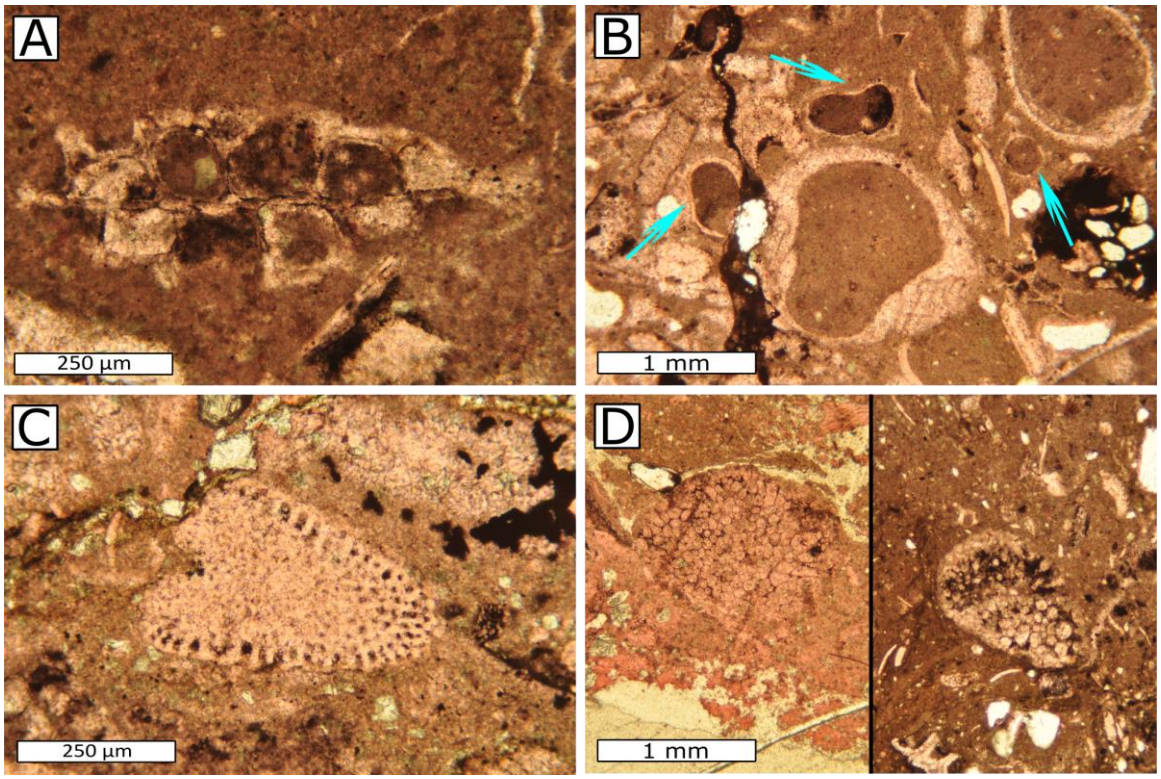

Figure 3.7. Thin-section photomicrograph of macrofossils in Unit 6 of Brent Crater sediment. All photos are taken under plane-polarized light of stained thin-sections. A) Bryozoan *Stictopora labyrinthica labyrinthica* Hall or *Stictopora labyrinthica tabulate* Ross. B) Fragments of calcareous worm tubes *Tymbochoos sinclairi* Okulitch. C) Fragment of dasycladacean algae. D) Photo pairing of fragments of cyanobacterium *Hedstroemia* aggregates.

3.4.1 Limestone

The ooid-bearing pack/grainstone (Unit 6a) contains micrite envelopes, syntaxial calcite cement, blocky calcite cement, and evidence of hardground development. A hardground surface separates the dolomite-free lithology and dolomitic lithology; along which clay accumulates (Fig. 3.6F; 3.8A).

3.4.2 Dolostone

Two types of planar-e dolomite are present in Brent Crater strata. Planar-e-1 dolomite is 20-150 μm in size and replaces calcite micrite in the bioclastic packstone of Unit 6e (Fig. 3.8A, B). Planar-e-2 dolomite is 10-60 μm in size and precipitates in the matrix of ooid-bearing pack/grainstone of Unit 6a. Some of the dolomite grains have black cores (Fig. 3.8C, D).

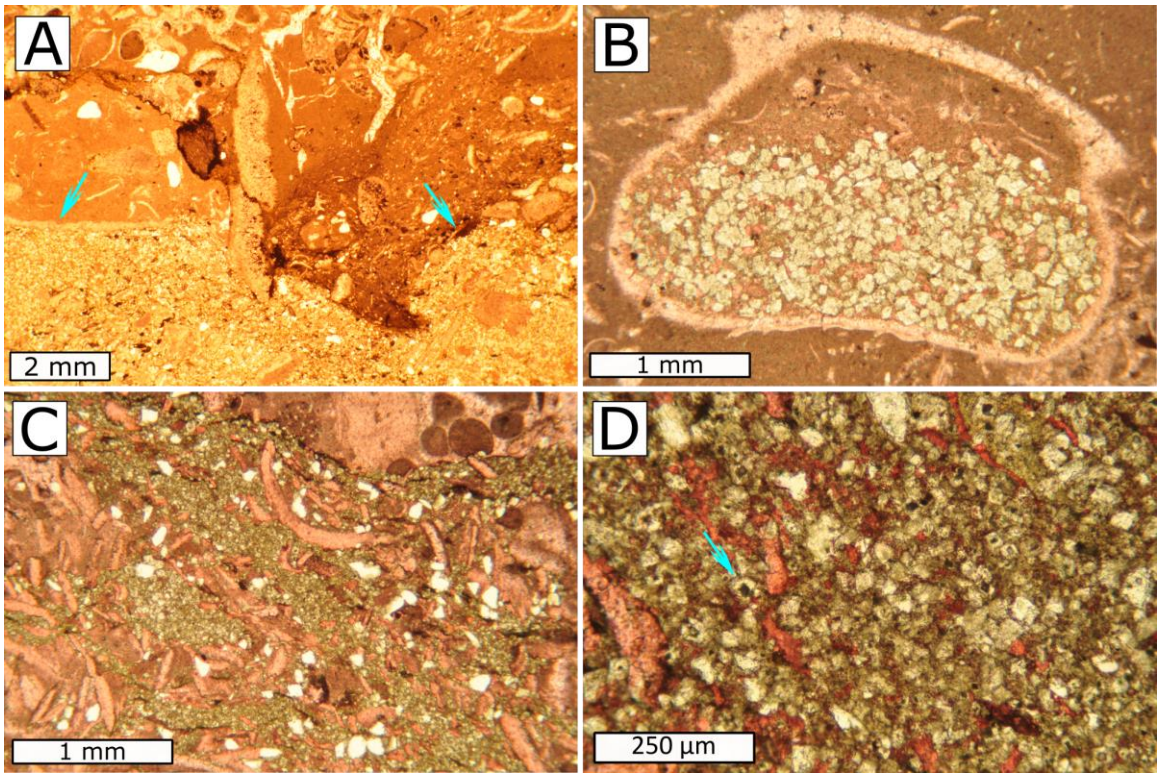

Figure 3.8. Thin-section photomicrograph of selective diagenetic features in Brent Crater sedimentary fill. All images are taken under plane-polarized light of stained thin-sections. A) Hardground (arrows) of Unit 6e; rock beneath hardground has been dolomitized severely. B) Dolomite rhombohedrals (white) precipitated in gastropod shell. C) Mosaics of dolomite precipitated in matrix of ooid-bearing pack/grainstone. D) Close-up view of photo “C” illustrating black core of some dolomite grains (arrow).

Chapter 4 Cedar Lake Outlier

4.1 Introduction

The Cedar Lake outlier (46° 01.405' N, 78° 29.247' W; Fig. 3.1A) is a small and thin sedimentary succession outcropping along the north margin of Cedar Lake (adjacent to the canoe put-in point near the Brent village) in Algonquin Park, Ontario. The outlier occurs ~ 5.7 km south of the center of Brent Crater. Two exposures occur within a distance of ~ 30 meters. The outlier is geographically bounded by gneisses of Mesoproterozoic age (Ontario Geological Survey, 2011), and is overlain by glacial-derived sediment, including boulder-size erratics.

4.2 Lithostratigraphy and facies

4.2.1 Locality A

A 2.9-meter-thick section was measured and subdivided on the basis of lithology, fossil content, and sedimentary structures (Fig. 4.1; Fig. 4.2A). The lower 60 cm (Unit 1) consist of feldspathic wacke and arenite. The middle interval (Unit 2) is 115 cm thick, composed of interbedded bioclastic sandy dolowacke/packstone and silty dolomudstone. The upper 115 cm (Unit 3) consist of dolomudstone. The following summarizes lithofacies types, their associations, and fossil content associated with each unit; and interpreted depositional environments. Details are summarized in Table 4.1.

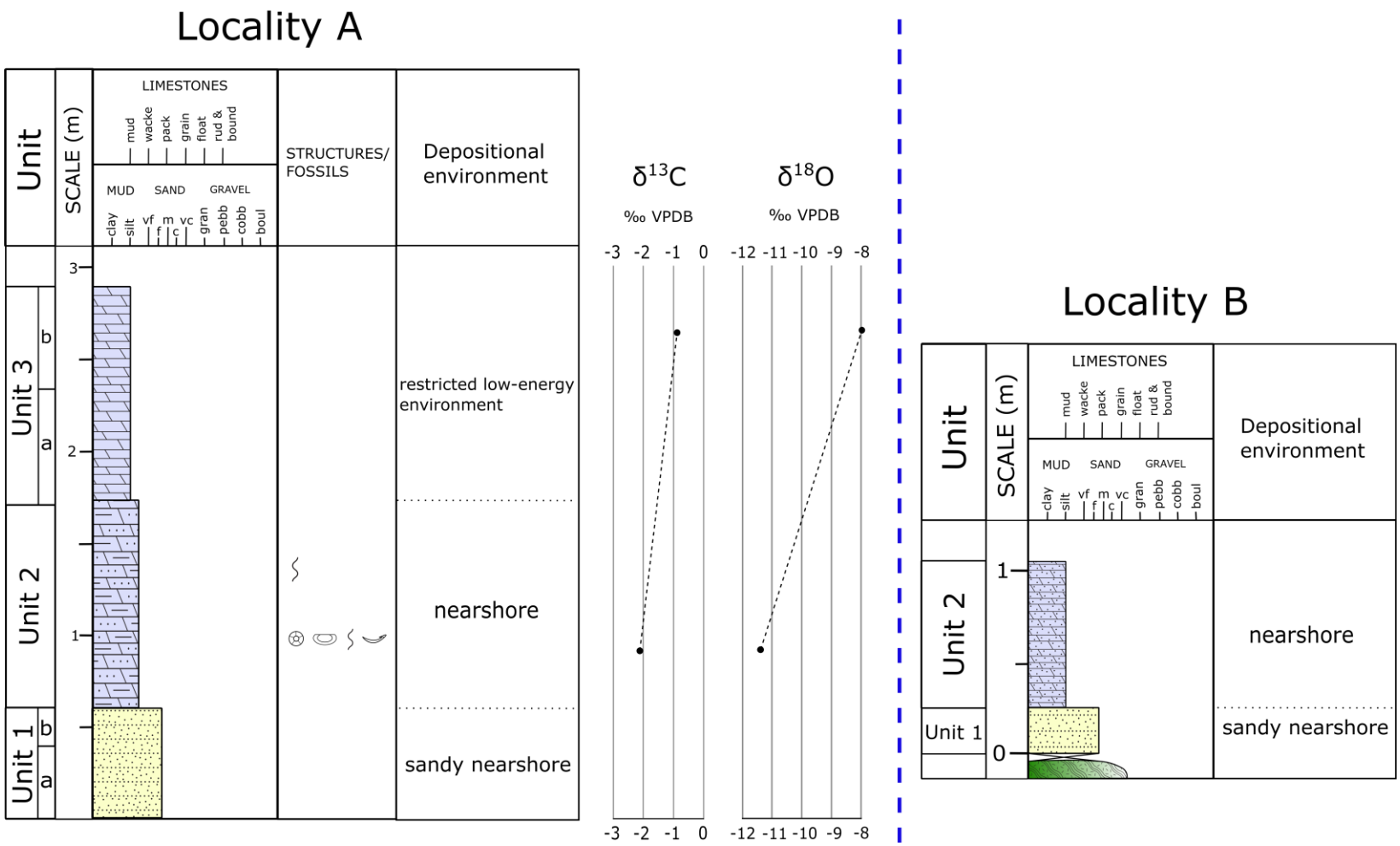

Figure 4.1. Stratigraphic attributes of the two sedimentary exposures of Cedar Lake outlier. Legend is in Fig. 2.2.

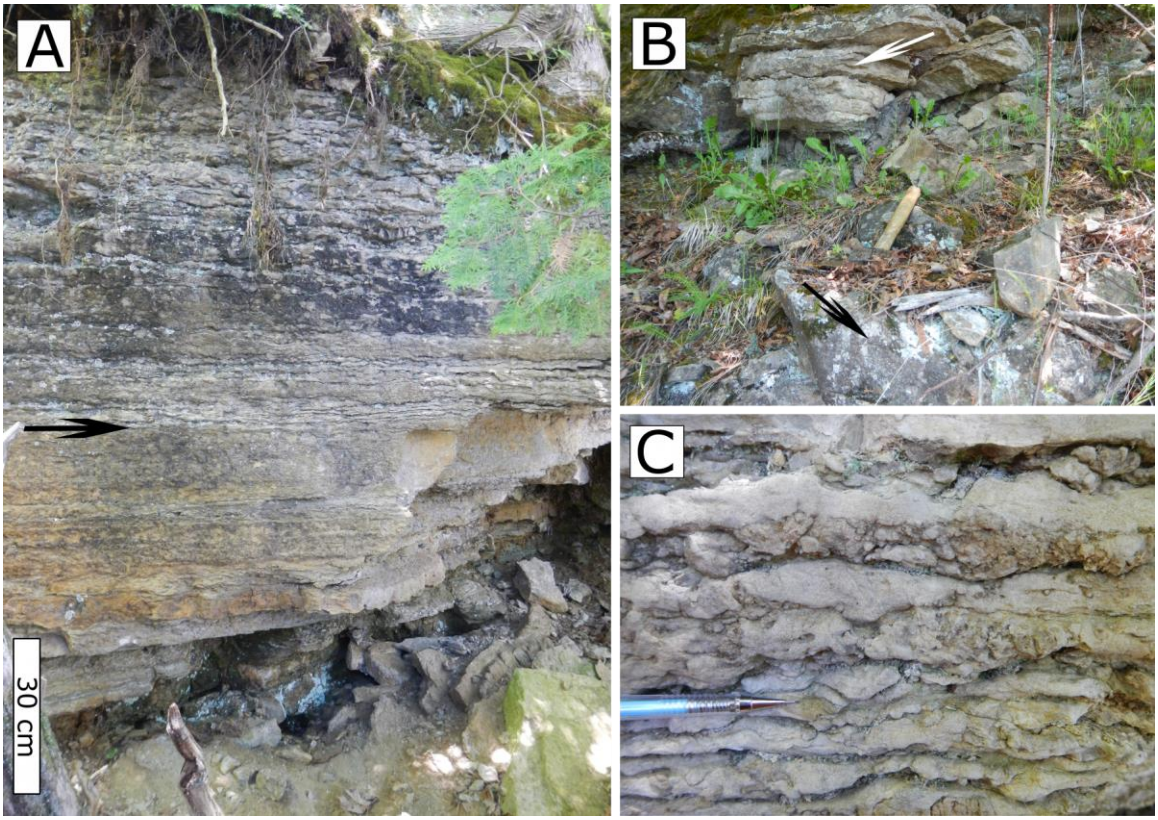

Figure 4.2. Field photo of the Cedar Lake outlier (Locality A). A) Lower and middle part of the succession; arrow indicates the contact between Units 1 and 2 strata. B) Sandstone (white arrow) of Unit 1 above Precambrian basement (black arrow); the contact is not exposed; hammer for scale is about 20 cm long. C) Interbedded bioclastic sandy dolowacke/packstone and silty dolomudstone of Unit 2; pencil for scale.

Litho-facies	lithology	Sedimentary features	Fossils and other textural attributes	Depositional environment	References
D1a	dolomudstone	thin- to medium-bedded, rare claystone	Rock is composed of 20-80 μm, planar dolomite fabrics	sabkha-type environment?	1
D1b	sandy dolomudstone		~ 20% of quartz and feldspar sands, angular to subrounded, and 80-1000 μm in size; dolomite crystals are 20-40 μm in size	close to source of siliciclastics	2
D2	interbedded sandy dolowacke/packstone and silty dolostone	burrows	ostracodes, crinoid ossicles, bivalves, trilobites (?), bryozoans (?)	abrupt fluctuations in depositional energy and habit, unknown salinity	
S1	greenish yellow feldspathic wacke		angular to subrounded, 80-550 μm sands; abundant clay minerals; dolomite in void space	deposition proximal to a source area	3
S2	feldspathic arenite		bimodal grain size: 1) 240-1200 μm and 2) 80-150 μm, but of similar roundness (angular to subrounded)	moderate grain segregation at source, during transport, or during deposition	3

Table 4.1. Summary of lithofacies types in Cedar Lake outlier. References: 1, Flügel, 2010; 2, Goldhammer, 2003; 3, Selley, 2000.

Unit 1

Description

Unit 1 is 60 cm thick, and divided into two successive lithofacies associations (1a-1b; Fig. 4.1). The lower 40 cm (Unit 1a) consist of a greenish yellow feldspathic wacke (lithofacies S1). Although contact with the underlying Precambrian basement is not exposed, basement rock outcrops adjacent to the section (Fig. 4.2B). Standard microscopy shows that sand grains are 80-550 μm in size, angular to subrounded, and there is an abundance of detrital clay minerals as matrix. Dolomite forms intergranular cement (Fig. 4.3A). Unit 1b is composed of thinly-laminated feldspathic arenite with dolomite cement. Sand grains are subangular to rounded.

Paleoenvironmental interpretation

Unit 1a represents a chemically and mechanically immature sedimentary rock, likely indicating either rapid accumulation of sediment with little segregation of clay and framework grains or incomplete weathering suggesting little to no transport. This is often associated with deposition or weathered residua proximal to or within a source area where little segregation of sediment sizes has occurred (Selley, 2000). Either possibility suggests that the Precambrian basement lies very close to the base of the outcrop exposure. Unit 1b is more mechanically mature (i.e., more reworked) than Unit 1a, suggesting either grain segregation at source, during transport, or during deposition.

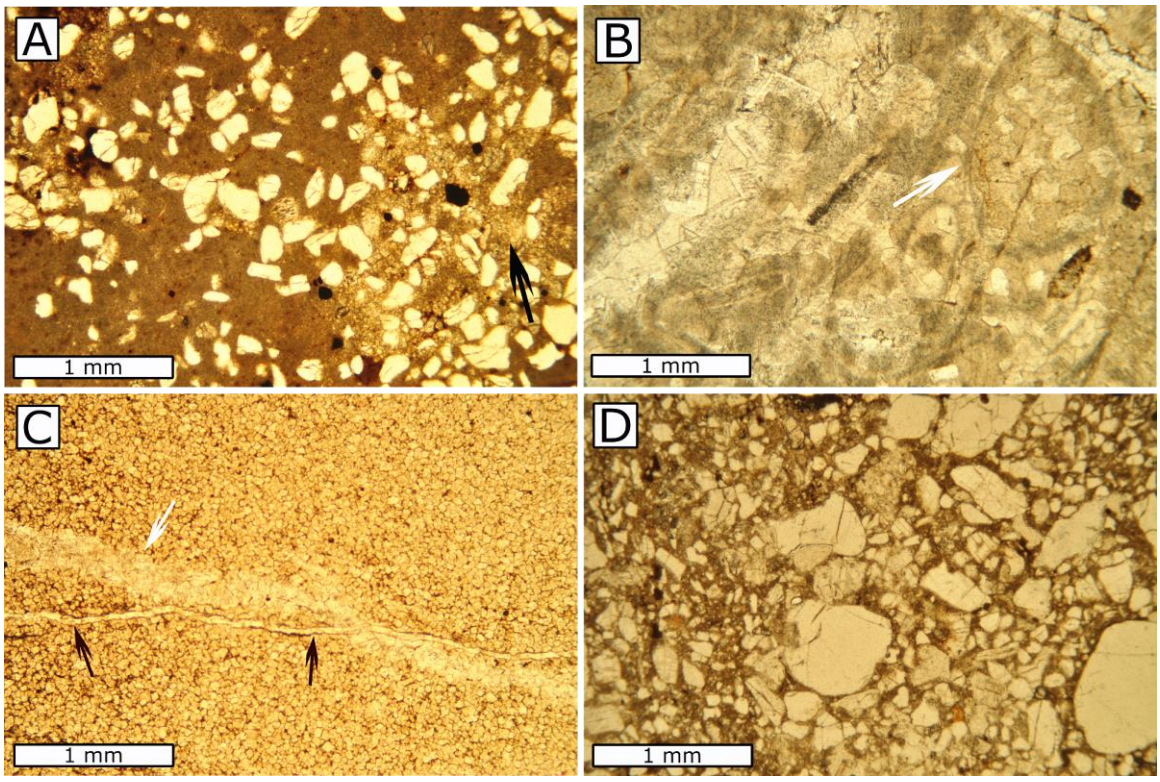

Figure 4.3. Thin-section photomicrograph of Cedar Lake outlier rocks. All photos are taken under plane-polarized light. A) Feldspathic wacke of Unit 1 at Loc. A; arrow indicates dolomite cement. B) Bioclastic dolowackstone of Unit 2 at Loc. A, arrow indicates an ostracode shell. C) Dolomudstone of Unit 3 at Loc. A is composed of fine-grained planar-s dolomite; fracture (white arrow) filled with coarse-grained nonplanar dolomite; vein dolomite is cross-cut by a later-stage thin fracture that is filled with calcite (black arrows). D) Feldspathic arenite of Unit 1 at Loc. B shows bimodal sand grain size.

Unit 2

Description

Unit 2 is 115 cm thick, and consists of interbedded bioclastic sandy dolowacke/packstone and silty burrowed dolomudstone (lithofacies D2; Fig. 4.2C). The thickness of beds varies between 3 and 20 cm. Two dolowacke/packstone samples from the lower part of Unit 2 shows that dolostone contains < 5% of sand grains (80-400 μm). Fossil preservation is poor due to dolomitization, but there are outlines of ostracodes and bivalves shells, crinoid ossicles, and possibly fragments of trilobites and bryozoans (Fig. 4.3B). Two types of dolomite are present: fine- to coarse-grained (sand size) crystalline dolomite and a strongly-burrowed silt-size crystalline dolomite.

Paleoenvironmental interpretation

The high-order alternating lithostratigraphy defined by grain size (sand vs silt) of siliciclastics, and the presence/absence of skeletal material suggest a record of abrupt fluctuations in depositional energy and habitat. Due to pervasive replacement dolomitization, it remains uncertain if the skeletal material was transported or represents *in situ* accumulation. Bioturbated silty dolomudstone illustrates a likely relative abundance of organic material within an otherwise low-energy environment.

Unit 3

Description

Unit 3 is 115 cm thick and composed of thin- to medium-bedded dolomudstone (lithofacies D1a). Dolostone in the lower 80 cm of this unit has wavy bedding planes and

beds with varying thickness (1-5 cm). Dolostone in the upper 45 cm is medium-bedded. Rare claystone layers are in the lower part of Unit 3. Standard microscopy of dolomudstone at 2.6 m shows that it is free of siliciclastic and skeletal material, and contains a fine-grained crystalline fabric (Fig. 4.3C).

Paleoenvironmental interpretation

Absence of siliciclastic material upsection suggests that accumulation of Unit 3 coincided with step-back or bypassing of a siliciclastic source. The fine-grained nature of this dolostone and absence of skeletal material may suggest a primary origin of dolomitization in an environmentally stressful hypersaline environment (Flügel, 2010). Rare thin beds of claystone near the base of the unit identify siliciclastic input, but of only the finest size fraction. Thus, Unit 3 may identify a sabhka-type environment wherein the clay-size material may represent aeolian deposits.

4.2.2 Locality B

Locality B is ~ 30 m away from Loc. A, and exposes a 1.05-m-thick section (Fig. 4.1). The unit divisions (1-3) of Loc. A are applied here, although there are slight variations in contained facies. At Loc. B, only the lower two units are exposed: the lower 35 cm (Unit 1) consists of feldspathic arenite, whereas the remaining 70 cm (Unit 2) consist of sandy dolomudstone. The following summarizes lithofacies types, their associations, and fossil content associated with each unit; and interpreted depositional environments. Details are summarized in Table 4.1.

Unit 1

Description

The lithology of Unit 1 is similar to Unit 1b at Loc. A. Microscopy shows that grain size of the feldspathic arenite (lithofacies S2) is bimodal: 1) 240-1200 μm; and 2) 80-150 μm (Fig. 4.3D). Grains of different sizes have similar roundness: angular to subrounded. The matrix is composed of clay mineral.

Paleoenvironmental interpretation

A bimodal grain size, including an abundance of angular clasts, suggests only moderate grain segregation at source, during transport, or during deposition; or mixing of two sediment sources. Grain size alone cannot define a specific depositional environment.

Unit 2

Description

Unit 2 is 70 cm thick and contains sandy dolomudstone (lithofacies D1b). Dolomite crystals have a fine (silt-size) crystalline texture. Sand grains make up ~ 20% of the whole rock, and are quartz and feldspar, angular to subrounded, and 80-1000 μm in size.

Paleoenvironmental interpretation

Unit 2 represents deposition in a nearshore carbonate environment proximal to a ready siliciclastic source.

4.2.3 Summary of depositional environments

Summary of depositional environments is shown in Fig. 4.1. Although the contact between basal sandstone of the outlier and Precambrian basement is not exposed at either locality, the lateral and vertical distribution of exposed sedimentary and underlying metamorphic rocks suggests that the base of Unit 1a at Loc. A is likely within 10-20 cm to the Precambrian basement. The outlier sections record net transgression of a restricted carbonate (dolomitic) environment across an initial terrigenous setting. Sandstone of Unit 1a (Loc. A) represents the most chemically and mechanically immature facies representing weathered residua locally overlying the Precambrian surfaces. Appearance of siliciclastic-bearing, then relatively pure dolostone (from Units 2 to 3) reveals decreased siliciclastic influence. Given this stratigraphic succession, the presence of fragmented crinoid ossicles in Unit 2, but their absence in Unit 3 may indicate an initial deeper facies registering more open circulation followed by shallowing yielding a muddy restricted subtidal flat.

4.3 Diagenesis

4.3.1 Petrography

Two types of dolomite fabrics are preserved in the Cedar Lake outlier. First, planar-s dolomite forms fine-grained (20-80 μm) fabric that dominates Unit 3 of Loc. A and Unit 2 of Loc. B. Second, at Loc. A, crystalline mosaics of fine- to coarse-grained (80-800 μm) crystalline nonplanar dolomite not only fills intergranular void space in feldspathic wacke of Unit 1, but also replaces limestone of Unit 2, and precipitates in fractures of Unit 3 (Fig. 4.3C). This suggests that planar-s dolomite in Unit 3 (Loc. A)

and Unit 2 (Loc. B) predates development of nonplanar dolomite at Loc. A if fracture-fill nonplanar dolomite is the same generation as nonplanar dolomite in Unit 2 (Loc. A). Or, there were two stages of nonplanar dolomitization at Loc. A. Vein dolomite of Unit 3 (Loc. A) is cross-cut by a thin (40 μm) vein calcite (Fig. 4.3C).

4.3.2 Geochemistry

Dolomites and fracture-fill calcite of Unit 3 (Loc. A) were analyzed (Table 4.2). There is no significant compositional difference between the planar-s and nonplanar dolomites with respect to major and minor elements (Table 4.2). Their common compositional ranges are near stoichiometric: $Ca_{51\text{-}52}Mg_{45\text{-}46}Fe_{02\text{-}03}Mn_{00\text{-}01}$.

A limited C and O isotope dataset of planar-s and nonplanar dolomites is available for Loc. A (Fig. 4.1). There is an apparent upsection increase (1.2‰) in $\delta^{13}C$ values from nonplanar to planar-s dolomite through the 1.7 m interval from Unit 2 to Unit 3. The $\delta^{18}O$ values are strongly negative relative to estimated values (-3 to -1‰) for dolomite if co-precipitated with Turinian marine brachiopod shells (-4‰ to -6‰ VPDB; Qing and Veizer, 1994; Shield et al., 2003) based on ~ 3‰ enrichment relative to marine calcite (Tucker and Wright, 2008; James and Jones, 2016). Such negative $\delta^{18}O$ values require a diagenetic fluid depleted in $\delta^{18}O$ relative to a normal shallow-water marine source, either of meteoric origin or elevated temperature. The former is likely given that planar-s dolomite crystals are very fine-grained and have subhedral fabric that are not typical of precipitation at elevated temperature (Mazzullo, 1992). Further information about origin of dolomite, and its relationship to dolostone in other outliers, is presented in the Discussion chapter.

Features	$CaCO_3$	$MgCO_3$	$FeCO_3$	$MnCO_3$	$BaCO_3$	$SrCO_3$
Planar-s dolomite	51.56%	44.90%	3.02%	0.46%	0.01%	n.d.*
Planar-s dolomite	51.26%	46.23%	2.10%	0.40%	0.01%	n.d.
Nonplanar dolomite (vein)	50.87%	45.50%	3.10%	0.52%	n.d.	n.d.
Nonplanar dolomite (vein)	51.44%	45.79%	2.34%	0.37%	0.02%	n.d.
Vein calcite	96.83%	1.53%	0.61%	1.01%	n.d.	n.d.
Vein calcite	96.93%	1.49%	0.64%	0.92%	0.01%	n.d.

* n.d. = not detected

Table 4.2. Major and minor elemental composition of calcite and dolomite in Cedar Lake outlier. Values are illustrated in molecular percentage.

Chapter 5 Manitou Islands

5.1 Local and general geology

The Manitou Islands are located in Lake Nipissing, Ontario, about 10 km offshore to the southwest of North Bay city (Fig. 1.1). Five islands are arranged in a concentric pattern. Lumbers (1971) provided the most recent and detailed information of the islands' geology (Fig. 5.1). The islands' orientation reflects distribution along a rim of a circular intrusive basement structure (Rowe, 1954; Lumbers, 1971), part of a series of syenitic intrusions in the region dated at 580-570 Ma (Bleeker et al., 2011). A low terraced island morphology is associated with islands underlain by remnants of Paleozoic strata capped by Quaternary glacial-derived sediment (Lumbers, 1971). Great and Little Manitou Islands offer the most extensive and best exposed stratigraphic sections (Fig. 5.1).

5.2 Lithostratigraphy and facies

5.2.1 Great Manitou Island

Introduction

Exposure of sedimentary rocks on Great Manitou Island occurs along the southwest margin of the island (Fig. 5.1) at 46° 16.337' N 79° 35.03' W. It is well hidden by trees, stepped back from the shoreline, and forms a low escarpment extending roughly parallel to the shoreline. Sedimentary rocks lie nonconformably on crystalline basement rocks that consist of altered Grenville hornblende gneiss and alkaline intrusive rocks. A composite section of 11.4 meters is exposed.

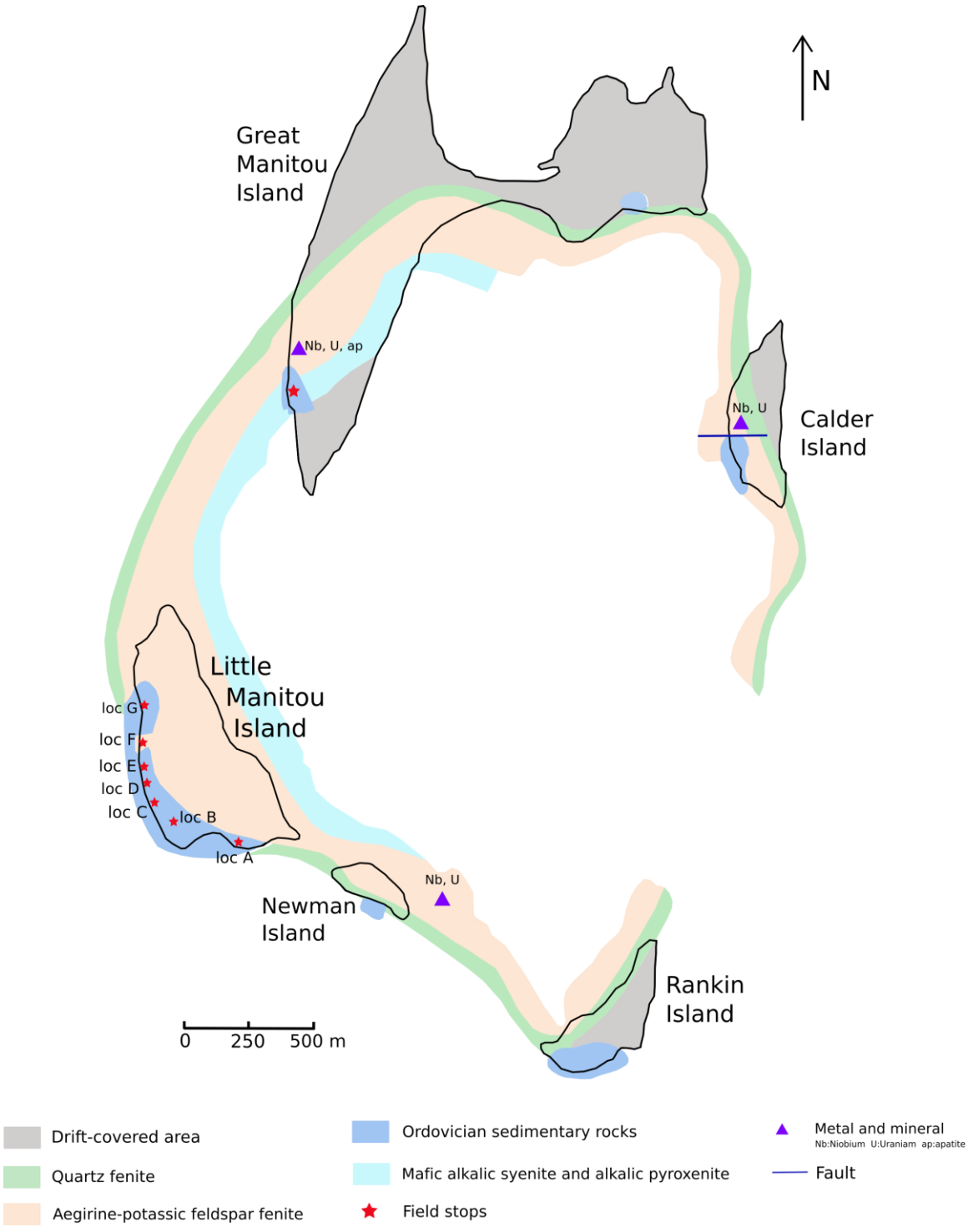

Figure 5.1. Location of outcrops studied on Manitou Islands. Map modified after Lumbers (1971).

The section is subdivided on the basis of lithology, fossil content, and sedimentary structures (Fig. 5.2). The lower 3.9 meters (Units 1-2) consist of siliciclastic breccia and pebbly dolostone, each with abundant fragments of basement rock. The upper 7.5 meters (Units 3-5) contain carbonate rocks including crystalline dolostone, bioclastic dolopackstone, lime mudstone, and bioclastic packstone. The following summarizes lithofacies types, their associations, and fossil content associated with each unit; and interpreted depositional environments. Details are summarized in Table 5.1.

Unit 1

Description

Unit 1 is 1.9 meters thick, and is divided into two successive coarse-grained lithofacies associations (1a and 1b, Fig. 5.2). There is an upsection decrease in basement-derived clasts abundance and size.

The lower 1.2 meters (Unit 1a) consist of framework-supported monomictic breccia with sandstone matrix (lithofacies C1). The breccia nonconformably overlies basement rocks, with syenite boulders up to 1 meter in diameter (Fig. 5.3A). The matrix of the breccia is a local bivalve-bearing quartz arenite with dolomite cement. Sand and silt grains are mostly quartz (< 2% microcline), and bimodal in size: 150-650 μm subangular to rounded sand; and 40-100 μm angular to subangular silt and sand. Whole shells of bivalves are rare to abundant, mostly 2-3 cm in size (Fig. 5.4A). Most bivalves have horizontal orientation, but some are oriented sub-vertically within the arenite matrix. Fragments of cryptostomid bryozoans are present, and are up to 2 mm in length. In the upper part of Unit 1a, clasts size has decreased to 10-30 cm.

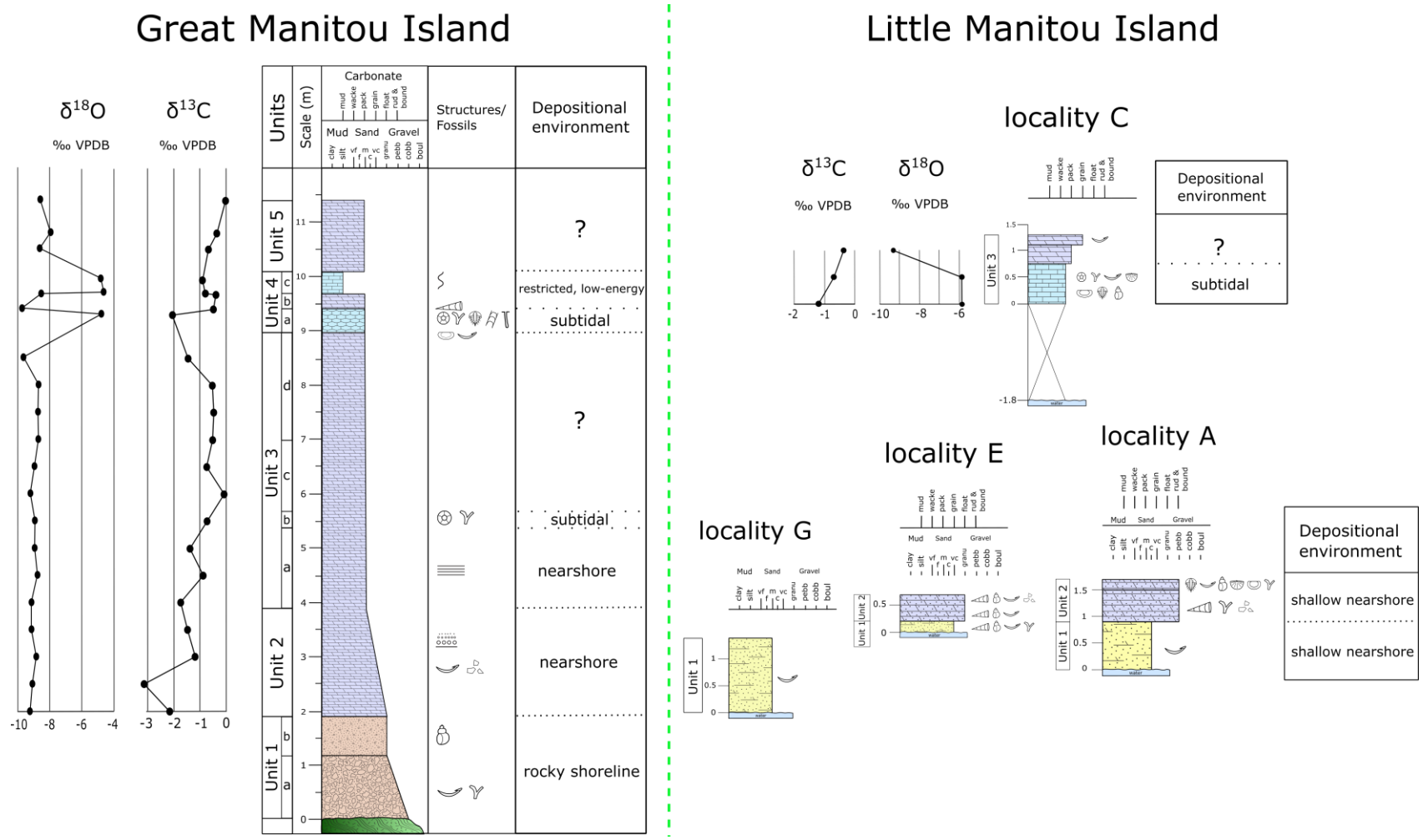

Figure 5.2. Stratigraphic attributes of the Great and Little Manitou islands sedimentary rocks. Legend is in Fig. 2.2.

Lithofacies types	lithology	Sedimentary features	Fossils and other textural attributes	Depositional environment	References
L1	lime mudstone	horizontal burrows	no skeletal material observed	low-energy fairweather conditions	1
L2	interlayered bioclastic packstone and lime mudstone with thin shale layers	medium-bedded hardground	crinoid ossicles, bryozoans, bivalves, brachiopod, ostracodes, calcareous algae *Vermiperolla*, and trilobites. Vertical and sub-vertical burrows	shallow, warm-water normal-marine, subtidal environment; varying water energy; changing patterns of riverine/storm influence from shore	1, 2, 3, 4
D2a	bioclastic dolopackstone 1		crinoid ossicles, bryozoans; syenite lithoclasts (up to 2 mm); nonplanar dolomite, 400-4000 μm	normal-marine, near a siliciclastic source	4
D2b	bioclastic dolopackstone 2		bryozoans, trilobites, < 1% lithoclasts	non-stenohaline, near a siliciclastic source	4, 5
D4	crystalline dolostone		planar-s to nonplanar texture, 400-1500 μm in size	not sure	
D5a	pebbly dolostone	normal grading	whole shells of bivalves	nearshore, close to source of siliciclastic input; waning energy, non-stenohaline	4, 5, 6
D5b	lilthoclastic bioclastic dolofloat/rudstone		orthocones, bivalves, and gastropods, trilobite bryozoans, none to rare (< 2%) crinoid ossicles; syenite clasts	nearshore, non-stenohaline environment with influence of siliciclastic source	4, 5
C1	framework-supported monomictic breccia with sandstone matrix	massive	framework: syenite up to 1 meter in size; matrix: quartz arenite with dolomite cement, bivalves and bryozoans	a mixture of regolith, alluvial, or deltaic deposits reworked in the nearshore-supratidal environment	7
C2	matrix-supported monomictic conglomerate with dolostone matrix	lamination	framework: 0.4-2 cm syenite and gastropod shells; matrix: nonplanar dolomite	a mixture of regolith, alluvial, or deltaic deposits reworked in the nearshore-supratidal environment	7
S1	bioclastic feldspathic arenite	thin-bedded	250-1600 μm subrounded to rounded sand, and 40-100 μm angular to subrounded silt and sand. Bivalves, orthocones, gastropods, and bryozoans.	undergone more than 1 cycles of weathering, erosion, transportation, and deposition. Deposited probably in a shallow nearshore environment	8

Table 5.1. Summary of lithofacies types on Great and Little Manitou Islands. References: 1, MacEachern et al., 2010; 2, Aguirre and Riding, 2005; 3, Mamet et al., 1984; 4, Flügel, 2010; 5, Goldhammer, 2003; 6, Boggs, 2011; 7, Melchin et al., 1994; 8, Selley, 2000.

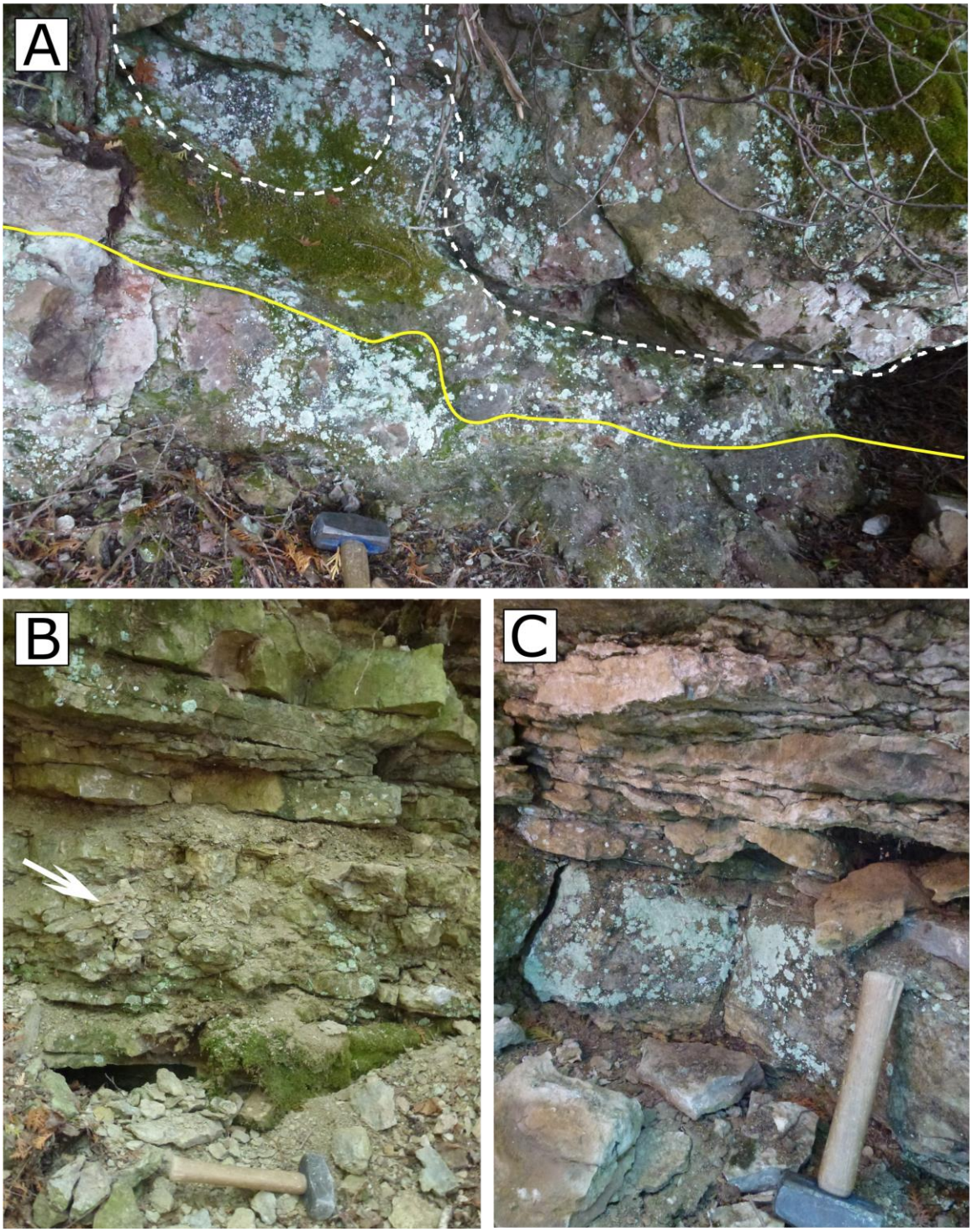

Figure 5.3. Field photos of the Great Manitou Island. A) the nonconformity boundary (solid line) between basement rock and Unit 1a of sedimentary succession; dashed lines illustrate boulders within Unit 1a. B) Unit 4a, nodular bioclastic packstone (arrow). C) Thin- to medium-bedded crystalline dolostone (Unit 5). The hammer for scale is 25 cm long.

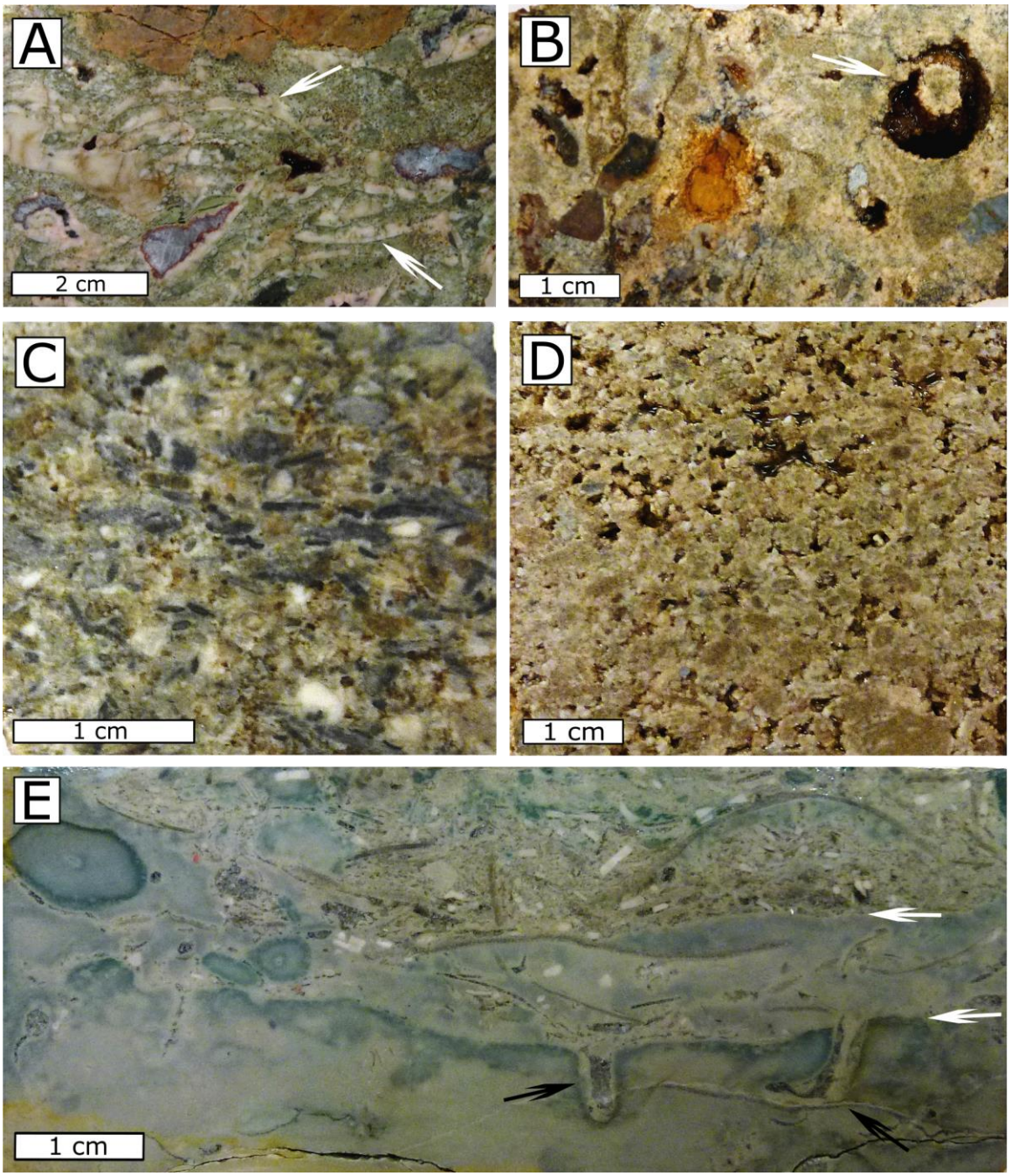

Figure 5.4. Slabbed rock sample of representative lithofacies on Great Manitou Island. A) Matrix of breccia of Unit 1a, arrows indicate bivalve shells. B) Conglomerate of Unit 1b, arrow indicates dissolved gastropod mold. C) Bioclastic dolopackstone of Unit 3b with fragments of bryozoans (platy, dark grey) and crinoids (white). D) Porous crystalline dolostone of Unit 3d, replaced primary grains are darker than the cement. E) Interlayered bioclastic pack/mudstone of Unit 4a; white arrows indicate 2 stages of hardground; black arrows indicate vertical/subvertical burrows.

Unit 1b consists of 70 cm of matrix-supported monomictic conglomerate with dolostone matrix (lithofacies C2). Basement clasts are sub-rounded to rounded, and 0.5-2 cm in size. The dolostone contains 3-15% quartz sand grains that exhibit a moderate sorting, and are 150-800 μm in size, fine- to coarse-sand texture. The sand grains are subrounded to rounded. Consistent orientation of long axis of clasts produces weak lamination. Whole shells of gastropods are present (Fig. 5.4B).

Paleoenvironmental interpretation

Fossil-bearing (gastropods, bivalves, and bryozoans) quartz sands forming matrix of breccia and conglomerate define a high-energy "rocky shoreline" setting, documenting marine transgression across crystalline basement. The compaction of whole shells of gastropods and bivalves and few obliquely oriented bivalves likely indicate rapid deposition, the latter possibly defining life-position fossil remains. The quartz arenite demonstrates an overall strong reworking by waves or currents in this setting.

Similar basal breccia/conglomerate facies overlying basement rocks have been noted in Turinian strata in the Lake Simcoe area (Melchin et al., 1994) and Manitoulin Island area (Brunton et al., 2009), and are also interpreted to have been deposited in a nearshore environment. In these regions, significant contrast in lithology, size, and shape of bedrock-lithology gravels and quartz/feldspar sands suggests a mixture of regolith, alluvial, or deltaic deposits reworked in the nearshore zone (Melchin et al., 1994). On the Manitou Islands, however, the quartz arenite reveals considerable mechanical maturity as a matrix suggesting greater extent of reworking during transgression. The predominant syenite composition of lithoclasts defines local derivation. Thus, a decrease in grain size

upsection coincident with the notable increase in roundness of syenite clasts from Units 1a to 1b suggests progressive burial of an initial irregular paleotopography, and increased transport from a more distal source in the area.

Unit 2

Description

Unit 2 is composed of 2 meters of pebbly dolostone (lithofacies D5a). The gradual boundary of Unit 2 with Unit 1 is defined to be at a level where the amount and size of lithoclasts decrease significantly. Pebbly dolostone beds display normal grading: clasts size decreases from 5 cm to 1 cm over some ~ 20 cm intervals. Whole shells of bivalves occur, with size up to 3 cm.

Paleoenvironmental interpretation

An abundance of granule to pebble size lithoclasts suggests that the depositional environment is still close to a basement source undergoing erosion. Repeated normal grading might indicate successive depositional events of waning energy (Boggs, 2011), or repeated transgressions that backstep the pebble source (Goldhammer, 2003). As the host sediment is dolostone, the latter explanation may serve better. The depositional environment is still likely nearshore and absence of crinoids likely illustrates that depositional environment doesn't have a normal-marine salinity (Flügel, 2010).

Unit 3

Description

Unit 3 is 5.05 meters thick, and divided into four successive lithofacies associations (Fig. 5.2). This unit contains interbedded crystalline dolostone and bioclastic dolopackstone. The first (lower) division, Unit 3a, consists of 1.4 meters of crystalline dolostone (lithofacies D4). Unit 3b is composed of 45 cm of bioclastic dolopackstone (lithofacies D2a). It contains very abundant fragmented benthic skeletal fossils, including crinoid ossicles and bryozoans, but replaced by dolomite (Fig. 5.4C). Dolomite crystals are medium to very coarse sand size. Syenite lithoclasts (< 3%) are up to 2 mm in size, angular in shape. Unit 3c, is 1 meter thick, and contains finely to medially crystalline dolomite. The uppermost subdivision of Unit 3 (Unit 3d) is 2 meters thick, and contains porous crystalline dolomite (Fig. 5.4D). Unit 3d is generally medium-bedded, except for one 80 cm-thick bed. There are very few (< 1%) lithoclasts in Unit 3d. Relic grain shapes are preserved despite dolomite replacement; these are large (0.8-3 mm) circular to elliptical bodies, and replaced by fine- to medium-grained dolomite crystals. Dolomite crystals between these bodies are medium- to coarse-sand in size.

Paleoenvironmental interpretation

Replacive dolomitization makes it difficult to interpret the depositional environment. Presence of sand-size basement lithoclasts suggests that the environment remains close to a ready basement source. The common presence of crinoid ossicles in Unit 3b suggests eventual development of a normal-marine subtidal setting (Flügel, 2010)

if they were not transported significantly. Dolomitization represented by Units 3c and 3b does not allow accurate assessment of primary facies.

Unit 4

Description

Unit 4 is 1.17 meters thick, and contains interbedded bioclastic packstone and lime mudstone, dolopackstone, and lime mudstone. Unit 4a is 42 cm thick, and consists of medium-bedded interlayered bioclastic packstone and lime mudstone with thin shale layers (lithofacies L2; Fig. 5.3B). The packstone contains abundant fragmented benthic skeletal material, including crinoid ossicles, bryozoans, bivalves, calcareous algae *Vermiperolla*, and trilobites. One sample collected shows vertical and sub-vertical burrows associated with a hardground (Fig. 5.4E). At the top of Unit 4a is a 2 cm-thick claystone bed. XRD analysis (Fig. 5.5) shows that the principal minerals are calcite, quartz, orthoclase, muscovite, rectorite, smectite-mica or smectite-illite, chlorite, and kaolinite.

Unit 4b consists of 30 cm of finely to coarsely crystalline bioclastic dolopackstone (lithofacies D2b). It contains abundant mm-scale fragmented benthic skeletal material, including bryozoans and trilobites. Less than 1% of the rock consists of basement-derived clasts. Unit 4c is 45 cm thick, and consists of thin-bedded burrowed lime mudstone (lithofacies L1). Burrows are horizontally-oriented, and 2 mm to 1 cm in size. No skeletal material is found.

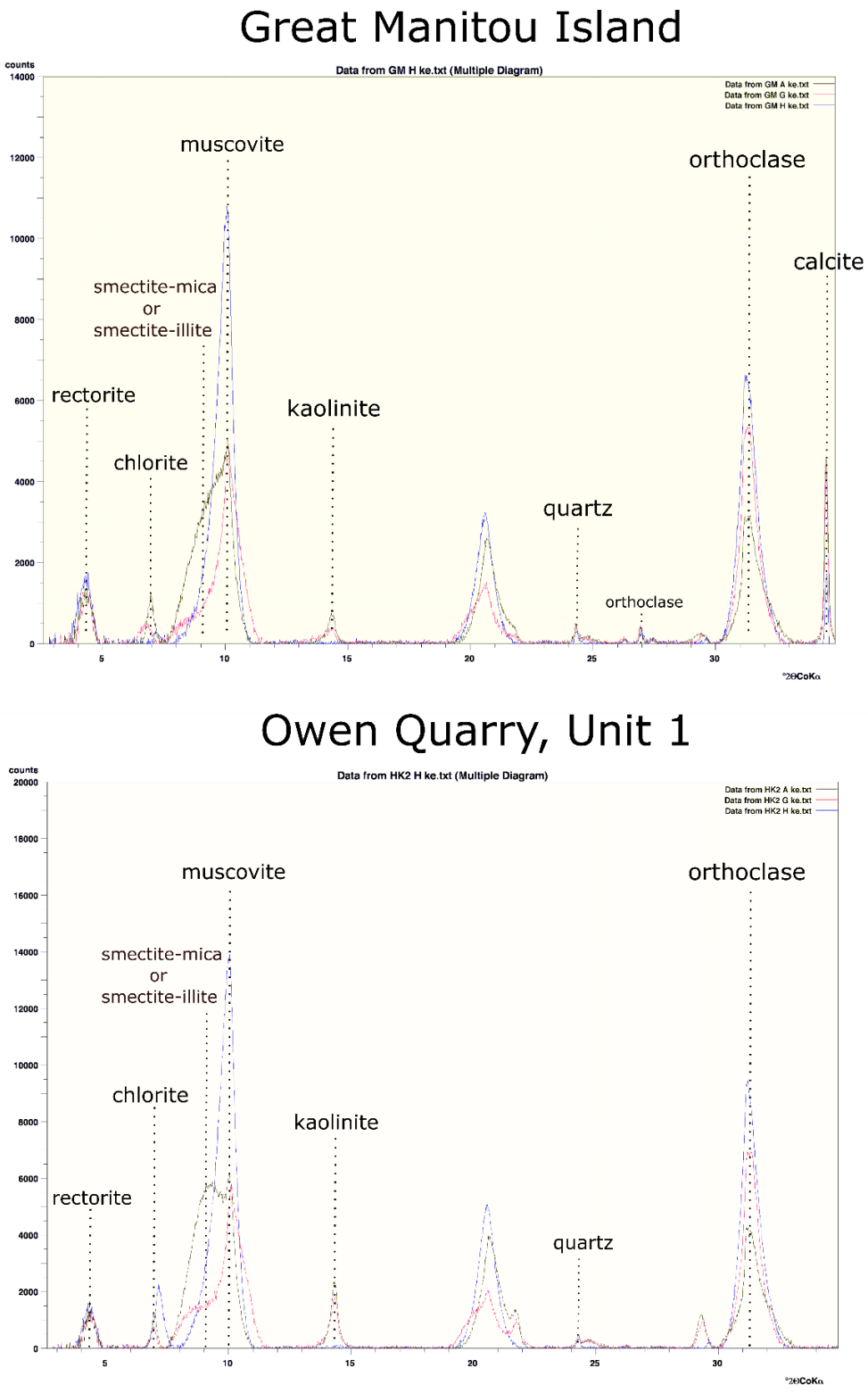

Figure 5.5. Sets of x-ray powder diffraction (XRD) lines of claystone from the Great Manitou Island and Owen Quarry outlier: green line, air-dried; red line, glycolated; blue line, heated (550 °C)

Paleoenvironmental interpretation

Facies of Unit 4a likely represents a low- to medium-energy, stenohaline, warm-water shallow marine environment: 1) the presence of abundant crinoid ossicles suggests a normal salinity (Flügel, 2010); 2) abundance of lime mud indicates a low energy environment, whereas vertical burrows suggest high levels of wave or current energy enabling loose or shifting substrate (MacEachern et al., 2010); and 3) Ordovician dasycladacean are common on shallow platforms (Mamet et al., 1984). Modern and ancient dasycladacean algae are favorable in warm-water environment (Aguirre and Riding, 2005). Occurrence of thin claystone in the fossiliferous subtidal facies may suggest changing patterns of riverine/storm influence from shore relative to carbonate production (Melchin et al., 1994). It does not have the typical characteristics of an altered volcanic ash, but could still be of aeolian origin.

The precursor limestone of Unit 4b was probably a bioclastic packstone. The low diversity of benthic biota and absence of crinoid ossicles suggest that the depositional environment may not have been of normal salinity (Flügel, 2010). Occurrence of lithoclasts indicates that there remains a ready basement source of sediment. The presence of horizontal burrows in Unit 4c identifies a stable seafloor with relatively available food source, likely in the fairweather conditions (MacEachern, 2010). In summary, carbonate production in Unit 4 shifts between high wave/current energy and fairweather conditions. Upsection, the environment changes from a normal-marine subtidal to a non-stenohaline subtidal environment.

Unit 5

Description

Unit 5 is 1.25 meters thick, and consists of medium-bedded crystalline dolostone (lithofacies D4; Fig. 5.3C). Dolomite crystals are medium- to coarse-sand size.

Paleoenvironmental interpretation

A paleoenvironmental interpretation is precluded due to the pervasive crystallinity of dolostone.

Summary of depositional environments

Summary of depositional environments is in Fig. 5.2. The Great Manitou Island section documents net transgression, with submergence and burial of paleotopography developed on a crystalline basement consisting of a syenitic intrusive body. With transgression, the depositional environment changes from nearshore/supratidal to shallow subtidal. Breccia and conglomerate of Unit 1 document the initial transgression with accumulation of fossiliferous, but mechanically immature siliciclastic sediment. Moving upsection, lithoclasts are reduced in size and the environment switched to carbonate represented by dolostone of Unit 2 that likely marks stepback of the siliciclastic source. Unit 3 rocks have been intensively dolomitized, but evidence for replaced crinoids in subdivision 3b suggests that continued transgression eventually allows development of normal-marine skeletal-bearing facies. Limestone of Unit 4 records abundant and diverse benthic fauna including crinoid ossicles and the calcareous algae *Vermiperolla*,

suggesting a normal-marine warm-water subtidal environment. Unit 5 forms the highest part of the section but dolomitization precludes paleoenvironmental interpretation.

5.2.2 Little Manitou Island

Any individual exposure of sedimentary rocks on Little Manitou Island doesn't exceed 1.7 meters, and the exposed sedimentary succession occurs as a low-lying escarpment mostly stepped back from the shoreline. Seven outcrops were measured to produce a > 3.5 m composite section (Fig. 5.2). The contact between sedimentary rocks and the basement is not exposed. Sedimentary rock types on Little Manitou Island include feldspathic arenite, bioclastic dolofloatstone/rudstone, interlayered bioclastic packstone and lime mudstone, and bioclastic dolopackstone. The composite succession is subdivided into 3 units on the basis of lithology, fossil content, and sedimentary structures.

Unit 1

Description

Unit 1 is exposed at localities A, E, and G, with maximum thickness of 1.4 meters at locality G. This unit consists of thin-bedded bioclastic feldspathic arenite (lithofacies S1; Fig. 5.6A). Few cm-size angular syenite clasts are present. Sand texture is bimodal: a coarser (250-1600 μm) fraction of subrounded to rounded sand, and a finer (40-100 μm) fraction of angular to subrounded silt and sand. Composition of sand grains include 80-90% quartz, 10-15% potassium feldspar, < 2% rutile, and < 2% syenite (Fig. 5.7A, B). Skeletal material is locally present, but not homogenous in distribution, rare to common, and

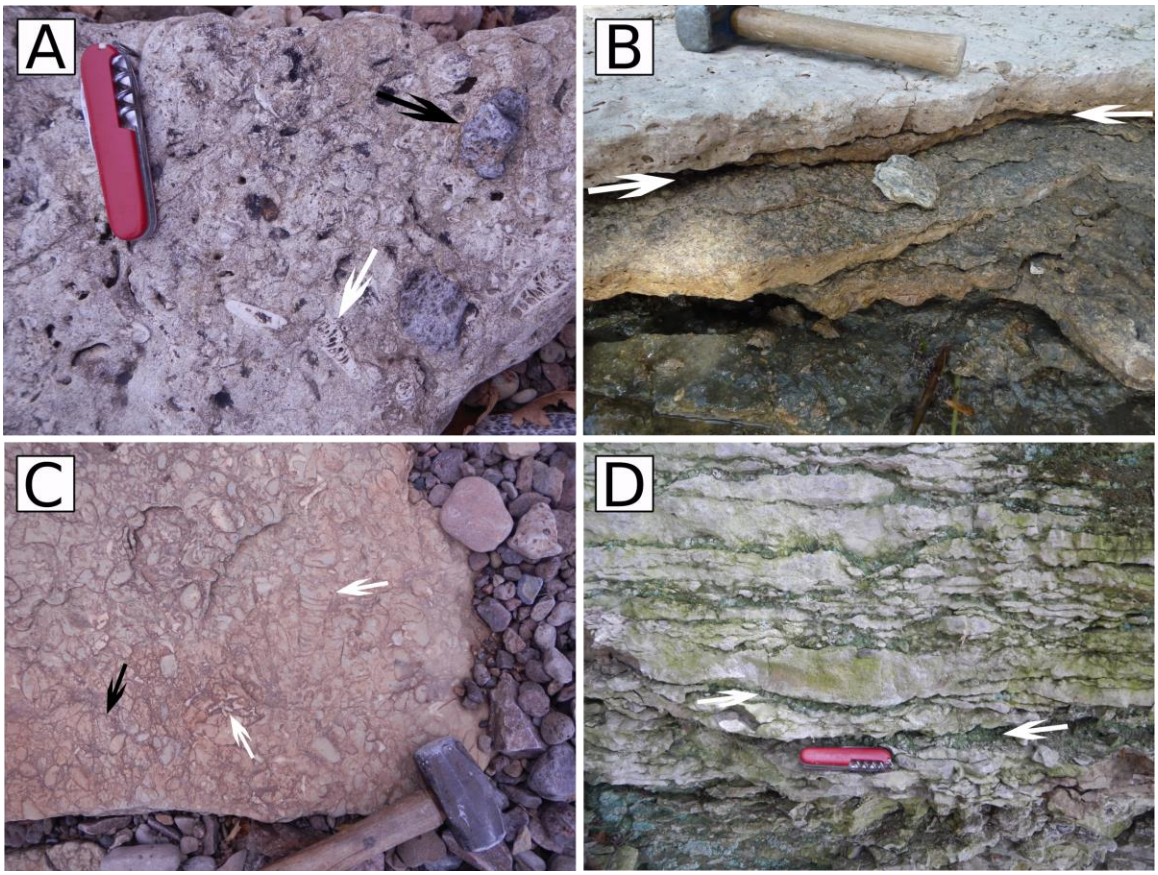

Figure 5.6. Field photo of lithofacies on Little Manitou Island. A) Lithoclasts-(black arrow) and orthocones (white arrow) bearing bioclastic sandstone of Unit 1. B) Boundary (arrows) between sandstone of Unit 1 and bioclastic dolorudstone of Unit 2. C) Bioclastic dolorudstone of Unit 2, fossils include bivalves (black arrow), orthocones (upper white arrow), and bryozoans (lower white arrow). D) Limestone of Unit 3 interlayered with thin claystone layers (arrows). Size of scale: knife is 9 cm long, and hammer is 20 cm long.

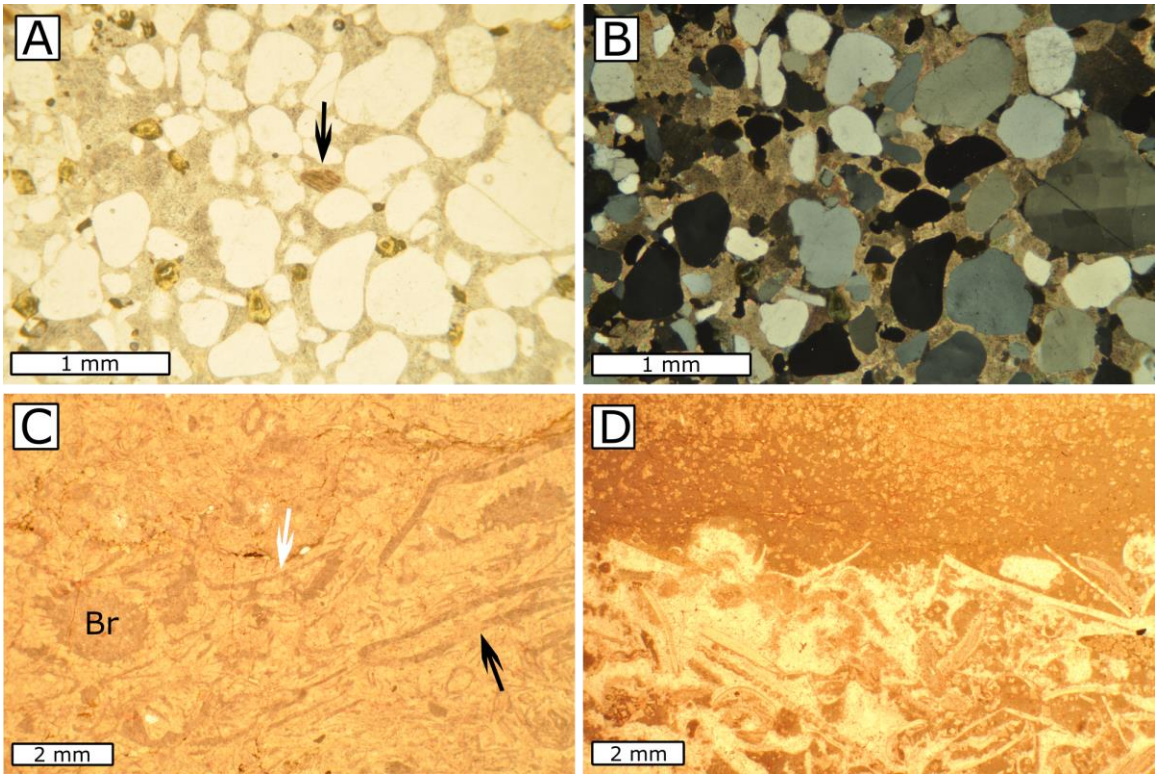

Figure 5.7. Thin-section photomicrographs of lithofacies on Little Manitou Island. A) Feldspathic arenite (Unit 1) (thin-section stained for K-feldspar); notice subrounded to rounded quartz (white), K-feldspar (yellow), and rutile (arrow); plane-polarized light image. B) Feldspathic arenite of Unit 1 (cross-polarized light image). C) Bioclastic dolorudstone of Unit 2 with abundant bryozoans (Br), trilobites (black arrow), and brachiopods (white arrow); plane-polarized light image. D) Interlayered bioclastic packstone and lime mudstone of Unit 3; both lithologies have been partially dolomitized; plane-polarized light image.

includes bivalves, small orthocones, gastropods, and bryozoans. Finely to coarsely crystalline dolomite forms intergranular cement, and has also precipitated in moldic pore space created by dissolution of bivalve shells and in cavities of orthocone shells. Rare large horizontal burrows (up to 1 cm in size), ellipsoid in cross-section are present, also filled with finely crystalline dolomite.

Paleoenvironmental interpretation

The quartz arenite facies characterizes a skeletal-rich shallow nearshore setting. The relatively diverse benthic faunal assemblage, yet absence of crinoid ossicles, may demonstrate non-stenohaline marine environment. Quartz grains are better-sorted and more rounded than lithoclasts, suggesting that the two are not from the same source: lithoclasts are reworked from exposed local basement whereas the source of the clean well-sorted quartz sand remains uncertain.

Unit 2

Description

Unit 2 is composed of lithoclastic dolostone with abundant benthic skeletal material. Dolomite is fine- to medium-crystalline. The lower contact of this unit is sharp and horizontal, and exposed at localities A and E (Fig. 5.6B). At locality E, Unit 2 consists of 50 cm of lithoclastic bioclastic dolofloatstone (lithofacies D5b). Fossils include orthocones, bivalves, and gastropods. Except for few (< 3%) cm-size lithoclasts, sand grains range from 400 to 800 μm in size, and are subrounded to rounded quartz and feldspar.

At locality A, Unit 2 consists of 60 cm of thin-bedded lithoclastic bioclastic dolorudstone (lithofacies D5b). Dolomite is fine- to medium-crystalline. Bioclasts include fragmented orthocones, gastropods, bivalves, ostracodes, bryozoans, and rare (< 2%) crinoid ossicles (Fig. 5.7C). This unit shows decreasing siliciclastic content upsection. In contrast to cm-size angular syenite (basement-derived) clasts, sand-size grains (< 3%) of quartz and feldspar are less than 400 μm in size, subrounded to rounded. Capping this initial dolostone is a 20-cm-thick interval of thin-bedded molluscan dolorudstone (lithofacies D5b; Fig. 5.6C) that contains abundant benthic skeletal remains of bryozoans, orthocones, ostracodes, bivalves, brachiopods, trilobites, and rare (< 2%) crinoid ossicles. Dolomite crystals display nonplanar texture and are 80 to 1200 μm in size.

Paleoenvironmental interpretation

The presence of angular basement-derived lithoclasts suggest that carbonate accumulation occurred within a relatively shallow-marine environment of siliciclastic (quartz, feldspar) sediment within which there were likely islands of Precambrian basement. Despite relatively abundant types of benthic fauna, the near absence of crinoids may suggest that the environment was not stenohaline (Flügel, 2010).

Unit 3

Description

Dolomitic limestone of this unit is exposed only at Loc. C, and is composed of thin-bedded interlayered dolomitic lime mudstone and bioclastic packstone (lithofacies

L2) with thin claystone layers (Fig. 5.6D). Bioclastic packstone contains abundant fragmented benthic skeletal material, including bivalves, bryozoans, crinoid ossicles, trilobites, ostracodes, and brachiopods (Fig. 5.7D). Dolomite crystals in the limestone will be further described in the latter content in this chapter.

Paleoenvironmental interpretation

Compared to the underlying facies (Unit 2), Unit 3 appears to represent a low-energy, stenohaline, shallow subtidal environment: 1) the presence of abundant crinoid ossicles suggests a normal salinity (Flügel, 2010); and 2) abundance of lime mud indicates a low energy environment. Occurrence of thin claystone may suggest changing patterns of riverine/storm influence from shore relative to carbonate production (Melchin et al., 1994), but may also be of an aeolian origin.

Summary of depositional environments

Summary of depositional environments is in Fig. 5.2. The Little Manitou Island succession documents net transgression resulting in development of a low-energy stenohaline setting, through a transition from higher energy nearshore siliciclastic-dominated facies. Absence of crinoids in this transitional phase likely illustrates fluctuating salinity.

5.2.3 Correlation of Great and Little Manitou islands strata

As is shown in Fig. 5.2, the stratigraphic successions on two islands can be partially correlated. Colquhoun (1958) mentioned 3 meters of calcareous/dolomitic

sandstone above 1.8 meters of conglomerate on Little Manitou Island. However, this is roughly the succession on Great Manitou Island and it is likely that the two sections were interchanged. Localities on the two islands are ~ 2 km apart.

Feldspathic bioclastic arenite (Unit 1) of Little Manitou Island is not directly represented in the section on Great Manitou Island. However, the quartz arenite matrix that constitutes the breccia of Unit 1a on Great Manitou Island, and contains apparent *in situ* bivalve remains, signifies a similar but higher energy siliciclastic facies maybe more proximal to islands as demonstrated by presence of admixed boulder-size basement clasts. Arenites on Little Manitou Island have coarser-grained sand grains and higher benthic biota diversity. Thus, transgression across basement with different paleotopography may explain the difference.

Dolofloat/rudstone of Unit 2 on Little Manitou Island is likely equivalent to dolostone of Unit 3 on Great Manitou Island. The bioclastic limestone and dolostone of Unit 3 on Little Manitou Island are similar to strata of Units 4 and 5 on Great Manitou Island based on lithology, skeletal material and $\delta^{13}C$ values (Fig. 5.2).

In summary, sedimentary rocks on Great and Little Manitou Islands represent a common regional depositional system with initial local differences influenced by paleotopography and supply of coarse-grained basement clasts greatly reduced with ongoing transgression.

5.3 Biostratigraphic indicators and age of outlier

One fragment of the bryozoan *Stictopora labyrinthica tabulata* Ross (Fig. 5.8A) observed from Unit 3b of Great Manitou Island is indicative of the equivalent Lowville-

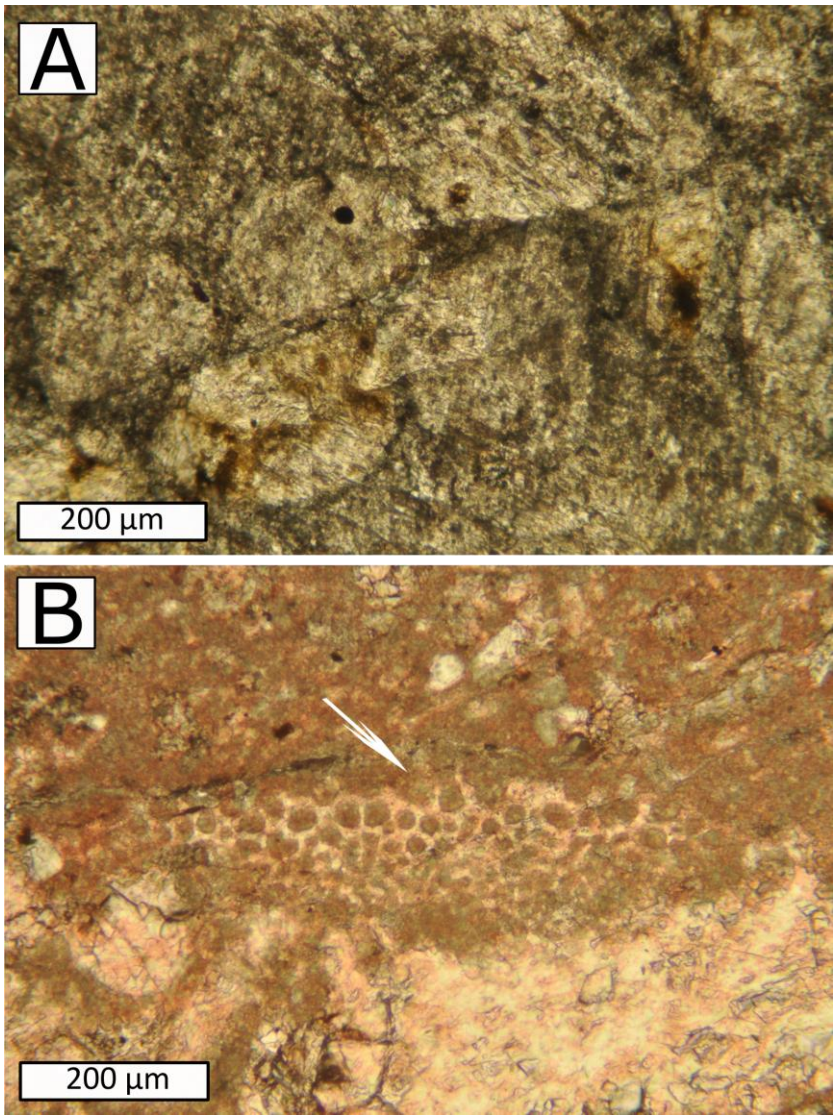

Figure 5.8. Thin-section photomicrographs of key fossils at Great Manitou Island. A) *Stictopora labyrinthica tabulata* Ross. B) *Vermiporella*? sp. (arrow).

Watertown interval of northern New York State (Ross, 1964). A fragment of a calcareous algae *Vermiporella*? (Fig. 5.8B) was observed in Unit 4a of Great Manitou Island. Regionally, calcareous algae occur in upper Gull River to Coboconk formations in the Lake Simcoe area (Grimwood et al., 1999; El Gadi, 2001) and Lowville to Watertown formations of northern New York State (Walker, 1972). Presence of calcareous algae in Unit 4 may indicate that the top of the succession still resides within the regional Blackriveran section.

5.4 Diagenesis

5.4.1 Introduction

Post-depositional (diagenetic) transformation of sediment to rock represented in the Manitou Islands outlier is described from petrographic and geochemical analyses. The post-depositional events represent surface (seafloor), shallow burial, and deep burial alteration wherein the top of the deep-burial zone is defined by onset of chemical compaction (pressure solution) of low-Mg calcite typically found at depth of > 300 meters (Neugebauer, 1991). Fig. 5.9 illustrates the interpreted relative timing and burial depth of diagenetic features.

5.4.2 Petrographic attributes

Limestone

Marine-derived diagenesis

Marine-derived diagenesis is documented in the Great Manitou Island succession, by the presence of burrows, hardground, and automicrite. Vertical and subvertical

burrows extend to a similar depth beneath the hardground in Unit 4a, and are filled with sediment of the overlying layer (Fig. 5.10A). Hardground is suggested by lithification of seafloor after burrowing and clasts in the overlying beds that are derived from the hardground (Fig. 5.4E). Automicrite occurs in the bioclastic packstone of Unit 4a, where it precipitates in intra- and interskeletal space cementing adjacent grains (Fig. 5.10B).

Shallow-burial diagenesis

In the Little Manitou Island section, shallow-burial diagenesis features include, in paragenetic order, syntaxial, bladed calcite cement, and blocky calcite cement.

Syntaxial calcite cement was observed in bioclastic packstone of Unit 3, where it occurs in optical continuity around trilobite fragments (Fig. 5.10C). Crystals are 200 to 300 μm long, 40 to 60 μm wide, and have a dull luminescence.

Bladed calcite cement precipitates in void space left by previous cement in the same lithofacies, including interskeletal and vuggy void space. Crystals range from 40 to 300 μm in length, and have dull luminescence (Fig. 5.10D, E). Horizontal and vertical fractures were both observed in the bioclastic packstone that are either empty or filled with calcite cement.

Blocky calcite I cement (40 to 2000 μm in size; Fig. 5.10D-F) is the last stage of calcite precipitation in limestone, in molds and intergranular void space of Unit 3. Crystals have medium luminescence. Their boundary between bladed calcite cement is distinguished by a thin layer of calcite with bright luminescence. Blocky calcite cement is cross-cut by wavy bedding-parallel stylolites. On the Great Manitou Island, blocky

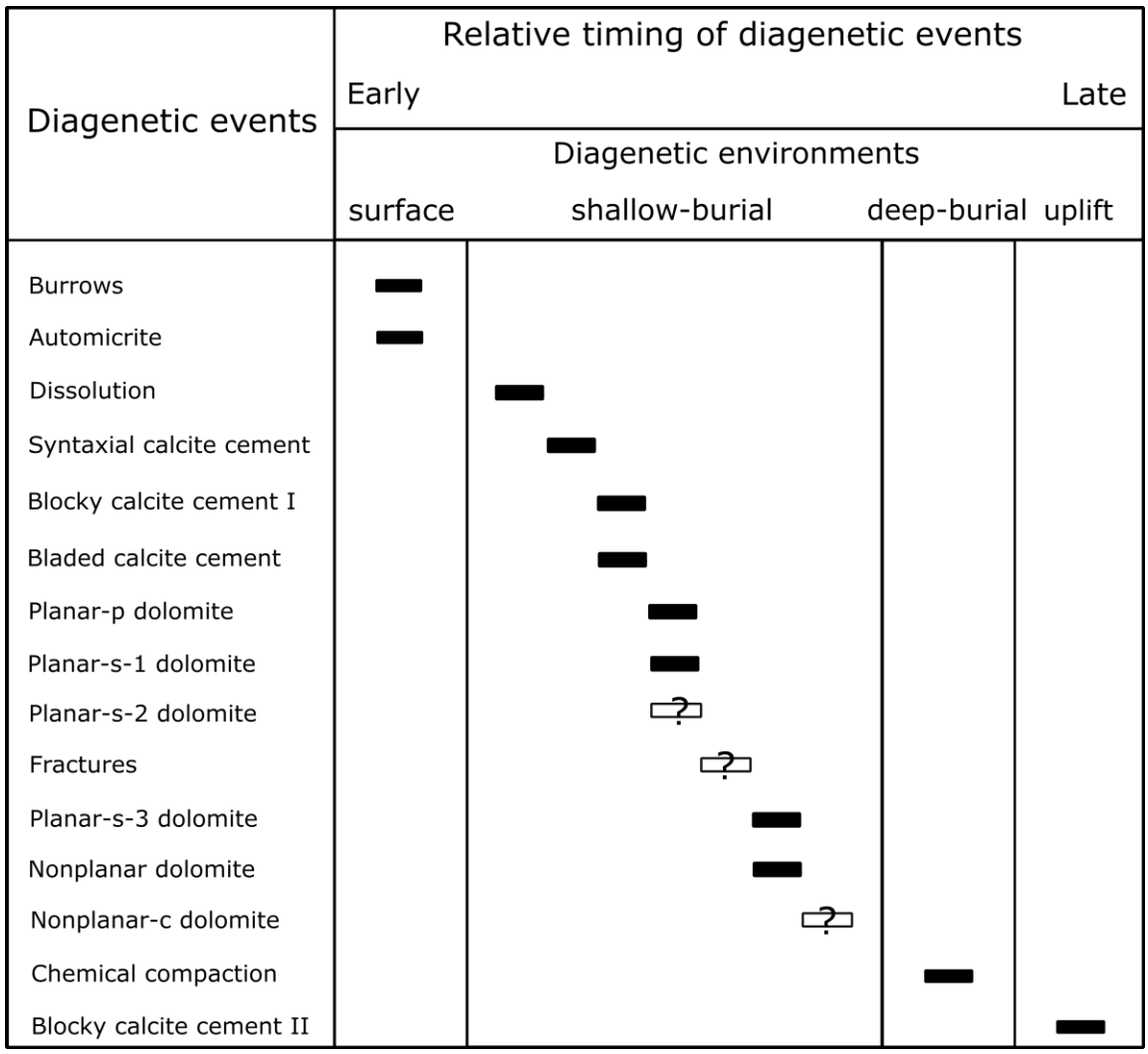

Figure 5.9. Diagenetic events and their relative timing of carbonate rocks and calcite/dolomite in siliciclastic rocks on Great and Little Manitou Islands. Based on petrographic and geochemistry study of samples.

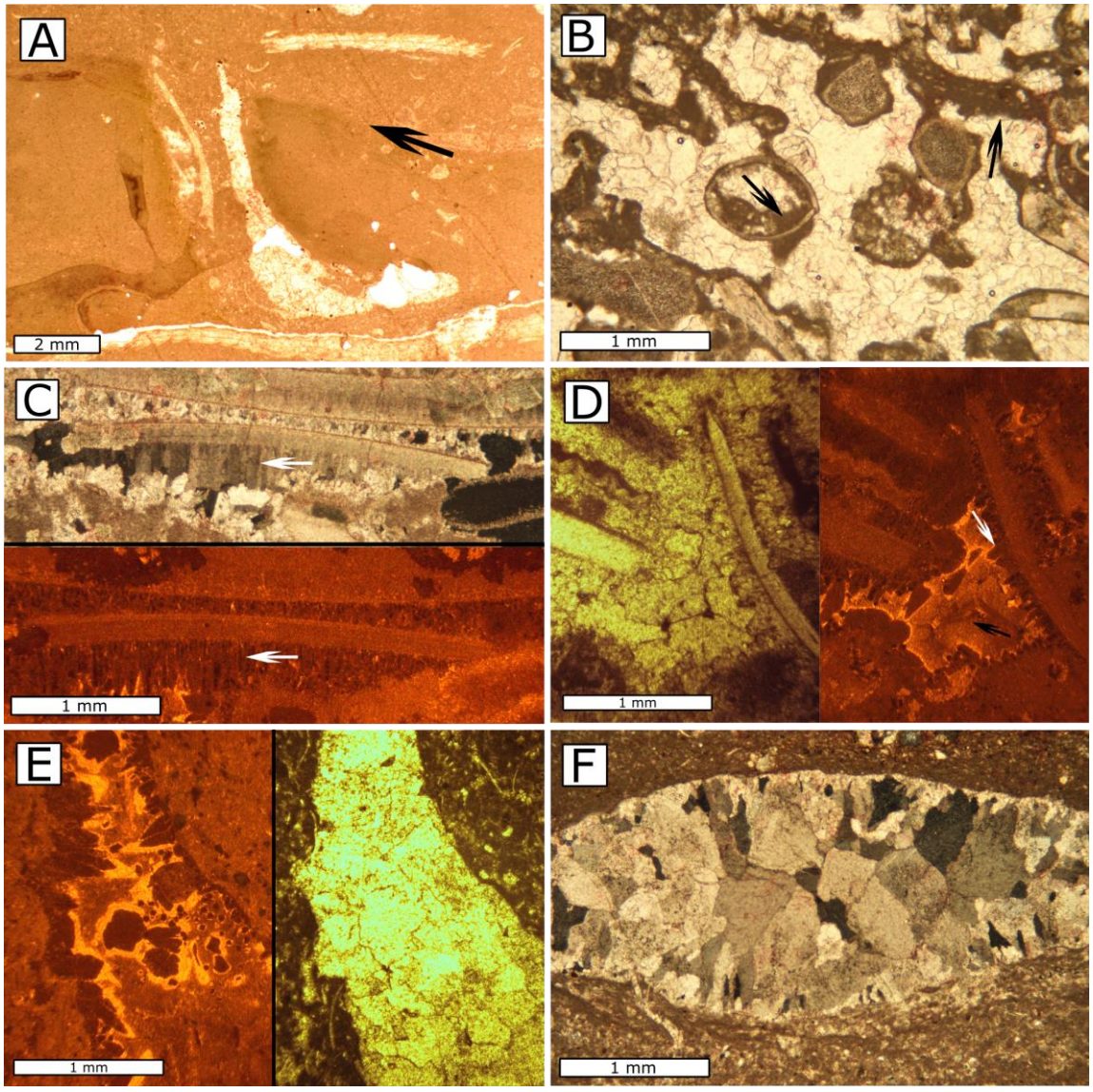

Figure 5.10. Thin-section photomicrographs of limestone diagenetic features on Manitou Islands. A) Burrow in interlayered bioclastic pack/wacke/mudstone of Unit 4a on Great Manitou Island; arrow indicates hard (firm?) ground, plane-polarized light image. B) Automicrite (arrows) and blocky calcite cement (pink color) of the bioclastic packstone on Great Manitou Island, plane-polarized light image of stained thin section. C) Photo pair illustrating syntaxial calcite cement (arrows) in bioclastic packstone of Unit 3 on Little Manitou Island; upper: cross-polarized light image; lower: CL image. D) Photo pair illustrating bladed calcite cement precipitates in interskeletal void space in bioclastic packstone of Unit 3 on Little Manitou Island, arrows indicate two stages of cement growth; left: plane polarized light image; right: CL image. E) Photo pair illustrating bladed calcite cement precipitates in vuggy void space of bioclastic packstone; left: CL image, right: plane-polarized light image. F) Blocky calcite I cement in bioclastic packstone of Unit 3 on Little Manitou Island, notice increased size of crystal from edge of the pore to the center; cross-polarized light image.

calcite I cement fills interskeletal and intraskeletal void space (Fig. 5.10B) in the bioclastic packstone lithofacies of Unit 4b after precipitation of automicrite.

Deep-burial diagenesis

Horizontal (bedding parallel) stylolites cross-cut blocky calcite I cement and micrite matrix in limestone.

Dolomitization

Five types of dolomite occur in the Great and Little Manitou sections. A summary of their textural attributes and distribution is presented in Table 2.3. The paragenetic order is illustrated in Fig. 5.9.

Planar-p dolomite occurs in bioclastic pack/wacke/mudstone of Unit 3 on Little Manitou Island, where crystals occur within the rock's matrix. Dolomite crystals are isolated or form small crystalline mosaics of euhedral rhombs, ranging in size from 80-500 μm. There is moderate degree of dedolomitization in which crystals are partially replaced by Fe-poor (pink staining) calcite (Fig. 5.11A). Dolomite crystals display complex luminescence characteristics (Fig. 5.11B) over a sampling distance of 4 cm: dolomite crystals vary from mostly non-luminescent to brightly luminescent, some show a non-luminescent core and bright rim. Planar-p dolomite is cross-cut by thin empty fractures that predate formation of stylolites. Stylolites display paleoporosity filled with pink-stained (Fe-poor) calcite.

There are three types of planar-s dolomite on the basis of distribution. Planar-s-1 dolomite occurs in the interlayered bioclastic packstone and lime mudstone of Unit 3 of

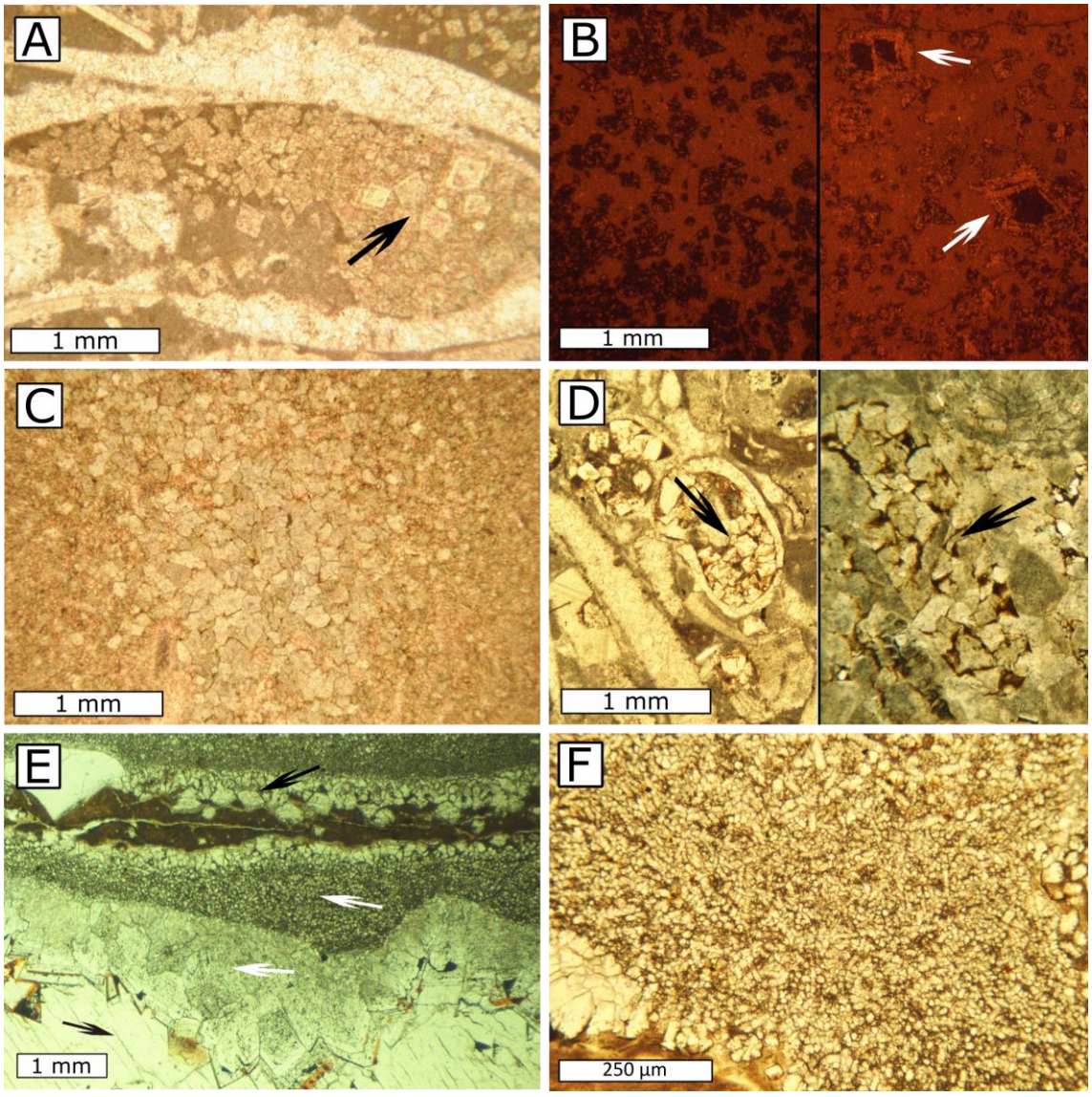

Figure 5.11. Thin-section photomicrographs of dolomite types on Manitou Islands (1). Photos A, C-F are taken under plane-polarized light. A) Planar-p dolomite (arrow) precipitates in intraparticle void space of ostracodes shells; dolomite has undergone dedolomitization. B) Photo pairing illustrating complex CL characteristics of planar-p dolomite; left: bright crystals with dull inclusions, right: bright crystals with dull cores (arrows). C) Planar-s-1 dolomite occurs in burrows of bioclastic pack/wacke/mudstone. D) Photo pair illustrating planar-s-1 dolomite features; left: it occurs in intraparticle void space of ostracodes of bioclastic packstone (red arrow), right: one patch of dolomite forming elliptical grains (blue arrow) in bioclastic dolopackstone. E) Planar-s-1 dolomite in clays (upper black arrow), planar-s-2 dolomite replaces bacterium tubes (upper white arrow), zoned saddle dolomite (lower white arrow), calcite precipitates in intergranular void space (lower black arrow), hematite (brownish) precipitates along the boundary of dolomite and calcite; image of polished thin section. F) Close-up view of planar-s-2 dolomite replacing bacterium tubes.

Little Manitou Island section, where dolomite forms crystalline mosaics that partially replace sediment in burrows (Fig. 5.11C). Crystals are 80-400 μm in size and non-luminescent. In bioclastic limestone of Unit 4a on Great Manitou island, planar-s-1 dolomite crystals form rounded patches (Fig. 5.11D left) within intraskeletal paleovoid space of ostracode shells, and resemble replaced primary grains in dolopackstone of Unit 3b (Fig. 5.11D right). This type of dolomite also precipitates in clay matrix of Unit 1a breccia of Great Manitou Island (Fig. 5.11E). Planar-s-1 dolomite is cross-cut by thin empty horizontal fractures.

Planar-s-2 dolomite is relatively fine-grained (5 to 40 μm) and replaces sinuous tubes, 5 to 20 μm in diameter (Fig. 5.11E, F), that may be of bacterial origin.

Planar-s-3 dolomite makes up most of the replacive dolomite on both Great and Little Manitou islands. Most of the dolomite crystals are fine- to coarse-grained, ranging from 80 to 1200 μm in size. Some dolomite crystals display cloudy cores and clear rims (Fig. 5.12A). Dolomite crystals are non-luminescent, precluding better discrimination between core and rim. Fe-poor (pink-staining), bright-luminescent blocky calcite II cement precipitates in intergranular void space of dolomite crystals.

There are two types of nonplanar dolomite. First, nonplanar-1 dolomite mosaics with crystals bearing normal extinction patterns define replacement texture and form intergranular cement in the breccia and sandstone (Fig. 5.12B) in both Great and Little Manitou islands sections. In the sandstone (including sandstone matrix of the basal breccia), intergranular and moldic void space is filled with this fine- to coarse-grained (80 to 1200 μm) anhedral dolomite. Nonplanar-1 dolomite crystalline mosaics are cut by

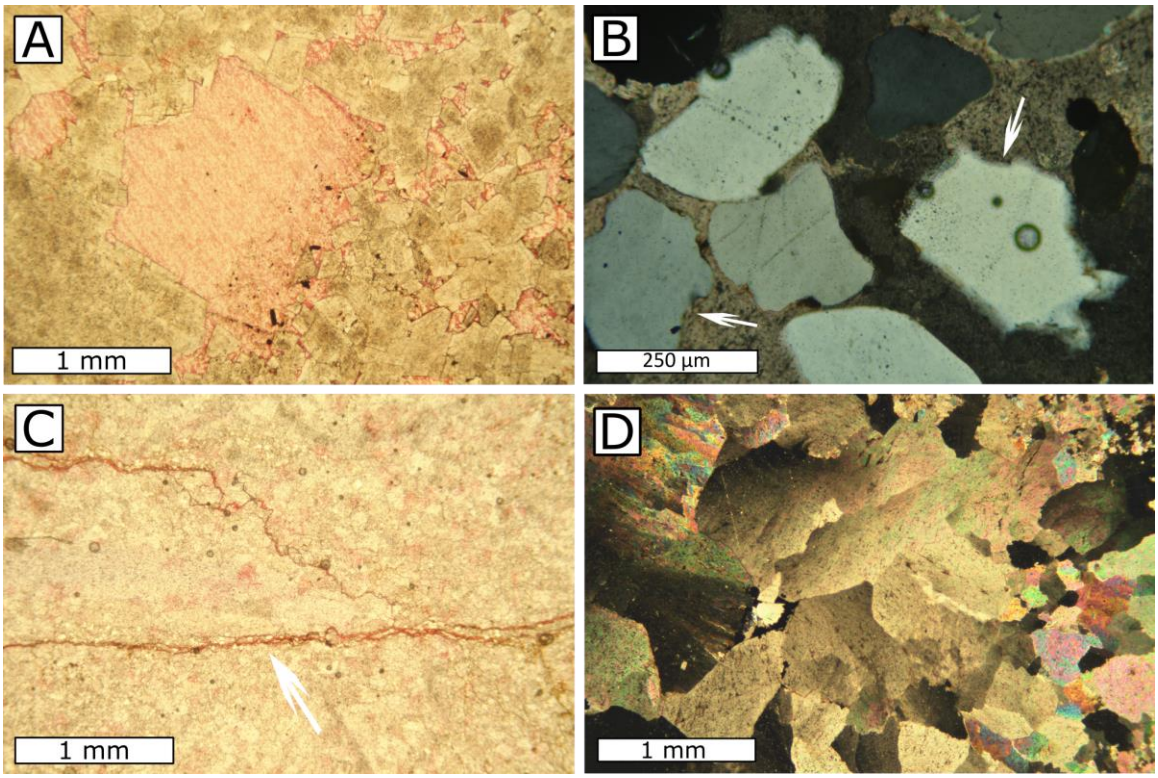

Figure 5.12. Thin-section photomicrographs of dolomite types on Manitou Islands (2). A) Planar-s-3 dolomite with dark core and clean rim, intergranular void space is filled with blocky calcite II cement; plane-polarized light image. B) Feldspathic arenite of Unit 1 on Little Manitou Island, arrows indicate replacement of quartz by nonplanar dolomite; cross-polarized light image. C) Nonplanar-1 dolomite is cross-cut by stylolites (arrow), which are dissolved and filled with calcite; plane-polarized light image. D) Nonplanar-c (saddle) dolomite from Unit 1a, Great Manitou Island shows sweeping extinction under cross-polarized light.

bedding parallel wavy stylolites (Fig. 5.12C) indicating that its origin predates deep-burial diagenesis.

The second type of nonplanar dolomite is saddle dolomite, and referred to formally as nonplanar-c dolomite. Here, it consists of medium- to coarse-grained (400 to 1600 μm) crystals with curved boundaries. This dolomite occupies paleo-moldic void space, has cloudy cores and clear rims (Fig. 5.11E), and displays sweeping extinction under cross-polarized light (Fig. 5.12D).

Blocky calcite II cement precipitates in any remaining paleoporosity following planar-s-3 (Fig. 5.12A) and nonplanar-c dolomites (Fig. 5.11E). Hematite has precipitated along the boundary between nonplanar-c dolomite and calcite II cement (Fig. 5.11E).

5.4.3 Geochemistry

Calcite

Major and minor elements

Late-stage blocky calcite II cement precipitated in intercrystalline void space of nonplanar-c dolomite and has a composition of $Ca_{98\text{-}99}Mg_{< 0.2}Fe_{< 0.6}Mn_{0.6\text{-}0.7}$.

Stable (C, O) isotopes

$\delta^{13}C$ and $\delta^{18}O$ values of micrite from limestones on both Great and Little Manitou islands were determined as part of a composite chemostratigraphic section (Fig. 5.2). In addition, this also allows examination of the character of marine versus burial diagenesis. $\delta^{13}C$ values range from -2.1‰ to -0.7‰ VPDB; and $\delta^{18}O$ values range between -4.6‰

and -5.9‰ VPDB, with values for Little Manitou limestone being ~ 1‰ more negative than those of Great Manitou limestone. The $\delta^{18}O$ range lies within that for Turinian marine brachiopod shells, -4‰ to -6‰ VPDB (Qing and Veizer, 1994; Shield et al., 2003). Thus, this may allow identification of temperature of early marine diagenesis. The equilibrium relationship between $\delta^{18}O$ of calcite, temperature, and $\delta^{18}O$ of water (Fig. 5.13) is adopted from Figure 23.4 of James and Jones (2016). Using a seawater $\delta^{18}O$ value of -1‰ to -3‰ SMOW for Turinian seawater (Shield et al., 2003), limestone on Great Manitou Island with $\delta^{18}O$ values of between -4.6‰ and -4.8‰ VPDB would have formed at temperature of between 22°C and 32°C. On Little Manitou Island, with $\delta^{18}O$ values more negative, ~ -5.9‰ VPDB, estimated water temperature is 29°C to 38°C.

Late-stage blocky calcite II cement precipitated in intercrystalline void space of nonplanar-c dolomite and has a more negative stable isotope value than calcitic micrite: a $\delta^{13}C$ value of -5.34‰ and $\delta^{18}O$ value of -6.5‰. These more negative values may identify either a meteoric source or elevated temperature, and evolvement of bacterial oxidation or sulfate reduction (James and Jones, 2016).

Strontium isotopes

$^{87}Sr/^{86}Sr$ isotope ratio of micrite from limestone of Unit 4a on Great Manitou Island is 0.70866, and blocky calcite II cement of Unit 1a on Great Manitou Island is 0.70864. The two values are similar and slightly higher than the value range estimated for Turinian seawater, 0.70788 to 0.7082 (Edwards et al., 2015). Interaction of fluid with shale associated with Unit 4a may have allowed fluid enrichment in ^{87}Sr (Banner, 1995).

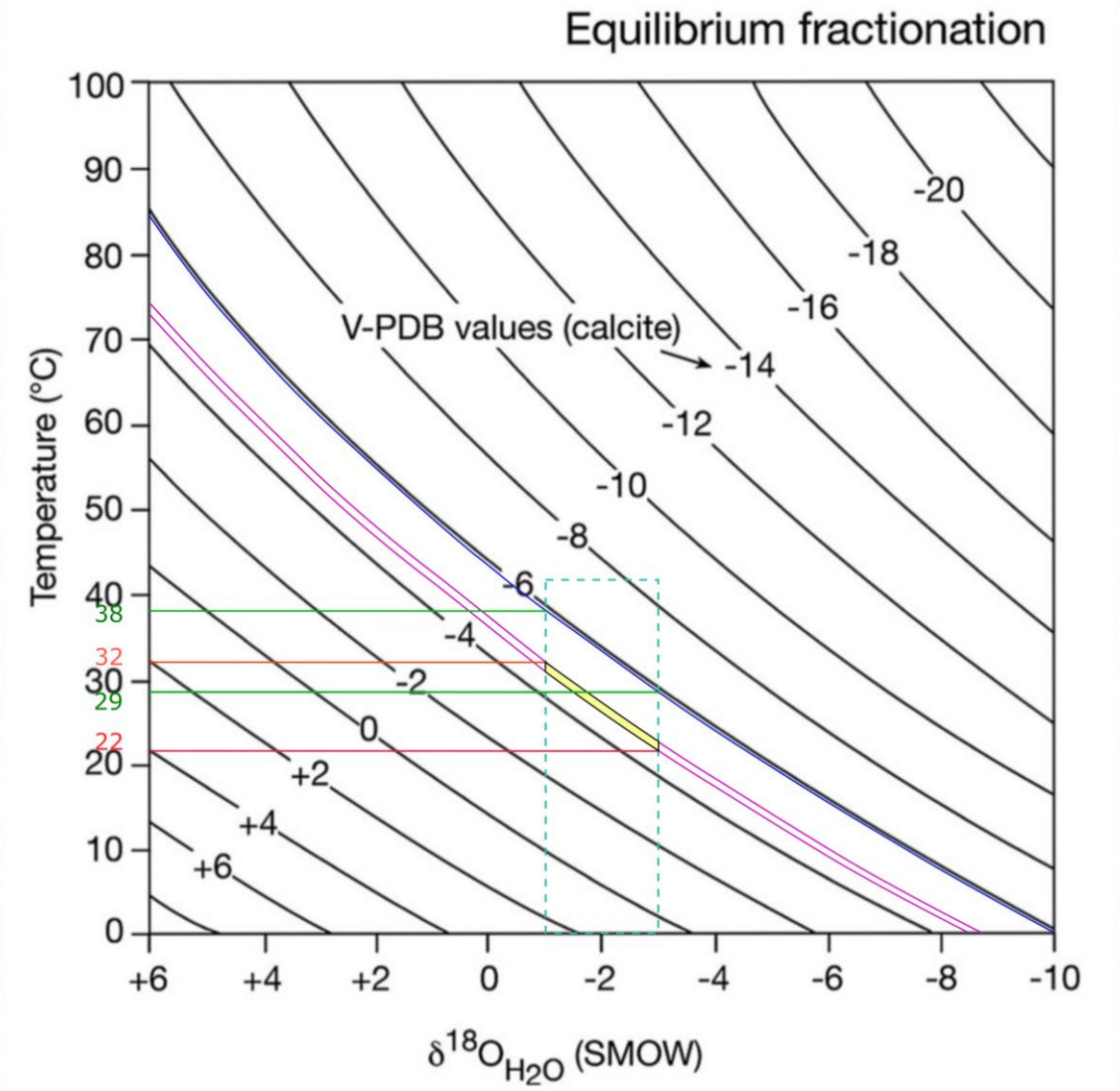

Figure 5.13. Equilibrium relationship between $\delta^{18}O$ of calcite, temperature, and the $\delta^{18}O$ of water, modified after James and Jones (2016). $\delta^{18}O$ of seawater is assumed to range from -1‰ to -3‰ SMOW (Shield et al., 2003). $\delta^{18}O$ of Great Manitou Island limestones ranges from -4.6‰ to -4.8‰ VPDB, whereas Little Manitou Island limestones is -5.9‰ VPDB. The plot shows that calcite is precipitated from water with temperature between 22°C and 32°C on Great Manitou Island, and between 29°C and 38°C on Little Manitou Island.

The fluid source of calcite II cement may be meteoric water that interacted with ^{87}Sr-rich aquifers.

Dolomite

Major and minor elements

Only planar-s-2, planar-s-3, and nonplanar-c dolomites were measured for major and minor elemental composition (Table 5.2) due to limited availability of polished thin-sections. The following mineral composition are defined for these three dolomite types. Planar-s-2 dolomite ($Ca_{49-50}Mg_{47-48}Fe_{02-05}Mn_{00-01}$) has a Fe-poor core and Fe-rich rim. Planar-s-3 dolomite has a relatively uniform composition of $Ca_{49-52}Mg_{46-50}Fe_{02-03}$. Nonplanar-c (saddle) dolomite is well zoned, with a Fe-poor core and Fe-rich rim, and shows variations in composition: $Ca_{49-51}Mg_{37-49}Fe_{01-10}Mn_{00-02}$.

Stable (C, O) isotopes

Isotope ratios of dolomite in a given unit were measured to generate a chemostratigraphic section (Fig. 5.2), and allow examination of dolostone diagenesis. $\delta^{13}C$ values of dolomite range from -3.1‰ to 0‰ VPDB. There is no obvious stratigraphic trend in $\delta^{13}C$, but two apparent positive excursions in the middle and upper parts of the section.

$\delta^{18}O$ values of planar-s-1, planar-s-3, and nonplanar-1 dolomite range from -8‰ to -9.4‰ VPDB, with values most negative in Unit 3d on Great Manitou Island. Nonplanar-c dolomite (-10.21‰ VPDB) of Unit 1a on Great Manitou Island has the most negative $\delta^{18}O$ value. There is great uncertainty in the composition of fluid from which

Description	$CaCO_3$	$MgCO_3$	$FeCO_3$	$MnCO_3$	$BaCO_3$	$SrCO_3$
Planar-s-2 dolomite (core)	49.50%	48.12%	2.05%	0.24%	0.04%	0.01%
Planar-s-2 dolomite (rim)	49.87%	44.23%	5.05%	0.77%	0.01%	n.d.*
Planar-s-2 dolomite (rim)	49.91%	44.08%	5.00%	1.00%	0.01%	n.d.
Planar-s-2 dolomite	49.31%	46.94%	3.27%	0.44%	0.01%	n.d.
Planar-s-2 dolomite	48.79%	47.44%	3.36%	0.41%	n.d.	n.d.
Planar-s-3 dolomite	52.38%	50.11%	2.08%	0.45%	0.03%	n.d.
Planar-s-3 dolomite	49.66%	47.47%	2.49%	0.34%	n.d.	n.d.
Planar-s-3 dolomite	50.19%	46.26%	3.05%	0.44%	n.d.	n.d.
Planar-s-3 dolomite (moldic void)	49.52%	47.49%	2.57%	0.40%	n.d.	n.d.
Planar-s-3 dolomite (moldic void)	50.00%	47.23%	2.36%	0.40%	n.d.	n.d.
Nonplanar-c dolomite	51.22%	37.57%	9.72%	1.47%	n.d.	n.d.
Nonplanar-c dolomite	50.85%	38.61%	8.73%	1.74%	0.02%	n.d.
Nonplanar-c dolomite	51.21%	42.11%	5.72%	0.92%	0.03%	n.d.
Nonplanar-c dolomite	49.09%	43.98%	5.45%	1.48%	n.d.	n.d.
Nonplanar-c dolomite	49.17%	48.68%	1.87%	0.27%	n.d.	n.d.
Nonplanar-c dolomite	49.40%	49.00%	1.39%	0.20%	n.d.	n.d.
Calcite Fe-poor zone	98.92%	0.12%	0.17%	0.75%	n.d.	0.03%
Calcite Fe-poor zone	98.56%	0.15%	0.52%	0.63%	0.07%	0.04%

*n.d.= not detected

Table 5.2. Major and minor elemental composition of calcite and dolomite on Manitou Islands. Values are illustrated in molecular percentage.

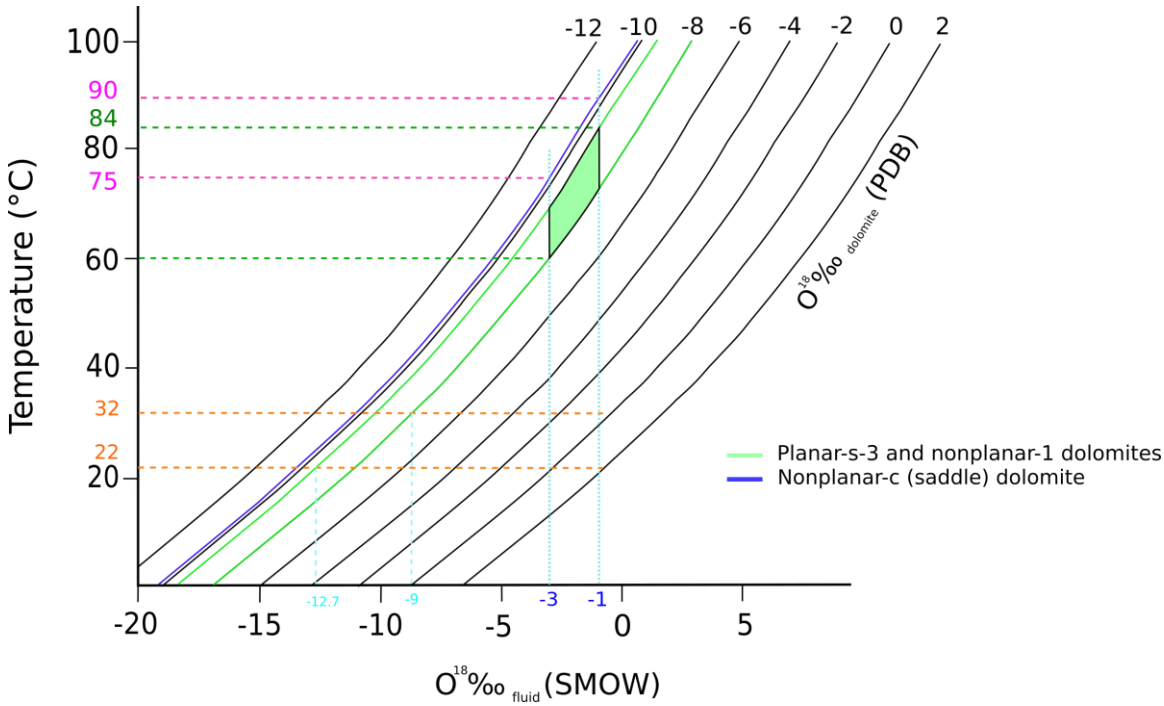

Figure 5.14. Estimated formation temperature and fluid $\delta^{18}O$ value of planar-s-3, nonplanar-1, and nonplanar-c dolomites on Great Manitou Island. The plot is modified after Nurkhanuly (2012), whose values are calculated using the equation: $10^3 \ln \alpha = 3.2 \times 10^2 T^{-2} - 3.3$ (Land, 1983).

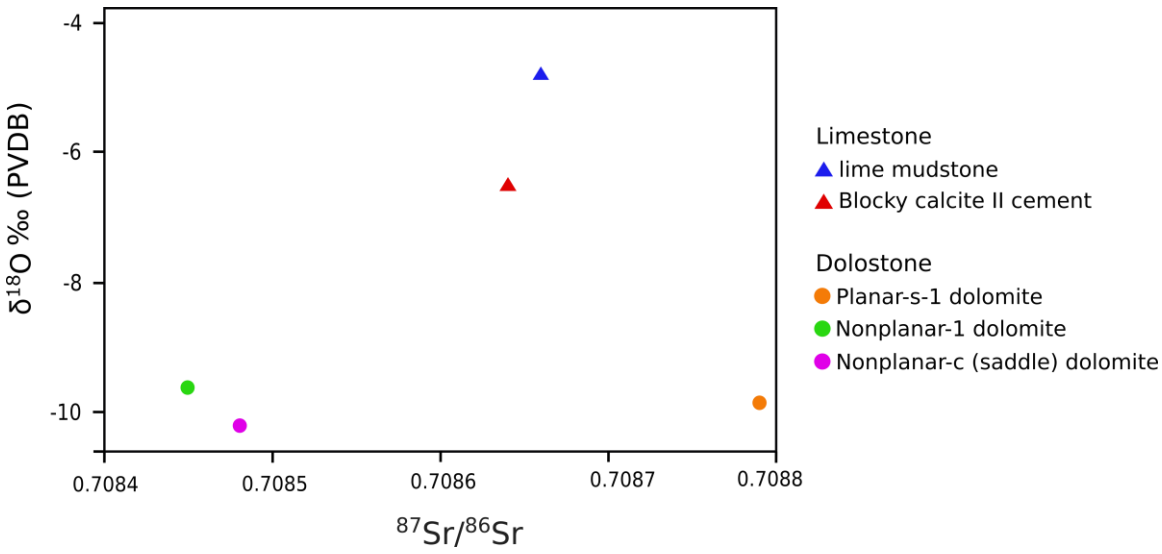

Figure 5.15. $\delta^{18}O$–$^{87}Sr/^{86}Sr$ plot of selective dolomite and calcite on Great Manitou Island.

dolomites precipitated. However, taking the same approach as presented in Chapter 2, the dolomite-water fractionation equation of Land (1983) is used to evaluate some endmember possibilities. If dolomite precipitated from seawater ($\delta^{18}O$ value: -1‰ to -3‰ SMOW), the estimated formation temperature of planar-s-3 and nonplanar-1 dolomites ranges from 60 to 84°C, and nonplanar-c dolomite ranges from 75 to 90°C (Fig. 5.14). If dolomite formed over a similar temperature range as limestone, 22-32°C (Fig. 5.13) on Great Manitou Island, planar-s-3 and nonplanar-1 dolomites would have precipitated from a fluid with $\delta^{18}O$ value of -9‰ to -12.7‰ SMOW (Fig. 5.14).

Strontium isotopes

Among samples collected from Great Manitou Island, strontium isotope ratios of planar-s-1 and nonplanar-1 dolomites of Unit 3d, and nonplanar-c dolomite were measured. The values are shown in Fig. 5.15.

All are well above the values of Turinian seawater (Edwards et al., 2015) indicating incorporation of radiogenic ^{87}Sr from passage of fluids interacting with either the basement or siliciclastics in shale layers and lithoclasts-rich lower succession strata. However, there are peculiar interstratigraphic similarities and intrastratigraphic contrasts. First, nonplanar-1 dolomite of Unit 3d has a similar $^{87}Sr/^{86}Sr$ value as nonplanar-c dolomite of Unit 1. Despite a stratigraphic separation of ~ 7 m, they probably precipitated from a similar diagenetic fluid. Second, although found in the same stratigraphic unit, planar-s-1 and nonplanar-1 dolomites have very different Sr isotope ratios, suggesting that they represent two stages of dolomitization. Third, blocky calcite cement precipitated

in intercrystalline void space of nonplanar-c dolomite has lower $^{87}Sr/^{86}Sr$ value than the host dolomite, but still significantly higher than Turinian seawater value.

5.2.4 Discussion

Limestone

Evidence of limestone diagenesis in the marine (or marine-derived) near-surface burial environment includes burrows, hardground, and automicrite cement. Input of meteoric-derived fluids likely causes dissolution of aragonitic skeletal material resulting in the subsequent precipitation of the initial syntaxial cement (James and Choquette, 1984). The subsequent bladed and blocky cements may identify deeper burial migration of fluids. However, this predates onset of stylolites that are commonly found no shallower than 300 m. A final stage of diagenesis is recorded by dissolution of dolostone along stylolites and filling of the paleoporosity by calcite cement. Timing of this remains uncertain but could document diagenetic processes during uplift leading to eventual exposure of the stratigraphic succession.

Dolostone

Planar-p, planar-s, and nonplanar dolomite types predate formation of stylolites, which indicates that they form during marine or shallow-burial diagenesis. An interpreted early dolomitization history is associated with planar-p and planar-s-1 dolomites because they selectively replace limestone in burrows and mud matrix (see Chapter 2). Later-stage planar-s-3 and nonplanar-1 dolomites may replace planar-p and planar-s-1 dolomites, thereby accounting for different fluid origins recorded by Sr-isotope ratios for

planar-s-1 and nonplanar-1 dolomites. Planar-s-1 dolomite resembles *dolomite D1* of Gingras et al. (2004), which forms mosaics in burrows, and is interpreted to have formed in the sulphate-reducing zone where burrow structures enhance bulk fluid flow through the matrix and enriches the substrate in organic and metallic material that is essential for dolomite precipitation (Gingras et al., 2004).

Planar-s-2 dolomite grows in clay-size sediment and replaces bacterium aggregation. Not enough information is available to evaluate the origin of this dolomite but, of note, low temperature dolomite has been precipitated in association with bacterial activity (Vasconcelos et al., 2005).

Nonplanar-c dolomite precipitates in moldic (bivalve) void space. It can be also referred to as saddle dolomite based on the evidence of its sweeping extinction under cross-polarized light. According to Spötl and Pitman (1998), formation of saddle dolomite requires minimum temperature of 60-80°C, a range in good agreement with the temperature estimation that nonplanar-c dolomite formed in the range of 75-90°C (Fig. 5.14). Hematite forms a thin coating on the surfaces of mosaics of nonplanar-c dolomite where overlain by late-stage calcite cement. As suggested by Frank (1981), hematite can be the oxidation and alteration product of ferroan dolomite. This suggests that the hematite in the outlier represents interaction of Ca-bearing fluids (associated with calcite precipitation) and the host dolostone.

Chapter 6 Owen Quarry Outlier

6.1 Local and general geology

The Owen Quarry outlier (46° 6.1' N, 79° 32.526' W) lies ~ 2.1 km west of Nipissing township, Ontario, and south of Lake Nipissing (Fig 1.1; Fig. 6.1). The outlier is bounded by granitic gneiss of Mesoproterozoic age (Lumbers, 1971). There are three outcrop exposures (Localities A-C) in the now abandoned quarry (Fig. 6.1). Locality A contains the principal exposure of a total thickness of 8.3 m. Locality B is ~ 20 m southeast of locality A, separated by vegetated land surface (Fig. 6.2A), whereas Locality C is ~ 51 m southwest of locality A along a heavily wooded escarpment. Contrasting bedding attitudes among the three localities imply local intervening faults, and the escarpment bounded by Paleozoic and Precambrian rocks likely defines the trace of a regional fault offsetting Paleozoic and Precambrian rocks (Lumbers, 1971).

6.2 Lithostratigraphy and facies

6.2.1 Locality A

Locality A contains 8.3 meters of dolostone subdivided into five units based on lithology, fossil content, and sedimentary structures (Fig. 6.3). The base of Locality A is 201±1 meters above sea level. Strata strike 338° and dip 10° to the northeast. The following summarizes lithofacies types, their associations, and fossil content associated with each unit; and interpreted depositional environments. Details are summarized in Table 6.1.

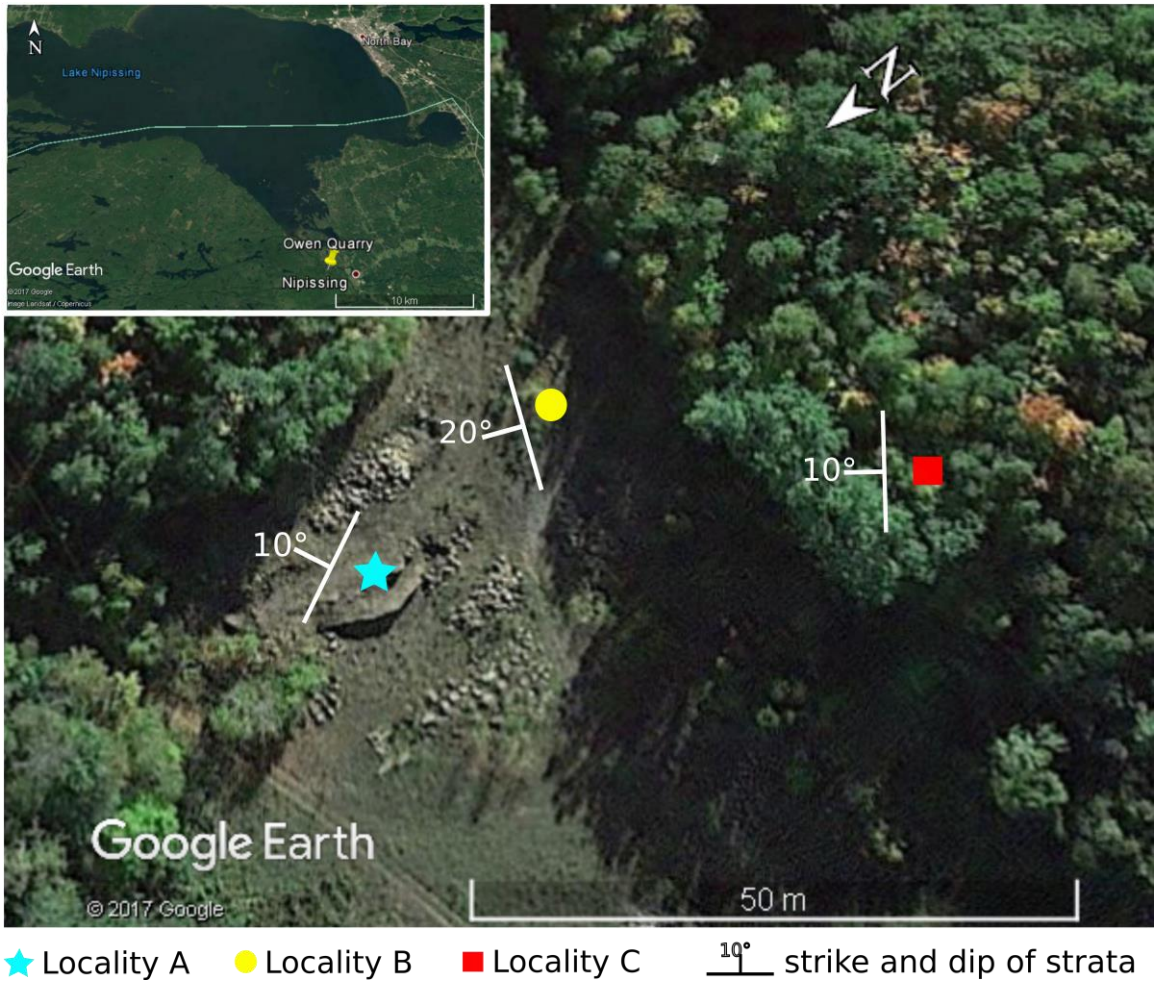

Figure 6.1. Location and bedding attributes (strike, dip) of three stratigraphic sections (coloured symbols) within the abandoned Owen Quarry: blues star, Loc. A; yellow circle, Loc. B; red square, Loc. C. Geographic location is shown in the inset image, and both images are derived from Google Earth.

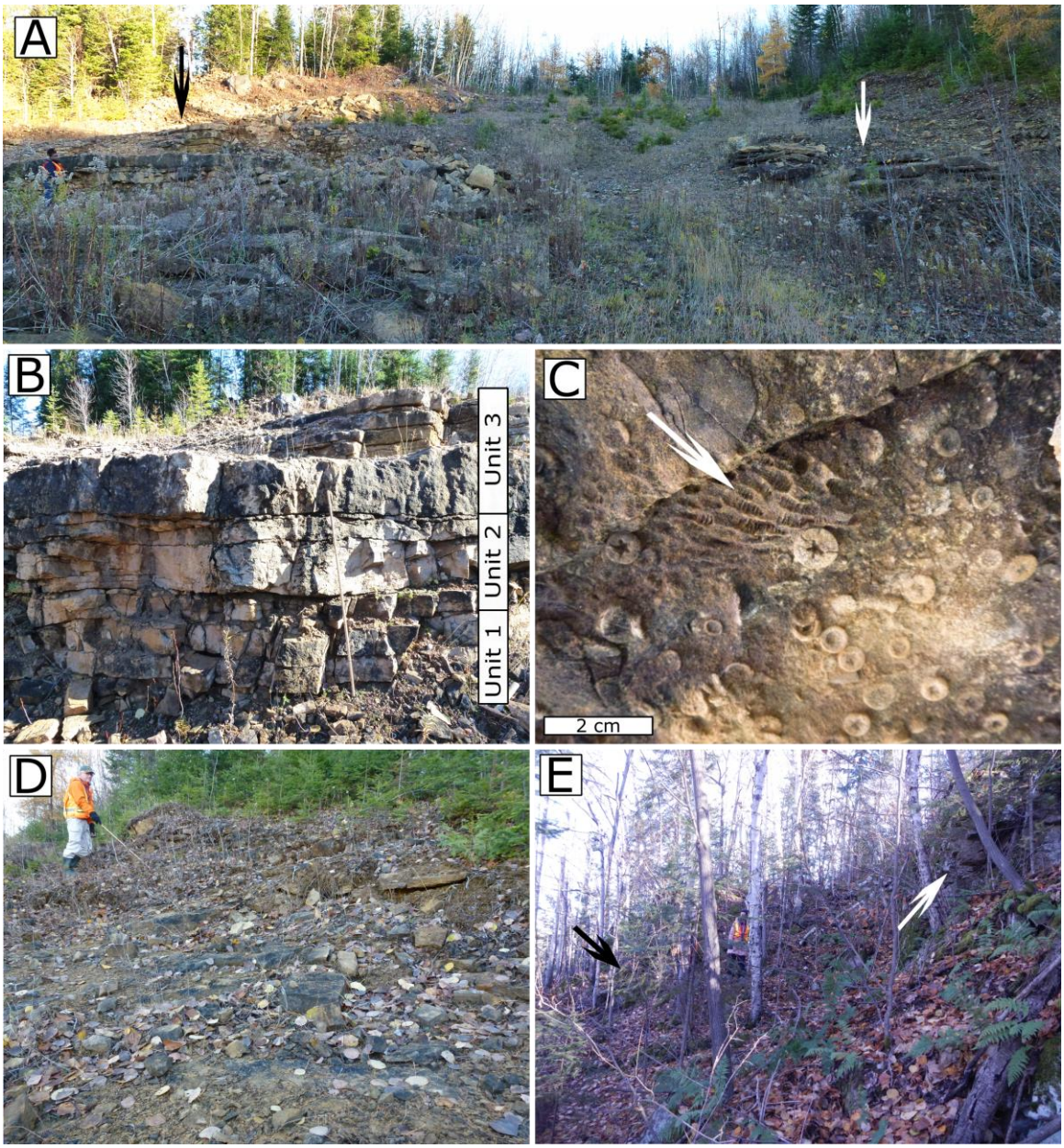

Figure 6.2. Field photos showing distribution of sedimentary rocks and representative lithofacies of Owen Quarry outlier. A) Field relationship between Locs. A (black arrow) and B (white arrow). B) Field view of lower three units of Loc. A. C) Bioclastic dolorudstone of Unit 2b of Loc. A, arrow indicates tabulate coral colonies. D) Field view of exposed entire Loc. B, person for scale. E) Field relationship of Loc. C dolostone (white arrow) and Precambrian basement (black arrow), person for scale.

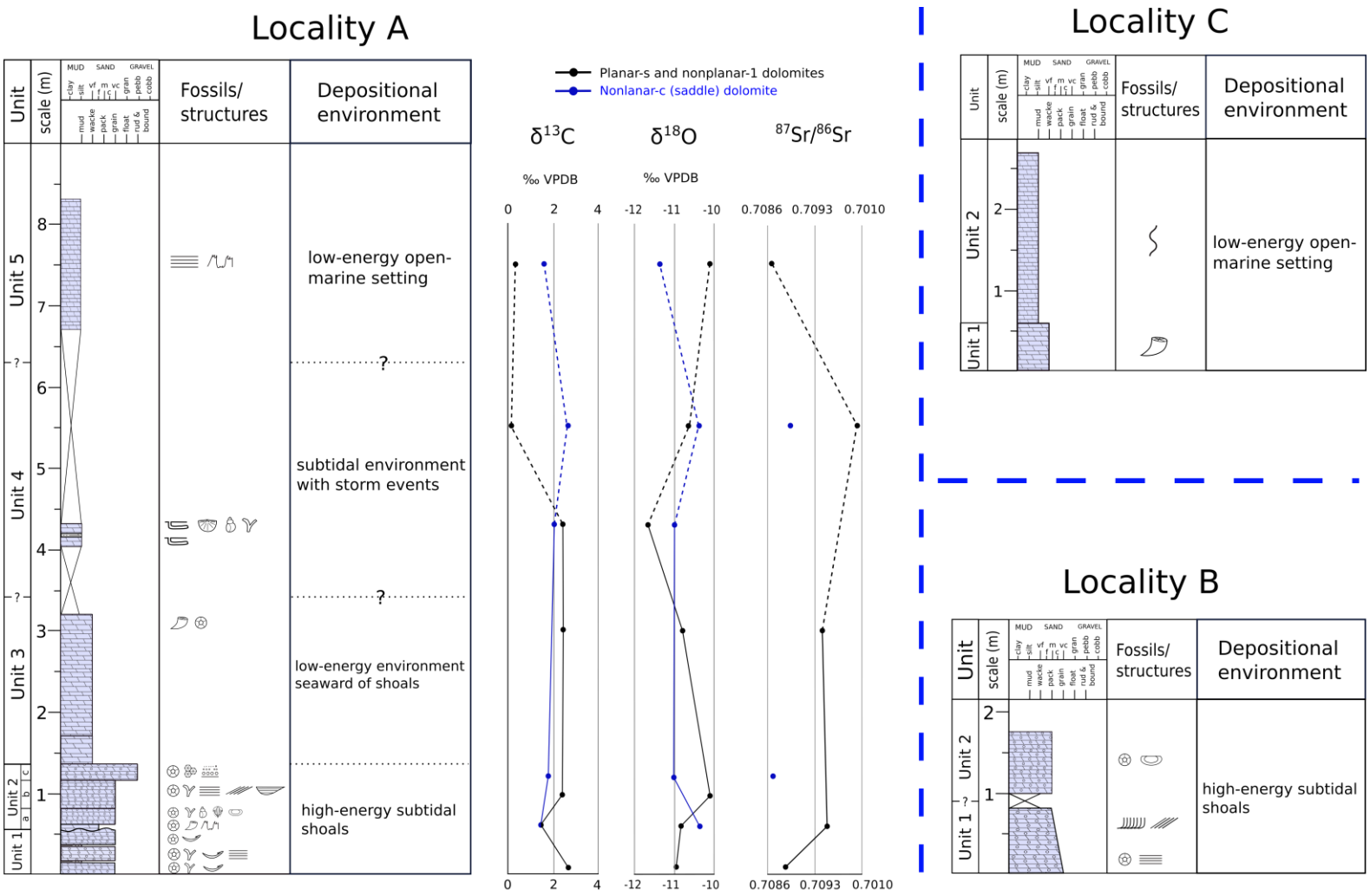

Figure 6.3. Stratigraphic attributes of the Owen Quarry outlier. Legend is in Fig. 2.2. Geochemical data for the upper part of Unit 4 is based on disturbed material (large quarry blocks) but similar in lithology to outcrop exposure lower in the unit.

Lithofacies type	Lithology	Sedimentary features	Fossils and detrital material	Interpretation	References
D1a	dolomudstone	medium-bedded	scarce crinoid ossicles and rugose corals; no siliciclastics	quiter, more open-marine environment	1
D1b	interbedded dolomudstone with claystone	thin-bedded, intense bioturbation	brachiopods, gastropods, crinoid ossicles, bryozoan and trace fossils *Chondrite, Palaeophycus, Bergaueria* are abundant	stenohaline, subtidal environment with wave/tide activities	2, 3
D4a	medium- to coarse-crystalline dolostone interlayered with dolomitic claystone	dolostone is medium-bedded, weakly laminated. Claystone is 2-cm-thick	fragmented crinoids, bryozoans, bivalves, rugose corals, and trilobites. Dolostone is composed of nonplanar, 150-2000 μm fabrics. < 1% to 10% detrital sand grains are 80-150 μm in size, subangular to rounded, main mineralogy of quartz and K-feldspar. Primary grains are probably ooids.	high-energy shoals in the stenohaline, subtidal environment with periods of increased siliciclastic input.	4, 5
D4b	channel with cross-laminated dolograinstone	cross-laminated	primary grains (ooids?), crinoid ossicles, bryozoans, ~ 2% of siliciclastics within the channel but ~ 10% outside of the channel	migrating tidal sand bars or bioclastic dunes in agitated shallow shelf	4, 6
D4c	cross-laminated fine- to medium-crystalline dolostone	medium-bedded; horizontal lamination, inclined lamination, and trough cross-lamination	crinoid ossicles, brachiopods, bivalves, bryozoans, and ostracodes; nonplanar to planar-s, 40-400 μm dolomite fabrics; primary grains (ooids?)	migration of small current ripples in subtidal sand shoals	7
D5	bioclastic dolorudstone	fining-upward	crinoid ossicles, tabulate coral colonies, ~ 8% siliciclastics	subtidal, warm-water environment	4

Table 6.1. Summary of lithofacies types in Owen Quarry outlier. References: 1, Holterhoff, 1997; 2, Cameron and Mangion, 1977; 3, Narbonne and James, 2017; 4, Flügel, 2010; 5, Ball et al., 1967; 6, Brookfield and Brett, 1988; 7, Boggs, 2011.

Unit 1

Description

Unit 1 (54 cm thick) contains abrupt and planar bedding contacts, except for the unit's upper boundary that is wavy and possibly an erosional surface. This unit is composed of weakly laminated medium-bedded medium- to coarse-crystalline dolostone (Fig. 6.4A) interlayered with 2 cm-thick dolomitic claystone (lithofacies D4a). It contains abundant benthic macrofossil remains including fragmented crinoid ossicles, bryozoans, bivalves, rugose corals, and trilobites. Dolostone is composed of nonplanar, 150-2000 μm fabrics with abundant crystal inclusions. There is common presence of rounded brownish outlines of dolomite-replaced grains (100-200 μm in size; Fig. 6.5A), which may have been ooids.

Siliciclastic grains represent no more than 10% of the rock. Grains are 80-150 μm in size, subangular to rounded, and consist of quartz and K-feldspar. XRD analysis of dolomitic claystone reveals that clay minerals include muscovite, rectorite, smectite-mica or smectite-illite, chlorite, and kaolinite (Fig. 5.5), and is similar to the claystone analyzed from Great Manitou Island (see Chapter 5).

Paleoenvironmental interpretation

Dolomite has replaced a precursor skeletal-rich limestone that may have contained ooids. Crinoid ossicles and rugose corals identify a stenohaline environment (Flügel, 2010), but one in which there was some influence from a siliciclastic source. If

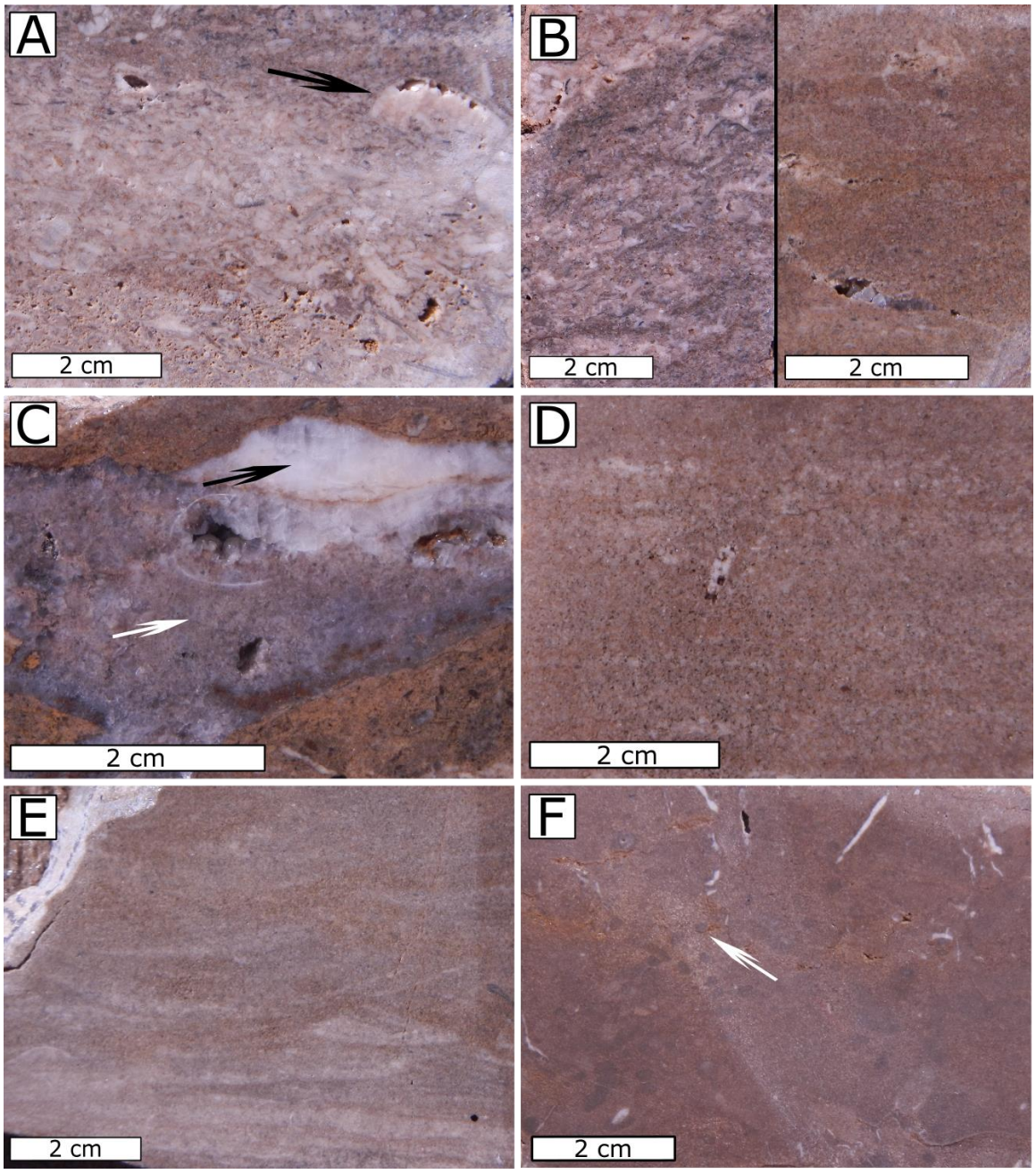

Figure 6.4. Slabbed rock sample of representative lithofacies in Owen Quarry outlier. A) Crinoidal dolograinstone of Unit 1, Loc. A; arrow indicates a bivalve shell. B) Photo pairing illustrating difference between lithofacies inside channel (left) and outside channel (right) of Unit 2b, Loc. A. C) Calcite (yellow arrow) and mixture of calcite and barite (red arrow) precipitated along fracture of fine-grained Unit 3, Loc. A. D) Weakly laminated dolostone of Unit 5, Loc. A. E) Trough cross-lamination of Unit 1, Loc. B. F) Horizontal burrows (arrow) in fine-grained dolostone of Unit 2, Loc. C.

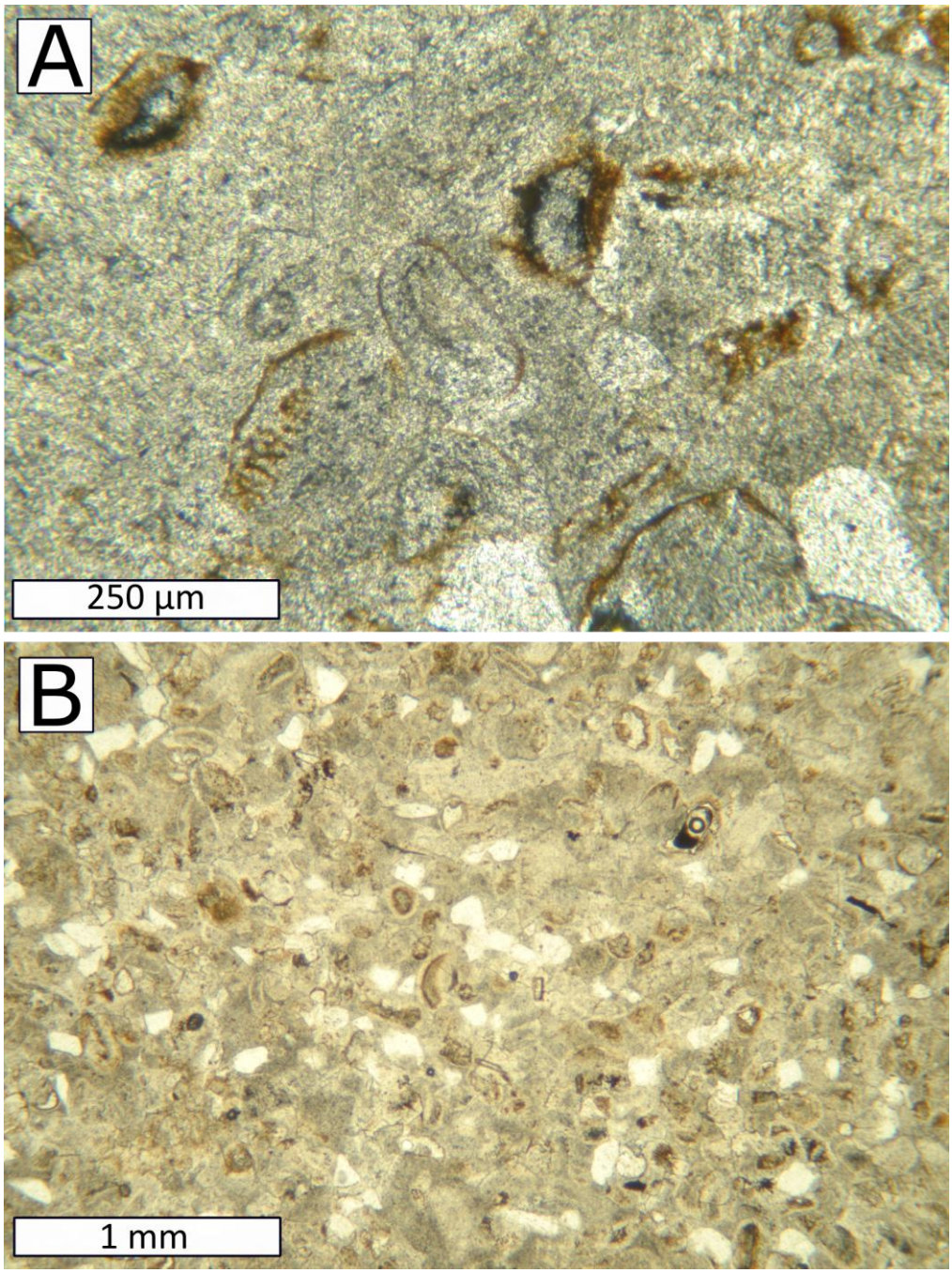

Figure 6.5. Thin-section photomicrograph of relic grains within dolostone in Owen Quarry outlier. A) In Units 1 and 2, Loc. A. B) In Unit 1, Loc. B.

the replaced circular grains were ooids, the paleofacies resembles lithofacies *SMF 15-C* of Flügel (2010), and characterizes high-energy oolitic-skeletal shoals along the margins and extending into the interiors of carbonate platforms (Ball et al., 1967). The thin interbedded siltstone layers document periods of carbonate production shut-down related to increased supply of fine-grained siliciclastics.

Unit 2

Description

Unit 2 is 81 cm thick, consisting of medium-bedded ooid-bearing coarsely crystalline dolostone. The unit contains three lithofacies associations (2a-2c, Fig. 6.3). The lowermost Unit 2a is 26 cm thick and contains dolograinstone with abundant fragments of bivalves, gastropods, trilobites, ostracodes, and crinoid ossicles. As in Unit 2a, there are beds with < 10% of fine-grained (80-150 μm) subrounded quartz and K-feldspar grains. In the upper part of Unit 2a, siliciclastic-bearing dolostone contains horizontally aligned grain fabric.

Unit 2b is 35 cm thick, and contains an oblique cross-section of a channel revealed by cross-bedded well-sorted coarsely crystalline (nonplanar, 150-2500 μm) dolograinstone (lithofacies D4b; Fig. 6.4B, left). The dolostone contains abundant fragmented crinoid ossicles and dolomite-replaced circular grains that may have been ooids. Dolostone beyond the channel's limits is finer-grained (nonplanar, 80-800 μm) and has a lower abundance of fossils but the same fossil types (Fig. 6.4B, right). Dolostone is composed of nonplanar, 150-2000 μm or planar-s, 150-300 μm fabric. There is only a

trace amount (~ 2%) of siliciclastics within the channel facies, much less than the content (~ 10%) beyond the channel's limits.

Unit 2c is a bioclastic dolorudstone (lithofacies D5) with large fragmented crinoid ossicles and minor tabulate coral colonies (Fig. 6.2C). Dolorudstone is composed of planar-s dolomite with crystals of 150-300 μm in size. Fossil fragments appear to decrease in size moving upsection. Unit 2c has a siliciclastic (quartz and K-feldspar) content (~ 8%) similar to the underlying unit.

Paleoenvironmental interpretation

Unit 2 is dominated by coarse-grained dolograinstone and dolorudstone representing original deposition in a shallow-water, stenohaline, high-energy subtidal environment. The abundance of crinoid ossicles demonstrates a normal-marine depositional environment (Flügel, 2010); the occurrence of tabulate corals refers to a warm-water, stenohaline environment (Flügel, 2010); and the likely original ooids indicate high-energy shoals along the margins and extending into the interiors of carbonate platforms (Ball et al., 1967). However, the minor amount of siliciclastics reveals that the depositional environment remained near a ready source of siliciclastics. Cross-bedded dolomite forming the channel in Unit 2b has a lithofacies similar to *Lithotype 7* of Brookfield and Brett (1988), related to migrating tidal sand bars or bioclastic dunes on an agitated shallow shelf.

Unit 3

Description

Unit 3 is at least 185 cm thick, with an upper limit defined by the base of a covered interval. The unit is composed of medium-bedded fine- to medium-crystalline dolostone with scarce fossil fragments (lithofacies D1a), but include crinoid ossicles and rugose coral fragments. The lower 0.5 m of Unit 3 contains a trace amount of siliciclastics, this fraction disappears higher in the unit. Dolomite crystalline mosaics define a planar-s fabric, with crystals of 40-250 μm in size. In the lower part of this unit, there is a local aggregation of vertical calcite microveins (Fig. 6.4C) that strikes 306°.

Paleoenvironmental interpretation

The relatively fine crystal size of dolomite may identify replacement of an original fine-grained limestone formed in a low-energy environment. Although fragments of crinoids and corals are present, their low abundance might indicate transport into a low-energy zone (see Deux Rivières outlier, Chapter 2). The initial very low siliciclastic content grading upsection to its absence denotes back-stepping of a siliciclastic source. The low abundance of crinoids in a likely deeper, more open-marine environment may suggest that only dense-fan crinoids are available within the craton interior region, which only live in high-energy, nearshore settings (Holterhoff, 1997).

Unit 4

Description

The interval occupied by Unit 4 has been greatly disrupted from blasting with disordered stacking of meter-scale blocks of interbedded dolostone and brown dolomitic claystone. There is, however, a small 25-cm thick exposure of *in situ* dolostone (from 4.05 m and 4.3 m) with an interbed of thin greenish brown claystone (lithofacies D1b). This exposure reveals that the blocks were part of a prominent interbedded dolostone/claystone stratigraphy. Based on the outcrop and blocks, dolostone beds are 10 to 20 cm thick, capped by brown dolomitic claystone. Abundant and superbly preserved trace fossils are associated with the dolostone-claystone boundaries.

Many of the blocks are fossil-bearing dolomudstone, composed of planar-s, fine-grained (40-160 μm) fabric with local fossil-rich layers. Fossils include fragmented to whole shells of brachiopods, gastropods, and crinoid ossicles; fragmented bryozoans; and abundant trace fossils (Fig. 6.6A). The intervening siltstone contains little skeletal fossil material. Claystone has the same mineral assemblage as that of Unit 1.

Three general types of trace fossil have been identified:

1) *Chondrites* isp.: branching shafts ~ 10 mm in diameter. One form (Fig. 6.6B) is similar to *Type A Chondrites* described by Pickerill et al. (1984) associated with Trentonian carbonates between Montreal and Quebec City;

2) *Palaeophycus* isp. (Fig. 6.6C): horizontal unbranched burrows passively filled with the same sediment as the surrounding matrix;

3) *Bergaueria* isp. (Fig. 6.6D): a cylindrical to hemispherical burrow fill. It has a circular to elliptical cross section and rounded base. *Bergaueria* normally display

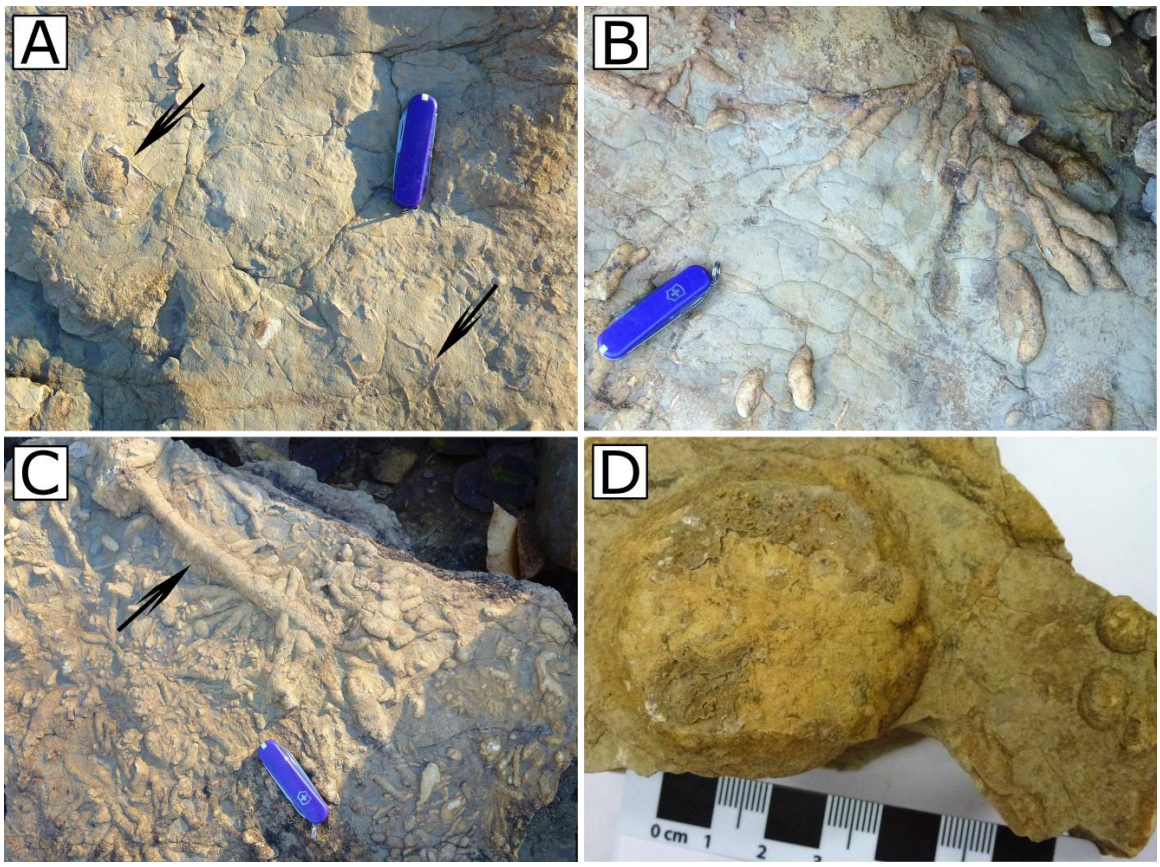

Figure 6.6. Field and hand specimen photos of Unit 4 of Loc. A, Owen Quarry outlier. A) Dolomudstone with scarce brachiopod whole shells (upper arrow) and fragmented bryozoan (lower arrow). B) Trace fossil *Chondrites* showing branching shafts. C) Trace fossil *Palaeophycus* (arrow). D) Trace fossil *Bergaueria* with two sizes. The knife for scale is 6 cm long.

diameters between 15 mm and 45 mm, and occur singly or in clusters (Alpert, 1973). In the Owen Quarry outlier, the example of *Bergaueria* display two diameters: 6 cm and 1 cm.

Paleoenvironmental interpretation

The common presence of crinoid ossicles within dolostone beds suggests a normal salinity during carbonate accumulation (Flügel, 2010). Therefore, the depositional condition for the dolostone is likely a stenohaline, subtidal environment with wave/tide activities. However, during inundation by clay-size siliciclastics, the environmental condition remains uncertain. Abundant trace fossils represent feeding/dwelling structures in response to increased abundance of organic material associated with the claystone. According to Bromley and Ekdale (1984), *Chondrites* isp. represents a complex deposit-feeding strategy, the burrows extending down into anaerobic sediment beneath oxygen-starved sea floors. *Palaeophycus* isp. is a dwelling burrow found in a wide range of environments from brackish-water to shoreface (Pemberton et al., 2001). *Bergaueria* isp. may represent a resting trace or dwelling burrow, and is a common element of the *Skolithos* ichnofacies that is indicative of normal-marine conditions on a wave- or tide-dominated shoreface (Pemberton et al., 2001).

A similar carbonate-claystone lithofacies suite has been recognized in northern New York State in the Trentonian Napanee to Sugar River formations, representing deeper water facies seaward of shoal systems (Cameron and Mangion, 1977). In the Kingston area, however, similar carbonate-siltstone interbeds are interpreted as storm-event beds of fossiliferous limestone separated by thin shaley beds that represent lower

rate of siliciclastic accumulation during intervals between storms (Narbonne and James, 2017).

Unit 5

Description

The uppermost unit (Unit 5) of Locality A is 160 cm thick, overlying the top of a covered interval representing Unit 4, and its upper surface being the present-day soil horizon. Unit 5 is composed of very hard thin-bedded, horizontally-laminated, medium-crystalline dolostone (lithofacies D1a; Fig. 6.4D). Dolomite crystalline mosaics are composed of planar-s fabric with fine- to coarse-grained (150-800 μm) crystals. Bedding planes are wavy, possibly reflecting stylolitic contacts or primary amalgamated beds. No skeletal fragments or internal sedimentary structures are evident. There is only a trace amount (< 1%) of subrounded quartz grains, 150-250 μm in size.

Paleoenvironmental interpretation

The crystalline dolostone provides no facies indicators allowing interpretation of a depositional setting.

6.2.2 Locality B

Locality B occurs a short distance (~ 20 m) from Loc. A but lateral continuity of strata is covered, and different stratal orientation suggests that it lies in fault contact with Loc. A. About 1.75 m of a poorly exposed succession of dolostone (Fig. 6.2D) is subdivided into two units based on lithology, fossil content, and sedimentary structures

(Fig. 6.3). The base of Locality B is 207 ±1 m above sea level. Locality B strata strike 296° and dip 20° to the northeast.

Unit 1

Description

This lower unit is 80 cm thick and composed of medium-bedded dolostone of fine- to medium-grained fabric (40-400 μm) (lithofacies D4c). The dolostone has horizontal lamination, inclined lamination, and trough cross-lamination (Fig. 6.4E). There is a relatively low abundance and diversity of benthic biota, including crinoid ossicles, bryozoans, brachiopods, bivalves, and ostracodes. There are abundant circular outliers of dolomite-replaced grains, possibly ooids (Fig. 6.5B), similar to those noted in the lower part of the section at Loc. A. The lower part of Unit 1 at Loc. B has relatively abundant (~ 40%) fine- to medium-grained (80-250 μm), subrounded quartz and K-feldspar grains, but siliciclastic content decreases to < 5% at the top of Unit 1.

Paleoenvironmental interpretation

Horizontal and inclined laminations indicate differential bedload transport and fluctuations in sedimentation conditions (Boggs, 2011). Trough cross-lamination can be produced by migration of dunes and ripples (Boggs, 2011). The common presence of crinoid ossicles indicates that the depositional environment is stenohaline (Flügel, 2010). Occurrence of siliciclastic grains, however, suggests a ready siliciclastic source near the depositional environment, but the importance of this source becomes diminished. This unit likely represents development of subtidal carbonate shoals with high-energy currents.

Unit 2

Description

Unit 2 is composed of coarsely crystalline dolostone with a nonplanar fabric, and crystal size ranges from 80 to1200 μm. Unit 2 appears to be massive and lacks obvious sedimentary structures. There are dolomite-replaced circular grains, interpreted as possible ooids, some crinoid ossicles, and disarticulated ostracode shells. Siliciclastic grains (quartz and K-feldspar) represent < 5% of the rock, 150-300 μm in size, subrounded to rounded.

Paleoenvironmental interpretation

Unit 2 displays a lower benthic biota abundance and diversity than that found in Unit 1, and may indicate a more restricted environment, with framework grains transported from an adjacent higher energy environment.

6.2.3 Locality C

Locality C is represented by a 3.7-m-thick exposure of a narrow vertical wedge of dolostone separated from an adjacent escarpment of Precambrian rocks by a narrow V-shaped gulley (Fig. 6.2E). The gulley is filled with gneissic boulders, gravel-size clasts of dolostone, and modern soil. The dolostone exposure is subdivided into two units based on lithology, fossil content, and sedimentary structures (Fig. 6.3). Locality C strata strike 310° and dip 10° to the northeast.

Unit 1

Description

This lower unit is 60 cm thick, and consists of massive finely crystalline dolostone (lithofacies D1a). There is scarce benthic material, probably fragmented rugose corals. Dolomite crystalline mosaics display a planar-s fabric, with crystal size between 80 and 250 μm. No siliciclastic grains are present.

Paleoenvironmental interpretation

If the abundance of finely crystalline dolostone reflects recrystallization of a finer-grained detrital component, then the host environment was of a low-energy depositional environment. However, there is little facies information to further interpret depositional conditions.

Unit 2

Description

Unit 2 consists of thinly-bedded to medium-bedded finely to medially crystalline dolostone (lithofacies D1a; Fig. 6.4F). Dolomite displays a planar-s fabric, with a greater size range of crystals, 80-400 μm, than that in Unit 1. There are abundant mm-scale horizontal burrows. No bioclasts or siliciclastic grains are present.

Paleoenvironmental interpretation

An abundance of horizontal borrows suggests a stable seafloor environment with available food source (MacEachern et al., 2010). A thin stratigraphic fabric suggests repetitive changes in depositional conditions, but no further interpretation is possible.

6.2.4 Stratigraphic relationship among Locs. A, B, and C

Although all sites contain dolostone, there are significant differences between Locs. A and B. At Loc. B, dolostone of Unit 1 contains up to 40% siliciclastic grains making this lithofacies a true mixed sediment not found anywhere in the succession at Loc. A. Evidence of horizontal and trough cross lamination in Unit 1 (Loc. B) is also absent in the lowermost unit of Loc. A. The stratigraphic succession at Loc. B also appears free of shale layers and bears less abundant benthic faunal fragments than rocks at Loc. A. The initial abundance of siliciclastics in Unit 1 (Loc. B) may indicate that this unit is older than Unit 1 (Loc. A), deposition having occurred within a more proximal position to a siliciclastic source. With transgression, siliciclastics were diminished in abundance and similarities in general lithologies become more apparent to Loc. A.

The above relative displacement is supported by GPS data that the base of Unit 1 (Loc. B) is ~ 6 m higher in elevation than the base of Unit 1 (Loc. A). As illustrated by the difference in bedding attributes between the two successions, a fault likely separates the two successions, and the sense of displacement is that Loc. A has moved vertically down relative to Loc. B given that Loc. A has lithofacies above those of Loc. B but at a lower elevation.

The dolomite texture, its hardness, and absence of fossils at Loc. C draw a comparison with Unit 5 of Loc. A. The base of Loc. C is ~ 6 m higher in elevation than the top of Loc. A, and has a different bedding attitude than Locs. A and B. Thus, a series of faults juxtapose the three dolostone localities. The succession at Loc. C lies faulted against the gneiss, the trace of the fault being a zone of weakness subsequently enhanced by erosion, forming the now present gulley. Succession at Locs. B and C are juxtaposed by a fault, now covered. And, as described above, Locs. A and B are structurally juxtaposed, the contact also covered. These faults characterize a NW-SE-oriented fault zone (Lumbers, 1971) with successive down-to-the-north displacement moving northeast away from the escarpment, itself the morphological expression of the Nipissing Fault forming a structural margin along the southern limit of the outlier (Lumbers, 1971).

6.2.5 Summary of depositional environments

Summary of depositional environments is in Fig. 6.3. Based on the above correlation among the three localities, the following depositional succession is interpreted. The lower 2 units of Locs. A and B represent a high-energy, stenohaline, subtidal environment with bioclastic-rich calcarenites, and presence of possible ooids. Loc. B strata demonstrate upsection loss of siliciclastics likely defining net transgression in a nearshore setting. Claystone intervals and prominent cross-section of a channel restricted to Loc. A may suggest periods of shut-down in carbonate production due to funnelling of siliciclastic fines focused along channel systems. Horizontal/inclined laminations and trough-cross lamination at Loc. B suggests a wave/storm-dominated environment. This

agrees with Brookfied and Brett's (1988) interpretation that similar lithofacies are linked to storm events.

Unit 3 of Loc. A is composed of fine-grained dolostone with very scarce fossils, and may represent a low-energy, more open-marine environment seaward of shoals. Unit 4 (Loc. A) is composed of heavily-burrowed carbonate with intervals of claystone indicating likely a stenohaline, subtidal environment related to storm events and intervals between storms in which siliciclastic accumulate (Narbonne and James, 2017). Burrowers occupied the seafloor during inter-storm periods. If correct, it suggests a possible deeper water setting, more distal to a cratonic siliciclastic source but adjacent to the seaward transition from carbonate to shale along the ramp. Trace fossils represent, collectively, a suite commonly associated with the *Cruziana* facies, usually positioned below fair-weather wave base (MacEachern et al., 2010).

Unit 5 of Loc. A and its possible lateral equivalent unit at Loc. C document reappearance of only dolostone. If dolomite replacement reflects the precursor limestone grain size, it denotes a possibly low energy setting.

6.3 Stratigraphic indicators and age of outlier

Conodonts

From samples of Unit 1 (Loc. A) four conodont species were recovered (McCracken, 2017). Species of stratigraphic significance include *Drepanoistodus suberectus* (Branson & Mehl), *Plectodina aculeata* (Stauffer), *Curtognathus* sp., and *Erismodus* sp.. The probable age ranges from *Plectodina aculeata* to *Plectodina tenuis*

zones of the Mid-Continent succession. This is equivalent to the Laurentian Blackriveran to Kirkfieldian stages (Table 1.1).

Macrofossils

Several macrofossils identified by the author from Unit 4 have biostratigraphic significance. The brachiopod *Dinorthis iphigenia media?* (or *minor?*) (Fig. 6.7A) suggests an age no older than the Rockland Formation of eastern Ontario (Wilson, 1946a). The ostracode *Eoleperditia fabulites* Conrad (Fig. 6.7B) was recovered from Blackriveran-Rocklandian strata across the mid-west USA and Ontario (Berdan, 1984). The rugose coral *Lambeophyllum profundum* (Conrad) (Fig. 6.7C) that is fairly common throughout Loc. A, occurs in Lowville through Rockland strata in eastern Ontario (Wilson, 1948). The cryptostomid bryozoan *Escharopora recta* Hall (Fig. 6.7D) was recovered from Unit 2, and suggests an age range equivalent to the Watertown to Hull strata of New York State (Ross, 1964). Based on macrofossils only, the succession likely straddles the Blackriveran-Trentonian boundary.

Colquhoun (1958) identified many more macrofossils from this outlier (see Appendix 2) but, unfortunately, without mentioning a stratigraphic position. His data, taxonomically updated, show that the entire fossil assemblage in the Owen Quarry outlier is mostly similar to that of the Rockland Formation in eastern Ontario.

$\delta^{13}C$ chemostratigraphic profile

$\delta^{13}C$ and $\delta^{18}O$ values of dolomicrite, or the finest size fraction available in a given unit, were determined from the section at Loc. A to generate a chemostratigraphic section

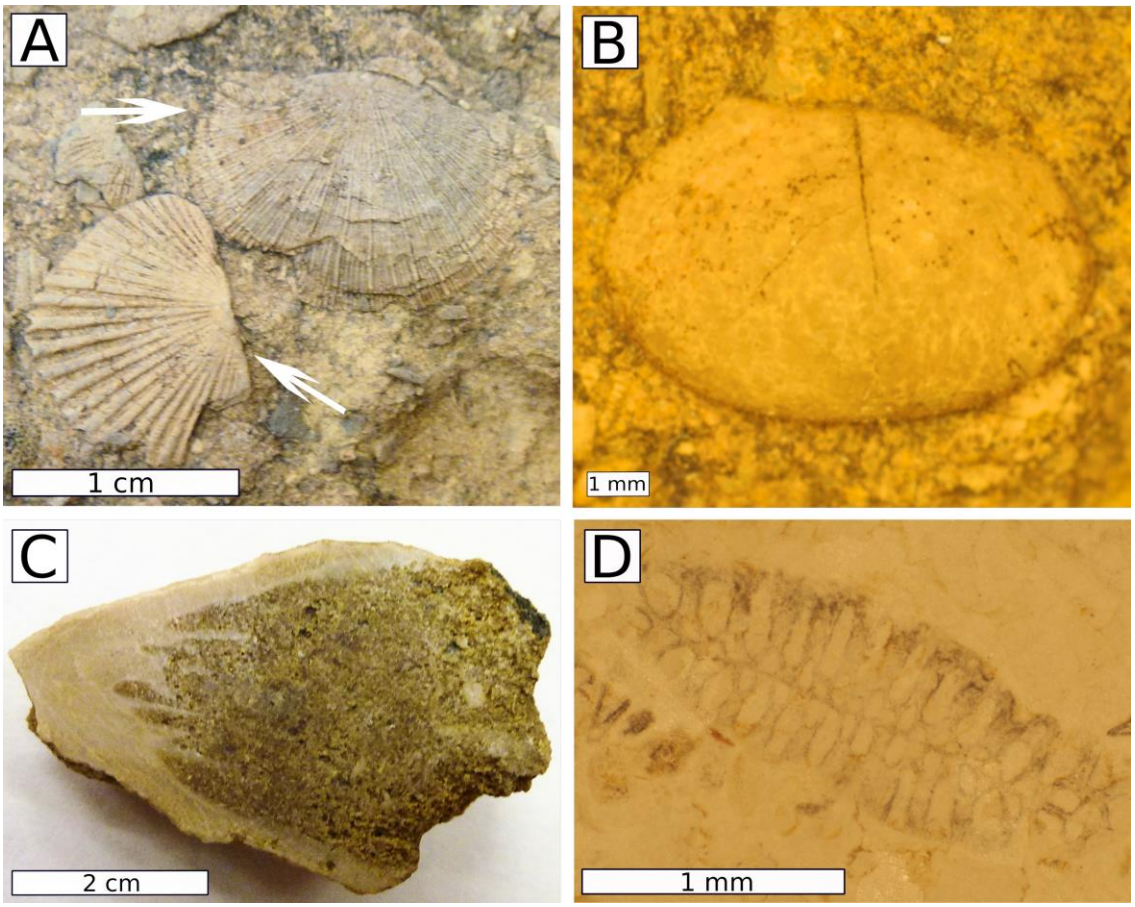

Figure 6.7. Critical macrofossils of the Owen Quarry outlier. A) Brachiopods *Dinorthis Iphigenia media*? (*minor*?) (lower arrow) and *Rafinesquina* sp. (upper arrow). B) Ostracode *Eoleperditia fabulites* Conrad. C) Rugose coral *Lambeophyllum profundum* (Conrad). D) Bryozoan *Escharopora recta* Hall.

(Fig. 6.3). $\delta^{13}C$ values range from 0.15‰ to 2.7‰ VPDB. Values are highest in the lower 3 meters, between 1.4‰ and 2.7‰, and decreases to close to 0‰ in the upper 5 meters. The basal 3 m may record the upsection tail of a positive excursion. If correct, an excursion may arise from two controls. First, it may reflect local water mass chemistry associated with rapid burial of organic matter related to transgression across the Precambrian surface. During Sr-isotope sample preparation, dissolution yielded a visually distinctive amount of organic material. A second control may be regional to global, part of the Guttenberg $\delta^{13}C$ excursion (GICE) well-documented across Northern America (Bergström et al., 2010). In both scenarios, however, the ultimate control is related to changing isotopic signature of seawater bicarbonate related to changes in the mass balance of organic carbon versus inorganic carbon related to burial of organic carbon and erosion of exposed limestone. ^{12}C is preferentially removed from seawater through incorporation into organic matter during biological metabolism. Burial of organic matter, rather than recycling through oxidation, promotes increase in seawater $\delta^{13}C$.

In North America, the GICE first appears in the upper *P. undatus* zone, and ends in the upper *P. tenuis* Zones (Young et al., 2005; Barta et al., 2007; Bergström et al., 2010). Specifically, in New York State, the GICE is present in the Napanee to lower Kings Falls formations; in southern Ontario, it occurs in the middle to upper Bobcaygeon Formation in Ontario (Barta et al., 2007); and in eastern Ontario, it has been documented from the Rockland and Hull formations (N. Oruche, Carleton University, written communication). In New York State and Ontario, the baseline $\delta^{13}C$ values are ~ 1‰ in pre-excursion strata; $\delta^{13}C$ approaches ~ 3‰ in the excursion peak; and post-excursion values are between 0‰ and 1‰ (Barta et al., 2007; Bergström et al., 2010). In cratonic

sections of North America, the GICE interval is generally ~ 5-10 meters thick (Bergström et al., 2010).

According to McCracken (2017), the conodont assemblage of Unit 1 (Loc. A) in the Owen Quarry may indicate an age as late as lower *P. tenuis* Zone, thus within the early GICE. Conodont analysis, macrofossil data, and $\delta^{13}C$ chemostratigraphy appear to fit together suggesting that the basal positive $\delta^{13}C$ excursion discovered in the Owen Quarry succession is part of the GICE. If correct, strata are equivalent to the upper Napanee/lower Hull formations of eastern Ontario (Barta et al., 2007).

6.4 Diagenesis

6.4.1 Introduction

Petrographic evidence suggests that the dolostone section in the Owen Quarry outlier represents a precursor limestone succession thoroughly dolomitized. Dolomite crystalline mosaics are cross-cut by bedding-parallel stylolites that indicates a minimum burial depth of 600 m (Machel, 2004). Several stages of dolomitization are recognized, and both calcite and barite are mineral phases that follow dolomitization. Faulting offsets all dolomitic units, and represents a diagenetic event prior to or after dolomitization. Fig. 6.8 illustrates the interpreted relative timing of diagenetic features.

6.4.2 Petrographic attributes

Dolostone

Five types of dolomite are recognized in the Owen Quarry outlier, their textural attributes are summarized in Table 2.3. The earliest stage of dolomitization is planar-p

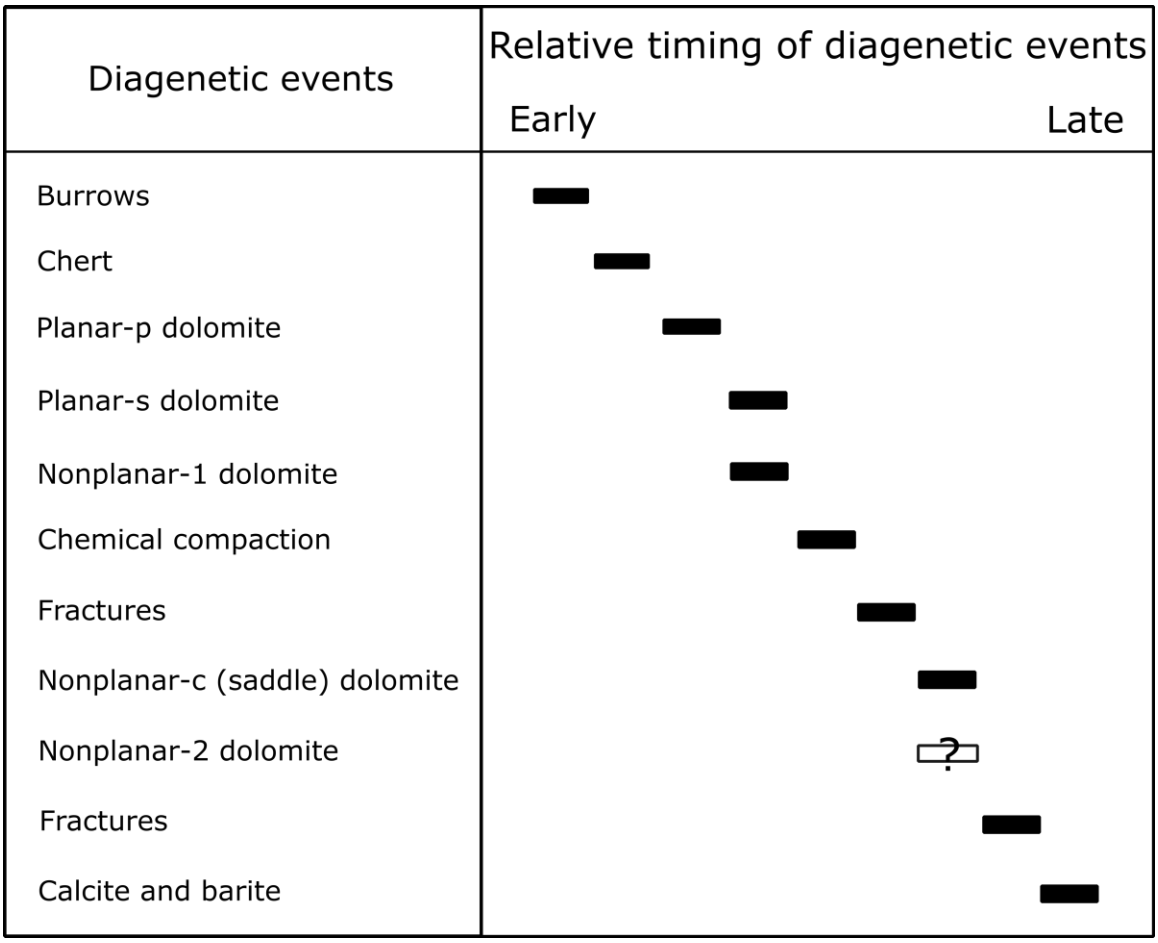

Figure 6.8. Diagenetic events and their relative timing within the Owen Quarry outlier. Based on petrographic and geochemistry study of samples.

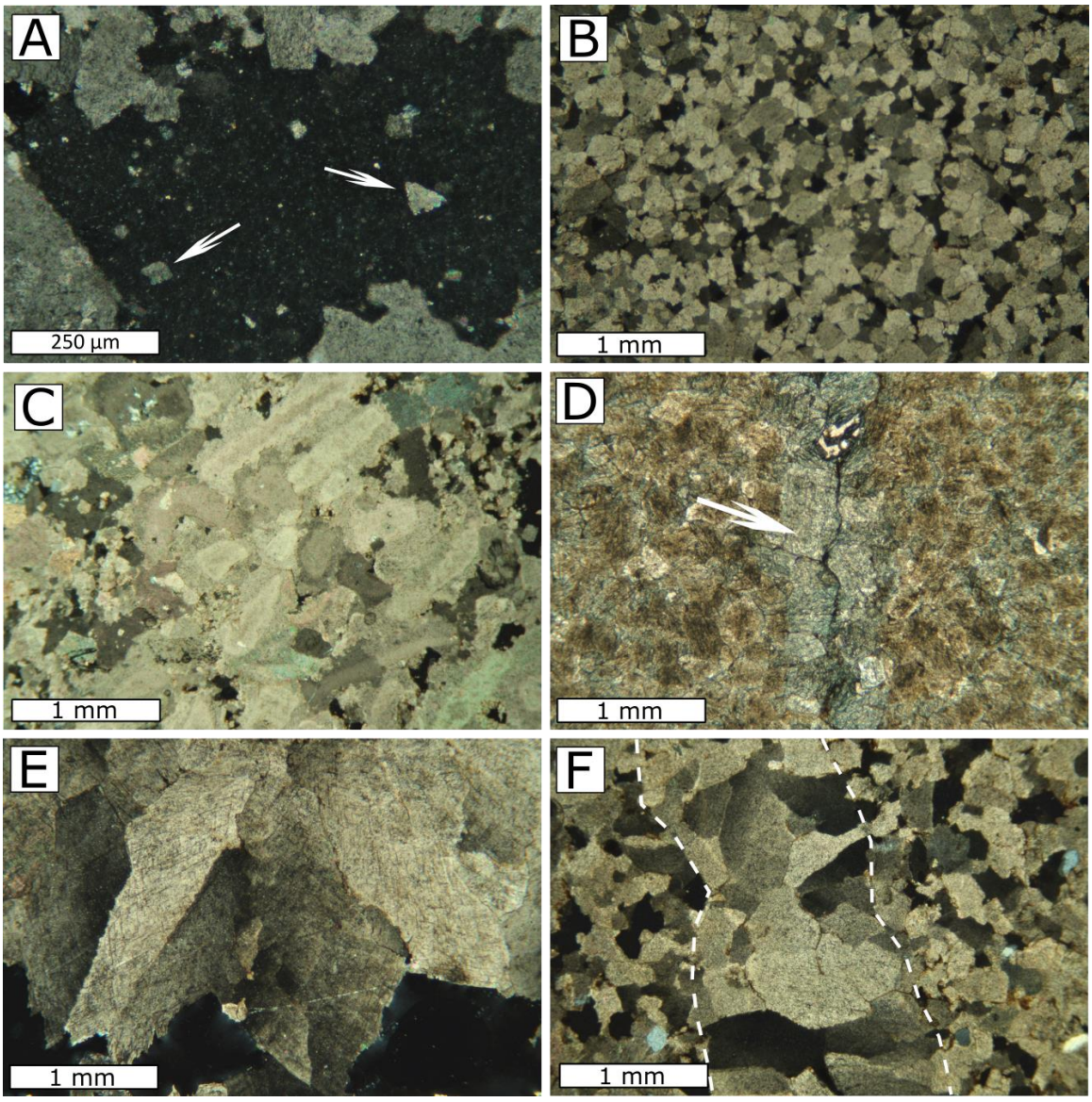

Figure 6.9. Thin-section photomicrographs of dolomite types of the Owen Quarry outlier. Pictures A-C and E-F are taken under cross-polarized light, D is plane-polarized light image of stained thin section. A) Planar-p dolomite within nonplanar-1 dolomite grains. B) Planar-s dolomite. C) Coarse-grained, nonplanar-1 dolomite replaces crinoid ossicles and bryozoans. D) Nonplanar-2 dolomite precipitates along fracture (arrows) and crystal boundary of planar-s dolomite grains, showing brighter blue color. E) Nonplanar-c (saddle) dolomite precipitates in paleovoid and shows sweeping extinction. F) Nonplanar-c dolomite precipitates along fractures.

dolomite that occurs as scattered, euhedral, fine to medium sand-size rhombs within coarser anhedral dolomite (Fig. 6.9A).

Planar-s dolomite has a crystal size ranging from 40 to 400 μm (Fig.6.9B), but typically characterizes the finer-crystalline dolostone. Dolomite crystals are non-luminescent.

Three types of nonplanar dolomite are present at Owen Quarry. Nonplanar-1 dolomite is finely to coarsely crystalline (80-2000 μm), but characterizes the coarser crystalline lithofacies. Dolomite crystals often form syntaxial growth around crinoid ossicles (Fig. 6.9C). Nonplanar-1 dolomite replaces locally silicified coral fragments and detrital quartz and feldspar grains in Unit 1 (Loc. A). Dolomite crystals are non-luminescent.

Nonplanar-2 dolomite precipitates within fractures or forms overgrowths (rims) of earlier dolomite crystals (Fig. 6.9D). In fractures, crystals are 200-500 μm in size. Based on stained thin-sections, nonplanar-2 dolomite has an elevated Fe content. Nonplanar-2 dolomite is also non-luminescent.

Saddle (nonplanar-c) dolomite crystals fill paleomolds and fractures (Fig. 6.9E, F), and have a milky white color (Fig. 6.4A) in hand specimen. This dolomite displays sweeping extinction under cross-polarized light, evidence that it is a form of saddle dolomite (Spötl and Pitman, 1998). Dolomite crystals are non-luminescent.

Calcite and barite

Calcite forms veins (Fig. 6.4C) and microveins (Fig. 6.10A, B), occupies intercrystalline void space in dolomite mosaics (Fig. 6.10C), and fills paleovoid space

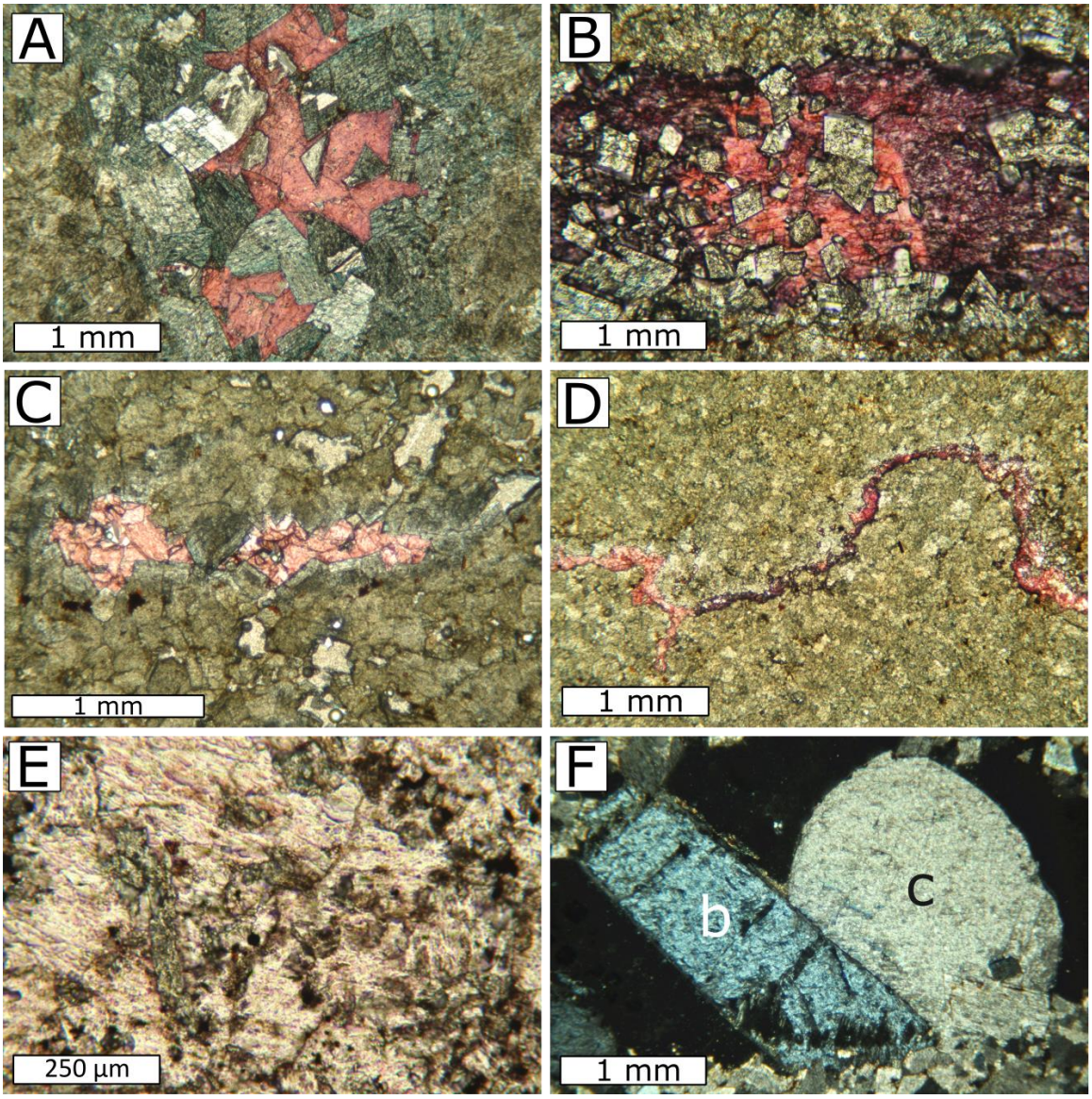

Figure 6.10. Thin-section photomicrograph of calcite and barite in Owen Quarry outlier. Photos A-E are plane-polarized image of stained thin sections. Photo E is cross-polarized image. A) Calcite grows along the fracture and causes dissolution of dolomite grains. B) Calcite composition changes during precipitation as shown by difference in staining color (pink and purple). C) Calcite precipitated in intergranular void space of dolomite. D) Calcite precipitated in dissolved stylolite. E) Anhedral barite grains (light blue) precipitated along with large calcite grains (pink). F) Euhedral barite (b) grows with calcite (c) in paleovoid.

developed along stylolites (Fig. 6.10D). Calcite crystals are equigranular, and 240 μm to 1 cm in size. Calcite-dolomite (planar-s) contacts are erosional, indicating dolomite dissolution prior to or during migration of Ca-bearing fluids. Dedolomitization of planar-s dolomite produces dolomite crystals "floating" within calcite crystalline mosaic. Stained thin-section illustrates alternating Fe-poor and ferroan calcite (Fig. 6.10B). Veins of calcite cross-cut saddle dolomite veins, calcite also precipitates in intercrystalline void space of saddle dolomite. Calcite crystals have an orange luminescence.

Barite forms a co-precipitate with calcite. Two types of barite crystals are present in strata at Loc. A. Type 1 (Fig. 6.10E) forms irregular or needle-shape crystals, 40-160 μm long, within vein calcite. Type 2 (Fig. 6.10F) forms large (2400 μm in length, 800 μm in width) prismatic crystals in moldic paleovoid space. Barite crystals are non-luminescent.

Stylolites

Bedding-parallel and bedding-oblique stylolites are present. The former possesses wavy and anastomosing wispy geometries. Wavy stylolites are associated with finely crystalline dolostone of Loc. A, but have been subject to dissolution, the paleovoid space filled with calcite cement. Anastomosing geometries develop in finely crystalline dolostone of Loc. C and are associated with Fe-oxide. In contrast, seismic stylolites occur oblique to bedding planes, and occur in the sand-rich, coarsely crystalline dolostone near the bottom of Loc. A that may be related to lateral compressional pressure gradients.

6.4.3 Geochemistry

Major and minor elements

Dolomite

Major and minor elemental compositions of dolomite, determined using electron microprobe, are provided in Table 6.2. Back-scattered imaging illustrates no grey-scale difference between planar-s and nonplanar-1 dolomite, suggesting homogeneous composition. Planar-s dolomite ($Ca_{49-51}Mg_{42-49}Fe_{01-07}$) is Fe-bearing and with very low Mn, Ba, and Sr content. The Fe content of planar-s dolomite increases from < 2 mol % in Unit 1 to > 4 mol % in Unit 5.

Nonplanar-1 dolomite ($Ca_{49-51}Mg_{43-47}Fe_{03-07}$) is also ferroan and has similar Mn, Ba, and Sr content as planar-s-1 dolomite. In non-porous zones, Fe content is relatively uniform through the succession. In porous zones, dolomite crystals tend to have clear rims that have $FeCO_3$ up to 2.5 mol % higher than cores (Fig. 6.11A).

Nonplanar-2 dolomite ($Ca_{50}Mg_{41-45}Fe_{04-08}$) is the most Fe-rich dolomite type in the outlier, and has relatively higher Mn content. Composition of nonplanar-2 dolomite varies within a microvein (Fig. 6.11B) with Fe content higher along the margin (6.8-8.1 mol %) than in the vein (4.7 mol %). Nonplanar-2 dolomite also forms a ~ 10 μm thick Fe-rich coating on planar-s dolomite crystals (Fig. 6.11C).

Nonplanar-c dolomite ($Ca_{48-51}Mg_{42-48}Fe_{02-07}$) displays no significant difference in elemental composition compared to planar-s and nonplanar-1 dolomite in the same stratigraphic unit. However, along void space margins, crystals show zones of varying Fe content (Fig. 6.11D). $FeCO_3$ increases from 2.8 mol % in the crystal core to 6.7 mol % in its rim.

Minerals	$CaCO_3$	$MgCO_3$	$FeCO_3$	$MnCO_3$	$BaCO_3$	$SrCO_3$
Dolomite						
Planar-s dolomite						
Loc. A						
Unit 2b	49.29%	48.81%	1.72%	0.18%	n.d. *	n.d.
Dedolomite, center, Unit 4	49.77%	45.53%	4.26%	0.44%	n.d.	n.d.
Dedolomite, rim, Unit 4	50.80%	41.88%	6.58%	0.73%	n.d.	n.d.
Dedolomite, rim, Unit 4	50.36%	43.29%	5.80%	0.53%	0.03%	n.d.
Unit 4	51.35%	45.57%	2.80%	0.26%	0.02%	n.d.
Unit 4	50.74%	44.45%	4.48%	0.33%	n.d.	n.d.
Unit 4	50.12%	45.67%	3.87%	0.34%	n.d.	n.d.
Near stylolite, Unit5	50.16%	44.53%	4.86%	0.41%	0.04%	n.d.
Unit 5	49.74%	45.32%	4.63%	0.30%	n.d.	n.d.
Porous, Unit 5	49.63%	45.02%	4.97%	0.38%	n.d.	n.d.
Loc. C						
Cloudy core, Unit 1	50.24%	47.69%	1.81%	0.26%	n.d.	n.d.
Unit 1	50.03%	47.61%	2.12%	0.23%	n.d.	n.d.
Nonplanar-1 dolomite						
Loc. A						
Porous, center, Unit 1	50.04%	46.84%	2.82%	0.30%	0.01%	n.d.
Porous, rim, Unit 1	49.64%	44.31%	5.27%	0.77%	0.01%	n.d.
Unit 1	50.29%	45.63%	3.74%	0.33%	0.01%	n.d.
Fe-rich band, Unit 1	50.02%	43.86%	5.50%	0.60%	0.02%	n.d.
Porous, unit 2b	49.99%	44.24%	5.14%	0.59%	0.04%	n.d.
Rim, unit 2b	49.85%	44.67%	4.91%	0.56%	0.01%	n.d.
Unit 2b	50.12%	46.32%	3.18%	0.37%	n.d.%	n.d.
Unit 2c	49.68%	45.81%	4.15%	0.36%	0.01%	n.d.
Porous, rim, Unit 2c	50.21%	43.53%	5.49%	0.75%	0.02%	n.d.
Porous, rim, Unit 2c	49.84%	43.08%	6.53%	0.55%	n.d.	n.d.
Unit 3	50.10%	45.76%	3.68%	0.45%	0.01%	n.d.
Loc. B						
Cloudy core, Unit 1	50.41%	45.75%	3.52%	0.32%	n.d.%	n.d.
Clear rim, Unit 1	49.83%	45.91%	3.92%	0.33%	0.02%	n.d.
Nonplanar-2 dolomite						
Loc. B						
Unit 1	50.09%	40.94%	8.20%	0.76%	0.01%	n.d.
Loc. C						

Vein, Unit 1	49.92%	42.57%	6.77%	0.74%	0.01%	n.d.
Vein, Unit 1	49.81%	44.91%	4.72%	0.55%	0.01%	n.d.
Vein, Unit 1	49.92%	41.16%	8.07%	0.85%	n.d.	n.d.
Crystal overgrowth, Unit 1	50.16%	42.34%	6.80%	0.69%	n.d.	n.d.
Nonplanar-c dolomite						
Loc. A						
Unit 2c	48.00%	47.39%	4.19%	0.41%	0.01%	n.d.
Unit 3	50.16%	45.13%	4.19%	0.52%	n.d.	n.d.
Rim, Unit 4	50.53%	43.20%	5.74%	0.53%	0.01%	n.d.
Rim, Unit 4	50.31%	45.04%	4.30%	0.33%	0.01%	n.d.
Rim, Unit 4	50.54%	42.53%	6.30%	0.62%	n.d.	n.d.
Cloudy center, Unit 4	50.10%	46.84%	2.77%	0.28%	0.01%	n.d.
Calcite						
Loc. A						
Unit 4	97.87%	0.61%	0.36%	1.11%	0.05%	n.d.
Unit 4	95.92%	0.93%	0.06%	3.03%	0.04%	0.02%
Unit 4	97.99%	0.36%	0.26%	1.36%	0.04%	n.d.
Unit 4	98.78%	0.28%	0.19%	0.74%	n.d.	n.d.
Unit 4	99.77%	0.01%	0.04%	0.17%	n.d.	n.d.
Barite						
Unit 3 (Loc. A)	1.09%	0.49%	0.25%	n.d.	94.53%	3.63%

* n.d. = not detected

Table 6.2. Major and minor elemental composition of dolomite, calcite, and barite in the Owen Quarry outlier. Values are illustrated in molecular percentage.

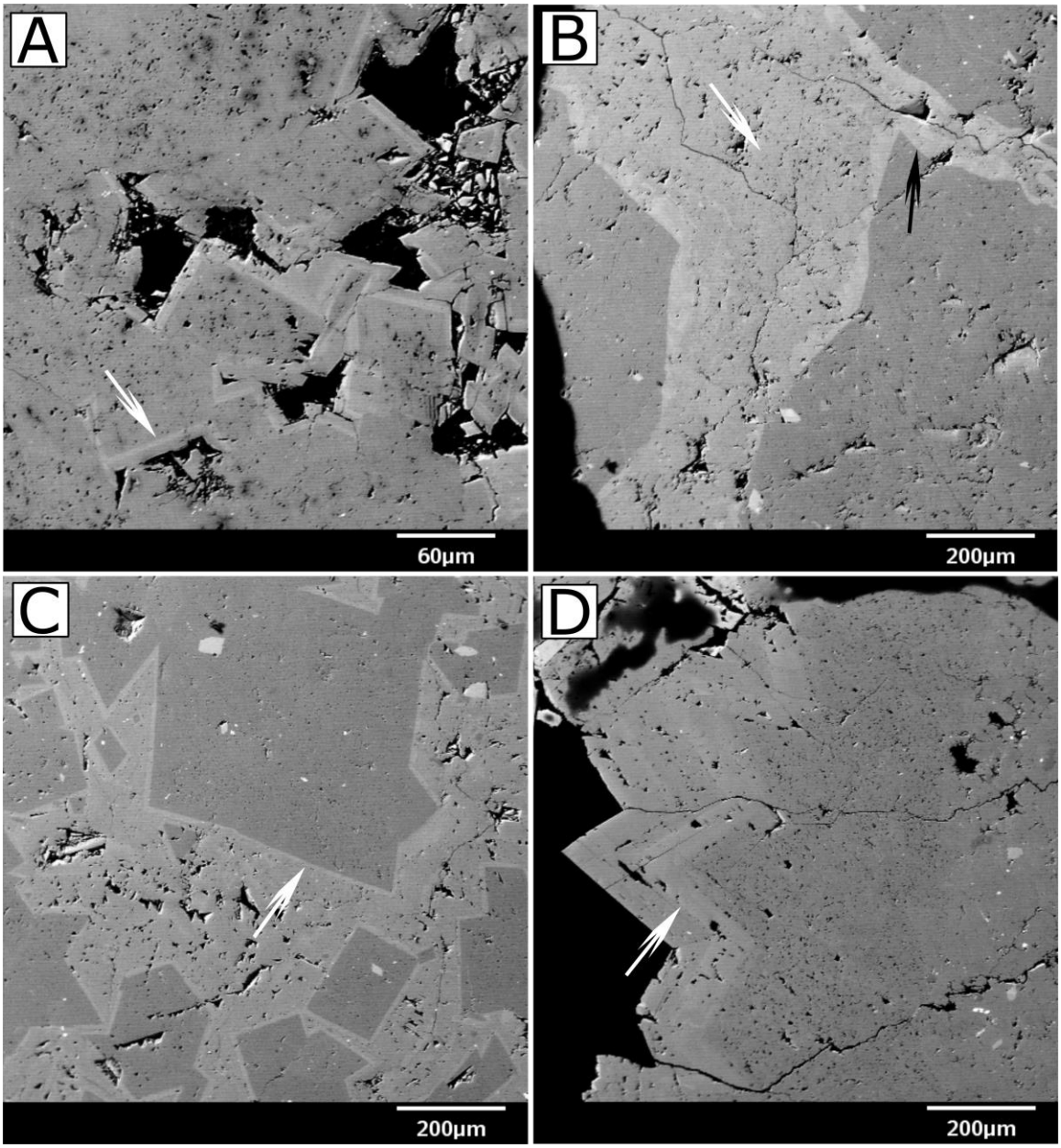

Figure 6.11. Back-scattered images of dolomite types in the Owen Quarry outlier. A) Fe-rich rim (arrow) of porous nonplanar-1 dolomite. B) Nonplanar-2 dolomite precipitated along a triple fracture; Fe content is highest along the edge (black arrow) and lower in the center (white arrow). C) Fe-rich nonplanar-2 dolomite precipitated along the surface (arrow) of planar-s dolomite grains. D) Compositional zonation of nonplanar-c dolomite, which has Fe-rich rim (arrow).

Calcite and Barite

Elemental compositions are provided in Table 6.2. Calcite ($Ca_{96-99}Mn_{00-03}$) occurs in intercrystalline void space within dolomite, and has very low Mg (0.1-0.9 mol %) and Fe (0-0.4 mol %) contents. Very pure calcite (99.77 mol % $CaCO_3$) is associated with void space in Unit 4, Loc. A. One large euhedral barite crystal was analyzed for elemental composition; its mineral composition is $Ba_{95}Sr_{03}Ca_{01}$.

Stable (C, O) isotopes

Dolomite

C and O isotope ratios of dolomite and calcite were determined and shown in Fig. 6.3. $\delta^{13}C$ values of planar-s and nonplanar-1 dolomites were summarized in previous section. $\delta^{13}C$ value of nonplanar-c dolomite doesn't follow the trend of the dolostone matrix above the carbon-isotope excursion peak, but remains relatively steady (1.4-2.6‰ VPDB) bracketing ~ 2‰. The relatively stable $\delta^{13}C$ value of nonplanar-c dolomite suggests that a similar fluid composition from which saddle dolomite precipitated had invaded the entire succession. In contrast, nonplanar-2 dolomite has a very low $\delta^{13}C$ value (-2‰ VPDB).

Planar-s, nonplanar-1, and nonplanar-c dolomites have similar $\delta^{18}O$ values: planar-s (-10.1 to -11.6‰ VPDB), nonplanar-1 (-10.1 to -10.9‰ VPDB), and nonplanar-c (-10.1 to -11.4‰ VPDB). Nonplanar-2 dolomite has a more positive $\delta^{18}O$ value (-9.7‰ VPDB). As with previous interpretations of fluid sources related to the other outliers (see previous chapters), possible solutions combining seawater source, elevated temperature, or meteoric-derived fluid are examined here (Fig. 6.12). If dolomite precipitated from

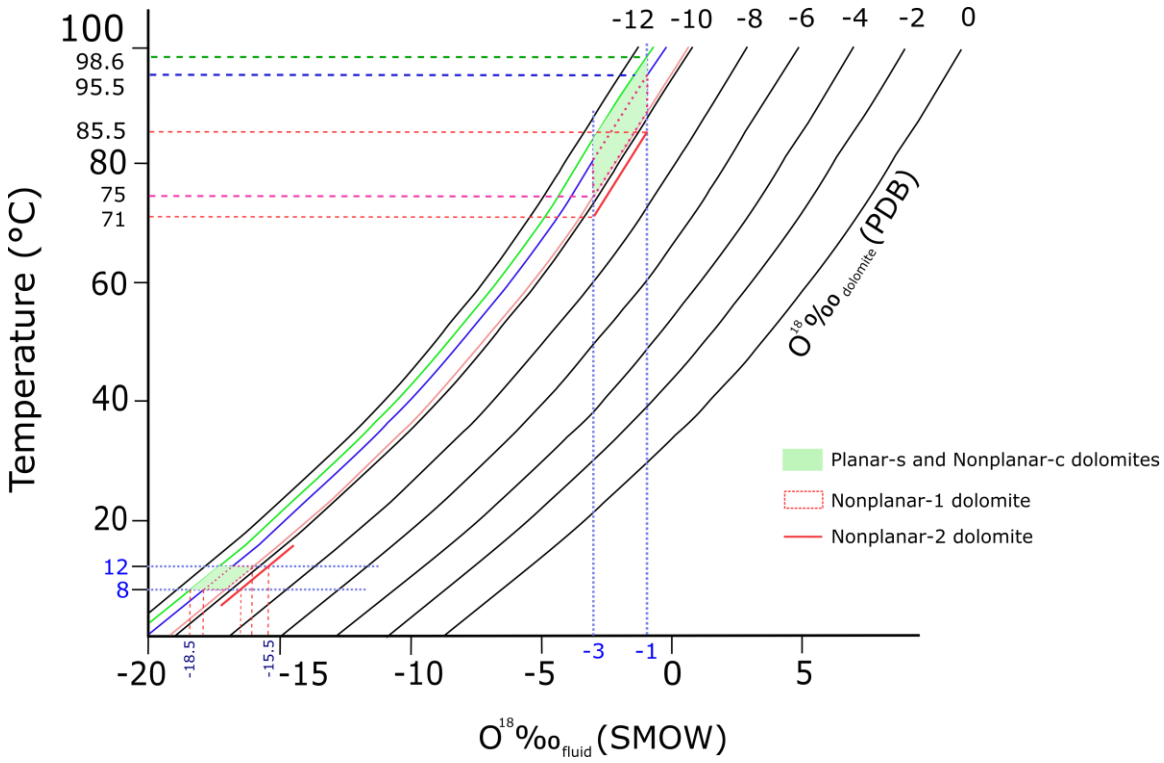

Figure 6.12. Estimated formation temperature and fluid $\delta^{18}O$ value of Dolomite types of Owen Quarry outlier. The plot is modified after Nurkhanuly (2012), whose values are calculated using the equation: $10^3 \ln \alpha = 3.2 \times 10^2 T^{-2} - 3.3$ (Land, 1983).

Late Ordovician seawater ($\delta^{18}O$ value: -1‰ to -3‰ SMOW), then the estimated formation temperature using the fractionation equation of Land (1983) reveals nearly similar ranges, from 71 to ~ 99°C, with nonplanar-2 dolomite precipitated at temperature that is about 4 to 13°C lower than other dolomite types. Using an interpreted seawater temperature of 8 to 12°C for depositional conditions during accumulation of the Late Ordovician of Bobcaygeon and Verulam formations in southern Ontario (Brookfield, 1988), the diagenetic fluid of dolomite types mentioned above should have a $\delta^{18}O$ value of -15.5 to -18.5‰ SMOW.

Calcite

The purest calcite analyzed has a $\delta^{13}C$ value of -7.46‰ VPDB and $\delta^{18}O$ value of -8.48‰ VPDB. Calcite precipitated with barite tends to have a more negative $\delta^{13}C$ value (-11.8‰ VPDB) yet a similar $\delta^{18}O$ value.

Strontium isotopes

Strontium isotope ratios of four types of dolomite and calcite were determined (Fig. 6.13). Values of planar-s, nonplanar-1, and nonplanar-c dolomites are illustrated in terms of their stratigraphic distribution (Fig. 6.3). Two samples of nonplanar-c dolomite show relatively consistent (0.7087-0.7089) ratios that are distinctly different from those of planar-s and nonplanar-1 dolomites in the same bed (Fig. 6.3). Due to the difficulty of sampling nonplanar-2 dolomite, the value may reflect a mixture of nonplanar-2 dolomite and the planar-s dolomite matrix. Nonplanar-2 dolomite has a $^{87}Sr/^{86}Sr$ value of 0.70856,

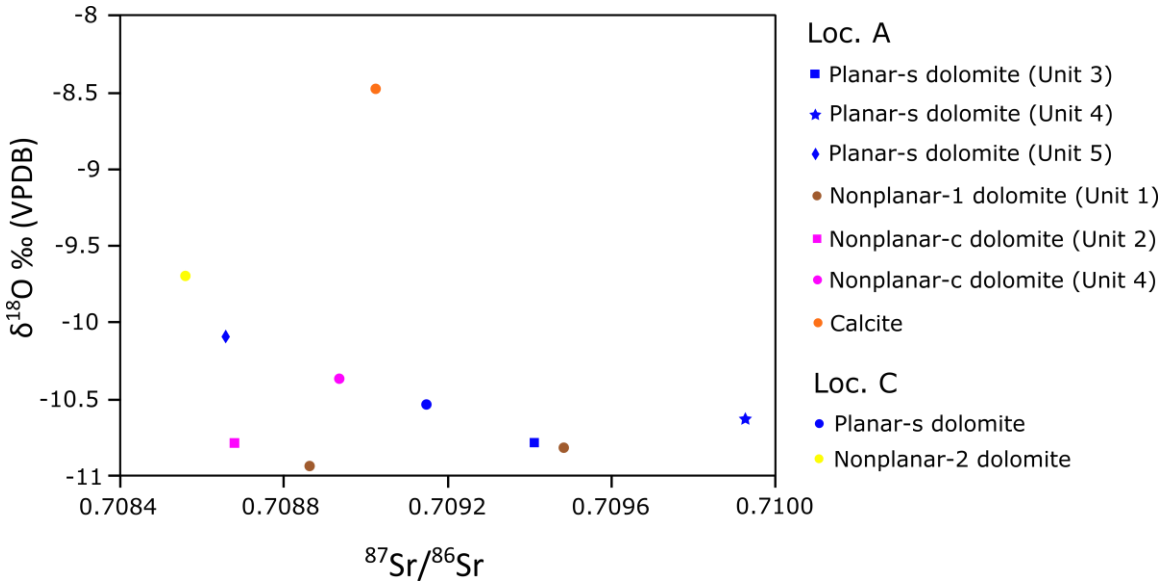

Figure 6.13. $^{87}Sr/^{86}Sr$-$\delta^{18}O$ plot of dolomite and calcite at Owen Quarry outlier.

which is the lowest among all dolomite types and is significantly lower than that of planar-s dolomite in the same unit (Fig. 6.13).

All dolomite samples measured have much higher $^{87}Sr/^{86}Sr$ values than Chatfieldian seawater (0.7079 to 0.70797; Edwards et al., 2015). An elevated ratio can represent interaction of fluid with siliciclastics, and especially fine-grained siliciclastics (Simo et al., 1994) such as those associated with Units 1 and 4 (Loc. A). In addition, fluid interaction with Precambrian gneisses will generate radiogenic ratios. Previous work measuring the Sr-isotope ratios of granitic and gneissic rocks of the Grenville orogen produced a range above 0.7200 (Davis et al., 1968; Krogh and Davis, 1969). A sample of granitic gneiss was collected from along the basement escarpment near the Owen Quarry outlier, and yielded a $^{87}Sr/^{86}Sr$ value of 0.7619.

Artificially decrepitated fluid inclusions

No fluid inclusion greater than 1-2 microns were noted. However, an experiment was carried out to identify fluid chemistry in these small inclusions. A fresh-fractured surface of a crystal mosaic of nonplanar-1 dolomite from Unit 2c (Loc. A) was analyzed by SEM to see if any evaporated deposits formed adjacent to inclusion cavities. Qualitative energy-dispersive X-ray spectroscopy (Fig. 6.14) illustrated that one such evaporated deposit produced an Mg-Ca-Cl spectrum. When compared to analysis of the adjacent dolomite, the energy peaks of Mg and Ca in the evaporated deposit were distinctly higher and a Cl peak was present. This illustrates that the evaporite contains all of these elements and the diagenetic fluid was a Mg-Ca-Cl brine.

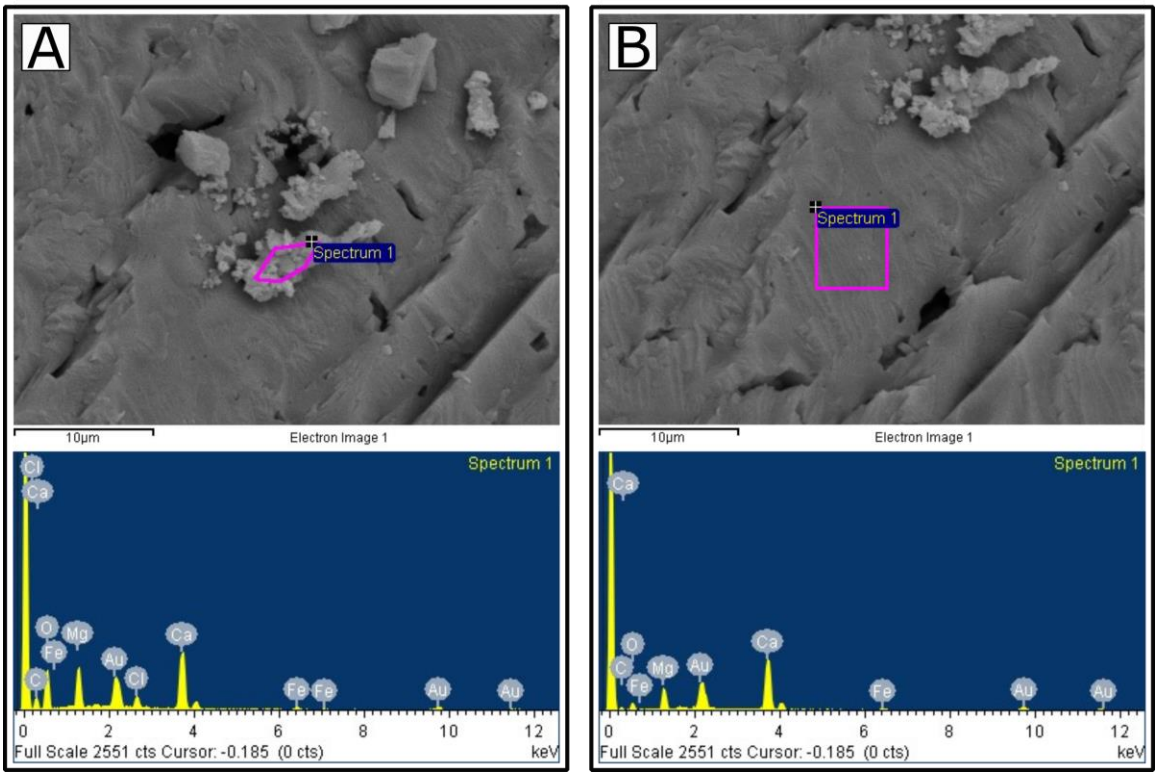

Figure 6.14. SEM-EDS analysis of fluid inclusion of dolomite in Owen Quarry outlier. A) Fluid inclusion suggested by presence of Chlorine. B) Nonplanar-1 dolomite grains; upper: secondary electron photomicrograph, lower: energy-dispersive X-ray spectroscopy.

6.4.4 Discussion

The initial stage of dolomitization is represented by planar-p dolomite, later likely replaced by planar-s and nonplanar-1 dolomite. $\delta^{13}C$ values of these dolomites fall within the range of Late Ordovician marine calcite, indicating that any recrystallization of limestone involved recycling the marine carbonate source. Differences in crystal size and texture may be related to the grain size of the precursor limestone. Planar-s and nonplanar-1 dolomites are cross-cut by stylolites, suggesting that they formed at a burial depth of less than 600 meters. A conodont color alteration index (CAI) for Unit 1 is 1.5 (McCracken, 2017). This suggests a maximum burial temperature of no more than 60°C (Legall et al., 1981).

On the basis of $\delta^{18}O$ values, planar-s and nonplanar-1 dolomites formed at temperature higher than 75°C if the fluid source was seawater or marine-derived fluids. This temperature discrepancy can be explained through the presence of nonplanar-c dolomite. Its petrographic habit defines saddle dolomite, and forms microveins that cross-cut earlier dolomites, and fills available intercrystalline pore space within these crystalline mosaics. Saddle dolomite is indicative of hydrothermal dolomitization, with formation requiring minimum temperature of 60-80°C (Spötl and Pitman, 1998). The calculated formation temperature (75-99°C) accommodates this if a marine-modified fluid was the source. Thus, sampling of planar-s and nonplanar-1 dolomites very likely involved either incorporation of rims of nonplanar-c dolomite (due to crystal size versus sampling tool), or the later dolomite recrystallized the precursor dolomite under higher temperature; evidence being similar $\delta^{18}O$ values among planar-s, nonplanar-1, and nonplanar-c dolomites.

As suggested by Davies and Smith (2006), hydrothermal dolomite in Upper Ordovician successions of New York State precipitated from $MgCl_2$-$CaCl_2$-NaCl-H_2O fluids interpreted to be likely marine-modified basinal brines. This appears to be in agreement with SEM analysis of an artificially decrepitated inclusion in nonplanar-1 dolomite. The interaction of dolomitizing fluids with either siliciclastics or basement rocks yields their radiogenic $^{87}Sr/^{86}Sr$ values. $^{87}Sr/^{86}Sr$ value of nonplanar-c dolomite is slightly higher in the clay-rich Unit 4, suggesting elevated ^{87}Sr likely absorbed onto clay particles. Nonplanar-c dolomite is Fe-bearing, with Fe-rich crystal rims. The likely source of Fe in diagenetic fluid is from the Precambrian basement that has abundant mafic minerals. Of interest, however, there is evidence of a ferruginization event influencing rocks exposed locally along the Precambrian escarpment. This may form a source of additional iron reworked by diagenetic fluids.

The amount of nonplanar-2 dolomite is very limited in the Owen Quarry outlier, and forms thin veins and rims of overgrowth on planar-s dolomite crystals. Fluids producing nonplanar-2 dolomite were likely fracture-related, then migrated into the adjacent host dolostone related to available intercrystalline permeability.

Calcite precipitated in remaining intercrystalline pores in dolomite is texturally and isotopically similar to the Upper Ordovician “late calcite” in the Manitoulin Island area studied by Coniglio et al. (1994). They interpreted that the pore water bicarbonate was affected by an organic carbon source, from bacterial or thermochemical sulphate reduction. Sulphate reduction is supported by the co-precipitation of barite and calcite: biogenic barium can be remobilized by sulphate reduction; afterwards, authigenic barite precipitates (Torres et al., 1996).

Chapter 7 Discussion

7.1 Regional correlation

The five outliers examined in this study lie within the Laurentian craton interior and, collectively, are well separated (~ 170 to ~ 300 km) from the erosional northern limit of the regional St. Lawrence Platform of the Appalachian Basin (southern Ontario) to the south; the Ottawa Embayment to the southeast; and, the northeastern erosional limit of the Michigan Basin to the southwest (Fig. 1.1). Comparing stratigraphy and depositional facies amongst the outliers with those of the regional platform successions that underlie these latter geologic basins enables improved understanding of cratonic patterns of transgression, structural development, and diagenetic systems.

Deux Rivières outlier

The Deux Rivières outlier is interpreted to be of Turinian age. Conodont data from Unit 5 and lithofacies of Unit 6 identify a likely correlation of the upper part of this outlier with the Blackriveran Watertown or Coboconk strata in southern and eastern Ontario (see Chapter 2).

A $\delta^{13}C$ profile through the outlier suggests that there may be a strong correlation with chemostratigraphic variation in the succession of Stewart Quarry (Rockland, eastern Ontario) in the Ottawa Embayment (N. Oruche, Carleton University, written communication; Fig. 7.1A). The lower 5 units of the outlier display a $\delta^{13}C$ profile similar to that associated with the uppermost Pamelia to Lowville formations of Stewart

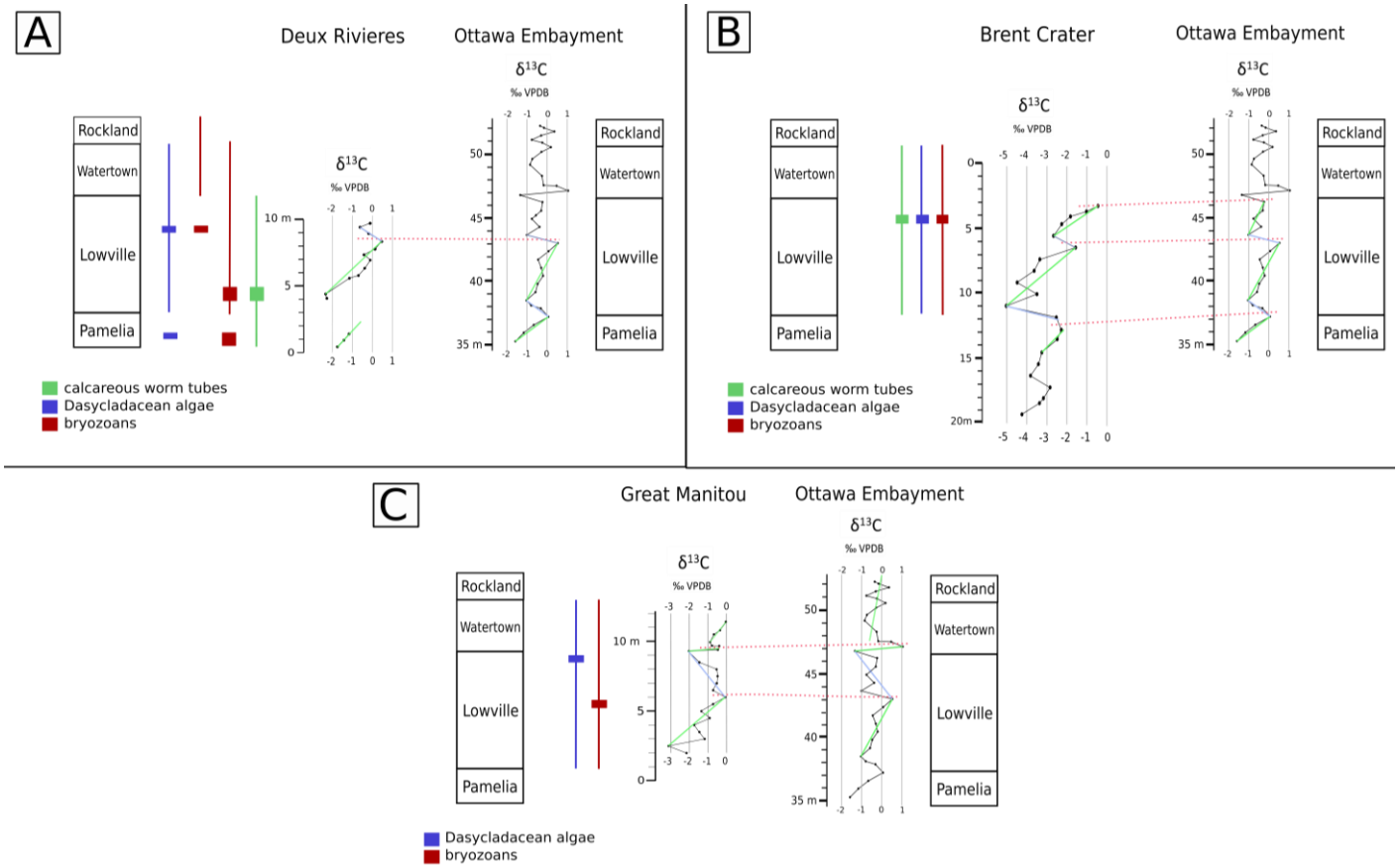

Figure 7.1. Correlation of $\delta^{13}C$ profiles and biostratigraphic indicators. The $\delta^{13}C$ profile of Ottawa Embayment (upper Pamelia to lower Rockland interval, Stewart Quarry) is unpublished data of Nkechi Oruche's PhD research. Colored rectangles represent stratigraphic distribution of fossils in studied outliers, whereas colored vertical lines represent known age range of the fossils elsewhere in eastern/southern Ontario and northern New York State. A) Deux Rivières outlier, B) Brent Crater sedimentary fill (upper 20 m), and C) Great Manitou Island section.

Quarry. The relatively long range of fossil types supports the general association of the outlier to the Blackriveran succession in the Ottawa Embayment (Fig. 7.1A and see also Chapter 2).

If the chemostratigraphic and macrofossil age determination is correct, then the silty/sandy dolostone of Units 1a-1b of the outlier may be equivalent to silty dolostone that characterize the uppermost lower Gull River Formation in the Lake Simcoe area (El Gadi, 2001) and upper Pamelia Formation of the Ottawa Embayment (Salad Hersi, 1997) (Fig. 7.2).

Following above correlation, the prominent arenite (Unit 2) in the outlier does not have an obvious equivalent unit in the St. Lawrence Platform. However, of significance, the boundary separating Pamelia and Lowville strata in eastern Ontario, southern Ontario, and New York State is a well-defined disconformity (Young, 1943; Cornell, 2001). In the Kingston area, for example, the boundary is an obvious paleokarst (G.R. Dix, verbal communication) denoting at least local uplift and dissolution. Correlation of $\delta^{13}C$ profile of the Deux Rivières outlier suggests that the Pamelia-Lowville boundary likely lies within the feldspathic arenite interval of Unit 2. If associated with regional uplift, the arenite of the Deux Rivières outlier may be a local craton-interior record of restricted transport of siliciclastics whereas in a paleoseaward direction only exposure and dissolution dominated. For example, the lowermost part of the Timiskaming outlier succession to the north is represented by thick interval of sandstone (Russel, 1984) that may be of similar age, and can act as a distant siliciclastic source of detrital grains in the Deux Rivières outlier. Again, the analogy with the Yates Formation (Permian, west Texas, New Mexico; see Chapter 2) remains a very reliable comparison.

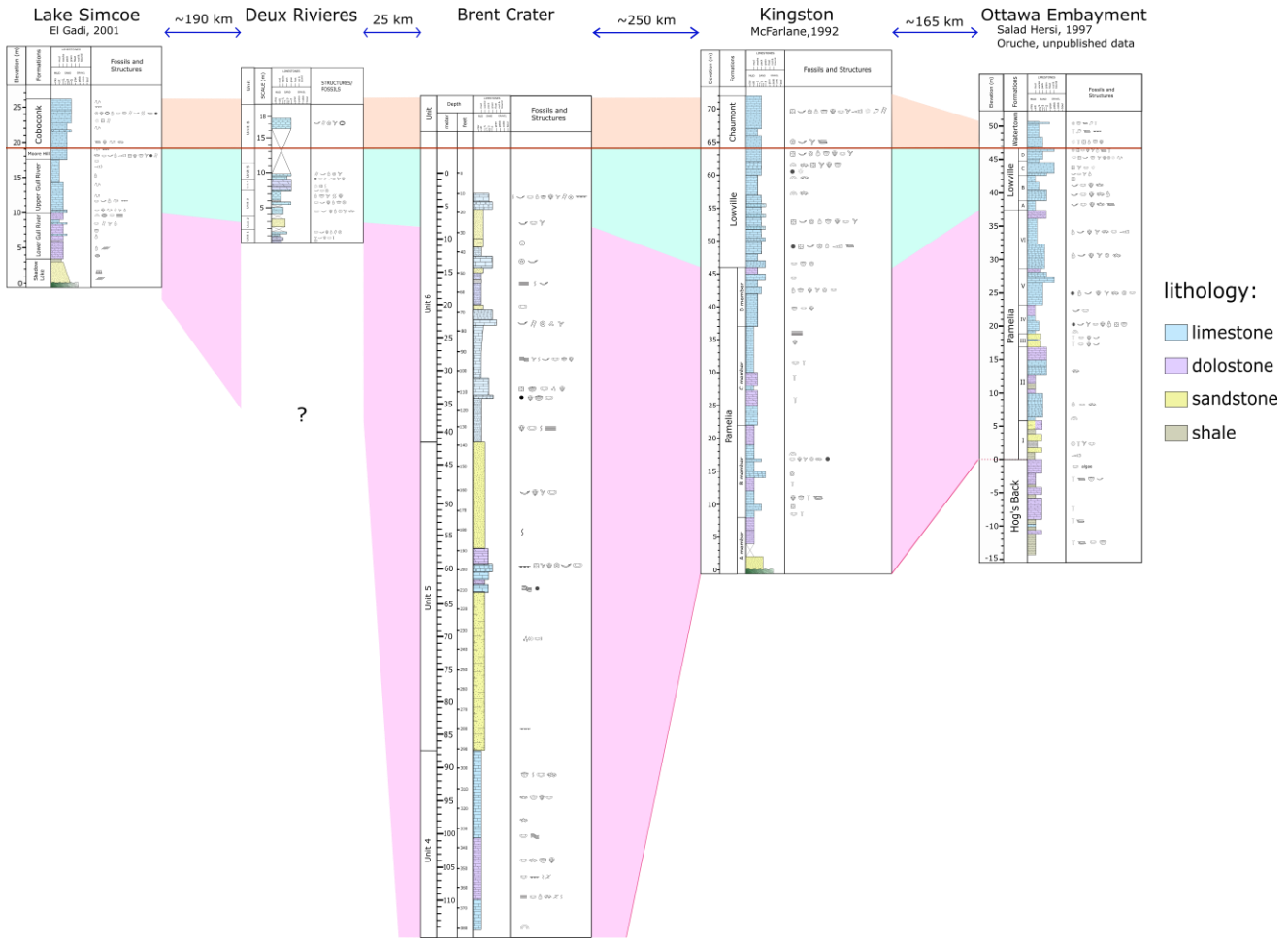

Figure 7.2. Regional correlation among Deux Rivières outlier, Brent Crater sedimentary fill, Lake Simcoe area, Kingston area, and Ottawa Embayment. Purple zone represents Pamelia (Shadow Lake + lower Gull River) Formation; blue zone represents Lowville (Upper Gull River) Formation; orange zone represents Chaumont (Coboconk) Formation. The red line across all columns is correlation datum represented by the Lowville-Chaumont (upper Gull River-Coboconk) Formation boundary.

Brent Crater outlier

Grahn and Ormö (1995) interpreted all of the Brent Crater sedimentary fill to be of Turinian age. This relies heavily on the presence and accurate taxonomy of fragmented chitinozoans in the lowermost sedimentary section. The stratigraphic affiliation is certainly supported for the upper part (Units 4 to 6) of the core with the occurrence of calcareous worm tubes *Tymbochoos sinclairi* Okulitch that identifies an equivalency with the Pamelia-Lowville succession of eastern Ontario. Unit 6 shows high orders of facies variations, with carbonate rocks deposited in nearshore to subtidal settings, and arenite intervals that suggest periods of relatively low sea level. However, due to limited core logging time and amount of sampled rocks, it is hard to confidently identify shallowing or deepening upward cycles.

A $\delta^{13}C$ profile through the upper 20 m of the of Brent Crater sedimentary succession is compared with strata of Ottawa Embayment. $\delta^{13}C$ correlation shows that the upper 20 m of the Brent succession are age-equivalent to the Pamelia-Lowville interval, and this correlation is also supported by biostratigraphic indicators (Fig. 7.1B). The presence of local ooid beds and absence of facies typical of Watertown/Coboconk Formation suggests the uppermost Brent succession remains equivalent to usually higher-energy Lowville Formation of eastern Ontario (Salad Hersi, 1997). The Pamelia-Lowville boundary suggested by $\delta^{13}C$ profile likely lies near the arenite interval of Unit 6d, which seems to be consistent with the regional disconformity along the Pamelia-Lowville boundary in New York State and eastern/southern Ontario (Young, 1943; Cornell, 2001).

Compared to the regional St. Lawrence platform in the Ottawa Embayment and Appalachian Basins, the Brent Crater succession contains an anomalously thick (~ 250 m)

equivalent succession. For example, Units 4-6b correspond to the Pamelia-Lowville succession of eastern Ontario but are 2-3 times the thickness of the latter, and this difference is even greater with respect to equivalent strata in the Lake Simcoe region that onlap the Precambrian interior (Grimwood et al, 1999; El Gadi, 2001) (Fig. 7.2). Part of the anomaly is attributed by a combined 39 m of sandstone (Units 5a, 5c) not found in these latter regions. In large marine impact structures in otherwise tectonically quiescent regions, sediment deposition can be controlled by local basement instability for several to tens of millions of years after impact before returning control to eustatic influence (Whalen et al., 2013). Rapid subsidence, but with sustained matching sedimentation rates, may explain the presence of the lower (Units 1-3) Brent succession that cannot be obviously correlated with strata along the regional platforms to the south.

Cedar Lake outlier

The Cedar Lake outlier is ~ 3 km south of the southern rim of Brent Crater. On the basis of lithology alone, the feldspathic arenite of Unit 1 at Cedar Lake is similar to Unit 5b of the Brent Crater succession. Limited exposure and absence of stratigraphically significant fossils in the Cedar Lake outlier preclude a well-defined regional correlation with other outliers or the St. Lawrence Platform.

Manitou Islands outlier

There are slight differences in lithofacies associations between the successions underlying Great and Little Manitou islands. This is probably due to difference in paleo-topography across a differentially eroded crystalline basement (see Chapter 5). In

addition, compared to other outliers, the initial setting is clearly more proximal to shore, forming a sandy to rocky nearshore environment.

On macrofossil assemblages alone, previous work (Colquhoun, 1958) suggested that the Manitou Islands sections were correlated with lower Trentonian (Rockland) strata. Discovery of the bryozoan *Stictopora labyrinthica tabulata* Ross, however, suggests a Blackriveran affiliation. Lithostratigraphic correlation with Turinian successions in the Lake Simcoe area (El Gadi, 2001) and northern limit of the Michigan Basin (Great La Cloche Island, Manitoulin Island area; Noor, 1989) regions may help to resolve this. Unfortunately, the Manitou Islands sections contain stratigraphically restricted distribution of dolostone, much of it being fabric destructive. Thus, poor preservation of original depositional attributes adds to the difficulty of lithic correlation.

In the Lake Simcoe area, the Blackriveran section contains three formations: Shadow Lake, Gull River, and Coboconk. The Shadow Lake Formation is characterized by conglomerate, sandstone, and siltstone that are deposited in transgressive nearshore-sabkha environments (Melchin, 1994; Grimwood et al., 1999). Unit 1 of Great and Little Manitou islands represents an equivalent lithofacies but wherein the basal bivalve-bearing sandy facies likely was subject to a greater influence of marine reworking. In central Ontario, the transition from lower to upper Gull River Formation strata reveals net transgression: from peritidal through subtidal conditions; from low benthic diversity in dolostone and lime mudstone of the lower Gull River Formation, through higher benthic diversity of the upper Gull River Formation, to fossiliferous wackestone through grainstone of the Coboconk Formation (Melchin, 1994; Grimwood et al., 1999; El Gadi, 2001).

The Manitou Islands sections reveal increased fossil diversity and abundance upsection, a similar transition from nearshore to subtidal settings. Units 2-3 of Great Manitou Island exhibit similar lithofacies to the lower Gull River Formation in the Lake Simcoe area and Gull River Formation in the Manitoulin Island area. Unit 4 shows greater lithofacies similarity to the upper Gull River Formation in the Lake Simcoe area. The Manitou Islands successions, however, do not have lithofacies similar to the Coboconk or Watertown Formation in southern and eastern Ontario, such as found at the Deux Rivières outlier (Unit 6). But this may reflect local influence on sedimentary facies.

$\delta^{13}C$ profiles assist in regional correlation. The preferred correlation of the Great Manitou Island section with the Ottawa Embayment succession is with the Lowville-lower Watertown interval, and this is supported by biostratigraphic indicators (Fig. 7.1C).

Owen Quarry outlier

Conodont data from Unit 1 (Loc. A) coupled with a ^{13}C profile (see Fig. 6.3) suggest that the entire stratigraphic interval may contain the post-peak portion of the local GICE record (see Chapter 6 for more review). This denotes an age equivalent to the lower Trentonian succession of southern/eastern Ontario and New York State (see Chapter 6), and draws obvious age comparison with the middle and upper Bobcaygeon Formation of southern Ontario and Rockland and Hull formations of the Ottawa Embayment (Table 1.1).

In southern Ontario, the middle Bobcaygeon Formation is a very distinctive unit consisting of peloidal wacke/pack/grainstone with prominent interbedded thin shale (Melchin et al., 1994). In Ottawa Embayment, the Rockland Formation has a similar

limestone-shale stratigraphic fabric, quite distinctive from succession beneath and overlying this interval. Thus, while the interbedded fabric in the Owen Quarry outlier could be a product of a local depositional system, this fabric defining Units 1-2 bear a striking similarity with lithofacies fabrics of the middle Bobcaygeon and Rockland formations in the Appalachian Basin and Ottawa Embayment, respectively. The interbedded claystone and fossiliferous limestone of Unit 4 (Loc. A) has not been recognized in any other outliers, but being similar to the Kirkfield Formation in southern Ontario (Melchin et al., 1994) and the Kings Fall Formation in the northern New York State (Cameron and Mangion, 1977), which is supported by the interval's overlap with the tail-end of the regional (North American) GICE peak.

Summary of regional correlation

In general, correlation of the five outliers with the St. Lawrence Platform to the south and southeast, and Michigan Basin to the southwest reveals that there was a relatively strong stratigraphic connectivity supporting previous interpretations that the crater-interior was once buried beneath a relatively continuous cover of Upper Ordovician strata (e.g. Hume, 1925; Caley and Liberty, 1957). However, this present study also reveals local variations in lithofacies patterns:

1. With regional transgression, some outliers (Deux Rivières and Brent Crater) document higher order controls (of indeterminate origins) were superimposed on net transgression across the craton interior.
2. Differences in lithofacies among interpreted contemporary outlier successions represent local spatial controls, especially basement paleotopography.

3. The Brent Crater succession is instrumental in illustrating how initial local basement tectonic instability (related to a meteoric impact), rapid subsidence, and basin fill (Units 1-3) could occur over a relatively small area within the craton interior. This initial local difference disappeared such that the record of regional transgression (Units 4-6) with superimposed higher-order patterns of changing accommodation space.

7.2 Preservation of Ordovician outliers

In general, among the five studied outliers, only the Owen Quarry outlier shows preservation of Trentonian (Chatfieldian) strata. Other outliers have uppermost strata that predate the Black River-Trenton boundary. Differential preservation of Late Ordovician strata along the OBG is common and has been considered a result of significant post-Ordovician erosion and offset across high-angle faults (Wilson, 1946b; Bleeker et al., 2011).

Two such controls are obvious: 1) most of the outliers (Manitou Islands, Owen Quarry, Brent Crater, and Cedar Lake) are in the center of the OBG, along the depression bounded by normal faults of the graben (Fig. 7.3A). 2) the Owen Quarry succession is clearly spatially associated with down-to-north faults peripheral to a regional graben fault defined by the escarpment of Precambrian rock (Lumbers, 1971). The presence of potential normal faults (Fig. 7.3B) is consistent with occurrence of vertical calcite/dolomite microveins, suggesting local extensional tectonism. 3) the Brent Crater succession represents local subsidence creating a significantly thick sedimentary repository compared to elsewhere along the craton-interior (Fig. 7.3C).

The Deux Rivières outlier is associated with one fault that defines its uplifted northwestern limit and another within the outlier itself that may extend across the Ottawa River. This latter fault represents a stress-relief feature separating slight variation in structural dip created during the local uplift of the stratigraphic succession. Today, the outlier is a local topographically elevated feature, but does lie lower than Precambrian basement exposed farther south and north of the river. Thus, although the Ordovician strata are locally uplifted, the outlier itself lies within a structural low.

For the Manitou Islands sections, lithostratigraphic correlation suggests that at least two faults cross-cut the sedimentary succession on Little Manitou Island and strata underlying both islands display gentle dips suggesting post-lithification movement. The preservation of the Manitou Islands sections may relate more with their spatial position within the core of the graben: the north and south structural limits of the graben form prominent escarpments (the north being a ski hill) in North Bay and the south bounds Lake Nipissing (Fig. 7.3A). In addition, the orientation of the islands and preserved Ordovician strata clearly reflects the influence of the rim of the underlying Neoproterozoic syenitic intrusion.

The Cedar Lake outlier is fault-bounded on the south according to Ontario Geological Survey (2011), suggesting down-fault preservation of sedimentary rocks. Regional topographic map also shows that this outlier has lower elevation than basement rock surrounding it.

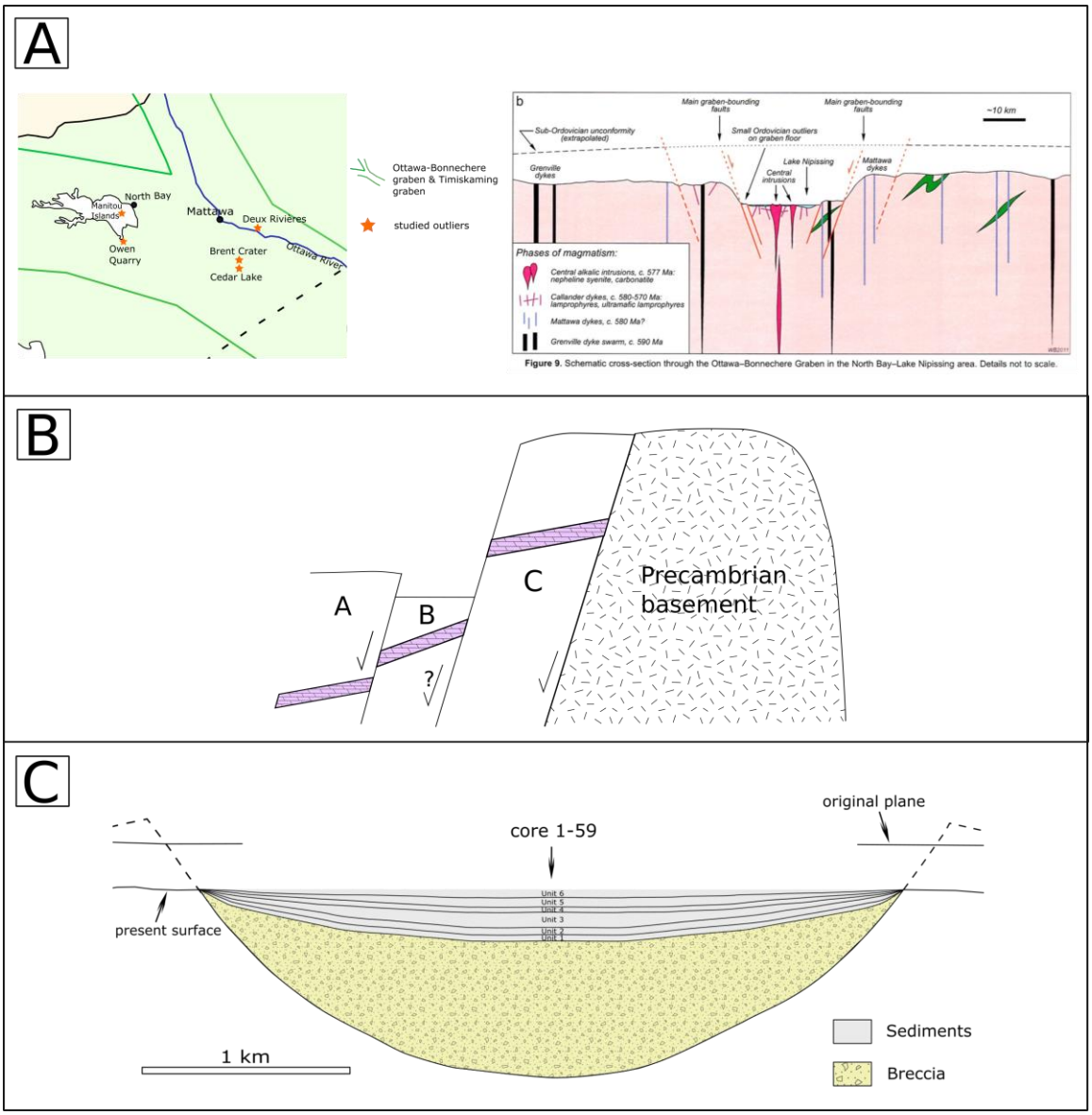

Figure 7.3. Structural development and preservation of outliers. A) left: most of the outliers are in the centre of the OBG; right: cross-section of the OBG near North Bay (Bleeker et al., 2011) shows Lake Nipissing is in a depression bounded by normal faults. B) Three subparallel normal faults accommodate different structural attributes of sections in the Owen Quarry outlier. C) Preservation of sedimentary rocks in the Brent impact crater.

7.3 Discussion of dolomitization

Examination of the outliers reveals several crystalline fabrics of dolomite, and different stratigraphic distribution patterns (Fig. 7.4). Each of these are discussed, followed by an attempt to integrate hydrology of dolostone formation.

7.3.1 Fabric-selective dolomitization

Selective dolomitization (Fig. 7.4A: 1-4) of fine-grained (micritic) matrix occurs in inter- and intraskeletal paleoporosity, burrows, and acts as partial replacement of skeletal allochems in the Deux Rivières outlier and Manitou Islands successions. Dolomite occurs as individual rhombs or in patches. Such local distribution suggests that Mg was supplied locally, derived from pore-fluids within the matrix, or from seawater pumped through burrows (Gingras et al., 2004). This type of dolomite, therefore, is both time- and spatial-limited in formation in response to the development of depositional and/or compactional burial environment. A greater presence may have once been developed, but subsequently hidden (or recrystallized) by subsequent pervasive dolomitization.

7.3.2 Pervasive dolomitization

Pervasive crystalline fabrics (Fig. 7.4A: 5-9) are associated with four different stratigraphic patterns: 1) development of dolostone beds overlying crystalline basement (Cedar Lake outlier; Fig. 7.4B-i); 2) development of dolostone beds overlying crystalline basement, but overlain by limestone (Manitou Islands outlier; Fig. 7.4B-ii); 3) individual dolostone beds abruptly bounded by limestone (Deux Rivières outlier and upper Manitou

Islands sections; Fig. 7.4B-ii); and 4) the entirely dolomitized Owen Quarry outlier, in fault contact with crystalline basement (Fig. 7.4B-iii). Potential controls on these stratigraphic patterns are discussed below.

Potential role of basement influence on dolomitization

The first two patterns may illustrate subsurface movement of dolomitizing brines along the surface of the Precambrian crystalline basement, which represents a prominent regional permeability boundary. Within the Cedar Lake outlier, coarsely crystalline, nonplanar dolomite occurs in the lower dolostone and sandstone beds lying above the crystalline basement. Higher in the succession, finely crystalline planar-s dolomite forms an individual bed, within which nonplanar dolomite occurs as microveins (Fig. 7.4B-i). Previous discussion (see Chapter 4) interpreted the possibility that the finely crystalline dolostone could be of near-surface shallow-burial origin related to meteoric diagenesis. The nonplanar dolomite, both in veins and basal beds of the outlier, represents precipitation from fluids of elevated temperature.

Likewise, dolomitization of the lower part of the Great and Little Manitou islands sections may demonstrate a similar relationship (Fig. 7.4B-ii). In this case, fluid flow may have been enhanced with greater initial permeability of the basal sandstone that overlies the basement. Evidence of limestone capping the dolomitized interval demonstrates some upper limit controlling fluid migration and dolomite formation (Fig. 7.4B-ii). The difference with the Cedar Lake outlier may be only that a once present limestone succession overlying the preserved dolostone was subsequently eroded.

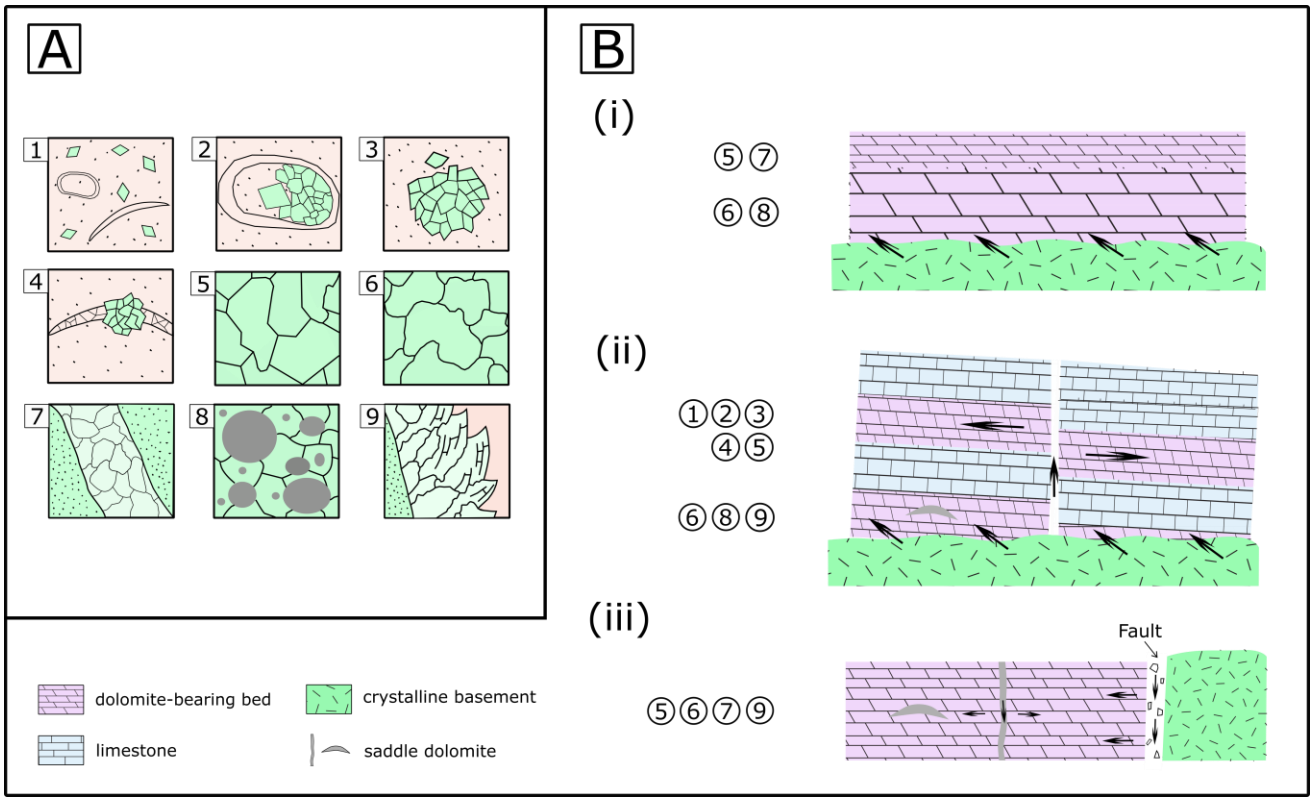

Figure 7.4. Summary of dolomite crystal features and stratal distribution. A) Dolomite crystal feature: 1, planar-p dolomite; 2, planar-s fabric in intraskeletal void space; 3, planar-s fabric within burrow; 4, planar-s fabric replaces skeletal material; 5, pervasive planar-s fabric; 6, pervasive nonplanar fabric; 7, nonplanar fabric in fracture; 8, nonplanar dolomite in sandstone; 9, nonplanar-c fabric in fracture or paleovoid space. B) Stratal distribution of different types of dolomite fabric (numbers correspond to those in (A); black arrows indicate path of fluid: i, basement-related distribution representing Cedar Lake outlier; ii, stratabound distribution combining Deux Rivières outlier and Manitou Islands sections; iii, fault-controlled distribution representing Owen Quarry outlier.

Discrete beds of stratabound dolomitization

In the Deux Rivières outlier, pervasive stratabound dolomitization (Fig. 7.4B-ii) resulted in a dolostone bed bounded abruptly by limestone. The precursor lithology of dolostone is most likely a limestone given the presence of skeletal benthic fauna that otherwise occur in limestone of equivalent Ordovician platforms. Petrographic analysis suggests that this pervasive dolomite may be a recrystallization product of precursor planar-p dolomite. Similar patterns of stratabound dolostone have been documented and modeled at various scales (e.g., Hollis et al., 2017; Gomez-Rivas et al., 2011). In Iran, for example, Cretaceous dolostone sheets are capped by nonporous lime mudstone, and extend away from faults (Lapponi et al., 2011).

Fault/fracture-controlled dolomitization

In the Owen Quarry and Cedar Lake outliers, microveins of dolomite cross-cut beds of dolostone illustrating two stages of fluid flow, the latter linked to structurally controlled fluid migration. Within the Owen Quarry succession, Fe concentrations appear to be higher in the upper part of the succession, and highest in Loc. C that is in fault contact to the crystalline basement. This pattern may suggest that dolomitizing fluid migrated along faults and fractures, then horizontally within individual beds (Fig. 7.4B-iii).

7.3.3 Integration of dolomitizing hydrological controls

In their study of dolomitization of Upper Ordovician strata in the Manitoulin Island area, Coniglio and Williams-Jones (1992) noted that pervasive dolomitization of

specific beds was one criterion for evidence of related fracture control of dolomitizing fluids. Additional criteria included: a) similar petrographic characteristics of dolomite in different stratigraphic units and lithofacies; and b) similar range of $\delta^{13}C$ and $\delta^{18}O$ values in different beds.

The stratigraphic patterns of dolomitization amongst the outliers may identify some variations on this theme; namely, either (1) long-distance migration of basin brines intersecting local faults within the early stage of the OBG development that redirects flow vertically; or (2) local mixing of marine and basin-derived fluids generated by local structural events within the graben. Both of these hypotheses are examined here.

First, stratabound and fracture-controlled dolomitization can be recognized in the same successions. For example, nonplanar dolomite lies along the base of the Cedar Lake and Manitou Islands sections, and higher in the section dolostone is cross-cut by nonplanar dolomite filling microveins. Although not saddle dolomite, the nonplanar fabric identifies likely elevated temperatures compared to planar fabrics (Sibley and Gregg, 1987), typical of basin brines.

Long-distance (many hundreds of km) migration of metal- and petroleum-bearing basin fluids was well-recognized in large sedimentary basins, often allied with orogenic phases along the Laurentian margin (Bethke and Marshak, 1990). Haeri-Ardakani et al. (2013) interpreted radially outward migration of dolomitizing brines from the center of the intracratonic Michigan Basin, and reaching the basin's present northern erosional limit in southern Ontario. $\delta^{18}O$ and $^{87}Sr/^{86}Sr$ values of their saddle dolomite are similar to those reported in this thesis from the Owen Quarry outlier section (Fig. 7.5). The outlier, although ~ 220 km from the northern limit (Georgian Bay) of the study area of Haeri-

Ardakani et al. (2013), it is possible that the outlier was along the migration pathway for these sedimentary brines from Michigan Basin.

Evidence of the second hypothesis is illustrated by the Owen Quarry outlier that is very clearly fault-bound, and ferrugineous nonplanar-2 dolomite may identify a direct link with fluids that migrate along the adjacent regional fault that bounds ferruginized basement rock. As concluded by Davies and Smith (2006), hydrothermal dolomitization shows a strong structural control by extensional and strike-slip faults, with fluid flow focused in the hanging wall in the former situation. This is represented well at the outlier. Along a large limestone outlier in the southern part of the graben, near Eganville, Ontario, crystalline mosaics of nonplanar dolomite and intercrystalline saddle dolomite produce narrow (meter-scale) vertical zones of dolomitization (Nurkhanuly and Dix, 2014).

The diagenetic fluid was interpreted to be a mixture of Late Ordovician marine-derived and basement-derived fluids, but reflecting structural control related to anticline development in a wrench-fault framework (Nurkhanuly and Dix, 2014). Thus, an alternative to pervasive dolomitization model of long-distance transport is local mixture of marine- and basement-derived fluids during local structural events along the axis of the graben.

With respect to the other outliers, if faults at the Manitou Islands (Lumbers, 1971) and the fault defining the northwest limit of the Deux Rivières outlier were fluid conduits for dolomitization, then they represent reactivated fault systems developed prior to dolomitization. The presence of saddle dolomite in Great Manitou Island section is in the porous breccia lying on the crystalline basement rock. This saddle dolomite has a

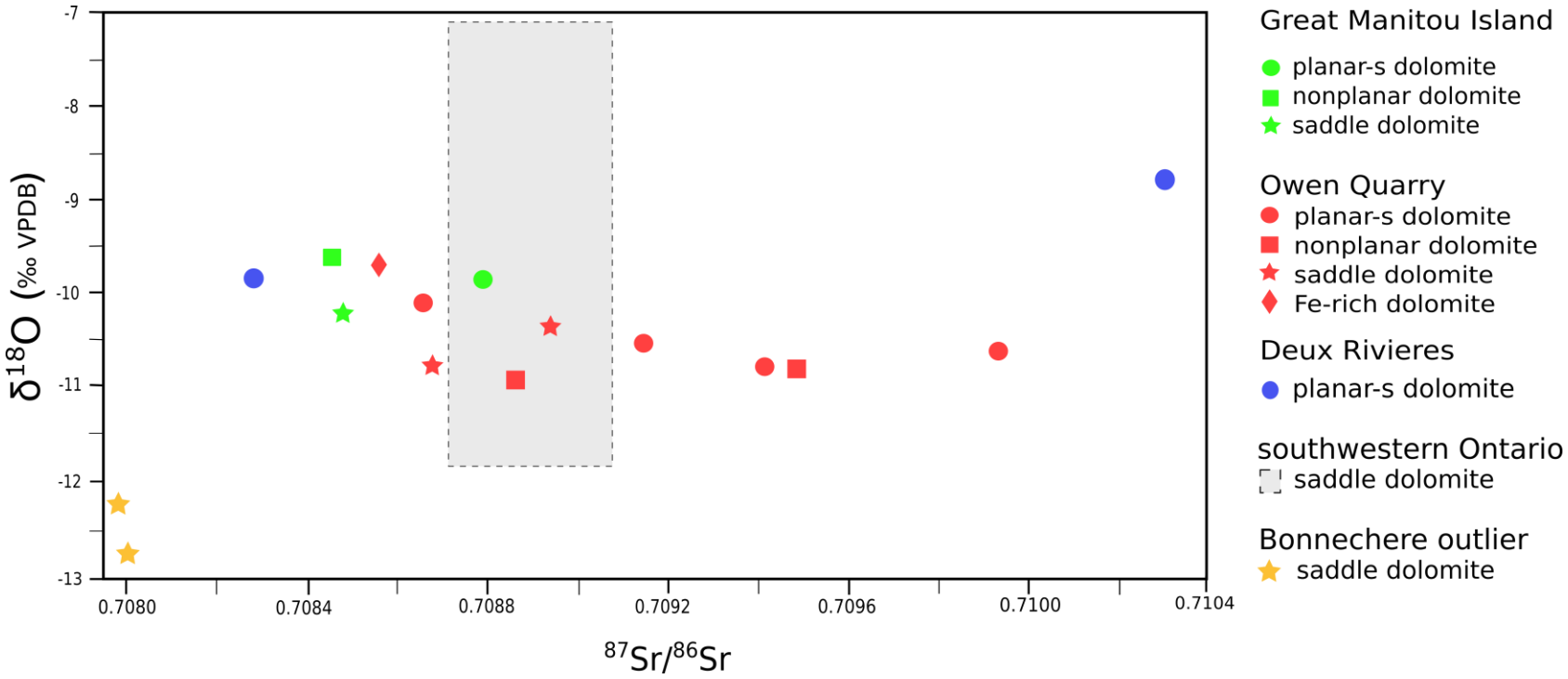

Figure 7.5. $^{87}Sr/^{86}Sr$-$\delta^{18}O$ plot of dolomite types in Great Manitou Island, Owen Quarry, and Deux Rivières outliers; and saddle dolomite from Trentonian strata in southwestern Ontario (Haeri-Ardakani et al., 2013) and from Rocklandian strata of Bonnechere outlier, Ontario (Nurkhanuly and Dix, 2014).

$^{87}Sr/^{86}Sr$ value in between those of Michigan Basin and Bonnechere outlier saddle dolomites (Fig. 7.5). The basement complex may represent a structural weakness along which structural control on hydrology may have been reactivated during the Paleozoic. As a result, brines from the Michigan Basin could have mixed with marine-derived fluid.

In summary, there appears to have been a combination of hydrological controls represented by stratigraphic patterns of dolomitization: 1) very local formation of dolomite in burrows that demonstrates Mg derived from seawater or pore water; 2) early near-surface burial dolomitization wherein Mg is derived from seawater or weathering and alteration; 3) later burial, regional to local migration of dolomitizing brines along the Paleozoic-Precambrian boundary that 4) may have intersected faults or fractures that allow vertical migration of fluids both near the basement but also higher in the stratigraphic section, promoting dolomitization of individual bed bounded by less permeable limestone.

Chapter 8 Conclusions

1) Integration of lithostratigraphic and biostratigraphic (conodonts, chitinozoans, macrofossils) datasets from previous work and this study indicate that the stratigraphic successions of five studied Paleozoic outliers within the northern Ottawa–Bonnechere graben fit the Upper Ordovician Mohawkian Series of North America. Specifically, all but the Owen Quarry outlier near Lake Nipissing are of Blackriveran (Turinian) age, whereas the Owen Quarry succession is interpreted to be equivalent to the lower Trentonian (Chatfieldian) succession of southern and eastern Ontario and northern New York State.

2) There were two broad controls influencing preservation of the Paleozoic outliers: 1) local and regional structural lows (Owen Quarry outlier, Cedar Lake outlier, Deux Rivières, and Manitou Islands) associated with graben faults; and 2) high rate of local subsidence (Brent Crater succession) due to basement instability following a meteorite impact.

3) The individual succession documents local variation of a common stratigraphic theme: net transgression across either an observed crystalline basement paleosurface, or siliciclastic-rich nearshore facies, yielding more open circulation and development of a normal-marine (carbonate) subtidal setting upsection. This study has demonstrated a strong regional stratigraphic connectivity among the outliers and with more distal Blackriveran and Trentonian strata of the St. Lawrence Platform to the south and

southeast. However, variations in lithofacies represent local controls, especially the influence of initial basement paleotopography. In detail:

a) The Deux Rivières outlier contains a 17-m succession of carbonate and siliciclastic rocks that document net environmental change from restricted nearshore to normal-marine conditions within a moderate- to high-energy subtidal setting.

b) About 250 m of sedimentary rocks are preserved in the center of Brent Crater. The lower ~ 140 m contain finely interlaminated sandstone, siltstone, dolostone, and lime mudstone suggesting a nearshore marine environment with variation of siliciclastic input. Abundant soft sediment deformation structures may indicate high slope steepness or earthquake events. A previous interpretation of a saline lake setting was based on the presence of gypsum layers viewed to be of depositional origin, but they represent sub-horizontal fracture fill deposits related to migration of saline burial fluids. The upper ~ 110 m of the Brent Crater succession are composed of marine carbonate and prominent sandstone intervals that represent deposition in nearshore to subtidal settings.

c) The very thin (< 3 m) Paleozoic succession at Cedar Lake is composed of sandstone, interbedded bioclastic sandy dolowacke/packstone and silty dolomudstone, and dolomudstone that suggest deposition in low-energy, restricted, shallow marine environment.

d) The stratigraphic successions on Great and Little Manitou islands document lithological change from initial fossiliferous basement breccia

or calcareous sandstone to dolostone and bioclastic limestone. It represents net transgression from nearshore to shallow subtidal setting.

e) The interpreted Trentonian Owen Quarry outlier is composed entirely of dolostone that has replaced precursor limestone. The succession contains a lower stenohaline high-energy subtidal facies, including channel deposits, influenced by storms. The middle part of the succession contains thin layers of heavily burrowed claystone and thicker beds of very fossiliferous dolostone. This interval may represent deeper water facies, with siliciclastic layers defining periods between storm deposition. The upper part of the succession contains dolomudstone suggesting a low-energy environment.

4) Diagenetic attributes of limestone reveal a relatively common succession among Blackriveran outliers: from surface to near-surface marine-derived (burrows, automicrite, micrite envelopes, blackened grains, hardgrounds), to shallow-burial (mechanical compaction, dissolution, cementation, fractures), then deep-burial (bedding-parallel stylolites) alteration.

5) All studied outliers have been variously dolomitized, either selectively or pervasively. Distribution of dolomite and geochemistry (C, O, Sr-isotopes) suggests three broad patterns: a) local selective dolomitization demonstrates Mg derived from seawater or pore water; b) early near-surface burial dolomitization resulted in fine-grained dolostone wherein Mg may have been derived from seawater or related to migration

of meteoric water in the burial environment; and c) much of the pervasive dolomitization may have been allied with regional migration of fluids along the basement interface, then refocused upsection along faults and fractures. $\delta^{18}O$ values of dolomite are more negative than Late Ordovician marine calcite, suggesting that the diagenetic fluid is either meteoric or hotter than surface conditions. Dolostone is more enriched in ^{87}Sr than Late Ordovician marine limestone, indicating interaction of dolomitizing fluids with continental basement or siliciclastic material. Presence of saddle dolomite in microveins and late-stage void-fills in the Great Manitou Island and Owen Quarry outliers supports migration of hydrothermal fluids along structural conduits, and elevated $^{87}Sr/^{86}Sr$ values indicate equilibration with basement or siliciclastic-bearing strata. Considering the paleogeographic proximity of these two outliers to the Michigan Basin (to the southwest), these late-stage hydrothermal fluids may be related to long-distance migration of Michigan Basin brines. Alternatively, they represent local mixture of marine- and basement-derived fluids during local structural events along the axis of the graben.

References

Alpert, S.P. 1973. *Bergaueria Prantl* (Cambrian and Ordovician), a probable actinian trace fossil. Journal of Paleontology, **47**: 919–924.

Aguirre, J., and Riding, R. 2005. Dasycladalean algal biodiversity compared with global variations in temperature and sea level over the past 350 Myr. Palaios, **20**: 581–588.

Andreason, M.W. 1992. Coastal siliciclastic sabkhas and related evaporative environments of the Permian Yates Formation, north Ward-Estes field, Ward County, Texas. American Association of Petroleum Geologists Bulletin, **76**: 1735–1759.

Anjos, S.M.C., De Ros, L.F., and Silva, C.M.A. 2003. Chlorite authigenesis and porosity preservation in the Upper Cretaceous marine sandstones of the Santos Basin, offshore eastern Brazil. *In* Clay Mineral Cements in Sandstones. *Edited by* R.H. Worden and S. Morad. International Association of Sedimentologists, Special Publication, **34**: 291–316.

Back, W., Hanshaw, B.B., Plummer, L.N., Rahn, P.H., Rightmire, C.T., and Rubin, M. 1983. Process and rate of dedolomitization: mass transfer and ^{14}C dating in a regional carbonate aquifer. Geological Society of America Bulletin, **94**: 1415–1429.

Ball, M.M. 1967. Carbonate sand bodies of Florida and the Bahamas. Journal of Sedimentary Research, **37**: 556–591.

Banner, J.L. 1995. Application of the trace element and isotope geochemistry of strontium to studies of carbonate diagenesis. Sedimentology, **42**: 805–824.

Barlow, A.E. 1899. Geology and natural resources of the area Included by Nipissing and Temiscaming map-sheets comprising portions of the District of Nipissing, Ontario and of the County of Pontiac, Québec. Report of the Geological Survey of Canada, **672**: 18–287.

Barta, N.C., Bergström, S.M., Saltzman, M.R., and Schmitz, B. 2007. First record of the Ordovician Guttenberg $\delta^{13}C$ excursion (GICE) in New York State and Ontario: local and regional chronostratigraphic implications. Northeastern Geology and Environmental Sciences, **29**: 276–298.

Berdan, J.M. 1984. Leperditicopid ostracodes from Ordovician rocks of Kentucky and nearby states and characteristic features of the order Leperditicopida. Geological Survey Professional Paper 1066-J, pp. 1–40.

Bergström, S.M., Schmitz, B., Saltzman, M.R., and Huff, W.D. 2010. The Upper Ordovician Guttenberg $\delta^{13}C$ excursion (GICE) in North America and Baltoscandia: Occurrence, chronostratigraphic significance, and paleoenvironmental relationships. Geological Society of America Special Papers, **466**: 37–67.

Bethke, C.M., and Marshak, S. 1990. Brine migrations across North America-the plate tectonics of groundwater. Annual Review of Earth and Planetary Sciences, **18**: 287–315.

Blackwell, W.H., Marak, J.H., Powell, M.J., and Martin, W.D. 1984. *Girvanella* (Cyanochloronta) in an Ordovician oncolite zone in eastern Indiana. Bulletin of the Torrey Botanical Club, **111**: 165–170.

Bleeker, W., Dix, G.R., and Davidson, A., and LeCheminant, A. 2011. Tectonic evolution and sedimentary record of the Ottawa–Bonnechere Graben: examining the Precambrian and Phanerozoic record of magmatic activity, faulting and sedimentation. Geological Association of Canada – Mineralogical Association of Canada – Society of Economic Geologists – Society for Geology Applied to Mineral Deposits Joint Annual Meeting, Ottawa 2011, Guidebook to Field Trip 1A, pp. 1–98.

Boggs Jr, S. 2011. Sedimentology and stratigraphy. Pearson Education. Upper Saddle River, N.J.

Borer, J.M., and Harris, P.M. 1991. Lithofacies and cyclicity of the Yates Formation, Permian Basin: Implications for reservoir heterogeneity. American Association of Petroleum Geologists Bulletin, **75**: 726–779.

Bromley, R.G., and Ekdale, A.A. 1984. *Chondrites*: a trace fossil indicator of anoxia in sediments. Science, **224**: 872–874.

Brookfield, M.E. 1988. A mid-Ordovician temperate carbonate shelf-the Black River and Trenton Limestone Groups of southern Ontario, Canada. Sedimentary Geology, **60**: 137–153.

Brookfield, M.E., and Brett, C.E. 1988. Paleoenvironments of the Mid-Ordovician (Upper Caradocian) Trenton limestones of southern Ontario, Canada: Storm sedimentation on a shoal-basin shelf model. Sedimentary Geology, **57**: 75–105.

Brunton, F., Turner, E. and Armstrong, D. 2009. A guide to the Paleozoic geology and fossils of Manitoulin Island and northern Bruce Peninsula, Ontario, Canada. Canadian Paleontology Conference Field Trip Guidebook No. 14, pp. 1–77.

Caley, J.F., and Liberty, B.A. 1957. The St. Lawrence and Hudson Bay Lowlands, and Paleozoic outliers. Geological Survey of Canada Economic Geology Series, **1**: 207–246.

Cameron, B., and Mangion, S. 1977. Depositional environments and revised stratigraphy along the Black River-Trenton boundary in New York and Ontario. American Journal of Science, **277**: 486–502.

Cocks, L.R.M., and Torsvik, T.H. 2011. The Palaeozoic geography of Laurentia and western Laurussia: a stable craton with mobile margins. Earth-Science Reviews, **106**: 1–51.

Colquhoun, D.J. 1958. Stratigraphy and paleontology of the Nipissing-Deux Rivieres outliers. Proceedings of the Geological Association of Canada, **10**: 83–93.

Coniglio, M., Sherlock, R., Williams-Jones, A.E., Middleton, K., and Frape, S.K. 1994. Burial and hydrothermal diagenesis of Ordovician carbonates from the Michigan Basin, Ontario, Canada. *In* Dolomites—A volume in honour of Dolomieu. *Edited by* B. Purser, M. Tucker and D. Zenger. International Association of Sedimentologists, Special Publication, **21**: 231–254.

Coniglio, M., and Williams-Jones, A.E. 1992. Diagenesis of Ordovician carbonates from the north-east Michigan Basin, Manitoulin Island area, Ontario: evidence from petrography, stable isotopes and fluid inclusions. Sedimentology, **39**: 813–836.

Cornell, S.R. 2001. Sequence stratigraphy and event correlations of upper Black River and lower Trenton Group carbonates of northern New York State and southern Ontario, Canada. M. Sc. thesis, Department of Geology. The University of Cincinnati University, Cincinnati, OH.

Chow, N., and Longstaffe, F.J. 1995. Dolomites of the Middle Devonian Elm Point Formation, southern Manitoba: intrinsic controls on early dolomitization. Bulletin of Canadian Petroleum Geology, **43**: 214–225.

Davis, G.L., Hart, S.R., Aldrich, L.T., Krogh, T.E., and Steuber, A. 1968. Geological history of the Grenville Province. Carnegie Institute Washington Yearbook, **66**: 52–536.

Davies, G.R., and Smith Jr, L.B. 2006. Structurally controlled hydrothermal dolomite reservoir facies: An overview. American Association of Petroleum Geologists Bulletin, **90**: 1641–1690.

Dix, G.R. 2012. The Sauk–Tippecanoe megasequence boundary in an interior structural corridor (Ottawa embayment) of the great American carbonate bank. *In* The great American carbonate bank: The geology and economic resources of the Cambrian–Ordovician Sauk megasequence of Laurentia, American Association of Petroleum Geologists Memoir 98. *Edited by* J.R. Derby, R.D. Fritz, S.A. Longacre, W.A. Morgan, and C.A. Sternbach. American Association of Petroleum Geologists, Tulsa, OK. pp. 545–557.

Dix, G.R., Coniglio, M., Riva, J.F., and Achab, A. 2007. The Late Ordovician Dawson Point Formation (Timiskaming outlier, Ontario): key to a new regional synthesis of Richmondian–Hirnantian carbonate and siliciclastic magnafacies across the central Canadian craton. Canadian Journal of Earth Sciences, **44**: 1313–1331.

Dix, G.R., and Jolicoeur C. 2011. Tectonostratigraphy of Upper Ordovician source rocks, Ottawa Embayment (eastern Ontario). Bulletin of Canadian Petroleum Geology, **59**: 7–26.

Dix, G.R., and Rodhan, Z.A. 2006. A new geological framework for the Middle Ordovician Carillon Formation (uppermost Beekmantown Group, Ottawa Embayment): onset of Taconic foreland deposition and tectonism within the Laurentian platform interior. Canadian Journal of Earth Sciences, **43**: 1367–1387.

Dott Jr, R.H. 1964. Wacke, graywacke and matrix—What approach to immature sandstone classification? Journal of Sedimentary Research, **34**: 625–632.

Dunham, R.J. 1962. Classification of carbonate rocks according to depositional texture. *In* Classification of carbonate rocks, a symposium, American Association of Petroleum Geologists Memoir 1. *Edited by* W.E. Hamm. American Association of Petroleum Geologists, Tulsa, OK. pp. 108–121.

Edwards, C.T., Saltzman, M.R., Leslie, S.A., Bergström, S.M., Sedlacek, A.R., Howard, A., ... and Young, S.A. 2015. Strontium isotope ($^{87}Sr/^{86}Sr$) stratigraphy of Ordovician bulk carbonate: Implications for preservation of primary seawater values. Geological Society of America Bulletin, **127**: 1275–1289.

El Gadi, M.S. 2001. Sedimentology and sequence stratigraphy of the Ordovician Black River and lower Trenton Groups, Lake Simcoe Area, Ontario. Ph.D. thesis, Department of Land Resource Science, University of Guelph, Guelph, ON.

Embry, A.F., and Klovan, J.E. 1971. A late Devonian reef tract on northeastern Banks Island, NWT. Bulletin of Canadian Petroleum Geology, **19**: 730–781.

Ettensohn, F.R. 2008. The Appalachian foreland basin in eastern United States. *In* The Sedimentary basins of the world, Vol. 5, The Sedimentary Basins of the United States and Canada. *Edited by* A.D. Miall. Elsevier. pp. 105–179.

Ettensohn, F.R. 2010. Origin of Late Ordovician (mid-Mohawkian) temperate-water conditions on southeastern Laurentia: Glacial or tectonic? Geological Society of America Special Papers, **466**: 163–175.

Ettensohn, F.R., and Brett, C.E. 2002. Stratigraphic evidence from the Appalachian Basin for continuation of the Taconian orogeny into Early Silurian time. Physics and Chemistry of the Earth, **27**: 279–288.

Evamy, B.D. 1969. The precipitational environment and correlation of some calcite cements deduced from artificial staining. Journal of Sedimentary Research, **39**: 787–821.

Flügel, E. 2010. Microfacies of carbonate rocks. Springer-Verlag Berlin Heidelberg.

Ford, M.J., Lall, R.A., and Bajc, A.J. 1984. Quaternary geology of Algonquin Park, North Central Part, Nipissing District, Ontario Geological Survey, Map P. 2703. Geological Series-Preliminary Map, scale 1:50000. Geology 1982, 1983.

Frank, J.R. 1981. Dedolomitization in the Taum Sauk Limestone (Upper Cambrian), Southeast Missouri. Journal of Sedimentary Research, **51**: 7–18.

Gbadeyan, R., and Dix, G.R. 2013. The role of regional and local structure in a Late Ordovician (Edenian) foreland platform-to-basin succession inboard of the Taconic Orogen, Central Canada. Geosciences, **3**: 216–239.

Gingras, M.K., Pemberton, S.G., Muelenbachs, K., and Machel, H. 2004. Conceptual models for burrow-related, selective dolomitization with textural and isotopic evidence from the Tyndall Stone, Canada. Geobiology, **2**: 21–30.

Goldhammer, R.K. 2003. Mixed siliciclastic and carbonate sedimentation. *In* Encyclopedia of sediments and sedimentary rocks. *Edited by* G.V. Middleton. Springer.

Gomez-Rivas, E., Corbella, M., Martín, J., Stafford, S., Griera, A., and Teixell, A. 2011. Origin and timing of stratabound dolomitization in the Cretaceous carbonate ramp of Benicàssim. MACLA. Revista de la Sociedad Española de Mineralogía, **15**: 103–104.

Goodwillie, J.M. 1893. A Geological sketch, with notes on the geology of the Manitou Islands of Lake Nipissing, Ontario. Science, **22**: 101–104.

Grahn, Y., and Ormö, J. 1995. Microfossil dating of the Brent meteorite crater, southeast Ontario, Canada. Revue de Micropaléontologie, **38**: 131–137.

Grieve, R.A.F. 2006. Impact structures in Canada. Geological Association of Canada. St. John's, NL.

Grimwood, J.L., Coniglio, M., and Armstrong, D.K. 1999. Blackriveran carbonates from the subsurface of the Lake Simcoe area, southern Ontario: stratigraphy and sedimentology of a low-energy carbonate ramp. Canadian Journal of Earth Sciences, **36**: 871–889.

Guilbault, J.P., and Mamet, B.L. 1976. Ordovician codiaceae (algae) from Saint Lawrence Lowlands. Canadian Journal of Earth Sciences, **13**: 636–660.

Haeri-Ardakani, O., Al-Aasm, I., and Coniglio, M. 2013. Petrologic and geochemical attributes of fracture-related dolomitization in Ordovician carbonates and their spatial distribution in southwestern Ontario, Canada. Marine and Petroleum Geology, **43**: 409–422.

Hartung, J.B., Dence, M.R., and Adams, J.A. 1971. Potassium-argon dating of shock-metamorphosed rocks from the Brent Impact Crater, Ontario, Canada. Journal of Geophysical Research, **76**: 5437–5448.

Herrmann, A.D., and Haupt, B.J. 2010. Toward identifying potential causes for stratigraphic change in subtropical to tropical Laurentia during the Mohawkian (early Late Ordovician). Geological Society of America Special Papers, **466**: 29–35.

Hollis, C., Bastesen, E., Boyce, A., Corlett, H., Gawthorpe, R., ... and Whitaker, F. 2017. Fault-controlled dolomitization in a rift basin. Geology, **45**: 219–222.

Holterhoff, P.F. 1997. Filtration models, guilds, and biofacies: Crinoid paleoecology of the Stanton Formation (Upper Pennsylvania), midcontinent, North America. Palaeogeography, Palaeoclimatology, Palaeoecology, **130**: 177–208.

Hume, G.S. 1925. The Paleozoic outlier of Lake Timiskaming, Ontario and Quebec. Geological Survey of Canada, Memoir 145. pp. 1–129.

James, N.P. 1972. Holocene and Pleistocene calcareous crust (caliche) profiles: criteria for subaerial exposure. Journal of Sedimentary Research, **42**: 817–836.

James, N.P., and Choquette, P. 1984. Diagenesis 9. Limestones-the meteoric diagenetic environment. Geoscience Canada, **11**: 161–194.

James, N.P., and Jones, B. 2016. Origin of carbonate rocks. John Wiley & Sons.

Kamo, S.L., Krogh, T.E., and Kumarapeli, P.S. 1995. Age of the Grenville dyke swarm, Ontario-Quebec: implications for the timing of Lapetan rifting. Canadian Journal of Earth Sciences, **32**: 273–280.

Kapp, U.S. 1975. Paleoecology of Middle Ordovician stromatoporoid mounds in Vermont. Lethaia, **8**: 195–207.

Karim, T., and Westrop, S.R. 2002. Taphonomy and paleoecology of Ordovician trilobite clusters, Bromide Formation, south-central Oklahoma. Palaios, **17**: 394–402.

Kay, G.M. 1942. Ottawa–Bonnechere graben and Lake Ontario homocline. Geological Society of America Bulletin, **53**: 585–646.

Keim, L., and Schlager, W. 1999. Automicrite facies on steep slopes (Triassic, Dolomites, Italy). Facies, **41**: 15–25.

Keith, B.D. 1988. Regional Facies of Upper Ordovician Series of Eastern North America. *In* The Trenton Group (Upper Ordovician series) of eastern North America: deposition, diagenesis, and petroleum. *Edited by* B.D. Keith. American Association of Petroleum Geologists Studies in Geology, **29**: 1–16.

Kennedy, M.J., and Droser, M.L. 2011. Early Cambrian metazoans in fluvial environments, evidence of the non-marine Cambrian radiation. Geology, **39**: 583–586.

Krogh, T.E., and Davis, G.L. 1969. Geochronology of the Grenville Province. Carnegie Institution of Washington Yearbook, **67**: 224–228.

Land, L.S. 1983. The application of stable isotopes to studies the origin of dolomite and to problems of diagenesis of clastic sediments. *In* Stable Isotopes in Sedimentary Geology. *Edited by* M.A. Arthur. Society of Economic Paleontologists and Mineralogists. Short Course Notes 10, p. 4.1–4. 22.

Lapponi, F., Casini, G., Sharp, I., Blendinger, W., Fernández, N., and Hunt, D. 2011. From outcrop to 3D modelling: a case study of a dolomitized carbonate reservoir, Zagros Mountains, Iran. Petroleum Geoscience, **17**: 283–307.

Lavoie, D. 1994. Diachronous tectonic collapse of the Ordovician continental margin, eastern Canada: comparison between the Quebec Reentrant and St. Lawrence Promontory. Canadian Journal of Earth Sciences, **31**: 1309–1319.

Lavoie, D. 1995. A Late Ordovician high-energy temperate-water carbonate ramp, southern Quebec, Canada: implications for Late Ordovician oceanography. Sedimentology, **42**: 95–116.

Lavoie, D. 2008. Appalachian foreland basin of Canada. *In* The Sedimentary basins of the world, The Sedimentary Basins of the United States and Canada. *Edited by* A.D. Miall. Elsevier. pp. 65–103.

Legall, F.D., Barnes, C.R., and Macqueen, R.W. 1981. Thermal maturation, burial history and hotspot development, Paleozoic strata of southern Ontario-Quebec, from conodont and acritarch colour alteration studies. Bulletin of Canadian Petroleum Geology, **29**: 492–539.

Liu, L., Wu, Y., Yang, H., and Riding, R. 2016. Ordovician calcified cyanobacteria and associated microfossils from the Tarim Basin, Northwest China: systematics and significance. Journal of Systematic Palaeontology, **14**: 183–210.

Logan, W.E. 1847. Geological Survey of Canada, Report of Progress for the Year 1845-46. Lovell & Gibson, Montreal. pp. 1–98.

Longman, M.W. 1980. Carbonate diagenetic textures from nearsurface diagenetic environments. American Association of Petroleum Geologists Bulletin, **64**: 461–487.

Lozej, G.P., and Beales, F.W. 1975. The unmetamorphosed sedimentary fill of the Brent meteorite crater, southeastern Ontario. Canadian Journal of Earth Sciences, **12**: 606–628.

Lumbers, S.B. 1971. Geology of the North Bay Area, Districts of Nipissing and Parry Sound, Ontario Dept. of Mines and Northern Affairs, Geological report, **94**: 1–112.

Lumbers, S.B. 1976. Mattawa-Deep River area (western half), District of Nipissing; Ontario Division of Mines, Preliminary Map P.1196.

MacEachern, J.A., Pemberton, S.G., Gingras, M.K., and Bann, K.L. 2010. Ichnology and facies models. *In* Facies models. *Edited by* N.P. James and R.W. Dalrymple. Geological Association of Canada, St. John's, Canada. pp. 19–58.

Machel, H.G. 1985. Cathodoluminescence in calcite and dolomite and its chemical interpretation. Geoscience Canada, **12**: 139–147.

Machel, H.G. 2004. Concepts and models of dolomitization: a critical reappraisal. Geological Society, London, Special Publications, **235**: 7–63.

Machel, H.G., and Mountjoy, E.W. 1987. General constraints on extensive pervasive dolomitization--and their application to the Devonian carbonates of western Canada. Bulletin of Canadian Petroleum Geology, **35**: 143–158.

Mamet, B., Roux, A., and Shalaby, H. 1984. Role des algues calcaires dans la sédimentation ordovicienne de la plate-forme du Saint-Laurent. Geobios, **17**: 261–269.

Mayall, M.J. 1983. An earthquake origin for synsedimentary deformation in a late Triassic (Rhaetian) lagoonal sequence, southwest Britain. Geological Magazine, **120**: 613–622.

Mazzullo, S.J. 1992. Geochemical and neomorphic alteration of dolomite: a review. Carbonates and evaporites, **7**: 21–37.

McCracken, A.D., 2017. Report on 2 Ordovician (Blackriveran to Kirkfieldian) conodont samples from unnamed strata in small outliers, central Ontario submitted in 2017 by George Dix (Carleton University) (VNR 330403-001-17-EXT.) NTS 31L-04, 31L-08. Con. No. 1814; Geological Survey of Canada, Paleontological Report 6-ADM-2017, 8 p.

McCracken, A.D., Armstrong, D.K., and Bolton, T.E. 2000. Conodonts and corals in kimberlite xenoliths confirm a Devonian seaway in central Ontario and Quebec. Canadian Journal of Earth Sciences, **37**: 1651–1663.

McFarlane, R.B. 1992. Stratigraphy, paleoenvironmental interpretation, and sequences of the Middle Ordovician Black River Group. Department of Geological Sciences, Queen's University, Kingston, ON.

Melchin, M. J., Brookfield, M.E., Armstrong, D.K, and Coniglio, M. 1994. Stratigraphy, sedimentology and biostratigraphy of the Ordovician rocks of the Lake Simcoe area, south-central Ontario. Geological Association of Canada–Mineralogical

Association of Canada Joint Annual Meeting, Waterloo 1994, Field Trip A4: Guidebook, pp. 1–101.

Millman, P.M., Liberty, B.A, Clark, J.F., Willmore, P. and Innes, M.J.S., 1960, The Brent Crater. Ottawa Dominion Observatory Publication, **24**: 1–43.

Murray, J.B., and Guest, J.E. 1970. Circularities of craters and related structures on earth and moon. Modern Geology, **1**: 149–159.

Narbonne, G.M., and James, N.P. 2017. Shallow neritic marine carbonates on a tropical Ordovician earth. Geological Association of Canada – Mineralogical Association of Canada Joint Annual Meeting, Kingston 2017, Guidebook to Field Trip #6, pp. 1–25.

Neugebauer, J. 1991. Some aspects of cementation in chalk. *In* Pelagic sediments: on land and under the sea. *Edited by* K.J. Hsü and H.C. Jenkyns, International Association of Sedimentologists, Special Publication, **1**: 149–176.

Nitecki, M.H., Webby, B.D., Spjeldnaes, N., and Yong-Yi, Z. 2004. Receptaculitids and algae. *In* The Great Ordovician Biodiversification Event. *Edited by* B.D. Webby, F. Paris, M.L. Droser, and I.G. Percival. Columbia University Press, New York. pp. 336–347.

Noor, I. 1989. Lithostratigraphy, environmental interpretation, and paleogeography of the Middle Ordovician Shadow Lake, Gull River, and Bobcaygeon Formations in parts of Southern Ontario. The University of Toronto, Toronto, ON.

Nurkhanuly, U. 2012. Structurally controlled hydrothermal dolomite, Eganville-Douglas Paleozoic outlier, Ottawa-Bonnechere graben, eastern Ontario. M.Sc. thesis, Department of Earth Sciences, Carleton University, Ottawa, ON.

Nurkhanuly, U., and Dix, G.R. 2014. Hydrothermal dolomitization of Upper Ordovician limestone, Central-East Canada: Fluid flow in a craton-interior wrench-fault system likely driven by distal Taconic Tectonism. The Journal of Geology, **122**: 259–282.

O'Neil, J.R., Clayton, R.N., and Mayeda, T.K. 1969. Oxygen isotope fractionation in divalent metal carbonates. The Journal of Chemical Physics, **51**: 5547–5558.

Ontario Geological Survey. 2011. 1:250000 scale bedrock geology of Ontario, Ontario Geological Survey, Miscellaneous Release–Data 126-Revision 1.

Osgood Jr, R.G., and Fischer, A.G. 1960. Structure and preservation of *Mastopora pyriformis*, an Ordovician dasycladacean alga. Journal of Paleontology, **34**: 896–902.

Pemberton, S.G., Spila, M., Pulham, A.J., Saunders, T., MacEachern, J.A., Robbins, D., and Sinclair, I. K. 2001. Ichnology and sedimentology of shallow marine to marginal marine systems: Ben Nevis and Avalon Reservoirs, Jeanne d'Arc Basin. Geological Association of Canada Short Course Notes, **15**: 1–343.

Percival, I.G. 1978. Inarticulate brachiopods from the Late Ordovician of New South Wales, and their palaeoecological significance. Alcheringa, **2**: 117–141.

Percival, I.G. 1999. Late Ordovician biostratigraphy of the northern Rockley–Gulgong volcanic belt. Quarterly Notes of the Geological Survey of New South Wales, **108**: 1–7.

Pettijohn, F.J., Potter, P.E., and Siever, R. 1972. Sand and sandstone. Springer-Verlag Berlin- Heidelberg.

Pickerill, R.K., Fillion, D., and Harland, T.L. 1984. Middle Ordovician trace fossils in carbonates of the Trenton Group between Montreal and Quebec City, St. Lawrence Lowland, eastern Canada. Journal of Paleontology, **58**: 416–439.

Plint, A. G. 2010. Wave-and storm-dominated shoreline and shallow-marine systems. *In* Facies models. *Edited by* N.P. James and R.W. Dalrymple. Geological Association of Canada, St. John's, Canada. pp. 167–199.

Pope, M.C., and Steffen, J.B. 2003. Widespread, prolonged late Middle to Late Ordovician upwelling in North America: A proxy record of glaciation? Geology, **31**: 63–66.

Qing, H., and Veizer, J. 1994. Oxygen and carbon isotopic composition of Ordovician brachiopods: Implications for coeval seawater. Geochimica et Cosmochimica Acta, **58**: 4429–4442.

Raaf, J.D., Reading, H.G., and Walker, R.G. 1965. Cyclic sedimentation in the Lower Westphalian of no Devon, England. Sedimentology, **4**: 1–52.

Ross, J.P. 1964. Champlainian cryptostome bryozoa from New York State. Journal of Paleontology, **38**: 1–32.

Rowe, R.B. 1954. Notes on geology and mineralogy of the Newman columbium-uranium deposit, Lake Nipissing, Ontario. Geological Survey of Canada Paper, 54.

Russell, D.J. 1984. Paleozoic geology of the Lake Timiskaming area, Timiskaming District. Ontario Geological Survey, Map P.2700, scale 1:50000.

Salad Hersi, O. 1997. Stratigraphic revision of the upper Chazyan to Trentonian succession, and sedimentologic and diagenetic aspects of the Blackriveran strata,

Ottawa Embayment, eastern Ontario, Canada. Ph.D. thesis, Department of Earth Sciences, Carleton University, Ottawa, ON.

Salad Hersi, O., and Dix, G.R. 2000. Blackriveran (lower Mohawkian, Upper Ordovician) lithostratigraphy, rhythmicity, and paleogeography: Ottawa Embayment, eastern Ontario, Canada. Canadian Journal of Earth Sciences, **36**: 2033–2050.

Salad Hersi, O., and Dix, G.R. 2006. Precambrian Fault Systems as Control on Regional Differences in Relative Sea Level Along the Early Ordovician Platform of Eastern North America. Journal of Sedimentary Research, **76**: 700–716.

Sandford, B.V. 1993a. St. Lawrence Platform– Introduction. *In* Sedimentary cover of the craton in Canada. *Edited by* D.F. Stott and J.D. Aitken. Geological Survey of Canada, Geology of Canada, No. 5, Ottawa, ON. pp. 709–722.

Sandford, B.V. 1993b. St. Lawrence Platform– Geology. *In* Sedimentary cover of the craton in Canada. *Edited by* D.F. Stott and J.D. Aitken. Geological Survey of Canada, Geology of Canada, No. 5, Ottawa, ON. pp. 723–786.

Satterly, J. 1943. Mineral occurrences in Parry Sound District. Ontario Department of Mines Annual Report 1942, **51**: 1–86.

Selley, R.C. 2000. Applied sedimentology. Academic Press.

Shen, Y., and Neuweiler, F. 2016. Taphocoenoses and diversification patterns of calcimicrobes and calcareous algae, Ordovician, Tarim Basin, China. Canadian Journal of Earth Sciences, **53**: 702–711.

Shields, G.A., Carden, G.A., Veizer, J., Meidla, T., Rong, J.Y., and Li, R.Y. 2003. Sr, C, and O isotope geochemistry of Ordovician brachiopods: a major isotopic event

around the Middle-Late Ordovician transition. Geochimica et Cosmochimica Acta, **67**: 2005–2025.

Sibley, D.F., and Gregg, J. M. 1987. Classification of dolomite rock textures. Journal of Sedimentary Research, **57**: 967–975.

Simo, J.A., Johnson, C.M., Vandrey, M.R., Brown, P.E., Giovanni, E., Castrogiovanni, ... and Boyer, J. 1994. Burial dolomitization of the Middle Ordovician Glenwood Formation by evaporitic brines, Michigan Basin. *In* Dolomites: A Volume in Honour of Dolomieu. *Edited by* B.H. Purser, M.E. Tucker, and D.H Zenger. International Association of Sedimentologists Special Publication, **21**: 169–186.

Sloss, L.L. 1988. Tectonic evolution of the craton in Phanerozoic time. *In* The Geology of North America, Volume D–2, Sedimentary Cover– North America Craton: U.S. *Edited by* Sloss, L.L, The geological Society of America. Boulder, CO. pp. 25–51.

Spötl, C., and Pitman, J.K. 1998. Saddle (baroque) dolomite in carbonates and sandstones: a reappraisal of the burial-diagenetic concept. *In* Carbonate Cementation in Sandstones: Distribution Patterns and Geochemical Evolution. *Edited by* S. Morad. International Association of Sedimentologists Special Publication, **26**: 437–460.

Steele-Petrovich, H.M., and Bolton, T.E. 1998. Morphology and palaeoecology of a primitive mound-forming tubicolous polychaete from the Ordovician of the Ottawa Valley, Canada. Palaeontology, **41**: 125–145.

Stott, D.F. 1991. Geotectonic correlation chart, Sheet 3, Southernmost Prairie Provinces, Hudson Platform and St. Lawrence Platform. *In* Sedimentary Cover of the North

American Craton: Canada. *Edited by* D.F. Stott an J.D. Aitken. Geological Survey of Canada, Geology of Canada, No. 5, Ottawa, ON.

Strasser, A. 1984. Black-pebble occurrence and genesis in Holocene carbonate sediments (Florida Keys, Bahamas, and Tunisia). Journal of Sedimentary Research, **54**: 1097–1109.

Swain, F.M., Palacas, J.G., and Kraft, J.C. 1966. High-calcium limestone deposits of Cumberland Valley, Pennsylvania. Ohio Journal of Science, **66**: 116–123.

Sweet, W.C. 1979. Late Ordovician conodonts and biostratigraphy of the western midcontinent province. *In* Conodont biostratigraphy of the Great Basin and Rocky Mountains. *Edited by* C.A. Sandberg and D.L. Clark. Brigham Young University, Geology Studies, v. 26, no. 3, p. 45–74.

Taugourdeau, P. 1965. Chitinozoaires de l'Ordovicien des U.S.A; comparaison avec les faunes de l'ancien monde. Rev. Inst. Fr. Petrole, Paris, **20**: 163–193.

Torres, M.E., Brumsack, H.J., Bohrmann, G., and Emeis, K.C. 1996. Barite fronts in continental margin sediments: a new look at barium remobilization in the zone of sulfate reduction and formation of heavy barites in diagenetic fronts. Chemical Geology, **127**: 125–139.

Tucker, M.E., and Wright, V.P. 2008. Carbonate sedimentology. John Wiley & Sons.

Vasconcelos, C., McKenzie, J.A., Warthmann, R., and Bernasconi, S.M. 2005. Calibration of the $\delta^{18}O$ paleothermometer for dolomite precipitated in microbial cultures and natural environments. Geology, **33**: 317–320.

Walker, K.R. 1972. Community ecology of the Middle Ordovician Black River Group of New York State. Geological Society of America Bulletin, **83**: 2499–2524.

Webby, B.D. 2004. Stromatoporoids. *In* The Great Ordovician Biodiversification Event. *Edited by* B.D. Webby, F. Paris, M.L. Droser, and I.G. Percival. Columbia University Press, New York. pp. 112–118.

Whalen, M.T., Gulick, S.P.S., Pearson, Z.F., Norris, R.D., Perez-Cruz, L., and Urrutia-Fucugauchi, J. 2013. Annealing the Chicxulub impact: Paleogene Yucatán carbonate slope development in the Chicxulub impact basin, Mexico. Deposits, Architecture and Controls of Carbonate Margin, Slope and Basinal Settings. SEPM Special Publication, **105**: 282–304.

Wilson, A.E. 1946a. Brachiopoda of the Ottawa Formation of the Ottawa–St. Lawrence Lowland. Geological Survey of Canada Bulletin, **8**: 1–149.

Wilson, A.E. 1946b. Geology of the Ottawa–St. Lawrence Lowland, Ontario and Quebec. Geological Survey of Canada, Memoir 241.

Wilson, A.E. 1948. Miscellaneous classes of fossils, Ottawa Formation, Ottawa–St. Lawrence Valley. Geological Survey of Canada Bulletin, **11**: 1–116.

Worden, R.H., and Morad, S. 2003. Clay minerals in sandstones: controls on formation, distribution and evolution. *In* Clay Mineral Cements in Sandstones. *Edited by* R.H. Worden and S. Morad. International Association of Sedimentologists Special Publication, **34**: 1–41.

Young, F.P., 1943, Black River Stratigraphy and faunas: I, American Journal of Science, **241**: 141–166.

Young, S.A., Saltzman, M.R., and Bergström, S.M. 2005. Upper Ordovician (Mohawkian) carbon isotope ($\delta^{13}C$) stratigraphy in eastern and central North America: Regional

expression of a perturbation of the global carbon cycle. Palaeogeography, Palaeoclimatology, Palaeoecology, **222**: 53–76.

Appendices

Appendix 1 Conodont Analysis

PALEONTOLOGICAL REPORT
RAPPORT DE PALÉONTOLOGIE

REPORT 6-ADM-2017

REPORT ON 2 ORDOVICIAN (BLACKRIVERAN TO KIRKFIELDIAN) CONODONT SAMPLES FROM UNNAMED STRATA IN SMALL OUTLIERS, CENTRAL ONTARIO SUBMITTED IN 2017 BY GEORGE DIX (CARLETON UNIVERSITY) (VNR 330403-001-17-EXT). NTS 31L-04, 31L-08. CON. NO. 1814

A.D. McCRACKEN

GEOLOGICAL SURVEY OF CANADA (CALGARY)
COMMISSION GEOLOGIQUE DU CANADA (CALGARY)

6-ADM-2017

Report on 2 Ordovician (Blackriveran to Kirkfieldian) conodont samples from unnamed strata in small outliers, central Ontario submitted in 2017 by George Dix (Carleton University) (VNR 330403-001-17-EXT). NTS 31L-04, 31L-08. Con. No. 1814

A. D. McCracken

All references to age determinations and paleontological data must quote the authorship of the report, and the unique GSC Curation Number of the fossil collection. If the report is cited in a publication, it should be included in the References Cited section as:

"McCracken, A.D., 2017. Report on 2 Ordovician (Blackriveran to Kirkfieldian) conodont samples from unnamed strata in small outliers, central Ontario submitted in 2017 by George Dix (Carleton University) (VNR 330403-001-17-EXT.) NTS 31L-04, 31L-08. Con. No. 1814; Geological Survey of Canada, Paleontological Report 6-ADM-2017, 8 p."

Reference to, or reproduction of, paleontological data and age determinations in publications must be approved by the author of the Paleontological Report prior to manuscript submission. If the author is not available, the Chief Paleontologist, Geological Survey of Canada (Calgary), should be consulted for possible revision.

Substantial use of paleontological and age data in publications should be reflected in the publications' authorship.

The two samples were submitted by George Dix, Carleton University. His submission application included this brief statement of objectives:

Several relatively small Ordovician outliers between Deux Rivieres and Lake Nipissing, central Ontario, represent erosional remnants of a stratigraphy that was once continuous with that in southern Ontario to the south, the Ottawa Embayment to the east, and a small fault-bound outlier to the north, the Timiskaming graben. One outlier, NW of Deux Rivieres was first described by Logan (1847), but contains very poor remains of macrofauna such that no biostratigraphic information has been obtained since. A second, south of Lake Nipissing, is part of a larger set including the Manitou Islands (Lake Nipissing) for which there is inconclusive biostratigraphy based on macrofauna. The two outliers are recognized have been interpreted to be of Late Ordovician in age, but whether they are of Blackriveran (Turinian) or Trentonian (Chatfieldian) or younger is not known. The objective is to obtain a conodont assemblage that will help resolve this problem. Ongoing M.Sc. research (Ms. He Kang, Carleton University) has

obtained a C13 profile from the Deux Rivieres outcrop showing a prominent positive excursion; conodont data will help to determine if this excursion is the GICE.

Material: 2 rock samples processed completely in the GSC laboratory.

GSC Curation Number: C-468313
Sample Bag A; station Deux Rivieres; latitude 46º 16' 52" N; longitude 78º 21' 42" W; NAD83; NTS 031-L-08. Con. No. 1814-1.

Fossils:
Belodina compressa (Branson & Mehl 1933)? - 1 specimen
Curtognathus sp. - 1 specimen
Drepanoistodus suberectus (Branson & Mehl 1933) - 1 specimen
Erismodus sp. - 9 specimens
Panderodus unicostatus (Branson & Mehl 1933) - 1 specimen
Plectodina aculeata (Stauffer 1930) - 8 specimens

Thermal: CAI 1.5.

Remarks: Probable age range *compressa* Zone to lower *tenuis* Zone (upper Blackriveran to Kirkfieldian)

The sample contains few elements, but is composed of six species. *Panderodus unicostatus* (Branson & Mehl) and *Drepanoistodus suberectus* (Branson & Mehl) are long-ranging taxa (upper Whiterockian to Middle Devonian for the former, upper Whiterockian through Richmondian for the latter).

Belodina compressa (Branson & Mehl)? and *Plectodina aculeata* (Stauffer) limit the age of this sample, although the two fibrous conodonts - *Curtognathus* and *Erismodus* do as well since they are typical of the Blackriveran to lower Shermanian strata. They can be dominant constituents of Fauna 7 (Sweet et al. 1971).

Plectodina aculeata ranges from Early Middle Ordovician (Champlainian); latest Chazyan through Kirkfieldian stages (Sweet in Ziegler, 1981, p. 277-280; *aculeata* to lower *tenuis* zones), or lowest Shermanian (Sweet 1982). Sweet (1984) showed the base of the *aculeata* Zone immediately below the base of Blackriveran.

Sweet (in Ziegler 1981) noted the Ontario occurrences of *Plectodina aculeata* included uppermost Chaumont and Rockland formations, Bobcaygeon and lower Verulam formations, Gull River and lower Bobcaygeon formations (Schopf 1966); Cloche Island formations and unnamed higher (pre-Cobourg) beds (Votaw 1971); upper Gull River, Coboconck, and mid-Kirk field formations (Winder et al. 1975). In Quebec, it was found in the Hull Limestone (Schopf 1966, Uyeno 1974), and at Globensky & Jauffred's (1971) Neuville section.

Belodina compressa (Branson & Mehl) ranges from Middle Ordovician (early Blackriveran to

mid-Shermanian). *Belodina compressa* evolved into *B. confluens* Sweet near the boundary between the *tvaerensis* and *superbus* zones in the mid-part of the Shermanian Substage (Sweet in Ziegler, 1981, p. 71-75).

Sweet (in Ziegler 1981) noted the species' Ontario occurrences included uppermost Chaumont and Rockland formations, Bobcaygeon and lower Verulam formations, upper Gull River and lower Bobcaygeon formations (Schopf 1966); Cloche Island formations and unnamed higher (pre-Cobourg) beds (Votaw 1971). In Quebec, it has been found in the Hull Formation (Schopf 1966, Uyeno 1974).

The fibrous genus *Erismodus* ranges from at least the base of the upper Whiterockian (= Chazyan) to about the middle of the Shermanian *tenuis* Zone (Sweet in Ziegler 1991, p. 55-58). Elements of *Erismodus* are relatively deeply excavated basally, whereas, in *Chirognathus*, the attachment surface is characteristically a scar-like area skewed to one side of the element. The fibrous genus *Ptilonconus* (cf. *Ptiloconus*? sp. of Schopf, 1966, Pl. 6, fig. 1) is regarded as a junior synonym of *Erismodus*. The two slender Sc elements are atypical of the genus *Erismodus*. They appear to be cordylodiform rather than eoligonodiniform. However, the Sa and Sb elements are typical of *Erismodus*.

The single *Curtognathus* element is asymmetrical - two small denticles on one lateral process, three on the other (further discussion below under GSC Curation Number C-468314).

GSC Curation Number: C-468314
Sample Bag B; station Owen Quarry; latitude 46º 06' 06" N; longitude 79º 32' 31" W; NAD83; NTS 031-L-04. Con. No. 1814-2.

Fossils:
Curtognathus sp. - 1 specimen
Drepanoistodus suberectus (Branson & Mehl 1933) - 4 specimens
Erismodus sp. - 1 specimen
Plectodina aculeata (Stauffer 1930) - 4 specimens

Thermal: CAI 1.5.

Remarks: Probable age range *aculeata* Zone to *tenuis* Zone (Blackriveran to Kirkfieldian)

The sample has fewer conodonts than the other, but the taxa are similar. The *Curtognathus* sp. element is symmetrical, with two small denticles on each lateral process. The base is typical of the genus - a scar-like area that is not excavated.

Uyeno (1974) illustrated "*Curtognathus*" *limitaris* Branson & Mehl (only two specimens were found in his Hull Formation samples). There is not enough material in these two samples to identify the taxa at the species level. *Curtognathus expansus* (Branson & Mehl) ranges from the *aculeata* to lower *tenuis* zones.

The single Sc element of *Erismodus* is eligonodiniform, with two small denticles on a short

anterolateral process, and a relatively deep base. Uyeno (1974) did not have an element that could be assigned to *Erismodus*.

Discussion on GICE

In their study, Young et al. (2005) noted that the Guettenberg carbon isotope excursion (GICE) began near the top of the *undatus* Zone (Turinian) with the heaviest C13 values within the tenuis Zone (Chatfieldian), and ended within the *tenuis* Zone. They found that the post-excursion values coincided with the base of the *confluens* Zone (also Chatfieldian).

The two species of significance herein to the GICE are *Belodina compressa*? and *Plectodina aculeata*. *Belodina compressa* ranges from the *compressa* Zone through the tenuis Zone (and presumably part of the evolution lineage to *B. confluens*). The species is represented here by only one robust element in GSC Curation No. C-468313. The most distinguishing feature between *B. compressa* and *B. confluens* is that the compressiform element in the former has a short straight anterobasal corner compared to the "smoothly arcuate anterior margin" in the latter (Sweet 1979, p. 59). This element is does not fit either definition convincingly. The elements of Uyeno (1974) that Sweet (1982) assigned to *B. compressa* do have this straight corner; the holotype of *B. confluens* (as *B. compressa* in Sweet & Bergström 1966) also has a straight (although more subtle) anterobasal portion of its arcuate margin. In the literature, other examples of the compressiform element in *B. confluens* have a more convincing arched anterobasal corner. It is unfortunate that there is only one specimen in this collection – the natural variation in a population might make a species interpretation more convincing. Hence I tentatively call this *B. compressa*? (i.e., with a queried species name).

Plectodina aculeata and *P. tenuis* (Branson & Mehl) overlap in range (Kirkfieldian-lowest Shermanian, Sweet 1982; lower part of the *tenuis* Zone, Sweet 1984) but differ in that the M element of the former is dichognathiform whereas in the latter it is cyrtoniodiform. Dichognathiform elements are also found in *Phragmodus undatus* Branson & Mehl as P elements – however, these two fragmentary elements in appear more robust than typical P elements of *P. undatus* (*P. undatus* and *P. aculeata* overlap in the *undatus* and lower *tenuis* zones).

The fibrous conodonts – *Curtignathus* and *Erismodus* also suggest a Blackriveran to lower Shermanian age.

In summary, I believe these are *B. compressa* and *P. aculeata* – if so, then these strata possibly date as pre-GICE, but could be as late as lower *tenuis* and thus within the early GICE.

REFERENCE LIST

Bergström, S.M. and Sweet, W.C.
1966: Conodonts from the Lexington Limestone (Middle Ordovician) of Kentucky, and its lateral equivalents in Ohio and Indiana. Bulletins of American Paleontology, v. 50, no. 229, p. 271-441.

Globensky, Y. and Jauffred, J.C.
1971: Stratigraphic distribution of conodonts in the Middle Ordovician Neuville section of Quebec. Geological Association of Canada, Proceedings, v. 23, p. 43-68.

Schopf, T.J.M.
1966: Conodonts of the Trenton Group (Ordovician) in New York, southern Ontario, and Quebec. New York State Museum and Science Service, Bulletin No. 405, 105 p.

Sweet, W.C.
1979: Late Ordovician conodonts and biostratigraphy of the western midcontinent province. *In* Conodont biostratigraphy of the Great Basin and Rocky Mountains. Sandberg, C.A. and Clark, D.L. (eds.). Brigham Young University, Geology Studies, v. 26, no. 3, p. 45-74.

Sweet, W.C.
1982: Conodonts from the Winnipeg Formation (Middle Ordovician) of the northern Black Hills, South Dakota. Journal of Paleontology, v. 56, p. 1029-1049.

Sweet, W.C.
1984: Graphic correlation of upper Middle and Upper Ordovician rocks, North American Midcontinent Province, U.S.A. *In* Aspects of the Ordovician System. Bruton, D.L. (ed.). Paleontological Contributions from the University of Oslo 295, p. 23-35.

Sweet, W.C., Ethington, R.L., and Barnes, C.R.
1971: North American Middle and Upper Ordovician conodont faunas. *In* Conodont Biostratigraphy. Geological Society of America, Memoir 127, p. 163-193.

Uyeno, T.T.
1974: Conodonts of the Hull Formation, Ottawa Group (Middle Ordovician), of the Ottawa-Hull area, Ontario and Quebec. Geological Survey of Canada, Bulletin 248, 31 p.

Votaw, R.B.
1971: Conodont biostratigraphy of the Black River Group (Middle Ordovician) and equivalent rocks of the eastern Midcontinent, North America. - Unpubl. Ph.D. Dissertation, Ohio State University, 170 p., 28 text-figs, 5 tables, 3 pl., Columbus, Ohio.

Winder, C.G., Barnes, C.R., Telford, P.G. & Uyeno, T.T.
1975: Ordovician to Devonian stratigraphy and conodont biostratigraphy of southern Ontario. - *In* Telford, P.G. (ed.), Field Excursions Guidebook, Part B: Phanerozoic Geology. - Geological Association of Canada, Mineralogical Association of Canada, Geological Society of America (North-Central Section), p. 119-160, 5 text-figs., Waterloo, Ontario.

Young, S.A., Saltzman., M.R., and Bergström, S.M.
2005: Upper Ordovician (Mohawkian) carbon isotope ($\delta^{13}C$) stratigraphy in eastern and central North America: Regional expression of a perturbation of the global. Palaeogeography, Palaeoclimatology, Palaeoecology, v. 222, p. 53-76.

Ziegler, W. (ed.)
1981: Catalogue of Conodonts. E. Schweizerbart'sche Verlagsbuchhandlung (Nägele u. Obermiller), Stuttgart, volume IV, 445 p.

Ziegler, W. (ed.)
1991: Catalogue of Conodonts. E. Schweizerbart'sche Verlagsbuchhandlung. (Nägele u. Obermiller), Stuttgart, volume V, 211 p.

Fig. 1. Middle and Upper Ordovician chronostratigraphic units (left two columns), conodont faunal units, conodont-based chronozones, Standard Time Units, North Atlantic conodont Zones. Figure is from Sweet (1979).

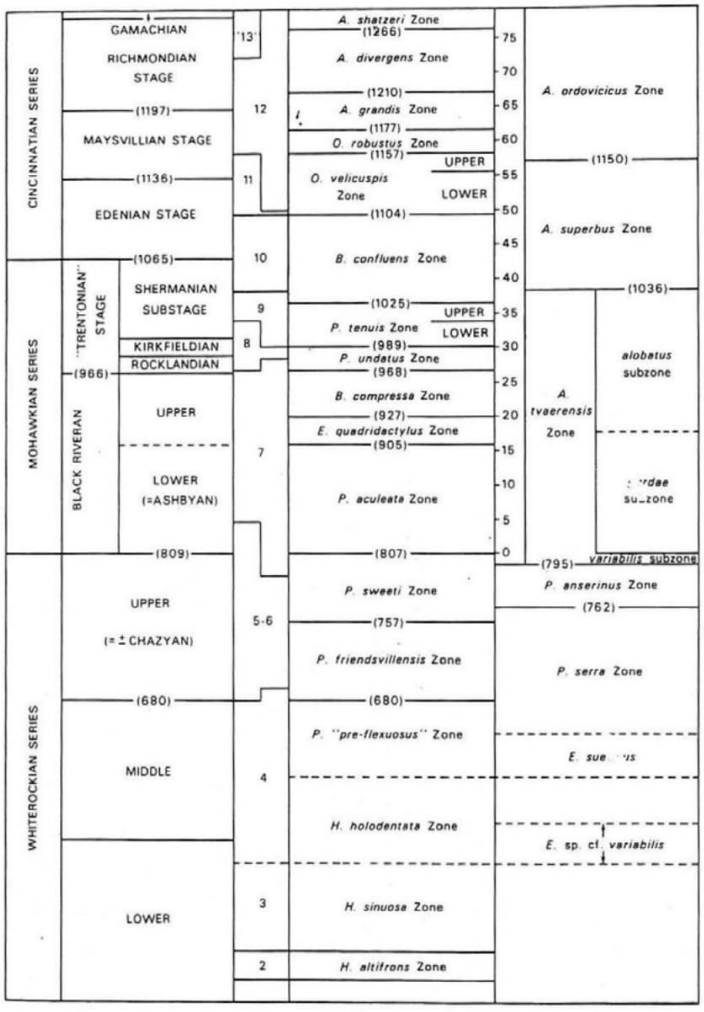

A.D. McCracken
Geological Survey of Canada (Calgary)
June 29, 2017
6-ADM-2017.docx

A.D. McCracken
Chief Paleontologist GSC (Calgary)

Appendix 2 Paleontology

(Compiled by Prof. George R. Dix; jointly interpreted with Ms. He Kang,
Department of Earth Sciences, Carleton University, 2017)

Fossil lists from previous work are presented with taxonomic names brought up to date on this basis of summaries of Ordovician stratigraphy of eastern Ontario (Fritz, 1957; Wilson, 1946a, 1947, 1948, 1951, 1956, 1961); summary of index fossils of North America (Shimer and Shrock, 1944); and, selected revisions of bryozoans (Blake, 1983). For each species, a stratigraphic range is shown that corresponds to "formations" of the Ottawa Embayment based on faunal succession (Wilson, 1921; 1946b), and, where applicable, reference is made to either Blackriveran or Trentonian affinities based on Shimer and Shrock (1944). All references are included in the main reference list of the thesis.

The Upper Ordovician "formational" succession defined by Wilson (1921; 1946b) for eastern Ontario is, from base to top:

Cobourg	
Sherman Fall	
Hull	
Rockland	base of Trenton succession
Leray	
Lowville	
Pamelia	base of Black River succession

For New York and eastern Ontario, subsequent work defined lithostratigraphic equivalents, replacing Leray with Watertown, Sherman Fall with Verulam, and Cobourg with Lindsay formations, although the specific boundaries are not equivalent (Liberty, 1965; Dix et al., 1997). In Wilson's collective work, she reported uncertainty about

stratigraphic affinity for a species by using a hyphen to link “formations”; the most common occurrence, unfortunately, being *Leray-Rockland* that signified uncertainty about whether a fossil belonged in uppermost Blackriveran or lowermost Trentonian strata.

Outliers on the Ottawa River between Deux Rivières and Mattawa

Introduction

In his report on the geology of the upper Ottawa River, Logan (1847) reported two areas of outliers upriver of what is now the townsite of Deux Rivières. The first was an outlier extending over a distance of about 2 miles (~ 4 km), above what was then known as Levier Rapids, now flooded. Today, the northern limit and thickest exposure of this outlier occurs ~ 4 miles (6 km) north of Deux Rivières (=Locality A, see below). Logan (1847) described a section of ~ 70 feet (21 m) with arenaceous brown limestone at the base succeeded by grey fine-grained limestone. Most of this stratigraphy is exposed at the outlier's northern limit.

The second outlier was encountered by Logan (1847) ~ 6 miles (10 km) south of Mattawa. The distance between localities A and B is ~ 15 km. Locality B contained two outcrops of limestone and large tabular blocks of limestone strewn along the shoreline (=Locality B; see below). With damming of the Ottawa River, Locality B was flooded. Bleeker (2012, written communication) reported the remains of a tiny outcrop of skeletal limestone.

Kay (1942) reported the occurrence of limestone blocks along the south side of the river north of Deux Rivières (=Locality C), approximately midway between the town site and Locality A. Colquhoun (1958) reported on the fossil assemblage in these blocks, and he thought that the blocks may represent remnants of blasting when a new rail bed was put in following valley flooding.

Locality A (Deux Rivières)

46° 16.875' N, 78° 21.711' W

north (Quebec) shore: strata display a rapid southward decrease in dip from northern limit of the outlier; the shoreline is underlain by carbonate rocks for several hundred metres.

From Logan (1847; p. 66), "Fossils are scarce . . . some remains of univalve [gastropods] and bivalve shells were too . . worn . . . but a peculiar coral . . resembles *Receptaculite de Neptune* of De Blainville." (Logan, 1847; p. 66). [Note: De Blainville is an incorrect authorship, it should be Defrance; Wilson, 1948]. In his summary of Paleozoic outliers, Ells (1896) referred to orthoceratites (cephalopod) in reference to the Deux Rivières outlier.

Present Study

Additional information is provided from thin-section petrography and conodont analysis. Thin sections reveal a cryptic fossil assemblage (see text) of bryozoans, calcareous algae, and cyanobacteria. In the following, fossils are reported relative to their height (DR2 = 2 m) above the base of the section; reference to text figures is made where appropriate. Only biostratigraphically critical fossils are illustrated, but references to sources from which comparisons were made are indicated.

DR2

<u>Bryozoan</u>

?Stictopora labyrinthica labyrinthica Hall.

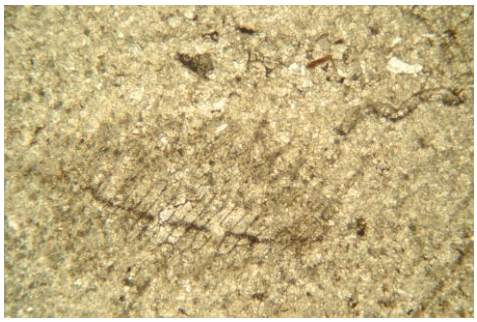

Oblique transverse section, wity mesotheca and extension of rectangular zooecia; magnification = 25x. Compare with Ross (1964; Plate 5, fig. 6).

DR5

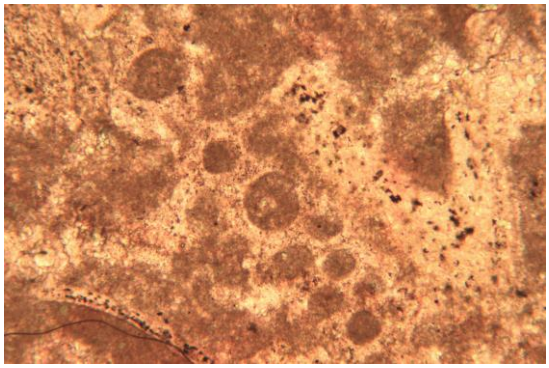

<u>*Calcareous Microfossil*</u>

Cyclocrinites (=Mastopora) sp. (Beadle, 1988). Osgood and Fisher (1960) provide a re-interpretation of an interpreted dasycladacean alga previously known under the genus *Nidulites*. However, other authors have moved this group in with receptaculitids, a problematic group of fauna or flora. Only a small fragment is present, showing large circular to ovoid pores that also occur in *C.* (=*M.*) *pyriformis.* Confirmation by Yuefeng Shen (Laval University). Magnification = 100x

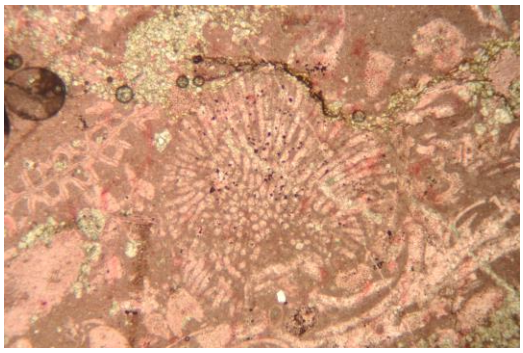

Hedstroemia sp.

Cyanobacteria; confirmation by Yuefeng Shen (Laval University), and see Johnson (1961; Plate 34, figs 1-5) for comparison**.** Thallus of intergrown rounded tubes. Thalli are irregular to rounded. Masses of this microbe is incorporated with laminar microbial micrite forming oncolites. Magnification =25x

<u>Bryozoan</u>

Stictopora sp., cf *S. labyrinthica labyrinthica* Ross (left side of above image). Similar form as illustrated in Blake (1983; Fig. 251, 1d) and Ross (1964; Plate 6, Fig 7). Magnification = 25x

DR7

Bryozoan

Stictopora labyrinthica labyrinthica, with prominent rectangular endozones; see Ross (1964; Plate 6)**.** Associated with lime mudstone that contains local transported ooid, and calcareous worm tube (upper part of photo).

Magnification =25x

Gastropod

Low, open-spired, rounded whorls.

Calcareous Worm tubes

Fragments of *Tymbochoos* sp. (Steele-Petrovich and Bolton, 1998) illustrating parts of small mounds and encrustations. Magnification = 25x

DR12

Bryozoans

Indeterminate forms: (1) encrusting (left image); and, (2) transverse section of a bifoliate (likely cryptostome) bryozoan illustrating hollow centre of a zoarial base encircled by radiating zooecia (compared with Blake, 1983; Fig. 224, fig. 5). Magnification = 25x (left), 100x (right)

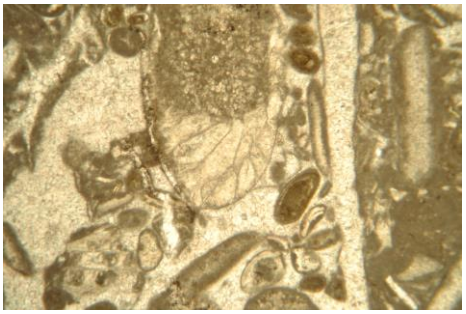

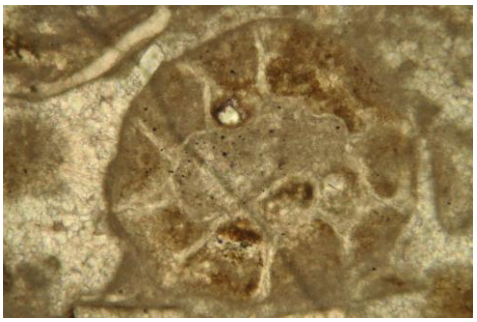

DR17

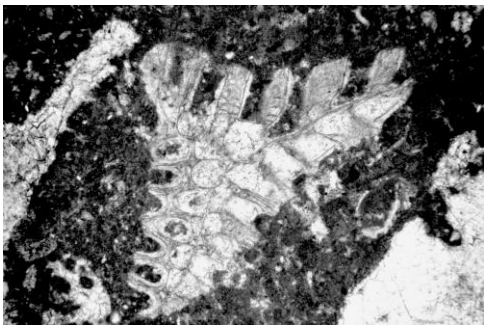

Bryozoa

Pachydictya acuta tabulata (see Ross, 1964; Plate 4, 5). The combination of bifurcating mesotheca and tabulae are unique to this species. Magnification = 25x

Algae (Dasycladacean)

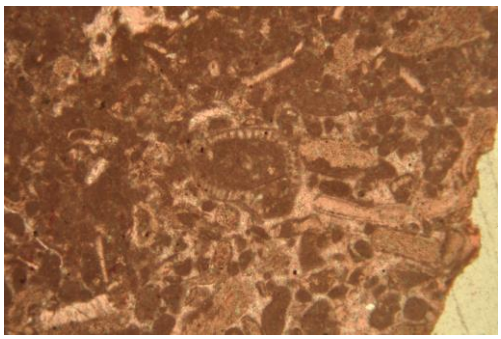

Vermiporella canadensis Horne and Johnson - various fragments including *V. canadensis* as identified by Yuefeng Shen (Laval University).

DR14

Hedstroemia sp.

Relatively common as small nodular forms, with one clast possessing a flat-floored geometry suggesting seafloor growth.

Girvanella sp.

Local, also incorporated within microbial micrite in oncolitic laminations

Oncolites

Microbial micrite with irregular porosity, along with irregular masses of *Girvanella* and *Hedstroemia*.

Rodophyte?

Transverse section, indeterminate affinity, illustrating concentric layer accumulation. Individual cells locally well separated by micrite; others are closely juxtaposed.

Vermiporella sp.

Several fragments, of which one is *Vermiporella canadensis* Horne and Johnson. Confirmation by Yuefeng Shen (Laval University).

Conodont Analysis

A sample of 1.9 kg of a skeletal-ooid grainstone was sent to the Biochronology Lab (GSC-Calgary, Dr. Sandy McCracken) for analysis. The results are shown in Appendix 1.

Interpreted Stratigraphic Affinity
Macrofossils

The presence of the bryozoans, *Stictopora labyrinthica labyrinthica* and *Pachydictya acuta tabulata*, suggest that the outcrop succession up to at least 7 m above the base is equivalent to Blackriveran strata in New York (Ross, 1964). This is further supported by the occurrence of fragments of calcareous worm tubes (*Tymbochoos*) that appear restricted to Black River strata, specifically the Pamelia and Lowville formations, in the Ottawa Valley (Steele-Petrovich and Bolton, 1998) and around Kingston, ON (Beddoes, 2009).

The calcareous algae define an Upper Ordovician association: a) *Mastapora* is a Caradocian (lower Upper Ordovician) genus, and b) *Vermiporella* ranges through the Upper Ordovician (Nitecki et al., 2004). The cyanobacterium or rivulariacean, *Hedstroemia*, occurs in Cambrian through Mesozoic strata (Nitecki et al., 2004). Logan's (1847) reference to a fossil that resembles *Receptaculites de Neptune* (Defrance*)* remains an uncertainty, although this fossil group can be used to distinguish Blackriveran and Trentonian strata (Shimer and Shrock, 1944).

Locality B: Ottawa River (East of Mattawa)

10 km south of Mattawa, ON, on the Ottawa River (Logan, 1847). Tabular blocks and two outcrops along the river shore were reported; the site is now flooded with river damming in the 1950s.

Logan (1847) referred to the limestone in outcrop and blocks as an encrinite, a grain-supported limestone composed nearly of only crinoid ossicles (Ausich, 1997). Later, Barlow (1899) provided paleontological data from identifications made by Dr. H.M. Ami, GSC paleontologist. His list follows:

Stratigraphic affinity*

Receptaculites occidentalis Salter	Leray/Rockland to Cobourg, (B)
Prasopora selwyni Nicholson	Hull, Sherman Fall, (T)**
Streptelasma corniculum Hall	Lowville to Cobourg, (B-T)
Strophomena incurvata Shepard	***
Rafiesquina alternata (Emmons)	Leray to Cobourg, (T)
Hesperorthis, sp. cf. *H. tricenaria* (Conrad)	Leray, Rockland, (B-T)
Anazyga recurvirostra (Hall)	Lowville to Cobourg, (B-T)
frondose and branching bryozoans	
gastropod (juveniles)	
trilobite fragment	

* "formation" names are from Wilson (1921; 1946b) whereas B (Black River), T (Trenton), B-T (Black River – Trenton), and R (Richmondian) are index references from Shimer and Shrock (1944) for North America.
** Ross (1967)
*** this species was defined by Shepard from rocks in northern Wisconsin interpreted at the time to have been Black River and Trenton strata but were shown later to be of a much younger Ordovician (Cincinnatian) age (Cooper, 1956; pg. 938-939); in addition, *S. incurvata* is of questionable status (Cooper, 1956).

Interpreted Stratigraphic affinity, Locality B

Barlow (1899) referred these rocks to the Trenton succession. The presence of the bryozoan *Prasopora selwyni* Nicholson, or *Prasoporina selwyni* (Nicholson) as reported by Fritz (1957) is stratigraphically significant. In New York, Ross (1967) showed that this species appears only during the late Trentonian, during the Denmarkian and

Cobourgian periods. Formations related to these periods are the Denley, Rust and Steuben formations (Brett and Baird, 2002). These strata are equivalent to the Hull (part), the overlying Sherman Fall (=Verulam), and Cobourg (=Lindsay) of eastern Ontario. Appearance of Trentonian rocks in eastern Ontario often coincides with an abrupt increase in the abundance of crinoids, with the upper Hull and Verulam representing encrinites accumulations.

Locality C

Colquhoun (1958) provided a fossil list for limestone blocks found along the southwest margin of the Ottawa River (see also Kay, 1942), ~ 3 miles or 5 km NW of Deux Rivières. Fossils were partly to extensively silicified, and recovered by acid leaching. This occurrence is ~ 2 km SE of Locality A on the Quebec side of the Ottawa River.

PORIFERA	
Receptaculites occidentalis Salter	Leray/Rockland, (B)
ANTHOZOA	
Streptelasma corniculum Hall	Leray/Rockland to Cobourg, (B-T)
Lambeophyllum profundum (Conrad)	Lowville to Leray/Rockland, (B)
ANTHOZOA	
Streptelasma corniculum Hall	Lowville/Leray to Cobourg, (B-T)
Lambeophyllum profundum (Conrad)	Lowville to Leray/Rockland, (B)
BRACHIOPODA	
Craniops trentonensis (Hall)	Leray/Rockland, (T)
Platystrophia amoena McEwan	Lowville/Leray to Cobourg
Hesperorthis tricenaria (Conrad)	Leray, Rockland, (B-T)
Dalmanella paquettensis (Sinclair)	Leray/Rockland
Dalmanella rogata (Sardeson)	Lowville to Cobourg
Dinorthis browni Wilson	Rockland to Cobourg
Dinorthis iphigenia media Wilson	Rockland/Hull
Dinorthis aff *subquadrata alternata* Wilson	Hull, Sherman Fall
Sowerbyella sericea (Sowerby)	Lowville/Leray to Cobourg
Sowerbyella punctostriata (Mather)	Leray?, Rockland, (lower T)*
Rafinesquina alternata (Conrad)	Leray to Cobourg
Rafinesquina alternata alta Wilson	Leray/Rockland
Rafinesquina alternata plana Wilson	Lowville to Cobourg
Rafinesquina alternata semiquadrata Wilson	Leray/Rockland, Hull
Rafinesquina lennoxensis Salmon	Leray/Rockland, Hull
Rafinesquina aff. *calderi* Wilson	Sherman Fall, Cobourg
Rafinesquina aff. *esmondsonis* borealis Wilson	Cobourg
Rafinesquina hullensis Wilson	Rockland, Hull
Rafinesquina opeongoensis Wilson	Rockland to Sherman Fall
Rafinesquina prestonensis Salmon	Sherman Fall
Rafinesquina rotunda Wilson	Cobourg
Rafinesquina subtrigonalis Wilson	Sherman Fall, Cobourg

Opikina gloucesterensis Wilson	Leray/Rockland
Opikina hemispherica Wilson	Leray/Rockland
Opikina platys Wilson	Leray/Rockland, Rockland
Opikina septata borealis Wilson	Leray/Rockland
Opikina sinclairi Wilson	Lowville to Hull
Strophomena billingsi Winchell and Schuchert	Leray/Rockland
Strophomena delicatula Fenton	Leray
Strophomena dignata Fenton	Leray
Strophomena venustrula Wilson	Pamelia to Rockland
Rostricellula ainsliei (Winchell)	Lowville, Leray, (B)
Rhyncotrema increbescens (Hall)	Lowville/Leray to Cobourg, (T)
Rhyncotrema intermedium Wilson	Leray
Rhyncotrema ottawaensis Billings	Leray/Rockland
Anazyga deflecta (Hall)	Leray
Anazyga recurvurostris (Hall)	Lowville to Cobourg, (B-T)

* *S. sericea* is a well-known lower Trenton fossil (Cooper, 1956), and Wilson's (1946a) reference to a Blackriveran form from the Lake Clear outlier seems incorrect given that the outlier contains "Utica shale" (Barlow, 1899) overlying encrinite (Dix, pers. obs, 2010).

GASTROPODA

Micropileus ottawanus Wilson	Lowville
Bucania halli Ulrich and Schofield	Lowville, Leray
Phragmolites compressus Conrad	Leray, Rockland, (T)
Sinuites cancellatus (Hall)	Rockland to Cobourg, (T-R)
Sinuites cancellatus liratus Wilson	Leray to Cobourg, (T)
Salpingostoma billingsi (Salter)	Lowville, Leray/Rockland
Loxoplocus (Lophospira) serrulatus (Salter)	Lowville to Hull, (B-T)
*Loxoplocus (Lophospira) milleri (*Salter)*	Leray, Leray/Rockland, (T)
Loxoplocus saffordi (Ulrich and Schofield)	Lowville, Leray/Rockland
Loxoplocus cf L. *ventricosa* (Hall)	Leray/Rockland, Hull
Hormotoma gracilis (Hall)	Lowville to Cobourg, (T-R)
Hormotoma aff. *trentonensis crassa* Wilson	Leray to Cobourg, (T)
Hormotoma salteri canadensis Ulrich and Schofield	Leray, Leray/Rockland
Hormotoma simplex paquettensis Wilson	Leray/Rockland
Liospira vitruvia Billings	Lowville to Cobourg, (B-R)
Eotomaria vitruvia (Billings)	Lowville to Leray/Rockland
Eotomaria supracingulata (Billings)	Leray, Leray/Rockland, (B)
Eotomaria dryope aff. *plana* Wilson	Leray, Leray/Rockland, (B)
Helicotoma planulata Salter	Lowville to Leray/Rockland, (B)
Trochonema umbilicum Hall	Leray, Rockland, (B-T)
Trochonemella arachne (Billings)	Lowville, Leray/Rockland
Gyronema semicarinatum (Salter)	Leray/Rockland
Halopea lavinia conica Wilson	Leray/Rockland
Halopea nereis spiralis Wilson	Leray/Rockland

* listed as *Lophospira helicteres*, but as indicated by Knight (1941) this is identical to *L. milleri*.

TRILOBITA	
Eoharpes sp. indet.	
Bathyurus aff. *bandifer* Sinclair	Leray
Bathyurus ingalli Raymond	Leray/Rockland, Hull
Bathyurus trispinosis Wilson	Leray/Rockland
Calliops narrawayi Okulitch	Leray/Rockland
Isotelus gigas DeKay	Lowville to Cobourg, (U. Ord)
Illaenus cf. *angusticollis* Billings	Leray
Calyptaulax calderi Wilson	Leray/Rockland
PELECYPODA	
Ctenodonta cf. *astartaeformis* Salter	Leray/Rockland to Cobourg
Ctenodonta contracta Salter	Leray, Leray/Rockland
Ctenodonta logani Salter	Leray/Rockland
Ctenodonta gibberula Salter	Leray/Rockland, (B)
Ctenodonta nasuta Hall	Pamelia to Cobourg, (B-T?)
CEPHALOPODA	
Zitteloceras hallianus (d'Orbigny)	Leray/Rockland, (T)
Gonioceras kayi Foerste	Leray/Rockland, (T)*
Michelinoceras aff. *sociale* Hall	Cobourg, (T)
Richardsonoceras cf. *simplex* (Billings)	Leray, (B)
Spyroceras cylindratum Foerste	Pamelia to Leray/Rockland
Spyroceras allumettense Foerste	Leray, Leray/Rockland

*from Kay (1942), but based on his interpretation that the Paquette Rapids section is Trentonian.

OSTRACODA
Aparachites sp.
Leperditella sp.
Leperditia sp.
Primitia sp.

Stratigraphic Affinity, Locality C

Colquhoun (1958) showed an interpreted strong association of the fossil assemblage with the "Rockland beds" (=lower Trenton) at the type section in Stewart Quarry (Rockland, ON). The above re-examination suggests that the fossils have a greater Blackriveran affinity. Some fossils lie within equivalent upper Ottawa Group strata, and may identify either misidentification or a more expanded range than recognized by Wilson's work.

Possibly supporting a Blackriveran association is the distribution of silicification. This diagenetic alteration is characteristic of sections at Paquette Rapids, Fourth Chute (Bonnechere River), and Braeside, all sections that the majority of workers (Kay, 1942 aside) consider to be of Blackriveran affinity (Billings, 1857; Flower, 1955; Cooper, 1956; Steele and Sinclair, 1971).

Relative Age of Stratigraphy at Localities A-C

Locality B is younger (=Trentonian) than the Blackriveran limestones at localities A and C. Locality A and C are not differentiated on fossil lists alone; instead, the former appears to grade upsection in lithofacies into what was a more skeletal-bearing, higher energy depositional system. This may indicate that the limestone blocks at Locality C represent facies younger than those exposed at Locality A.

Locality D (Manitou Islands)
eastern part of Lake Nipissing; 46° 15'43"N, 79° 34'28.4"W;
within Manitou Islands Provincial Park (restricted access)

Part 1
Murray (1853) reported fossiliferous strata from several of the Manitou islands. On the southwestern end of the western most island (unnamed by Murray), he noted the occurrence of *Actinoceras tenuifilum* (Hall) that at the time was viewed characteristic of Black River strata in New York, and known from the Watertown beds in New York and their equivalent in Ontario (Flower, 1955). From Iron Island, he also referred to abundant sandstone, with fragments of fossiliferous limestone along the beach. Fossils were considered to be of Chazyan aspect. This association often encompassed what are now lower Blackriveran strata (see Cooper, 1956). Unfortunately, he did not list the fossil names.

Part 2
On the most southerly of the Manitou islands, Barlow (1899) documented remains of the cephalopod *Vaginoceras multitabulatum* (Hall). This species, which is very common in upper Blackriveran (=Watertown) strata in New York, has a Blackriveran to lower Trenton range (Flower, 1955).

From the larger islands, Barlow (1899) reported the following fossils.

<u>Little Manitou (McDonald's) Island</u>

Palaeophlym or *Columnaria*	
Amplexopora sp.	(Ord)
Coscinopora ? sp.	
Rhombotrypa quadrata (Rominger)	(R)
Pachydictya acuta Hall	(T)
Sowerbyella ? sp.	

Anazyga recurvirostra (Hall)	Lowville to Cobourg, (T)
Hesperorthis tricenaria Conrad	Leray, Rockland, (B-T)
Rafinesquina cf *R. alternata* (Emmons)	(T-R)
Trochonema umbilicatum Hall	Leray, Rockland, (B-T)
orthoceratites (up to 2 m in length)	

<u>Great Manitou (Newmans) Island</u>

Stromatocerium rugosum Hall	Leray-Rockland, (B)
Favistella halli (Nicholson)	(B-T)
crinoids	
Escharapora falciformis (Nicholson)	(Maysvillian)
Rafinesquina cf *R. alternata*	(T-R)
Anazyga recurvirostra Hall	Lowville to Cobourg, (T)
Lophospira bicincta (Hall)*	Lowville to Rockland, (T)
Lophospira sp., cf *L. helicteres* Salter*	Leray, Rockland, (T)
Maclurea ? sp.	
Actinoceras sp. cf *A. bigsbyi* Salter	Lowville to Rockland, (B)
Endoceras sp.,	
Orthoceras sp.	

* from Knight (1941) - The genus *Lophospira* Whitfield was proposed with two "types" designated: *Murchisonia milleri* Hall or *M. bicincta* Hall, and *M. helicteres* Salter. Later, Oehlert in 1888 designated the former (*M. milleri*) as genotype. Thus, the two lophospirids above are the same species, with an age range of Black River – Trenton (Wilson, 1951).

Part 3

Colquhoun (1958) re-examined the fossil assemblage on Little and Great Manitou Islands.

Little and Great Manitou Islands

(not distinguished by individual island)

Clematischnia succulens Hall	burrows (not age-significant)
Lambeophyllum profundum (Conrad)	Lowville to Leray/Rockland, (B)
Lyopora halli (Nicholson)	Leray
Tetradium cellulosum (Hall)	Pamelia to Hull, (B-T)
Tetradium clarki Okulitch	Pamelia to Leray
Tetradium cf. *T. fibratum* Safford	Pamelia to Leray/Rockland, (B-R)
Craniops sp. indet.	
Hesperorthis tricenaria (Conrad)	Leray, Rockland, (B-T)
Dalmanella rogata (Sardeson)	Lowville to Cobourg
Sowerbyella sericea (Sowerby)	Lowville/Leray to Cobourg*
Rafinesquina alternata plana Wilson	Lowville to Cobourg
Rafinesquina alternata platys Wilson	Leray
Rafinesquina lennoxensis Salmon	Leray/Rockland, Hull
Rafinesquina praedeltoidea Wilson	Cobourg
Rostricellula ainsliei (Winchell)	Lowville, Leray, (B)
Rhyncotrema increbescens (Hall)	Lowville/Leray to Cobourg, (T)

Rhyncotrema intermedium Wilson	Leray
Opikina platys Wilson	Leray/Rockland, Rockland
Opikina sinclairi Wilson	Lowville to Hull
Anazyga deflecta (Hall)	Leray
Anazyga recurvurostris (Hall)	Lowville to Cobourg, (B-T)
Several cryptostome bryozoan (no species defined): Phyllodictya, Rhinidictya, Pachydictya, Esharopora, Ulrichostylus	
Phragmolites compressus Conrad	Leray, Rockland, (T)
Hormotoma salteri canadensis Ulrich and Schofield	Leray, Leray/Rockland
Liospira progne (Billings)	Lowville to Cobourg, (B-T)
Liospira vitruvia Billings	Lowville to Cobourg, (B-R)
Helicotoma planulata Salter	Lowville to Leray/Rockland, (B)
Trochonema umbilicum Hall	Leray, Rockland, (B-T)
Subulites cf. S. canadensis Ulrich and Schofield	Lowville, Leray/Rockland, Hull?

TRILOBITA

Bathyurus ingalli Raymond	Leray/Rockland, Hull
Bathyurus spiniger (Hall)	Lowville to Hull, (B)
Bathyurus trispinosis Wilson	Leray/Rockland
Isotelus cf. I. iowaensis (Owen)	(R)
Isotelus cf. I. latus Raymond	Leray
Ceraurus dentatus Raymond and Barton	Leray to Hull
Ceraurus cf. C. pleurexanthemus Green	Lowville/Leray to Cobourg, (B-T)

CEPHALOPODA

'Spyroceras' cf. S. paquettensis (Billings)	?
Sactoceras cf S. ehlersi Foerste	?
Sactoceras cf. *S. josephianum* Foerste	Pamelia/Lowville to Cobourg, (B)
Monomchites decrescens (Billings)	B (Frey, 1995)
Richardsonoceras falx (Billings)	Leray, Leray/Rockland
Ormoceras allumettense (Billings)	Leray, (B)
Actinoceras cf. A. tenuifilum (Hall)	(B-Watertown)*
Actinoceras cf. A. bigsbyi Bronn	(B)
Actinoceras cf. A. billingsi Foerste	Leray/Rockland
Vaginoceras multicameratum (Hall)	(B, T?)**
Leuerthoceras cf. L. hanseni Foerste	(U Ord)

* Flower (1957); A. tenuifilum (Hall) and A. bigsbyi Bronn are synonyms (Foord, 1889);
** Flower (1955)

Leperdita sp.

Ctenodonta astartaeformis Whiteaves	Leray/Rockland, Rockland

Stratigraphic affinity, Manitou Islands

The islands appear to have an upper Blackriveran biotic assemblage. Iron Island contains fossils considered by Murray (1853) to have a Chazyan aspect. It must be remember that this term was used in a much less restricted manner compared to now, and likely included strata equivalent to the lower Blackriveran succession of New York.

Locality E (Owen Quarry)

abandoned quarry south of Lake Nipissing, ~ 3 km west of Nipissing, ON;
46° 6.1' N, 79° 32.526' W; see Colquhoun (1958; p. 88-89); named after owner of property.

ANTHOZOA

from Colquhoun (1958):

Lyopora halli (Nicholson)	Leray
Lambeophyllum profundum (Conrad)	Leray/Rockland, (B)

Discussion based on the present study:

Three different forms of *Lambeophyllum* sp. were recovered, with these corals common in the carbonate succession beneath the shale-bearing interval.

Lambeophyllum? apertum (Billings)

Small, yet very broad (=flat; Wilson, 1948), turbinate calice, displaying rapid expansion. Billings (1865; p. 102, Fig. 89) described this form from interpreted Blackriveran strata at Paquette Rapids, upper Ottawa Valley; Okulitch (1938) re-assigned it to his *Lambeophyllum* genus, but with hesitation, and Wilson (1948) retained the association and "query". But these subsequent publications all deal with the same locality (Paquette Rapids); thus, this is the first time that the species has been found elsewhere. Wilson (1948) referred the Paquette Rapids section to an uncertain Leray-Rockland affinity. Kay (1942) is the only author to interpret the Paquette Rapids section as Trentonian. Scale = mm.

Lambeophyllum? sp.

A conical or funnel-shaped cross-section with an apparent basal central boss. In the United States, Elias (1983) reported a large number of specimens of a form that was similar to *Lambeophyllum profundum* (Conrad), yet differed in two respects: the calice was conical rather than funnel shaped (see Wilson, 1948), and some forms contained a central basal boss not reported for *L. profundum*. Elias (1983) queried the allocation to *Lambeophyllum* despite the general similarity in form.

Lambeophyllum profundum (Conrad)

Specimen similar in form as figured by Wilson (1948; Plate 15, figs. 8-11). Elias (1983) noted that this species allocation is often made by form alone, rather based on growth stages. The recovered speciment best fits *L. profundum* as figured by Wilson (1948).

Lichenaria sp. cf. L. globularis
Small, encrusting specimen, similar in form and cross-sectional structure to that figured by Elias (2008; Fig. 1) and illustrated by Okulitch as reported in Bassler (1950; Plate 11, fig 1-3; Plate 15, fig 8-9). Image: left, cross-section growth position; right, top view

BRACHIOPODA

from Colquhoun (1958):

Platystrophia aff. *amoena* McEwan	Leray/Rockland, Rockland, Sherman Fall
Glyptorthis aff *bellarugos* (Conrad)	Lowville/Leray, Leray/Rockland, (B-T)
Dalmanella rogata (Sardeson)	Lowville through Cobourg
Dinorthis pectinella (Emmons)	Lowville through Sherman Fall, (T)
Sowerbyella punctostriata Mather	Leray, Rockland, (T)
Rafinesquina esmondsonis borealis Wilson	Cobourg
Rafinesquina prestonensis Salmon	Sherman Fall
Strophonema aff *dignata* Fenton	Leray
Strophonema aff *magna* Wilson	Rockland
Trigammaria aff *trigonalis prima* Wilson	Rockland
Rhyncotrema i*ncrebescens* (Hall)	Lowville through Cobourg, (T)

Discussion based on the present study:

According to the Treatis of Invertebrate Paleontology, the latest revision of strophomenid brachiopods (*Rafinesquina*, *Trigammaria* and *Strophomena*) places the latter two as subgenera of *Strophomena*. Rafinisquinids display considerable variation in form resulting in great potential for over speciation (Wilson, 1946; p. 54). Furthermore, all three require careful examination of external and internal morphologies in order to correctly identify and distinguish species and even subgenera. Thus, this study tentatively identifies (sub)genera in common with Colquhoun (1958), including *Sowerbyella.* But specific affinities are not possible. Note that in the above list the two rafinesquinids are associated with much younger stratigraphy in eastern Ontario, well separated from the others suggesting either an incorrect identification or a much greater faunal range.

Strophomena or Trigammaria
pedicle valve, ventral interior: spade shaped valve, with stout cardinal processes and much reduced muscle ridge and median septum, the latter extending anteriorly beyond the terminus of the muscle ridge. This specimen fits that figured by Cooper (1956) of *S. inspeciosa* Willard (Plate 264, Fig. 21) and description of Willard (1928; Plate 2, Fig. 13) of a ventral interior referenced to this species. *S. inspeciosa* is

associated with rocks equivalent to the Blackriveran- lower Trentonian succession in New York (Cooper, 1956).

Strophonmena sp. B
Pedicle, ventral interior, and brachial exterior: elliptical muscle ridges recurved posteriorly, leaving a medial gap. Width = 7 cm

Strophomena sp. C
pedicle valve, interior: showing elliptical muscle ridges; variation of similar geometries are associated with Cooper's (1956; Plate 257, fig. 10) subspecies of *S. auburnensis nasuta* from the Tyrone Formation, Trentonian strata equivalent to the Napanee through lower Hull Formation (Cooper, 1956). Scale = mm.

Strophomena sp. D
pedicle, ventral interior: oblate spherical shaped muscle ridges, thickened laterally, recurved into median gap, with space in between. Similar geometries are associated with Cooper's (1956; Plate 257, fig. 9, 10) subspecies of *S. auburnensis nasuta* from the Tyrone Formation, Trentonian strata equivalent to the Napanee through lower Hull Formation (Cooper, 1956). Scale = mm

?Dinorthis sp.
pedicle valve: similar in form illustrated by Cooper (1956; Plate 57A)
Width of shell = 2 cm.

?Plectorthis sp.
pedicle valve: similar in form illustrated by Wilson (1946a; Plate II, Fig. 5b). Scale = mm.

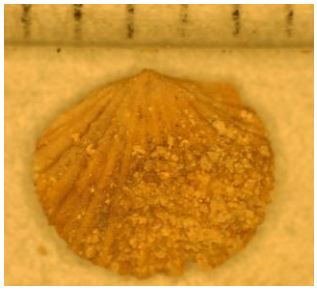

Hesperorthis sp.
forms similar to those illustrated by Cooper (1956; Plates 51-54).
Maximum width of shell = 17 mm.

Sowerbyella sp.
fragment of brachial valve; similar in form as *S. sericea* figured by Wilson (1946; Fig. 26), and elongated forms illustrated by Cooper (1956: Plate 196, Fig. 27).
Scale = mm.

<u>Proposed stratigraphic affinity:</u>
The present study adds no new biostratigraphic information to Colquhoun's (1958) study. From comparison with Wilson's work, and incorporating the uncertainty of her Leray/Rockland association, the brachiopod assemblage suggests a correspondence to Rockland-age strata. Colquhoun (1958; Table 3) illustrated similarly a strong correspondence among brachiopod fauna with Rockland beds at the formation's type section in eastern Ontario, but this is assuming a correct species identification and shifting the Leray-Rockland uncertainty to Rockland affinity at Paquette Rapids.

BRYOZOA
From Colquhoun (1958):
Dianulites rocklandensis Wilson Leray, Rockland (most abundant)

Discussion based on this study:
Three types of bryozoans are recognized:

1. a low encrusting to domal form (*Dianulites rocklandensis*) as illustrated by Wilson (1921). Width of zoaria = 2 cm

2. two types of erect bryozoan forms, with internal structure lost through dolomitization: (left) the more common and larger forms are long (< 5-6 cm) cylindrical branching forms; and, (right) dumbbell-shaped stick fragments of the segmented *Arthroclema* Billings (see Blake, 1983; Fig. 272, 2b, c; also Lobdell, 1992; Plate 1, fig. 15). Individual segments are 2-3 mm in length and 0.5 to 0.75 mm in width, but widening with matching terminal flanges at either end of a segment. At least one articulation facet is visible on a given segment. Zoecial details are lost through dolomitization but the form and size fits Billings' (1865; p. 54) *A. pulchella* collected from "Trenton limestone, City of Ottawa". Segments are ~ 4 mm in length.

Proposed stratigraphic affinity
The defined bryozoans identify a Trentonian affinity with an important stratigraphic link to fossil material in eastern Ontario. Blake (1983) refers to additional Trentonian material from the Decorah Shale whereas Lobell's (1992) material comes from younger Richmondian strata from in the mid-west USA. The genus has an Upper Ordovician range (Blake, 1983).

TRILOBITA

From Colquhoun (1958):

Illaenus aff *americanus* Billings — Leray, Sherman Fall, Cobourg, (T)

Calyptaulax aff *calderi* Wilson — Leray/Rockland

Discussion based on this study:

Only a fragment of what might be part of a pustulose glabella was recovered; pustular surfaces are common in several trilobite groups.

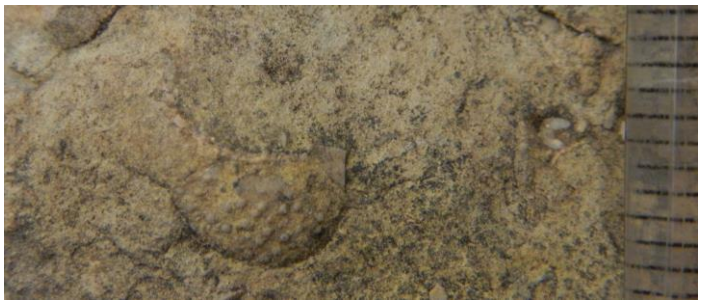

Proposed stratigraphic affinity:

Assuming the correct identification of *C.* aff. *caldera*, this species restricts the association to the uncertain Leray/Rockland succession.

PELECYPODA

From Colquhoun (1958):

Ctenodonta gibberula Salter — Leray/Rockland, (B)

Discussion based on the present study:

The above genus was not recognized. Instead, the cast of another pelecypod was recovered. Its form is most similar to Ulrich's (1894) *Sphenolium striatum* (Plate 36, Fig. 44, 45). *Sphenolium* Miller as figured by Ulrich (1894) differs from Upper Ordovician defined type species *S. cuneiforme*, *S. richmondense* and *S. faberi (*see Miller, 1889; Kriz and Steinova, 2009). Wilson (1956; Plate 1, figs 10 and 11) figured a specimen referred to *Cuneamya* sp., noting its form similar to *Sphenolium parallelum* described by Ulrich (1884). As noted above in comparison with Miller's (1889) documentation, and discussion by Kříž and Steinová (2009), the reference of Ulrich's specimen to *Sphenolium* becomes unclear.

(left) scale = mm; (right) width = 20 mm

Proposed stratigraphic affinity:
Despite the uncertainty described above, Ulrich's (1894) material comes from the *Fusispira* and *Nematopora* beds of Late Ordovician age in Minnesota, a stratigraphic affinity recognized to be equivalent to the present-day Galena Formation, which is equivalent to the lower Trentonian strata of New York (Agnew et al., 1955). This association fits with the uncertain Leray/Rockland placement of *Ctenodonta gibberula*.

NAUTILOIDEA
From Colquhoun (1958):
Richardsonoceras falx Billings

Discussion based on this study:
Two fragments of nautaloids were recovered.
Richardsonoceras falx.
Colquhoun (1958) recorded *Cyrtoceras falx* Whiteaves, but Billings (1857) is the correct authorship, whereas an authorship to Whiteaves would be in reference to *C. cuneatum* (Whiteaves, 1906). Whiteaves (1906) speculated that *C. cuneatum* may be of a different genus. The present study recovered one specimen of *R. falx*, an internal cast with no ultrastructure preserved. In comparison with specimens figured by all previous workers (including that of Billings) the specimen is unique in preserving much more of the narrowing and curved posterior end. Scale = mm

Zitteloceras sp.
Only a very small part of the exterior is exposed in a rock slab, but is distinctive with its crenulated frills (see Steele and Sinclair, 1971; Plate 11, figs. 17, 18). Scale = mm

Proposed stratigraphic affinity:
Billings' specimen of *R. falx* came from strata exposed at Paquette Rapids, ON, in which there has been debate of Blackriveran versus Trentonian affinity.

ARTHROPODA
Ostracoda
Discussion based on this study:

Two large smooth ostracodal forms were recovered:

Several large (cm-scale) smooth shelled ostracodes are typical in coarse-grained rudstones, and interpreted as leperditicopid ostracodes. Of these, however, the following is recognized:

Eoleperditia fabulites (Conrad, 1843)
Very similar in form to that illustrated by Berdan (1984; Plate 1, fig. 8).

Proposed stratigraphic affinity:
E. fabulites has been recovered from Blackriverian-Rocklandian strata across the mid-west USA and Ontario (Berdan, 1984).

ECHINODERMATA
Crinoidea
Discussion based on this study:
Crinoid ossicles are abundant in the coarse-grained skeletal limestones of the quarry. Some columnals several cm in length are preserved. The following example matches closesly with *Schizocrinus nodosum* Hall (see Hall 1847) with its double pattern of alternating nodose columnals with the larger diameter primary columnals.

?Cystoidea
Several examples of small cups, plates, and attached columnals suggest an association with cystoids, possibly the Glyptocystidae (see Kesling, 1967). All scales = mm.

References:

Ausich, W.I. 1997. Regional encrinites: a vanished lithofacies. In: *Paleontological events: stratigraphic, ecologic and evolutionary implications*, p. 509-519. Columbia University Press, New York.

Barlow, A.E., 1899. Nipissing and Timiskaming Map-Sheets. Geological Survey of Canada, Ottawa.

Beadle, S.C., 1988. Dasyclads, cyclocrinitids and receptaculitids: comparative morphology and paleoecology. Lethaia, v. 21, 1-12.

Beddoes, P.A., 2009. Urban coastal geology and management, Kingston region. Lake Ontario, B.Sc. (Hons) thesis, Carleton University.

Billings, E. 1858. Report of Progress of the Geological Survey of Canada, 1857, pp. 147-192.

Blake, D.B., 1983. The order Cryptostomata. In:Treatise of Invertebrate Paleontology, Part G (revised). Edited by R.S. Boardman et al.. Geological Society of America and University of Kansas, pp. 441-592.

Colquhoun, D.J., 1958. Stratigraphy and paleontology of the Nipissing-Deux Rivieres outliers. Proceedings of the Geological Association of Canada.

Cooper, G.A., 1956. Chazyan and Related Brachiopods. Smithsonian Institutions, Washington, 1245 pp.

Ells, R.W., 1896. Palaeozoic outliers in the Ottawa River Basin. Transactions of the Royal Society of Canada, Second Series, vol 2, section IV, pp. 137- 149.

Foord, A.H. 1889. Catalogue of Fossil Cephalopoda in the British Museum (Natural History), Part 1. Taylor and Francis, London, 344 pp.

Flower, R.H., 1955. Status of Ednoceroid classification. Journal of Paleontology, v. 29, 329-371.

Flower, R.H., 1957. Studies of Actinoceratida. New Mexico State Bureau of Mines and Mineral Resources, Memoir 2, 73 pp.

Fritz, M.A., 1957. Bryozoa (mainly Trepostomata) from the Ottawa Formation (Middle Ordovician) of the Ottawa-St. Lawrence Lowland. Geological Survey of Canada Bulletin 42.

Kay, G.M., 1942. Ottawa-Bonnechere graben and Lake Ontario homocline. Bulletin of the Geological Society of America, v. 53, 505-546.

Kesling, R.V., 1967. Cystoids, In: Echinodermata 1. Beaver, H.H. and 10 others. *Treatise of Invertebrate Paleontology, Part S*. Geological Society of America, Kansas, pp. S85-S268.

Knight, J.B. 1941. *Paleozoic Gastropod Genotypes*. GSA Special Paper 32, Washington, USA, 510 pp.

Logan, W.E., 1847. Report on Progress of the Geological Survey of Anada, 1845-1846, 40-51.

Murray, A., 1853. Progress Report of the Geological Survey of Canada, 1853, pp. 59-124.

Nitecki, M.H., Webby, B.D., Spjeldnaes, N., and Yong-Yi, Z., 2004. Receptaculitids and Algae. In: The Great Ordovician Biodiversification Event. Edited by B.D. Webby, F.Paris, M.L. Droser, and I.G. Percival. Columbia University Press, pp. 336-347.

Osgood, R.G., and Fisher, A.G., 1960. Structure and preservation of Mastopora pyriformis, an Ordovician dasycladacean algae. Journal of Paleontology, v. 34, 896-902.

Ross, J.P., 1964. Champlainian cryptostome bryozoan from New York State. Journal of Paleontology, v. 38, 1-32.

Steele, H.M., and Sinclair G.W., 1971. A Middle Ordovician fauna from Braeside, Ottawa Valley, Ontario. Geological Survey of Canada Bulletin 211, 42 pp.

Steele-Petrovich, H.M., and Bolton, T.E. 1998. Morphology and palaeoecology of a primitive mound-forming tubicolous polychaete from the Ordovician of the Ottawa Valley, Canada. Palaeontology 41, pp. 125-145.

Wilson, A.E., 1921. A range of certain Lower Ordovician faunas of the Ottawa Valley with dscriptions of some new species. Geological Survey of Canada, Victoria Museum Bulletin 33, pp. 19-57.

Wilson, A.E., 1946a. Brachiopoda of the Ottawa Formation of the Ottawa-St. Lawrence Lowland. Geological Survey of Canada Bulletin 8.

Wilson, A.E., 1946b. Geology of the Ottawa-St. Lawrence Lowland, Ontario and Quebec. Geological Survey of Canada Memoir 241.

Wilson, A.E., 1947. Trilobita of the Ottawa Formation of the Ottawa-St. Lawrence Lowland. Geological Survey of Canada Bulletin 9.

Wilson, A.E., 1948. Miscellaneous classes of fossils: Ottawa Formation, Ottawa-St. Lawrence Lowland. Geological Survey of Canada Bulletin 11.

Wilson, A.E., 1951. Gastropoda and Conularida of the Ottawa Formation of the Ottawa-St. Lawrence Lowland. Geological Survey of Canada Bulletin 17.

Wilson, A.E., 1956. Pelecypod of the Ottawa Formation of the Ottawa-St. Lawrence Lowlands. Geological Survey of Canada Bulletin 28, 98 pp.

Wilson, A.E., 1961. Cephalopoda of the Ottawa Formation of the Ottawa-St. Lawrence Lowland. Geological Survey of Canada Bulletin 67, 106 pp.

Appendix 3 Carbon and Oxygen Isotopes

Deux Rivières outlier (analyzed at Queen's University)

Sample ID	elevation (meter)	$\delta^{13}C$ ‰ vs VPDB	$\delta^{18}O$ ‰ vs VSMOW	$\delta^{18}O$ ‰ vs VPDB
C1	0.4	-1.7	21.9	-8.7
C2	0.95	-1.4	22.4	-8.2
C3	1.4	-1.1	26.4	-4.4
C4	4.1	-2.2	26.3	-4.4
C5	4.4	-2.3	26.1	-4.6
C6	5.65	-1.1	24.4	-6.3
C7	5.85	-0.7	26.0	-4.7
C8	6.4	-0.4	26.2	-4.5
C9	7	-0.1	26.4	-4.3
C10	7.4	-0.4	25.7	-5.0
C11	8.45	0.5	20.7	-9.8
C12	9	-0.2	25.7	-5.0
C13	9.5	-0.6	26.2	-4.5
C14	9.8	-0.1	26.0	-4.7
D1	4	-1.1	28.8	-2.0
D2	7.85	0.2	22.6	-8.0

Brent Crater (analyzed at Queen's University)

Sample ID	elevation (feet)	elevation (meter)	$\delta^{13}C$ ‰ vs VPDB	$\delta^{18}O$ ‰ vs VSMOW	$\delta^{18}O$ ‰ vs VPDB
C20	10.3	3.09	-0.5	26.4	-4.3
C21	11.8	3.54	-1.0	26.3	-4.5
C22	13	3.9	-1.8	26.3	-4.5
C23	15	4.5	-2.3	26.1	-4.6
C24	18	5.4	-2.7	26.7	-4.1
C25	21	6.3	-1.6	26.2	-4.6
C26	24	7.2	-3.4	25.4	-5.3
C27	27	8.1	-3.6	25.5	-5.3
C28	30	9	-4.5	27.7	-3.1
D23	33	9.9	-3.5	29.4	-1.4
C29	36	10.8	-5.0	27.6	-3.2
C30	39	11.7	-2.5	27.8	-3.0
C31	42.2	12.66	-2.3	26.2	-4.5
C32	44.6	13.38	-2.5	26.2	-4.6
C33	48	14.4	-3.3	23.3	-7.4
D24	51	15.3	-3.4	29.6	-1.2
D25	54	16.2	-3.8	28.5	-2.3
D26	57	17.1	-2.8	24.1	-6.6
D27	59.8	17.94	-3.2	29.7	-1.2
D28	61	18.3	-3.4	29.5	-1.3
C34	64	19.2	-4.2	29.2	-1.7
C35	67	20.1	-3.9	23.7	-6.9
C36	70	21	-3.6	26.0	-4.8
C37	73	21.9	-2.2	27.1	-3.7
C38	76	22.8	-1.7	27.9	-2.9
D29	79	23.7	-1.4	29.4	-1.5
C39	82	24.6	-1.9	25.3	-5.4
C40	85	25.5	-0.7	27.5	-3.3
C41	88	26.4	-1.9	26.0	-4.7
C42	91	27.3	-1.3	28.5	-2.3
C43	94	28.2	-1.2	25.8	-5.0
C44	97	29.1	-1.0	25.1	-5.6
C45	100	30	-0.7	29.5	-1.4
C46	103	30.9	-0.9	28.5	-2.3
C47	106	31.8	-2.0	25.3	-5.4
C48	109.5	32.85	-0.6	29.0	-1.9
C49	112	33.6	-1.8	25.0	-5.7
C50	115	34.5	-1.8	24.8	-5.9

C51	118	35.4	-0.1	28.1	-2.7
C52	121	36.3	-0.2	28.2	-2.6
C53	124	37.2	-0.7	26.5	-4.3
C54	127	38.1	-1.1	27.4	-3.4
C55	130	39	-0.4	27.6	-3.2
C56	190	57	-1.0	27.9	-2.9
C57	193	57.9	-2.1	25.5	-5.3
D30	196	58.8	-1.5	29.1	-1.7
C58	199	59.7	-2.2	26.6	-4.2
C59	202	60.6	-3.1	27.3	-3.5
C60	205	61.5	-3.5	25.6	-5.1
D31	208	62.4	-1.6	29.3	-1.6
C61	211	63.3	-3.9	25.4	-5.3
C64	291	87.3	-2.9	25.5	-5.3
C62	293	87.9	-3.1	27.2	-3.6
C63	296	88.8	-3.6	26.9	-3.9
C65	299	89.7	-3.2	26.0	-4.8
C66	302	90.6	-3.4	26.1	-4.7
C67	305	91.5	-3.8	25.8	-5.0
C68	308	92.4	-3.8	25.9	-4.9
C69	311	93.3	-2.7	26.2	-4.6
C70	314	94.2	-1.9	26.9	-3.9
C71	317	95.1	-2.0	26.6	-4.2
C72	320	96	-1.3	26.3	-4.5
C73	323	96.9	-2.0	25.9	-4.9
C74	326	97.8	-1.4	25.4	-5.4
C75	329	98.7	-2.3	25.5	-5.3
C76	332	99.6	-3.7	25.4	-5.4
C77	334	100.2	-2.3	25.8	-4.9
C78	338	101.4	-2.0	28.7	-2.2
C79	341	102.3	-2.5	26.7	-4.0
C80	344	103.2	-1.9	28.1	-2.7
C81	347	104.1	-1.5	26.8	-4.0
C82	350	105	-1.4	26.6	-4.1
C83	353	105.9	-7.3	27.9	-2.9
C84	356	106.8	-8.8	25.7	-5.0
C85	359	107.7	-7.4	27.7	-3.1
C86	362	108.6	-8.3	25.9	-4.9
C87	365	109.5	-8.4	25.4	-5.3
C88	368	110.4	-9.2	25.0	-5.8
C89	370.6	111.18	-7.6	26.7	-4.1

C90	371	111.3	-8.8	25.2	-5.6
C91	373	111.9	-9.3	25.1	-5.6
C92	376	112.8	-9.9	25.2	-5.6
C93	378	113.4	-10.8	25.7	-5.0
C94	381.6	114.48	-18.0	27.6	-3.2
C95	385	115.5	-7.3	26.9	-3.9
C96	388.4	116.52	-6.8	22.9	-7.7
C97	391	117.3	3.1	23.7	-7.0
C98	401.8	120.54	-9.7	26.3	-4.5
C99	418.5	125.55	1.6	25.4	-5.3
C100	443.3	132.99	3.5	24.9	-5.9
C101	454.8	136.44	-0.4	20.8	-9.8
D43	482.8	144.84	3.5	22.8	-7.8
C102	493.9	148.17	3.5	24.4	-6.3
D44	498.6	149.58	3.4	27.3	-3.5
D33	501	150.3	2.4	26.0	-4.7
D32	504	151.2	2.2	27.7	-3.1
D34	508.2	152.46	1.7	28.3	-2.5
D35	512.1	153.63	2.0	27.4	-3.4
D36	518.6	155.58	3.8	26.3	-4.5
D37	534	160.2	1.4	25.3	-5.4
D38	549.3	164.79	-0.4	26.6	-4.2
D39	565	169.5	2.0	27.6	-3.3
D40	580	174	-2.5	27.2	-3.6
D41	584	175.2	0.3	27.8	-3.0
D42	593	177.9	-5.7	25.6	-5.2
D45	608.5	182.55	-5.7	27.7	-3.1
D46	611	183.3	-12.7	25.4	-5.4
D47	626	187.8	-13.7	26.6	-4.2
D48	647.5	194.25	-15.7	26.8	-4.0
D49	654	196.2	-15.8	27.2	-3.6
D50	666	199.8	-16.7	27.7	-3.1
D51	669	200.7	-12.4	26.9	-3.9
D52	679.3	203.79	-17.1	27.5	-3.3
D54	689.3	206.79	-18.1	26.8	-4.0
D53	690.1	207.03	-17.6	27.4	-3.4
C103	700	210	-17.8	24.6	-6.1
D55	707	212.1	-18.0	27.3	-3.5
D56	710	213	-18.4	25.7	-5.0
D57	713.2	213.96	-18.2	26.8	-3.9
D58	719.6	215.88	-18.1	25.0	-5.8

D59	723.5	217.05	-18.0	24.4	-6.3
D60	729	218.7	-17.6	28.2	-2.6
D61	733.5	220.05	-18.0	26.4	-4.4
D62	739.9	221.97	-17.0	24.7	-6.1

Cedar Lake outlier (analyzed at Queen's University)

Sample ID	Elevation (cm)	$\delta^{13}C$ ‰ vs VPDB	$\delta^{18}O$ ‰ vs VSMOW	$\delta^{18}O$ ‰ vs VPDB
CR5	91	-2.105	19.212	-11.354
CR8	264	-0.905	22.702	-7.969

Great Manitou Island
(analyzed at Queen's University)

Sample ID	elevation (meter)	$\delta^{13}C$ ‰ vs VPDB	$\delta^{18}O$ ‰ vs VSMOW	$\delta^{18}O$ ‰ vs VPDB
D3	2	-2.2	21.3	-9.2
D4	2.5	-3.1	21.5	-9.1
D5	3	-1.2	21.7	-8.8
D6	3.5	-1.5	21.4	-9.1
D7	4	-1.7	21.4	-9.1
D8	4.5	-0.9	21.8	-8.8
D9	5	-1.4	21.6	-8.9
D10	5.5	-0.7	21.6	-8.9
D11	6	-0.1	21.4	-9.2
D12	6.5	-0.7	21.6	-9.0
D13	7	-0.5	21.9	-8.7
D14	7.5	-0.5	21.8	-8.8
D15	8	-0.5	21.9	-8.7
D16	8.5	-1.4	20.9	-9.7
D17	9.3	-2.1	26.0	-4.8
D18	9.4	-0.5	20.8	-9.7
D19	9.67	-0.4	22.1	-8.5
C15	9.7	-0.8	26.1	-4.6
C16	9.95	-0.9	25.9	-4.8
D20	10.5	-0.7	22.0	-8.6
D21	10.8	-0.3	22.7	-8.0
D22	11.4	0.0	22.0	-8.6

(analyzed at University of Ottawa)

Sample ID	Type	$\delta^{13}C$ ‰ vs VPDB	$\delta^{18}O$ ‰ vs VPDB
GM5Ca	late-stage calcite cement	-5.34	-6.5
GM5Do	Saddle dolomite	-2.85	-10.21
GM14Do, grey	planar-s-1 dolomite	-0.90	-9.84
GM14Do, white	planar-s-2 dolomite	-0.81	-9.62

Little Manitou Island (analyzed at Queen's University)

Sample ID	elevation (meter)	$\delta^{13}C$ ‰ vs VPDB	$\delta^{18}O$ ‰ vs VSMOW	$\delta^{18}O$ ‰ vs VPDB
C17	0	-1.2	24.8	-5.9
C18	0.5	-0.7	24.8	-5.9
C19	1	-0.4	21.3	-9.3

Owen Quarry outlier
(analyzed at Queen's University)

sample	description	elevation (cm)	$\delta^{13}C$ ‰ vs VPDB	δ18O ‰ vs VPDB
HK 1	nonplanar-1 dolomite	7.5	2.66	-10.95
HK 9	nonplanar-1 dolomite	97	2.39	-10.10
HK 12	planar-s dolomite	300	2.44	-10.79
1401-15-a	planar-s dolomite	575	0.15	-10.64
HK 14	planar-s	750	0.33	-10.10
HK 14	saddle dolomite	750	1.571	-11.363
1401-1-b	porous dolomite	60	1.47	-10.83
HK7	nonplanar-1 dolomite	60	1.43	-10.35
1401-3	single crinoid	120	1.76	-11.01
1401-15-a	doo vein, nonplanar-c	575	2.65	-10.37
1401-11-b	planar-s dolomite	575	2.39	-11.659
1401-11-b	saddle dolomite, nonplanar-c	430	2.05	-10.99
1401-3	saddle dolomite, nonplanar-c	120	1.78	-10.79
HK 16-c	nonplanar-1 dolomite	Loc B	-1.93	-9.14
HK 16-a	saddle vein dolomite	Loc B	2.54	-10.12
1401-15-c	nonplanar-2 dolomite vein	Loc C	-2.03	-9.70
HK 20-a	planar-s dolomite	Loc C	-0.20	-10.55
1401-14	calcite with barite	430-670	-11.80	-8.39
1401-14	pure calcite	430-670	-7.46	-8.48
1401-15-a	calcite in dolomite vein	575	-3.29	-7.86

Appendix 4 Strontium Isotope

Sample	Description	$^{87}Sr/^{86}Sr$ (mean)	Valid values	Standard error (absolute)
Owen Quarry				
HK 14	planar-s dolomite	0.70866	100	9.19e-006
HK 20	planar-s dolomite	0.70915	100	6.93e-006
1401-1-b	nonplanar-1 dolomite	0.70949	99	7.06e-006
HK 1	nonplanar-1 dolomite	0.70887	100	8.86e-006
1401-14	late-stage calcite	0.70903	100	8.68e-006
1401-15-a	planar-s dolomite	0.70993	100	7.96e-006
1401-15-a	saddle dolomite	0.70894	99	8.07e-006
1401-3	saddle dolomite	0.70868	99	7.46e-006
HK 12	planar-s dolomite	0.70941	100	8.18e-006
1401-15-c	Fe-rich dolomite vein	0.70856	111	1.12e-005
Owen gneiss	granitic gneiss	0.76191	100	9.47e-006
Deux Rivières outlier				
DR 2	planar-s-2 dolomite	0.71035	99	9.01e-006
DR 5	wackestone	0.70832	100	8.19e-006
DR 7	lime mudstone	0.70877	100	5.88e-006
DR 9	lime mudstone	0.70851	100	1.31e-005
DR 11	planar-s-3 dolomite	0.70827	100	1.05e-005
DR 12	ooid-bearing grainstone	0.70813	98	1.26e-005
Great Manitou Island				
GM5Ca	late-stage calcite	0.70864	100	9.84e-006
GM5Do	saddle dolomite	0.70848	99	1.01e-005
GM14Grey	grey dolomite	0.70879	99	4.15e-005
GM14White	white dolomite	0.70845	100	8.92e-006
GM15	limestone	0.70866	100	8.99e-006
Owen gneiss	granitic gneiss	0.76191	100	9.47e-006